FABRICATION AND CHARACTERIZATION OF CIPROFLOXACIN LOADED NIOSOMES FOR TRANSTYMPANIC DELIVERY

A Thesis Submitted to Rhodes University in
Fulfilment of the Requirements for the Degree of

MASTER OF SCIENCE (PHARMACY)

In

PHARMACEUTICS

By

Asavela Mhlanga

NOVEMBER 2021

Faculty of Pharmacy
Rhodes University
Makhanda
South Africa

ABSTRACT

Ciprofloxacin (CPH) is a broad-spectrum antibiotic used to treat bone, joint, and skin infections. It is commercially available as an extended-release tablet and as a cream dosage form. CPH is a bactericidal active pharmaceutical ingredient (API) of the fluoroquinolone drug class. It inhibits deoxyribonucleic acid (DNA) replication by inhibiting bacterial DNA topoisomerase and DNA gyrase enzymes. Common adverse effects include nausea, vomiting, unusual fatigue, pale skin, and may increase the risk of tendinitis, which could be a major concern. CPH is, according to the Biopharmaceutics Classification System (BCS), classified as a BCS class IV drug exhibiting low oral bioavailability, low solubility, and intestinal permeability. CPH was chosen as a good candidate for the study because of its stability in solutions, its low molecular weight (331.4 g/mol), and its moderate lipophilicity (log P = 0.28) [16].

The use of conventional ear drops in the ear is effective, avoids hepatic first metabolism and extensive protein binding and may reduce adverse effects as a low dose may be used to achieve a therapeutic effect. However, conventional ear drops and oral antibiotics have a long onset of action and have to be taken/applied in short intervals. For convenience and assurance of a long residence time in the ear, CPH may be delivered by using a niosomal formulation, a liquid at room temperature, to allow administration into the ear without the need to constantly apply the ear drops for long periods of time.

A simple, rapid, precise, accurate, reproducible, and specific reversed-phase high-performance liquid chromatography (RP-HPLC) method using ultraviolet (UV) detection for the quantitation of CPH was developed and optimized using a central composite design (CCD). The method was validated using International Conference on Harmonisation (ICH) guidelines and was found to be linear, precise, accurate, and specific for the analysis of CPH. Since the method is specific, it was used to quantify CPH in commercial and experimental formulations and monitor CPH released during *in-vitro* release testing.

The compatibility of CPH and potential excipients was investigated during preformulation studies using Fourier transform infrared spectroscopy (FT-IR) and differential scanning calorimetry (DSC) to identify and select suitable excipients for use during formulation

development activities. No apparent interactions were evident between CPH, and the excipients tested.

The probe sonication method was used to manufacture CPH loaded niosomes using different surfactants/surfactant combinations, and a combination of Tween® 80: sodium lauryl sulfate (SLS) was found to be the best composition in terms of both entrapment efficiency and Zeta potential. The limits for the independent input variables used for the manufacture included amplitude, sonication time, and amount of cholesterol were determined.

Design of experiments (DOE) was used to design the study. The input variables investigated included amplitude, amount of cholesterol, and sonication time. The output or responses monitored included Zeta potential, vesicle size, polydispersity index (PDI), and entrapment efficiency. Non-ionic surfactant systems are predominantly stabilized by steric stabilization, and there is only a minor electrostatic element from adsorbed hydroxyl ions. With the inclusion of SLS it is to be expected that Zeta potential will be a contributing factor.

DOE using Box-Behnken design (BBD) and response surface methodology (RSM) in addition to Artificial Neural Networks (ANN) were used for the optimization of the formulation. The optimized formulation had a composition of 1 g cholesterol, 1 g of Tween® 80, 1 g of SLS and was prepared at an amplitude of 11.294 % with a sonication time of 3.304 minutes. The formulation exhibited zero-order release kinetics and had an average pH of 7.45. The formulation was stored at 4 ℃ and 25 ℃ and was assessed for vesicle size, entrapment efficiency, Zeta potential, colour, lamellarity, and PDI every 7 days for 4 weeks. The lead formulation stored at 4 ℃ was more stable than the formulation at 25 ℃ in terms of entrapment efficiency, PDI and vesicle size during the 4-week period.

CPH loaded niosomes for transtympanic delivery in the treatment of otitis media were developed and optimized. The technology exhibits sustained release of CPH and has the potential for further development and optimization.

ACKNOWLEDGEMENTS

My supervisor, Prof SMM Khamanga. Thank you for giving me the confidence to do postgraduate studies. Thank you for your assistance, advice, and patience in my years of study.

My co-supervisor, Prof RB Walker, thank you for the advice, providing me with materials and facilities, and lastly, thank you for your patience and guidance.

Rhodes University Finance office and the Hillensberg trust, thank you for giving me an opportunity to complete my studies. I would not have made this far without your continued financial support.

Dr BA Witika, Dr S Melamane, Dr M Chikukwa, and Dr P Ntemi for their constant guidance and assistance.

Rhodes University Faculty of Pharmacy postgraduates, thank you for your advice and support.

Miss SP Tyobashe, thank you for your constant support and assistance; I would not have made it this far without you.

Mr S Ngxingo, Mr T Fleck, Mr X Rasana, Ms L Emslie, Mrs T Kent, Mr Baa, and Dr S Abboo for their unlimited assistance, providing me with the materials required and assisting me with instruments.

Pharmacy undergraduate students, it has been a pleasure working with you guys. I have learnt as much from you as you have from me.

To all the teachers and lecturers, I have ever come across in my academic career, you all have profoundly affected me and how I see the outside world. Thank you all, and I would not be here if not for your hard work and dedication.

DEDICATION

To my family

Thank you for the constant love and support. Even when I felt overwhelmed and ready to give up, you were always there for me. I appreciate your unwavering support and never-ending love.

Jesus Christ, my saviour

Nokuba ndihamba emfuleni wethunzi lokufa,
Andiyi koyika bubi, ngokuba unam wena.
Intonga yakho, umsimelelo wakho, uyandithuthuzela.

To my brother

Zamxolo Hope Mhlanga (1980 -2020)

It is on days like these that I think about you the most. You have always been there for me from the first time I arrived at this university. I wish you were here to celebrate this achievement. Thank you for your love and support. I am lucky to have a guardian angel like you; this is your achievement. I dedicate this to you. Te amo Hermano.

STUDY OBJECTIVES

Otitis media is an inflammation of the tympanic membrane and the middle ear commonly caused by *Streptococcus pneumonia* and affects the outer and middle ear. Otitis media is a major chronic disease in low- and middle-income countries with Sub-Saharan Africa and South Asia having the highest incidence [1]. Otitis is associated with complications like hearing loss, decreased learning ability and low educational achievement. Symptoms include loss of balance, fever, and fluid draining from the ear(s) [1]. Typical management of bacterial ear infections in South Africa usually requires an oral course of a broad-spectrum antibiotic for 14 days which may be changed to intravenous (IV) injection if the signs and symptoms do not disappear within a few days of commencing treatment [2]. Ear drops are also available and to date, many products used for bacterial ear infections are administered locally in the ear [3]. The main limitation with ear drops is the tympanic membrane's low permeability, which presents a potential barrier for transtympanic drug diffusion [4]. However, local antibiotic delivery across an intact tympanic membrane using niosomes may be considered a promising alternative to systemic antibiotics for treating bacterial ear infections [5].

Local niosomal treatment will exhibit advantages over the conventional ear drops such as enhanced availability of the API at the site of action, complete eradication of pathogenic bacteria, and thus, a reduced likelihood of recurrent infection and risk of developing antibiotic resistance [4, 5].

Topical formulations using niosomes to deliver poorly permeable drugs through the tympanic membrane are based on non-ionic surfactants and can entrap hydrophilic and hydrophobic drugs [6]. Niosomes have several advantages over conventional ear drops, such as biocompatibility, biodegradability, non-immunogenicity, and structural stability which can improve antimicrobial activity and therapeutic potency of antibiotics. The ability of these deformable vesicles to cross the stratum corneum because of their elasticity has been intensively studied [7]. It has been shown that upon non-occlusive application, niosomal vesicles significantly enhance the transdermal delivery of drugs that would otherwise penetrate poorly [6]. Given the potential of these vesicles to increase transdermal drug delivery, they may also be effective in the tympanic membrane. The ability of niosomes as carriers for compounds, such as enoxacin [8], febuxostat [9], atenolol [10], lacidipine [11], and anticancer agents [12] has been reported. Since these elastic vesicles move towards areas of high-water

content, it would be expected that a niosomal formulation could potentially enhance the flux of antibiotics across an intact tympanic membrane into the affected area [7].

CPH is a synthetic broad-spectrum bactericidal fluoroquinolone antibiotic. It acts by inhibiting the bacterial DNA gyrase, resulting in the degradation of bacterial DNA by exonuclease activity [13]. It is a widely used antibiotic for systemic and topical treatment of otitis media in adults and children [13, 14]. Despite being contraindicated for systemic use in children because of its effect on bone growth plates, CPH has been approved for topical treatment of ear infections in paediatric patients [15].

The objectives of this study were to:

1. Develop and validate a high-performance liquid chromatographic (HPLC) method with UV detection for the accurate and precise quantitation of CPH.
2. Conduct preformulation studies to investigate the potential for CPH-excipient interactions using FT-IR spectroscopy and DSC methods and determine the compatibility of CPH with excipients in the study.
3. Evaluate CPH release and fit *in-vitro* release data to different kinetic models.
4. Investigate factors that affect CPH release from niosomes and identify aspects of formulation and manufacture requiring further studies.
5. Conduct stability assessment of the formulations at 4 ºC and 25 ºC for 4 weeks and monitoring vesicle size, Zeta potential, polydispersity index (PDI), colour, lamellarity, membrane permeability, surface morphology, and entrapment efficiency.

TABLE OF CONTENTS

LIST OF TABLES

CHAPTER ONE

CHAPTER TWO

CHAPTER THREE

CHAPTER FOUR

CHAPTER FIVE

LIST OF FIGURES

CHAPTER ONE

CHAPTER TWO

CHAPTER THREE

CHAPTER FOUR

CHAPTER FIVE

ABBREVIATIONS

3D	Three dimensional
ACN	Acetonitrile
AIDS	Acquired Immune Deficiency Syndrome
ANN	Artificial Neural Network
ANOVA	Analysis of variation
API	Active pharmaceutical ingredient
AUC	Area under curve
BBD	Box-Behnken Design
BCS	Biopharmaceutical classification system
BFGS	Broyden Fletcher Goldfard Shano
CBZ	Carbamazepine
CCD	Central Composite Design
CI	Confidence interval
CNS	Central nervous system
CPE	Chemical penetration enhancer
CPH	Ciprofloxacin
CV	Coefficient of variation
Df	Degree of freedom
DNA	Deoxyribonucleic acid
DOE	Design of experiment
DSC	Differential scanning calorimetry
FDA	Food & Drug Administration
FT-IR	Fourier-transform infrared spectroscopy

GC	Gas chromatography
GFR	Glomerular Filtration Rate
GIT	Gastrointestinal tract
HLB	Hydrophilic-lipophilic balance
HPLC	High pressure liquid chromatography
ICH	International Conference on Harmonization
INR	International Normalized Ratio
IR	Infrared
IS	Internal standard
IV	Intravenous
LC	Liquid chromatography
LOD	Limit of detection
LOQ	Limit of quantification
LUV	Large uni-lamellar vesicle
MSE	Mean square error
MW	Molecular weight
NMR	Nuclear Magnetic Resonance
NPC	Normal-phase chromatography
PAR	Peak area ratio
PDI	Polydispersity index
PKa	Acid dissociation constant
PRESS	Predicted error sum of squares
R_s	Resolution factor
R_t	Retention time
RPC	Reverse phase chromatography

RP-HPLC	Reverse-phase high pressure liquid chromatography
RSD	Relative standard deviation
RSM	Response surface methodology
SEC	Size-exclusion chromatography
SD	Standard deviation
SLS	Sodium lauryl sulfate
TEM	Transmission electron microscope
USP	United States Pharmacopoeia
UTI	Urinary tract infection
UV	Ultraviolet
VIF	Variance Inflation Factor

CHAPTER ONE

CIPROFLOXACIN

1.1 INTRODUCTION

Otitis media is an infection of the middle ear that usually begins due to upper respiratory tract pathogens entering the middle ear via the Eustachian tube, leading to inflammation and effusion. Although it may occur at any age, it is most frequently diagnosed in children. Current therapy for otitis media usually includes an oral course of a broad-spectrum antibiotic. A significant proportion of antibiotics prescribed (≥ 25 %) are dispensed to treat otitis media. Systemic administration of broad-spectrum antibiotics against an infection with such high prevalence and recurrence is believed to be partially responsible for the emergence of drug-resistant strains of pathogenic bacteria [4]. Furthermore, the systemic administration of antibiotics often results in side effects, including diarrhoea, dermatitis, vomiting, and oral thrush [4, 5].

Local and sustained delivery of active therapeutics directly to the middle ear for the treatment of otitis media could potentially minimize systemic exposure and side effects and allow for substantially higher middle ear drug concentrations than systemic administration [17]. However, although only about 100 μm thick, the tympanic membrane presents a barrier impermeable primarily to all but the smallest lipophilic molecules [18] (**Figure 1.1**).

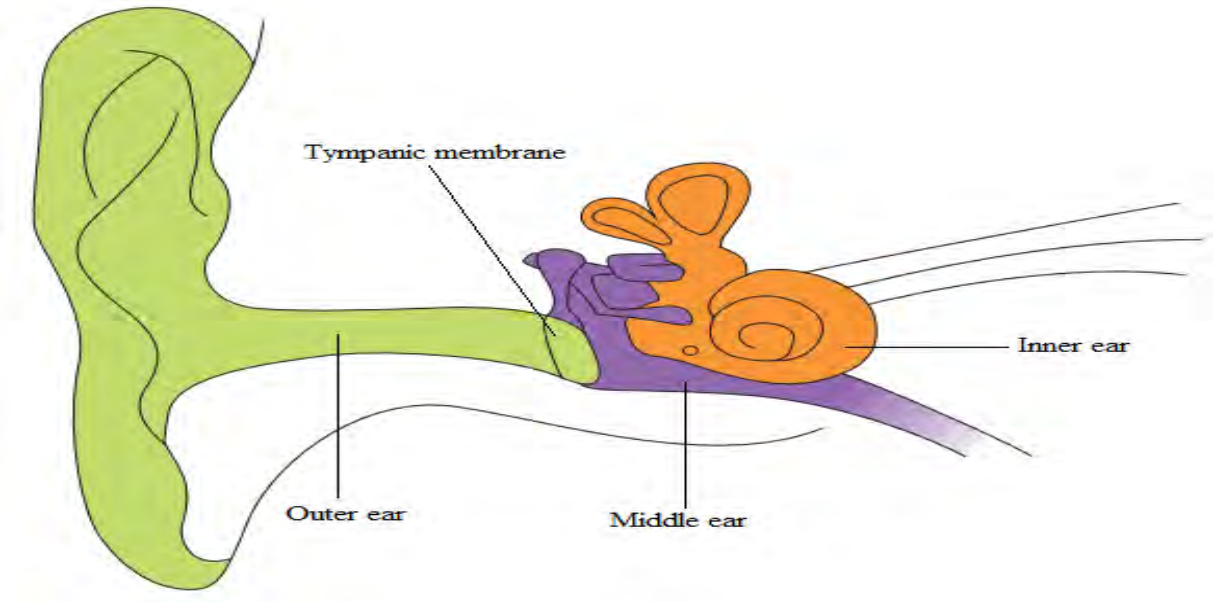

Figure 1.1 The structure of the ear (Adapted from [18]).

Strategies have been extensively explored to overcome the tympanic membrane barrier, these include chemical additives, iontophoresis, and micro-injection [19]. Chemical permeation enhancers (CPE) have emerged as an effective means of enhancing small molecule flux across the tympanic membrane. By reversibly increasing the permeability of the tympanic membrane, CPE significantly improve the transtympanic delivery of molecules that would otherwise permeate poorly, and a formulation combining both CPE and antibiotics could potentially enhance drug flux across the intact tympanic membrane into the middle ear [20-22].

There are two main routes of transdermal permeation of drugs: the transcellular/transappandageal route, through which substances infiltrate the keratocytes, appendages, and intercellular lipids, subsequently pass through the stratum corneum and are then transported to the systemic circulation. The drug needs to diffuse through hydrophilic and hydrophobic areas, and therefore, it may not apply to most drugs [23]. The second and most likely route taken by drugs when penetrating the stratum corneum is via a tortuous pathway through the lipids surrounding the keratocytes, known as the intercellular route (**Figure 1.2**) [24]. Niosomes have been proven to be effective in transdermal and could be effective in transtympanic delivery as the two membranes share many structural similarities [24].

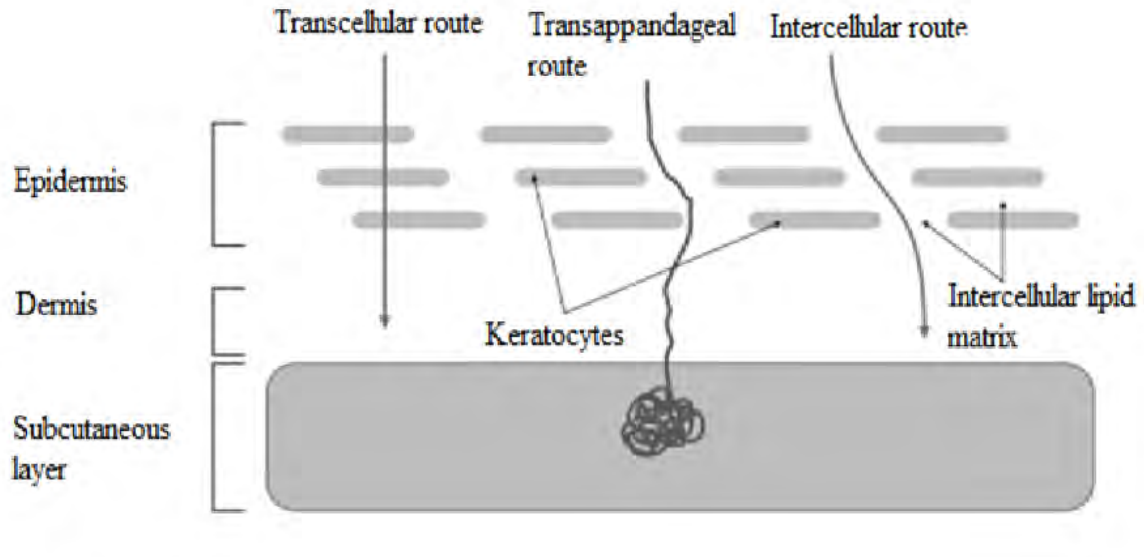

Figure 1.2 Main routes of transtympanic permeation (Adapted from [24]).

Novel vesicular drug delivery systems aim to deliver the drug at a rate directed by the body's need during treatment and channel the active entity to the site of action. Bingham first reported the biological origin of these vesicles in 1965, and the vesicles have been given the name Bingham bodies. Several novel vesicular drug delivery systems have emerged since,

encompassing various routes of administration, to achieve targeted and controlled drug delivery [25]. Targeted drug delivery is a mode of delivering the therapeutic agent to the tissues of interest while reducing the relative concentration of the therapeutic agent in remaining tissues, which improves the therapeutic efficacy and reduces side effects. Drug targeting means the delivery of drugs to receptors, organs, or any other specific part of the body to which one wishes to deliver the entire drug [26]. Paul Ehrlich developed the targeted drug delivery system in 1909, which delivered the therapeutic agent directly to diseased cells. Since then, many carriers were utilized to deliver the drug to the target site; these include immunoglobulins, serum proteins, synthetic polymers, microspheres, liposomes, niosomes, and erythrocytes. Among different carriers, vesicular drug delivery systems are found to be well renowned [27]. These systems have also been used to improve drug molecules' therapeutic index, solubility, stability, and rapid degradation [25-27]. The different types of vesicular carriers are shown in **Table 1.1**.

Table 1.1 The different types of lipid and non-lipid-based vesicular carriers (Adapted from [27]).

Lipid-based vesicular carriers	Non-lipid-based vesicular carriers
Liposomes	Niosomes
Enzymosomes	Bilosomes
Sphingosomes	Aquasomes
Pharmacosomes	
Emulsomes	
Ethosomes	
Transfersomes	
Virosomes	

Niosomes are vesicular systems comprising a bilayer made up of non-ionic surfactants and were primarily launched to the market in 1987 by Lancôme [28]. Due to their deformable nature, they act as excellent carriers for loading both hydrophilic and lipophilic drugs. These vesicles are biocompatible, biodegradable, non-immunogenic, and enhance permeation of drugs across the tympanic membrane by disrupting the lipids due to the presence of a surfactant and the flexible nature of the vesicle [29]. Another mechanism regarding alteration of the barrier function is the adsorption and fusion with the tympanic membrane surface, followed by the modification of the tympanic membrane lipids. The discovery of niosomes,

due to their deformability, can pass through skin pores 5 – 10 times lesser than their size, makes the relative molecular mass limit of the drugs that penetrate the skin reach up to 1 million g/mol and enables the administration of macromolecular drugs such as peptides and proteins [29, 30].

1.2 PHYSICOCHEMICAL PROPERTIES

1.2.1 Description

CPH was discovered in 1983 when the pharmaceutical company Bayer published *in-vitro* potency data for CPH, a fluoroquinolone antibacterial having a chemical structure differing from that of norfloxacin by the presence of a single carbon atom. The oral tablet form of CPH was approved in October 1987, just one year after the approval of norfloxacin [30].

CPH is a faint to light yellow crystalline powder which is practically insoluble in water [31]. CPH has a chemical formula of $C_{17}H_{18}FN_3O_3$ and is chemically known as 1-cyclopropyl-6-fluoro-4-oxo-7-piperazin-1-quinoline-3-carboxylic acid. The chemical structure of CPH is shown in **Figure 1.3**. CPH has a molecular weight of 331.34 g/mol, dissociation constant (pKa) of 6.09, a partition coefficient of 0.28 [32] and is available commercially in South Africa as Cipro Bay®, Austell-Ciprofloxacin®, Biotech Ciprofloxacin®, Cifran®, Ciploxx®, Ciprofloxacin Actor®, Cipro-Hexal®, Ciprol®, CPL Alliance Ciprofloxacin®, Dynafloc®, Cifloc®, Ciprogen®, Orpic®, Loxip®, Sabax® Ciprofloxacin® and Spec-Topistin® [33].

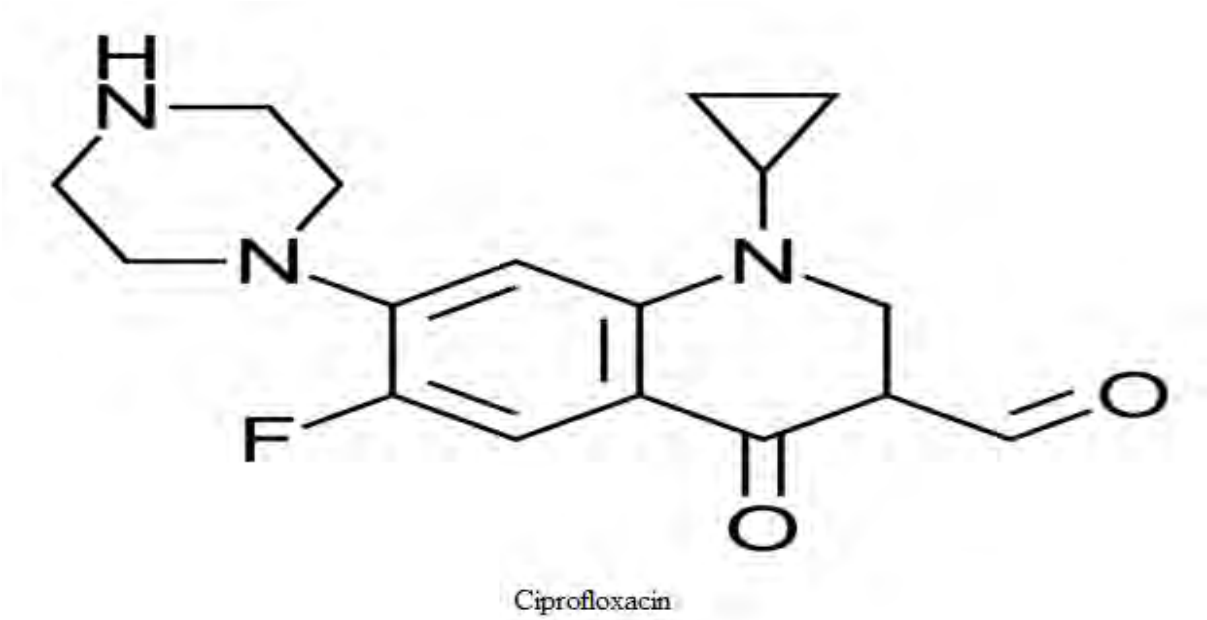

Figure 1.3 Chemical structure of CPH (Adapted from [32]).

1.2.2 Isomerism

CPH does not have any known isomers [34].

1.2.3 Solubility

CPH is poorly soluble in water, practically insoluble in dehydrated alcohol and dichloromethane, and soluble in dilute hydrochloric acid. The solubility of CPH is summarized in **Table 1.2** [31].

Table 1.2 Solubility of CPH in different solvents [31].

Solvent	Solubility mg/ml
Water	1.35
DMSO	< 1
0.1 N HCl	25
Ethanol	< 1

1.2.4 Dissociation constant (pKa)

The pKa of CPH is 6.09, pKa 5.76 (carboxylic acid group) and pKa 8.68 (piperazinyl ring) [31].

1.2.5 Biopharmaceutical classification system

The Biopharmaceutical classification system (BCS) classifies API according to their gastrointestinal permeability and aqueous solubility [35]. CPH is classified as a BCS class IV compound exhibiting low water solubility and gastrointestinal permeability [36, 37]. CPH does not exhibit high solubility at all pH values between 1 to 7.5 and has a bioavailability of less than 90% [37].

1.2.6 Partition coefficient

The partition coefficient is defined as the concentration ratio between two media at equilibrium [38]. Substances tend to distribute between two partially miscible solvents, and the ratio of API concentrations in the organic phase and aqueous phase is known as partition coefficient [39]. Log P represents the logarithm of the partition coefficient for an API between octanol and water [40]. CPH has a log octanol/water partition coefficient (log P) of 0.28 [41].

1.2.7 Hygroscopicity

CPH is slightly hygroscopic [42].

1.2.8 Stability

The degradation of CPH was carried out in alkaline conditions (0.1 N NaOH at 70 ℃ for 4 hours), acidic conditions (0.1 N HCl at 70 ℃ for 4 hours), and oxidative degradation (3 % H_2O_2 at 70 ℃). Degradation of the drug product was carried out as per the International Council for Harmonisation (ICH) guidelines. It was found that in alkaline conditions, i.e., in 0.1 N NaOH at 70 ℃ for 4 hours, the degradation of CPH was about 24 %. In acidic conditions (0.1 N HCl at 70 ℃ for 4 h), the degradation was somewhat slower than in alkaline conditions, and it was found to be about 20 %. Oxidation degradation (3 % H_2O_2 at 70 ℃ for 4 h) of CPH was somewhat significant compared to acidic and alkaline conditions and was found to be about 40 %. The percentage of drug degradation under UV radiation for 5 days and in thermal conditions at 60 ℃ for 24 hours was about 30 % and 10 %, respectively. CPH was stable at ambient temperature and when stored at 2 - 5 ℃ [30].

1.2.9 Polymorphism

There are no known polymorphs of CPH known in literature [31].

1.2.10 Melting point

CPH has a melting point range of 255-257 ℃ [31].

1.2.11 Ultraviolet (UV) spectrum

CPH was detected and quantified at a wavelength of 277 nm (lambda max = 278nm) [43].

1.2.12 Infrared (IR) spectrum

Infrared (IR) spectroscopy is used in the identification, and structural elucidation of compounds wherein molecules absorb electromagnetic radiation at frequencies correlating to the vibration of the functional groups and chemical bonds resonate at different frequencies [44, 45]. These frequencies are determined and assessed using IR spectroscopy [46]. The IR spectrum may be used as a fingerprint for identification by comparing the spectrum of an unknown compound with a reference spectrum [45]. FT-IR spectroscopy is also used to determine API-excipient compatibility [46]. The FT-IR spectra of CPH (Sigma-Aldrich®, St. Louis, Missouri, USA) is shown in **Figure 1.4**. The spectrum was generated using a Perkin Elmer® Spectrum 100 FT-IR ATR spectrophotometer (Beaconsfield, Buckinghamshire, England). The scanning range was between 4000 and 650 cm^{-1}, and the resolution was 4 cm^{-1}. In the FT-IR spectra of CPH, the two characteristic peaks at 3500.00 and 3450.44 cm^{-1} respectively were assigned to OH stretching vibrations (intermolecular hydrogen bonding). Another band at 2980.66 cm^{-}

[1] represents alkenes and aromatic C-H stretching. The bands at 1745.67 and 1712.34 cm[-1] indicated carbonyl C = O stretching and quinolones, respectively, while the band at 1435.55 cm^{-1} was assigned to C - O vibrations. The strong band at 1300.54 cm^{-1} represents the OH group's bending vibration, which indicates the presence of carboxylic acid. In addition, the band at 1000.37 cm^{-1} was assigned to the C-F group (**Table 1.3**) [47].

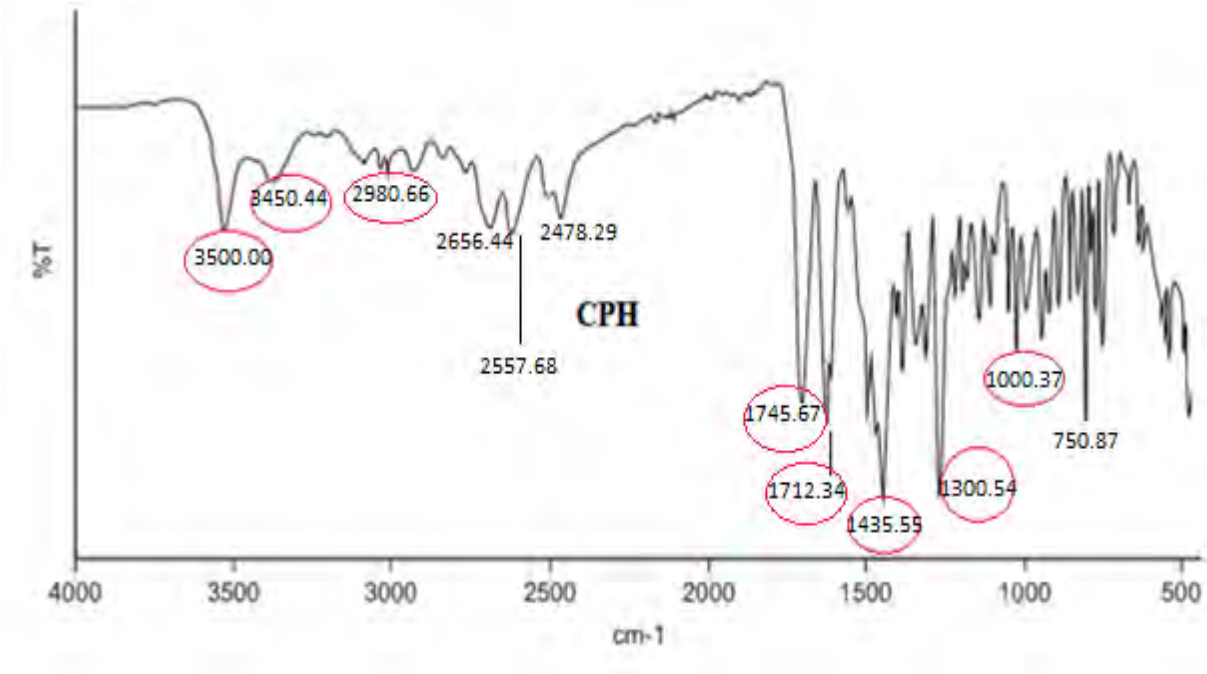

Figure 1.4 FT-IR spectrum of CPH.

Table 1.3 CPH prominent FT-IR peaks.

Peaks (cm^{-1})	**Groups**	**Peak assignment**
3500-3450	Hydroxyl group	O-H stretching vibration, intermolecular H-bond
3000-2950	Aromatics and cyclic alkenes	Alkene and C-H stretching
1750-1700	CO group of acid	C = O stretching vibration
1650-1600	Quinolones	δ N-H bending vibration
1450-1400	Carbonyl group	υ C-O
1300-1250	Hydroxyl group	δ O-H bending vibration
1050-1000	Fluorine group	C-F stretching

1.2.13 Differential scanning calorimetry

DSC was used to identify CPH. The melting point of CPH was established using a TA Model Q100 Differential Scanning Calorimeter, which is fitted with an RCS (90) refrigerated cooling system (New Castle, Delaware, USA). Approximately 2.5 to 5 mg of the sample was weighed into an aluminium pan and sealed with an aluminium disc, and an empty aluminium pan was used as a reference. The DSC scan was produced by heating the sample from 30 ℃ to 450 ℃ at a rate of 10 ℃/min with gas nitrogen purge at a flow rate of 20 mL/min used to cool the system to 15 ℃. The thermogram was analyzed using TA Universal Analysis 2000 software (New Castle, Delaware, USA). The generated thermogram is shown in **Figure 1.5**. CPH showed a sharp melting exotherm at 323.15 ℃, therefore positively identifying CPH. The enthalpy of the reaction was 145.38 J/g with an area of 395.68 mJ.

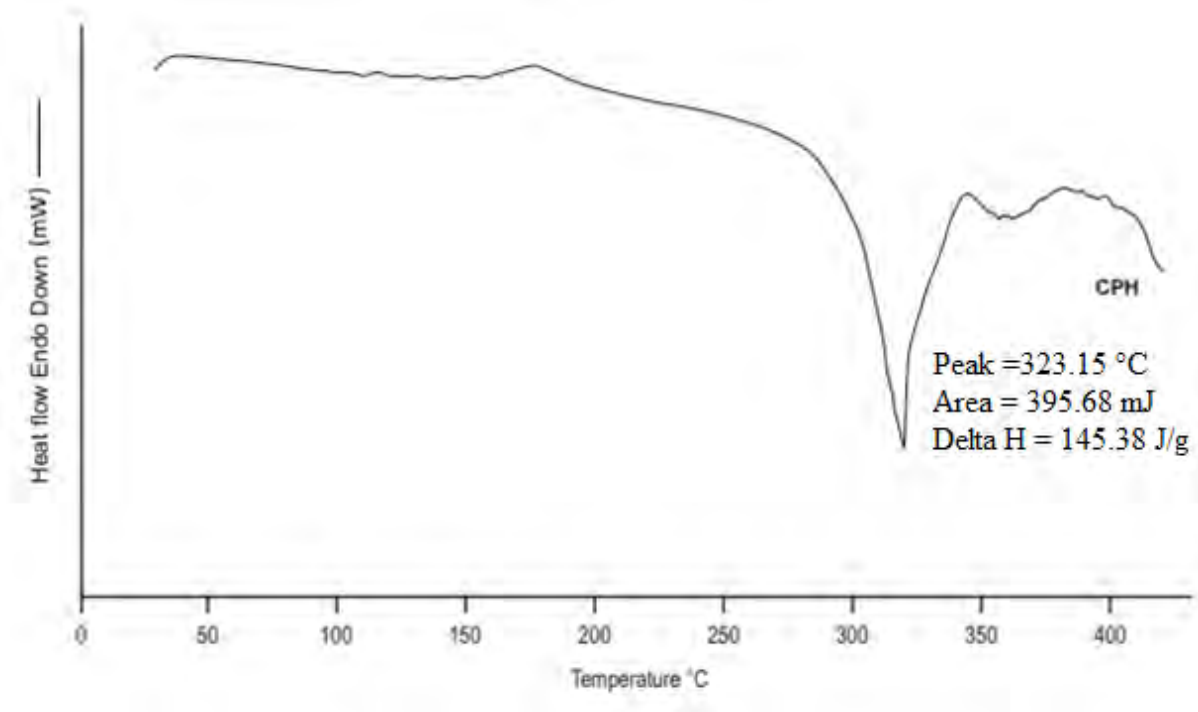

Figure 1.5 CPH DSC thermogram.

1.3 SYNTHESIS

1.3.1 Synthetic pathway

2, 4-dichloro-5-fluorobenzoylchloride is condensed with diethyl malonate using magnesium ethoxide in ether to produce diethyl 2, 4-dichloro-5-fluorobenzoylmalonate, which is partially hydrolysed and decarboxylated with p-toluene sulfonic acid-water, yielding ethyl 2, 4-dichloro-5-fluorobenzoylacetate. Condensation of this with triethylorthoformate in refluxing acetic anhydride affords ethyl 2-(2, 4-dichloro-5-fluorobenzoyl)-3-ethoxyacrylate, which is treated with cyclopropylamine in ethanol to give ethyl 2-(2, 4-dichloro-5-fluorobenzoyl)-3-cycloporpylaminoacrylate. Cyclization of ethyl 2-(2, 4-dichloro-5-fluorobenzoyl)-3-cycloporpylaminoacrylate with NaOH in refluxing dioxane then yields 7-chloro-1-cyclopropyl-6-fluoro-1, 4-dihydro-4-oxoquinoline-3-carboxylic acid, which is finally condensed with piperazine in hot DMSO to yield CPH [48]. A schematic representation of the synthesis pathway of CPH is shown in **Figure 1.6**.

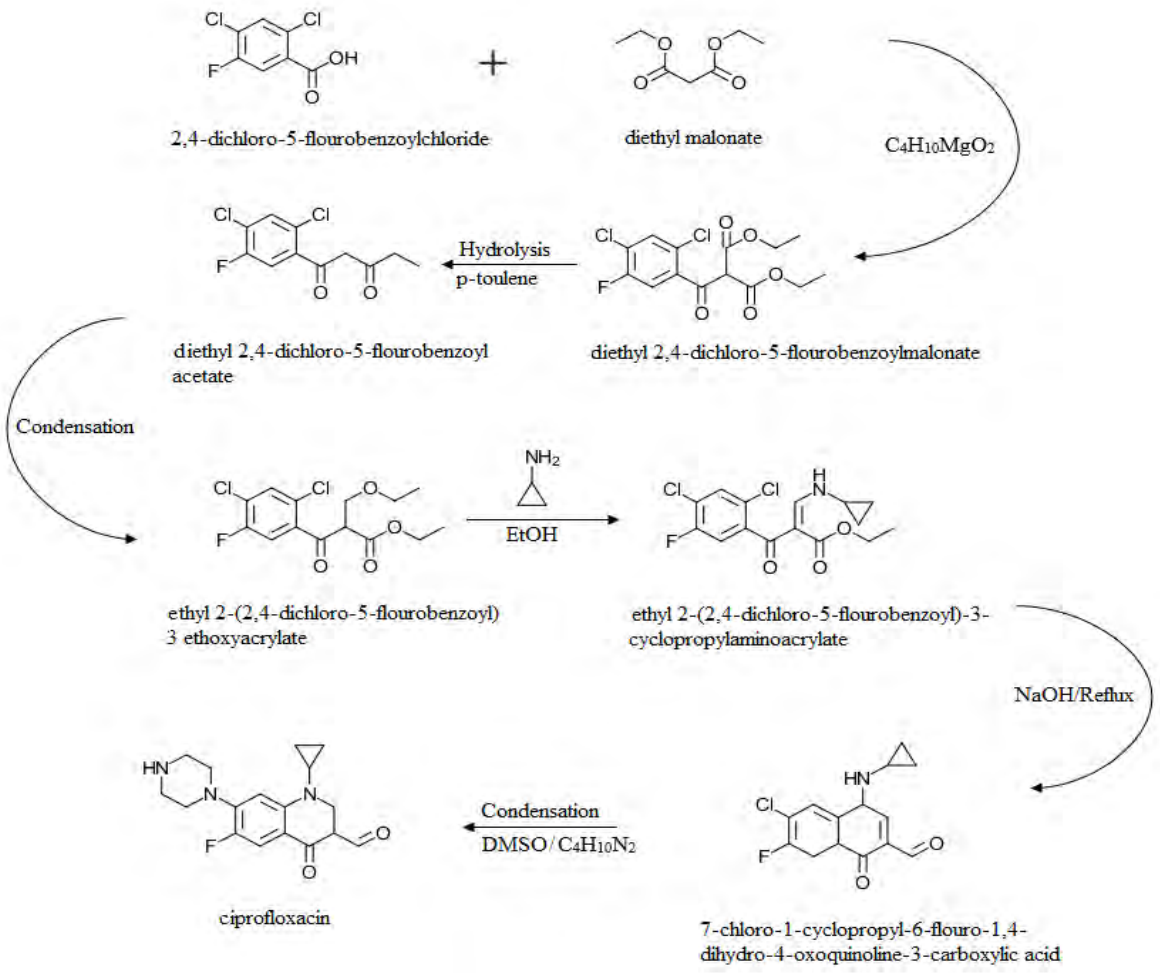

Figure 1.6 The synthesis pathway of CPH [48].

1.3.2 Structure-activity relationship

Hooper [49] reported the essential functional groups for CPH antibacterial activity. These functional groups exist in a special spatial arrangement, as shown in **Figure 1.7.**

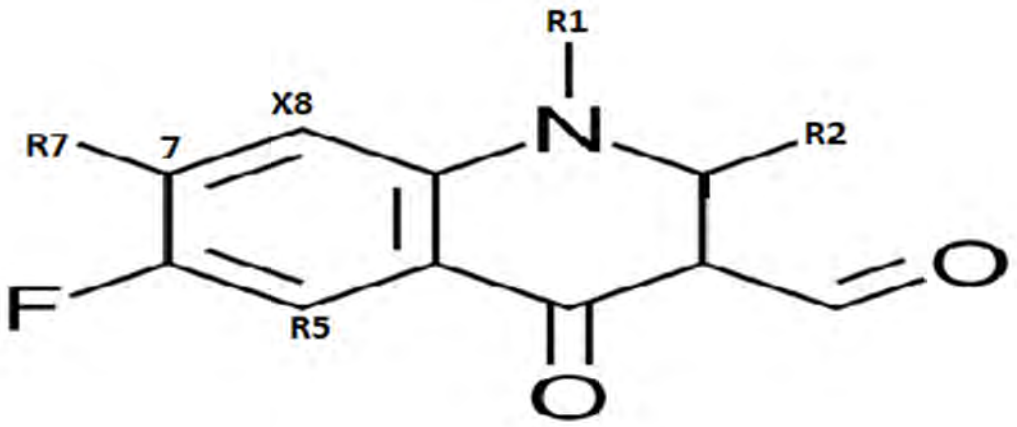

Figure 1.7 Chemical structure of CPH – an annotated diagram of the primary structures for antibacterial activity [49].

The fluorine group (R6) control is responsible for gyrase and bacterial potency. The fluorine group is 5 - 100× more active than other groups. Structure-activity relationships show that antibacterial activity is related to nitrogen heterocyclic moiety, which is present at the C-7 position of fluoroquinolones. Literature shows that introducing modifications at nitrogen moiety significantly affects the antibacterial potential of fluoroquinolones. The R7 group controls potency, spectrum, and pharmacokinetics. The 5 - 6 membered rings are the most active. For oral activity: CF, CCl > N > COMe > CH, the X8 group controls pharmacokinetics and anaerobe activity. For the best anaerobe activity, the order is as follows, CCl > CF > COMe >> CH > N. The R1 group controls potency and has some effect on pharmacokinetics. O or N groups at R1 reduce activity. H is optimal in the R2 group. This group is close to the gyrase binding site. The carboxylic group is essential for gyrase binding and bacterial transport [49].

1.4 CLINICAL PHARMACOLOGY

1.4.1 Mechanism of action

CPH is a second-generation fluoroquinolone that is active against many gram-negative and gram-positive bacteria [50]. It produces its action through inhibition of bacterial DNA gyrase and topoisomerase IV. CPH binds to bacterial DNA gyrase with 100 times the affinity of mammalian DNA gyrase. There is no cross-resistance between fluoroquinolones and other classes [51].

1.4.2 Clinical indications

CPH is used to treat infections caused by sensitive organisms of the urinary, gastrointestinal, and lower respiratory tracts, skin and soft tissue, and bone. It is the drug of choice for typhoid fever [33].

1.4.3 Off-label use

CPH has been effective in the treatment of isopropiasis, which is a parasitic intestinal infection. CPH is also used in the prevention of isopropiasis from reoccurring [52].

1.4.4 Contraindications

CPH is contraindicated in patients with a known allergy to CPH or other quinolones [33].

1.4.5 Precautions and warnings

1.4.5.1 Pregnancy

CPH is a category C medication, and cartilage damage has been reported in animals. Most studies reported no increased chance of congenital disabilities when women took CPH or other quinolone antibiotics during the first trimester of pregnancy [33]. These studies included women receiving CPH for only five to seven days. The effects of long-term use in pregnancy are not well known [53].

1.4.5.2 Lactation

CPH is excreted in breast milk, and use is not recommended [33].

1.4.5.3 Paediatric patients

Studies have shown damage to the cartilage of weight-bearing joints in immature animals. Therefore, only use in patients under 18 years old for severe infections when there are no other alternatives [33].

1.4.5.4 Geriatric patients

Older patients are particularly at risk of neurotoxicity [33].

1.4.5.5 Renal impairment

Patients with renal impairment should not use ciprofloxacin. If the benefit outweighs the risk, the administered dose must be 50 – 75 % of the original dose for stage 5 chronic kidney failure. If the glomerular filtration rate (GFR) < 10 mL/min, the dose must be 50 % of original dose [33].

1.4.5.6 Hepatic impairment

Use of CPH in hepatically impaired patients is not recommended [33].

1.4.6 Drug interactions

CPH is an inhibitor of hepatic microsomal enzymes. When taken concurrently with theophylline, the clearance of theophylline is reduced, leading to increased serum levels of theophylline in the blood. CPH tends to induce an increase in anticoagulant effects, and therefore the International Normalized Ratio (INR) should be monitored. Concurrent use of sucralfate, antacids containing aluminium, calcium or magnesium, or oral iron, zinc, or magnesium supplements reduce the absorption of CPH. Concomitant use of CPH with glibenclamide may result in hypoglycaemia. Probenecid interferes with the renal secretion of CPH and may increase CPH concentrations [33].

1.4.7 Adverse effects

1.4.7.1 Hepatic

CPH can cause raised liver enzymes, hepatic necrosis, and interstitial nephritis [54].

1.4.7.2 Dermatological

Hypersensitivity reactions have been reported, including skin rash, urticaria, pruritus, and photosensitivity reactions. Hypersensitivity reactions commonly present themselves as a maculopapular rash which may lead patients to stop treatment. This rash is considered an immune-mediated hypersensitivity reaction due to an increase in the percentage of activated

T-helper and T-suppressor lymphocytes and an increase in serum concentrations of immunoglobulin E immediately after the rash appears [55].

1.4.7.3 Gastrointestinal

CPH is generally well tolerated. The most frequent adverse effects are gastrointestinal disturbances such as abdominal pain, nausea, vomiting, and diarrhoea. Pseudomembranous colitis has also been reported but rarely occurs [33].

1.4.7.4 Musculoskeletal and neurological

The use of CPH has been associated with central nervous system (CNS) effects like headache, dizziness, restlessness, drowsiness, insomnia, tremor, agitation, and confusion. Seizures and hallucinations are rare but may occur more commonly in patients with underlying CNS diseases [33].

1.5 CLINICAL PHARMACOKINETICS

1.5.1 Dosage and administration

The CPH adult (over 18 years) oral dose is 250 -750 mg twice daily, depending on the nature and severity of infection. Prolonged therapy (4 - 6 weeks) is required in bone infections, chronic prostatitis, and invasive salmonellosis in Acquired Immunodeficiency Syndrome (AIDS) patients [33]. For urinary tract infection (UTI), an oral dose of 250 – 500 mg twice a day (250 mg as a single dose or twice daily for 3 days in acute uncomplicated cystitis in non-pregnant women). For meningococcal prophylaxis, an oral dose of 500 mg is administered as a single dose. In the case of renal impairment, if GFR 10 - 50 mL/min (stage 5 chronic kidney failure), give 50 – 75 % of the dose. If GFR < 10 mL/min, take 50 % of original dose [33].

1.5.2 Overdose

The overdose concentration for CPH has not yet been determined [56].

1.5.3 Absorption

1.5.3.1 Systemic Circulation

CPH has an oral bioavailability of 70 – 80 %. The drug is widely distributed with good penetration of tissues and bone and has a half-life of 4 – 5 hours, slightly longer in renal failure. The drug is metabolised in the liver, 40 – 50 % of an oral dose is excreted unchanged in the urine, small amounts are excreted in the bile, and 20 – 35 % of an oral dose is excreted in the faeces in 5 days [33]. In an otic solution, maximum plasma concentrations of CPH are expected

to be less than 5 ng/mL after administration of 0.25 mL otic solution (total dose, 0.5 mg CPH). After multiple doses of CPH immediate-release tablets, CPH area under the curve (AUC) (0 to 12 hours) was 13.7 µg x hr/mL with a 500 mg dose administered every 12 hours the AUC (0 to 24 hours) was 31.6 µg x hr/mL with a 750 mg dose administered every 12 hours. Food tends to delay absorption by 1 hour (tablet), but the extent of absorption is not affected. When a CPH immediate-release tablet is given concomitantly with food, there is a delay in the absorption of the drug, resulting in peak concentrations that occur closer to 2 hours after dosing rather than 1 hour, whereas there is no delay observed when a CPH oral suspension is given with food. The overall absorption of CPH tablets or suspensions, however, is not substantially affected. The pharmacokinetics of CPH given as the suspension is also not affected by food. Extended-release tablets may be administered with or without food. The renal clearance of CPH is approximately 300 mL/min or 22 L/hour [56].

1.5.4 Distribution

When CPH is intravenously administered, its plasma concentration is best characterized by a one-compartment open model undergoing first-order elimination [57]. The volume of distribution ranges between 2.1 and 2.7 L/kg. The plasma protein binding degree of CPH to serum proteins is 40 % [56].

1.5.5 Metabolism and elimination

The pharmacokinetic parameters of CPH in adults are summarized in **Table 1.4.**

Table 1.4 Pharmacokinetic parameters of CPH in adults**.**

Drug	Bioavailability (%)	Protein binding (%)	Volume of distribution (L/kg)	Half-life (hrs)	Clearance (L/Hr)	Main route of distribution
CPH	70 – 80	20 – 40	2.1 - 2.7	4 – 6	35	Renal

The primary route of elimination for CPH is the renal route. CPH has three metabolites, namely, desethylene ciprofloxacin, sulfonyl ciprofloxacin, and oxo ciprofloxacin. 40 – 50 % of a CPH dose is eliminated unchanged renally, small amounts in the bile, and 20 – 35 % is excreted in the faeces in ≈ 5 days [57].

1.6 CONCLUSIONS

CPH is a fluoroquinolone antibiotic that acts by inhibiting DNA gyrase, interfering with the reproduction of bacterial DNA. It is used mainly against *Enterobacteriaceae, P. Aeruginosa, Haemophilus*, and *Legionella* species but has no beneficial activity against *S. Pneumonia*. CPH is a well-tolerated antibiotic with the most common adverse effects: pain, nausea, vomiting, and diarrhoea and does not cause bloating, indigestion, or loss of appetite as associated with other antibiotics [58].

Patients usually discontinue their otitis media treatment regimen due to a severe rash; therefore, the delivery of CPH in a dosage form and route that will allow the administration of lower dosages may reduce the prevalence of this and many other adverse effects. CPH is currently available as tablets and an IV infusion [33]. As a result, the drug passes through the gastrointestinal tract (GIT) into the systemic circulation. The administration of CPH via a route that avoids the GIT membrane passage would be preferable because 50 % of an oral dose of CPH is excreted unchanged in the urine. The high concentrations of drug lost in the urine warrant high oral doses, e.g., 250 mg, 500 mg, and 750 mg. High doses may also induce adverse effects such as insomnia, agitation, and abdominal pains. Patient adherence is essential in the treatment of otitis media. Patient inconvenience and challenges associated with the use of currently available technologies may be reduced by the development of novel methods which may improve patient adherence to the medication regimen.

Niosomes share the same general preparation methodology as other lipid vesicles and can be prepared as uni- or multi-lamellar vesicles. Niosomes, like liposomes, are vesicular systems composed mainly of non-ionic surfactants and cholesterol bilayers. Compared with liposomes, these vesicular systems exhibit preferred characteristics, such as high chemical stability, low cost, easy handling, and storage [26, 27]. Surfactants used in the manufacture of niosomes are biodegradable, non-immunogenic, and biocompatible. Several methods of preparation can be used to prepare niosomes. These include but are not limited to handshaking, ether injection, and reverse-phase evaporation. All these methods require several excipients and sophisticated machinery [27]. In this study, the probe sonication method will be used to prepare the niosomes; this is an environmentally friendly method and will only require three reagents: water, cholesterol, and the surfactant(s) (non-ionic), and a probe sonicator. The method is quick, and from this method, large uni-lamellar vesicles (LUVs) can be prepared. Unlike conventional liposomes, these vesicles will possess an infrastructure that can entrap drugs with

a wide range of solubility and consequently improve the bioavailability of the drug while also minimizing adverse effects [27]. Additionally, these vesicles will not require any special storage conditions as they can be stored at room temperature (25 °C).

CPH is classified as an intermediate between BCS class IV with low water solubility. Low water solubility may present a challenge in incorporating CPH into topical formulations. Due to their flexible nature, depending on the nature of the active ingredient, niosomes will cross the tympanic membrane quicker than conventional eardrops. This will improve the onset of action, and patients will be relieved of pain quicker than they usually would from conventional eardrops or oral dosage forms.

In conclusion, scientists are interested in using new drug delivery systems to treat infectious diseases, including intracellular infections, considering the emergence of antibiotic resistance. Liposomes can improve the efficacy and safety of antibiotics; however, they have low stability during storage and administration. Considering these problems, developing novel drug delivery systems is essential. Niosomes, compared to liposomes, exhibit higher chemical stability, are less expensive, and will be able to cross the tympanic membrane quicker and more efficiently, improving drug delivery and performance.

CHAPTER TWO

REVERSED-PHASE HIGH-PERFORMANCE LIQUID CHROMATOGRAPHY METHOD DEVELOPMENT AND VALIDATION

2.1 INTRODUCTION

Chromatography exists in various forms and separates organic and inorganic compounds from mixtures or solvents [58]. All chromatographic techniques make use of a stationary and mobile phase that carries analytes and passes through a stationary phase that may adsorb the compounds to different extents depending on their relative affinity for the stationary and mobile phase [59]. Liquid chromatography (LC) is commonly used for analysis during the different stages of pharmaceutical development, synthesis, isolation, pharmacological testing, dosage form development, and quality control of the manufactured product, amongst others [60]. High-performance liquid chromatography (HPLC) can separate and identify compounds present in any sample that can be dissolved in a liquid in trace concentrations as low as parts per trillion. Because of this versatility, HPLC is used in a variety of industrial and scientific applications. HPLC can be used to analyze a wide range of molecules including, polymers, macromolecules, ionic species, molecules with high molecular masses, and those containing specific functional groups [61].

HPLC uses similar principles to gas chromatography (GC). However, GC possesses better column efficiency and speed of analysis. RP-HPLC is commonly used in pharmaceutical sciences research [62]. Although there are numerous types of chromatographic methods, several factors are common to all types. All chromatographic systems have a mobile and a stationary phase. Regardless of the type of chromatography, samples are dissolved in the mobile phase, which travels through the stationary phase. Separation is possible because different compounds have different affinities for the mobile and stationary phases, affecting their distribution between the two phases and their resulting behaviour in the system [63].

LC is classified according to the interaction between the stationary phase and analytes of interest and how efficiently the analytes are separated [64]. The separations are generally classified as ion exchange [65], normal-phase [66], size-exclusion [67] and reverse-phase chromatography (RPC) [68, 69].

Ion-exchange chromatography is based on electrostatic interactions between charged protein groups and solid support material (matrix). Matrix has an ion load opposite to that of the protein to be separated, and the affinity of the protein to the column is achieved with ionic interactions. Proteins are separated from the column by changing pH, ion salts concentration, or the buffer solution's ionic strength [70]. Positively charged ion-exchange matrices are called anion-exchange matrices and adsorb negatively charged proteins. Matrices bound with negatively charged groups are cation-exchange matrices and adsorb positively charged proteins [71, 72].

Normal phase chromatography (NPC) uses a polar stationary phase bonded to silica backbone support and non-polar mobile phases. This mode of separation is primarily used for the separation of non-ionic compounds [73-75]. In NPC, the dominant interactions between the solute and the stationary phase that cause retention and selectivity are polar. Highly hydrophilic substances will interact more strongly with polar stationary phases and will be retained for longer [75].

Size-exclusion chromatography (SEC), also known as molecular sieve chromatography, is a chromatographic method in which the size separates molecules in solution, some cases molecular weight or how efficiently they penetrate the pores of the stationary phase [76]. Separation occurs when molecules of different sizes are included or excluded from the pores within the matrix. Small molecules diffuse into the pores, and their flow through the column is retarded according to their size, while large molecules do not enter the pores and are eluted in the column's void volume. Consequently, molecules separate based on their size as they pass through the column and are eluted in order of decreasing molecular weight (MW) [77].

In RPC, the mobile phase is very polar – water or mixtures of water with polar, water-miscible solvents – and the stationary phase is non-polar, often an 18-carbon-long hydrocarbon attached to the surface of silica or closely related material. RPC is commonly used in pharmaceutical sciences as excellent resolutions for closely related molecules that are structurally distinct [77, 78]. Additionally, since only a small volume of sample is injected into the system, the low aqueous solubility of the analytes does not limit separations—the analytes partition between the mobile and stationary phases. The more hydrophobic the analytes are, the more retained they will be in the stationary phase. The more polar they are, the more they will prefer the mobile phase [79].

Method validation is the process used to confirm that the analytical procedure employed for a specific test is accurate, robust, specific, and reproducible within the specified range of operation. Method validation can be used to judge the reliability, quality, and consistency of analytical results. It is an integral part of any good analytical practice [80].

2.2 PRINCIPLES OF REVERSE PHASE HPLC (RP-HPLC)

RP-HPLC is used for preparative, quantitative, and qualitative separations to analyze substances, including compounds that decompose on vaporization [64]. RPC has found both analytical and preparative applications in biochemical separation and purification. Molecules that possess some degree of hydrophobic character, such as proteins, peptides, and nucleic acids, can be separated by RPC with excellent recovery and resolution [81].

Separation is achieved using silica-based support bonded to compounds that impart varying degrees of hydrophobicity to the stationary phase [82]. Compounds are separated based on their different migration rates as they flow through the column after loading onto the system and are transported by the mobile phase through the column by gravity or hydrostatic pressure [83, 84]. The mobile phase flows through the column and into a detector before running to waste or being recycled [85]. The stationary phase is packed in the column onto which the analyte(s) adhere at different degrees, resulting in different transfer rates that facilitate the separation [84]. The mechanism of RPC is complex, and sample components are retained through non-specific hydrophobic interactions with the stationary phase. With this separation mode, the more polar the solute, the lower the retention. A more polar mobile phase results in increased solute retention, and to achieve separation, the compound must partition from the column towards the organic component of the mobile phase [86-88].

The use of reversed-phase mode in preparative separations provides several benefits over normal phase methods. In addition to eliminating solubility issues often experienced in non-polar normal phase solvents, the utilization of RPC uses fewer toxic solvents than those associated with the normal phase and provides timely sample recovery [89]. Additionally, reversed-phase columns exhibit more extended durability and better stability than normal phase columns making their use economically viable [90].

2.2.1 Column Selection

An essential component of an RP-HPLC is the column. Columns are the main components in HPLC because the column is responsible for separating the sample components. The sample passes through the column with the mobile phase and separates its components when it comes out from the column. Generally, silica gel is filled in the HPLC columns because of its particle size and porosity, which helps separate components. It is also an inert material that does not react with mobile phases. Therefore, silica columns can be used to analyze compounds of different chemical natures. The material filled in HPLC columns is known as the stationary phase [91].

A stable column must be used to develop an efficient, rugged, and reproducible method [92]. Separation of sample components in reversed-phase columns also occurs based on the polarity of the sample components, but it happens just opposite of the normal phase HPLC columns. Therefore, this type of chromatography is known as RPC [91, 92].

HPLC columns are usually packed with pellicular or porous particles. Pellicular particles are made from polymer or glass beads. Pellicular particles are surrounded by a thin uniform layer of silica, polystyrene-divinyl-benzene synthetic resin, alumina, or another type of ion-exchange resin. The diameter of the pellicular beads is between 30 and 40 μm [93]. Porous particles are more commonly used, have diameters between 3 to 10 μm and are made up of silica, polystyrene-divinyl-benzene synthetic resin, alumina, or another type of ion exchange resin. Silica is the most common type of porous particle packing material.

Partition HPLC uses liquid bonded phase columns, where the liquid stationary phase is chemically bonded to the packing material. The packing material is usually hydrolyzed silica which reacts with the bond-phase coating. The most common bond-phase coatings are siloxanes [91-94]. The most common stationary phases used are with non-polar functional groups such as propyl (C3), octyl (C8), and octadecyl (C18) functionalities bonded as a thin layer onto the silica backbone support [64, 95]. Octadecyl silyl (or C18) is commonly used as it is a highly robust hydrophobic phase, which produces good retention with hydrophobic (non-polar) analyte molecules. In general, shortening the alkyl chain will shorten the retention time (R_t) [96].

Spherical particles produce more efficient columns and are preferred over irregularly shaped particles [97]. Usually, HPLC has a guard column ahead of the analytical column to protect and extend the life of the analytical column. The guard column removes particulate matter, contaminants, and molecules that bind irreversibly to the column and has a stationary phase similar to the analytical column. The most common HPLC columns are made from stainless steel, but they can also be made from thick glass, polymers such as polyetheretherketone, a combination of stainless steel and glass, or a combination of stainless steel and polymers [97, 98]. Typical HPLC analytical columns are between 3 and 25 cm long and have 1 to 5 mm diameter. Particles that pack the columns have a typical diameter between 3 to 5 µm [100]. Liquid chromatographic columns will increase efficiency when the packed particles' diameter inside the column decreases [101].

Silica-based stationary phases dissolve at high temperatures and in solutions of pH > 8 [102, 103]. When dissolved, the silica support collapses, reducing column efficiency and increasing peak symmetry [99, 104].

2.2.2 Methods of Detection

A detector in HPLC is placed at the end of the analytical column. The function of the detector is to examine the solution eluting from the column [105]. An electronic signal is proportional to the concentration of individual components of the analyte [106, 107]. The detector turns a physical or chemical attribute into a measurable signal corresponding to concentration or identity [108]. Different types of detectors, such as UV or fluorescence detectors, can be coupled to HPLC. UV detectors are often preferred because they are cheaper and more readily available [109, 110]. The ideal detector must exhibit high sensitivity for the analyte of interest, specificity, insensitivity to temperature, and mobile phase flow rate changes. The physicochemical properties, the concentration of the compound(s) of interest, and system sensitivity should be considered when selecting a method of detection. Detectors should also exhibit a high degree of sensitivity for the analyte of interest, specificity, insensitivity to temperature, and mobile phase flow rate changes [111].

2.2.3 Mobile Phase Selection

Mobile phase composition is crucial as it may affect the selectivity and separation of analytes using HPLC [88]. The mobile phase in RP-HPLC usually consists of a water/aqueous solution (commonly an aqueous buffer) and an organic modifier. Solvents commonly used for RP-

HPLC mobile phase include methanol, ethanol, propanol, and acetonitrile (ACN), water, or buffer [92, 103]. When ionizable compounds are analyzed, buffers and other additives may be present in the aqueous phase to control retention and peak shape [105]. Solvent selection may be one of the most critical parameters in an HPLC separation due to its effect on selectivity. Selectivity may be the most effective tool for optimizing resolution. Changing the organic modifier within a mobile phase can alter the selectivity of the separation and the retention characteristics.

Its composition and temperature play a significant role in the separation process by influencing the interactions between sample components and the adsorbent. These interactions are physical in nature, such as hydrophobic (dispersive), dipole-dipole, and ionic, most often a combination [112].

2.3 ANALYSIS OF CIPROFLOXACIN (CPH)

Several analytical methods for the quantitation of CPH in different dosage forms and matrices and the conditions for these separations have been reported and are summarized in **Table 2.1**. CPH has been analyzed in dosage forms and biological fluids; the preferred analysis method is RP-HPLC as specified in the British Pharmacopoeia [113]. This chapter aims to develop and validate a selective, precise, rapid, and accurate RP-HPLC method to analyze CPH in pharmaceutical formulations.

CPH was analyzed using a UV-Vis detector at 278 nm. The λmax used was identified from the data listed in **Table 2.1**.

Table 2.1 RP-HPLC methods used for the analysis of CPH.

Sample matrix	Column	Mobile phase	Flow rate	λ nm	R_t(minutes)	Internal standard	Reference
Human plasma and pharmaceuticals	RP C18 column (4.6x150mm,5µm)	Acetonitrile: Acetic acid solution (pH=3±0.1) (16:84 v/v)	1 ml/min	280	6.5	-	[113]
Pharmaceutical formulations	C18(4.6x150mm,3.5µm)	0.025M Phosphoric acid solution (pH=3±0.1): Acetonitrile 60:40 v/v	1 ml/min	278	2.5	-	[114]
Ciprofloxacin tablet	C18(125mmx4.5mm, 5µm)	0.025M Orthophosphoric acid solution (pH=3±0.1) + Triethylamine	2 ml/min	278	1.70-1.75	-	[115]
Ciprofloxacin in drug and serum	C18 column	Phosphate buffer: Acetonitrile: Methanol (81:5:14) v/v	1.5 ml/min	270	8.03-12.79	-	[116]
Ciprofloxacin in Jiaozuo seawater	C18 column (Hitachi, Japan) (250mmx4.6mm, 5µm)	25mM Orthophosphoric acid solution (pH=2.4) with Triethylamine: Acetonitrile (82:18v/v)	0.8 ml/min	280	6.5	-	[117]
Human plasma	C18 Bonda pack column (250mm x3.9mm, 5µm)	Acetonitrile: potassium dihydrogen phosphate (20:80 v/v)	1.5 ml/min	276	9.064	-	[118]
Human plasma	ACE® 5 C18 column (250mm x4.6mm,5µm)	Phosphate buffer (pH =2.7): acetonitrile (77:23 v/v)	1.5 ml/min	277	3.26	Sulfadimidine sodium	[110]
Human plasma	C18 µ-Bonda pack column (250mm x 3.9mm)	Acetonitrile: potassium dihydrogen phosphate (pH=3) 20:80v/v	1.5 ml/min	276	5.382	Phenacetin	[119]
Tablet	Inertsil C18(250mm x4.6, 5µm)	Phosphate buffer: acetonitrile 82:18v/v	1.0 ml/min	316	5.6	-	[120]

2.4 EXPERIMENTAL

2.4.1 Chemicals and reagents

All reagents were of analytical grade and were used without further purification. CPH was purchased from Sigma Aldrich® (St Louis, USA). The internal standard (IS), carbamazepine (CBZ), was purchased from Sigma Aldrich® (St Louis, USA). HPLC grade acetonitrile (ACN) 200 far UV Romil-Sp STM Super Purity solvent was purchased from Microsep® (Port Elizabeth, Eastern Cape, South Africa). HPLC grade water was initially purified by reverse osmosis using a Millipore® Milli-RO 15 water purification system consisting of Organex-Q, Super-C carbon, and two Ion-X ion-exchange cartridges. NaOH (0.1 M) was prepared by dissolving 0.4 g of NaOH pellets (Rochelle Ltd, Johannesburg, South Africa) in 100 mL of HPLC grade water in a 400 mL A-grade volumetric flask.

2.4.2 Instrumentation and analytical conditions

The HPLC system for the analysis of CPH was comprised of a Model 2695 Alliance Separations® module (Milford, Massachusetts, USA) fitted with a Model 2487 Waters® Dual -wavelength detector, and data capture and analysis were achieved using Waters® Empower 3 Data acquisition software (Milford, Massachusetts, USA). All samples were sonicated using a Branson® B12 sonicator (Danbury, Connecticut, USA) during solution preparation. The chemical reagents and formulations were weighed using a Model AG135 Mettler Toledo® top loading balance (Mettler®, Zurich, Switzerland). Before analysis, the solutions were agitated using a Model G560E Vortex Genie-2 mixer (Bohemia, New York, USA).

2.4.3 Sample preparation

CPH samples were prepared using calibrated A-grade glassware. Sample loss was minimized by limiting the number of manipulations and dilutions. The samples were completely mixed and dissolved using ACN and 0.0175 M phosphate buffer in a 40/60 v/v ratio [121].

2.4.4 Preparation of stock solutions

Stock solutions containing 1000 µg/mL CPH and 500 µg/mL CBZ were prepared on a daily basis by weighing approximately 100 mg of CPH into a 100 mL A-grade volumetric flask and 50 mg of CBZ into a 100 mL A-grade volumetric flask. The stock solution of CPH was made up to

volume with a 40/60 v/v solution of ACN and 0.0175 M phosphate buffer and was mixed with a vortex mixer. Different analytical standards were prepared by serial dilution to produce CPH solutions of 0.1, 0.2, 0.4, 0.6, 0.8, 1, 2, 5, 10, 20, 50, 80 and 120, 150 and 250 µg/mL. A 1 mL aliquot of the CBZ stock solution was transferred into a 10 mL A-grade volumetric flask and a volume of CPH stock solution corresponding to the required concentration of the analytical standard. The solutions were then transferred into an amber vial and sealed, and the contents were mixed using a Model G-560E Vortex Genie-2 mixer (Bohemia, New York, USA). The 0.1 M NaOH used for pH adjustments was prepared daily by dissolving 400 mg of sodium hydroxide pellets in 100 mL HPLC grade water.

2.4.5 Preparation of mobile phase

The mobile phase for the analysis of CPH was comprised of different ratios of ACN: 0.0175 M phosphate buffer and investigation of molarity and the pH of the mobile phase. The final mobile phase composition was ACN: 0.0175 M phosphate buffer in a ratio of 40:60 v/v. The mobile phase was prepared by weighing 2.38 g of potassium dihydrogen phosphate (AnalaR, Wadesville, Gauteng, South Africa) using a model AG135 Mettler Toledo® top loading balance (Port Elizabeth, Eastern Cape, South Africa) into a 1000 mL A-grade volumetric flask made up to volume with HPLC grade water to produce a 0.0175 M phosphate buffer. The mobile phase was prepared by transferring 600 mL of the solution into a 1000 mL A-grade measuring cylinder and making up to volume with ACN. The mobile phase was transferred into a 2000 mL Schott Duran® glass bottle (Bestenheid, Wertheim, Germany). The pH of the mobile phase was measured using a model GLP 21 Crison® instruments pH meter (Barcelona, Catalonia, Spain) and was adjusted to pH 3 using a 0.1 M NaOH solution. A Labcon® Laboratory Magnetic Stirrer hotplate (Maraisburg, Gauteng, South Africa) was used to mix the mobile phase during pH adjustment. The mobile phase was prepared daily and not recycled during analysis.

2.4.6 Degassing

The mobile phase in an HPLC system is typically made up of any combination of four solvents: methanol, buffer, ACN, and water. The solvents used to make mobile phases absorb oxygen and nitrogen [122]. The solubility of nitrogen and oxygen in water and ACN is low, and therefore the solution becomes supersaturated, resulting in bubble formation. Bubble formation upon mixing two solvents can lead to several problems in HPLC analysis which can be prevented by degassing

the mobile phase. Air bubbles passing through the detectors can lead to spurious peaks and can also modify the flow of the mobile phase through the column due to the creation of dead volumes [122].

It is only necessary to remove a fraction of the dissolved air to bring it below the super saturation level in the mobile phase. Some of the most widely used methods to degas a mobile phase are:

a) ***Helium purging*:** helium is bubbled through the solvent and removes up to 80 % of dissolved air.
b) ***Vacuum degassing*:** the solvent is exposed to a vacuum, and the reduced pressure removes more than 60 % of the dissolved air.
c) **S*onication*:** ultrasonic baths as a stand-alone technique only remove up to 30 % dissolved air.

Vacuum degassing removes more than 60 % of dissolved air. The mobile phase is passed through porous polymer tubing placed in a vacuum chamber inside the HPLC instrument. The porosity of the tubing allows air expulsion through the walls, but the liquid is retained in the tubing. On-line vacuuming degassing makes use of thin-walled porous tubing that permits dissolved air to be pulled through the pores in the tubing when under vacuum [122, 123]. Vacuum filtration is performed by drawing a vacuum with a simple vacuum pump or water aspirator [122]. Degassing of mobile phase was conducted by filtration under vacuum and on-line vacuum filtration. The mobile phase was degassed by filtration through a 0.45 μm Millipore® Corporation HVLP Durapore membrane filter (Milford, Massachusetts, USA) and an Eyela® Aspirator-degasser A-2S (Bunkyo-Ku, Tokyo, Japan).

2.4.7 Choice of internal standard (IS)

The IS is a compound that is very similar but not identical to the chemical species of interest. The chosen IS is incorporated before sample preparation and analysis. The IS needs to provide a signal similar to the analyte signal in most ways but sufficiently different so that the instrument readily distinguishes the two signals [124,125]. The IS was added to analyte solutions before analyzing these studies to minimize injection and sample handling errors. IS are used to determine the concentration of other analytes by calculating the peak area ratio (PAR). The requirement for IS selection is that it should be similar to the analyte and have a similar retention time (R_t). It must be stable under the specified conditions for analysis,

completely resolved from and chemically similar to the analyte of interest. Generally, IS with the same functional groups and activity are considered the most appropriate [126]. The conditions use for these chromatographic studies are listed in **Table 2.2.**

Table 2.2 Chromatographic conditions for the trial RP-HPLC analysis of CPH and selection of IS.

Detector	Model 2489 UV/Vis detector
Detector wavelength	278 nm
Flow rate	1.0 mL/min
Injection volume	1.0 µL
Mobile phase composition	ACN: 0.0175 M phosphate buffer 40:60 v/v
Column temperature	40 °C
Mobile phase pH	3.0
Mode	Isocratic

The compounds evaluated as potential IS included hydrochlorothiazide, lamotrigine, and CBZ. The criteria used for selecting the IS were based on R_t and resolution of CPH and the IS. Solutions of CPH and IS were mixed in a 1:1 ratio prior to RP-HPLC analysis. The resolution between CPH and potential IS was acceptable if the resolution factor ≥ 2. The chromatogram showed resolved CPH and IS peaks between 3.5 and 10 minutes.

The results of this assessment are listed in **Table 2.3** and reveal that CBZ was the most suitable IS with a R_t of 5.3 minutes and a resolution factor of 5.7 indicating adequate separation between the peaks.

Table 2.3 R_t for potential IS.

Internal standard	R_t (min)	Time between CPH and IS (min)	R_t between 3 and 10 minutes	Time between $R_t \geq 2$ minutes
Hydrochlorothiazide	> 10	-	No	Yes
Lamotrigine	> 10	-	No	Yes
CBZ	5.3	1.6	Yes	No

R_t shorter than three minutes are not desirable as interference with peaks resulting from excipients in the solvent front would preclude accurate analysis of CPH formulations. The R_t of the potential IS was used as the primary criterion for qualifying the IS.

Approximately 50 mg CBZ and 100 mg of CPH were transferred into two separate 100 mL A-grade volumetric flasks and were dissolved in the mobile phase to produce stock solutions. The stock solutions were ultra-sonicated for 15 minutes using a Branson® B12 sonicator (Danbury, Connecticut, USA). For RP-HPLC analysis, a 1 mL aliquot of each stock solution was transferred into a 10 mL A-grade volumetric flask and made up to volume with the mobile phase. The mixture was thoroughly mixed using a Model G-560E Vortex Genie-2 mixer (Bohemia, New York, USA). After mixing, the solution was transferred into a 2 mL amber vial and analyzed by RP-HPLC. A typical chromatogram depicting the separation of CPH and CBZ at 278 nm is depicted in **Figure 2.1.**

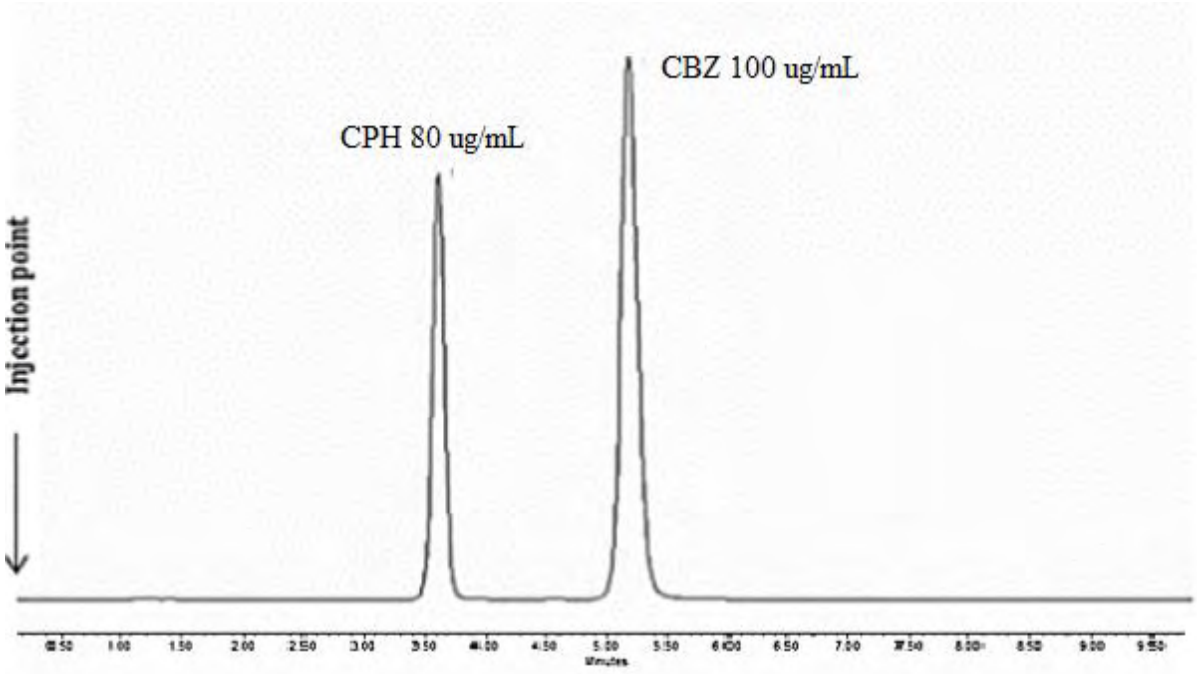

Figure 2.1 Typical chromatogram depicting CPH at 3.7 minutes and CBZ at 5.3 minutes.

2.4.8 System Suitability Testing

2.4.8.1 Number of theoretical plates (N)

The number of theoretical plates measures the efficiency of a column. It is an indication of the suitability of a column to produce peaks that are narrow with adequate resolution. The theoretical plate number (*N*) is expressed by **Equation 2.1** [127]:

$$N = 16(\frac{Rt}{W})^{1/2}$$

Equation 2.1

Where,

N = number of theoretical plates,
R_t = R_t of test peak and
w = peak width at baseline.

2.4.8.2 Peak asymmetry factor (Peak tailing)

This study determined the peak shape by calculating the peak symmetry factor using the equation shown in **Equation 2.2**.

$$A_2 = \frac{B}{A}$$

Equation 2.2

Where,

A = peak width to the tailing edge at 10% peak height, and
B = peak width to the leading edge at 10% peak height.

Peak asymmetry factor values < 1.50 are considered acceptable, and a value of 1.00 is indicative of symmetrical peaks. Values > 1.50 indicate poor peak asymmetry, which could result in the calculation of an inaccurate plate number, poor resolution, poor R_t reproducibility, and undetected minor bands located under the tail of the peak [88]. Peak asymmetry factor values between 0.95 and 1.10 indicate values between 0.95 and 1.30 indicate good column performance and new columns. Another parameter used to determine peak shape is the peak tailing factor (PTF) calculated using **Equation 2.3** [88, 128].

$$PTF = \frac{A+B}{2A}$$

Equation 2.3

Where,

PTF= Peak tailing factor,

A = peak width to the tailing edge at 10% peak height, and

B = peak width to the leading edge at 10% peak height.

2.4.8.3 Resolution factor

The resolution factor (R_s) measures the extent and quality of separation between the analyte and the IS peaks. R_s is calculated by dividing the difference in peak R_t by the average peak width and considers efficiency, selectivity, and retention as shown in **Equation 2.4**.

$$R_s = \frac{RT_2 - RT_1}{0.5(TW_1 - TW_2)}$$

Equation 2.4

Where,

TW_1 = width of the first peak at baseline,

TW_2 = width of the second peak at baseline.

RT_1 = R_t of first peak and

RT_2 = R_t of second peak.

A good separation is indicated by R_s values > 2.0 and poor separation by values < 1.5 [88] and can be calculated using **Equation 2.4**.

2.4.8.4 Capacity factor

The capacity factor (*K'*) measures the amount of time the sample component resides in the stationary phase relative to its time in the mobile phase. *K'* is influenced by the mobile phase composition, age of the column, and column temperature [88, 129] and is calculated using **Equation 2.5**.

$$K' = \frac{V_1 - V_0}{V_0}$$

Equation 2.5

Where,

V_0 = Void volume of the column, and

V_1 = R_t of the analyte (retention time × flow rate).

The void volume of a column is determined using the R_t of uracil, as reversed-phase columns do not retain it. A K' value ≥ 2.0 is desirable and chromatographic conditions < 2.0 are regarded as unacceptable [130].

2.4.9 Method Development using Central Composite Design (CCD)

2.4.9.1 Selection of factor levels for CCD model

The minimum and maximum levels for each factor for the design of experiments and CCD were initially based on Scherer's analytical method for CPH [114]. Initially, a trial analysis of CPH was undertaken using a mobile phase of ACN: 0.0175 M phosphate buffer in a ratio of 40:60 v/v adjusted to pH of 3 at a flow rate of 1.0 mL/min. Separation was achieved using a Phenomenex® 150 x 4.6 mm 5µm C18 column, and the eluent was monitored at 278 nm. A typical chromatogram of the trial analysis is depicted in **Figure 2.2.**

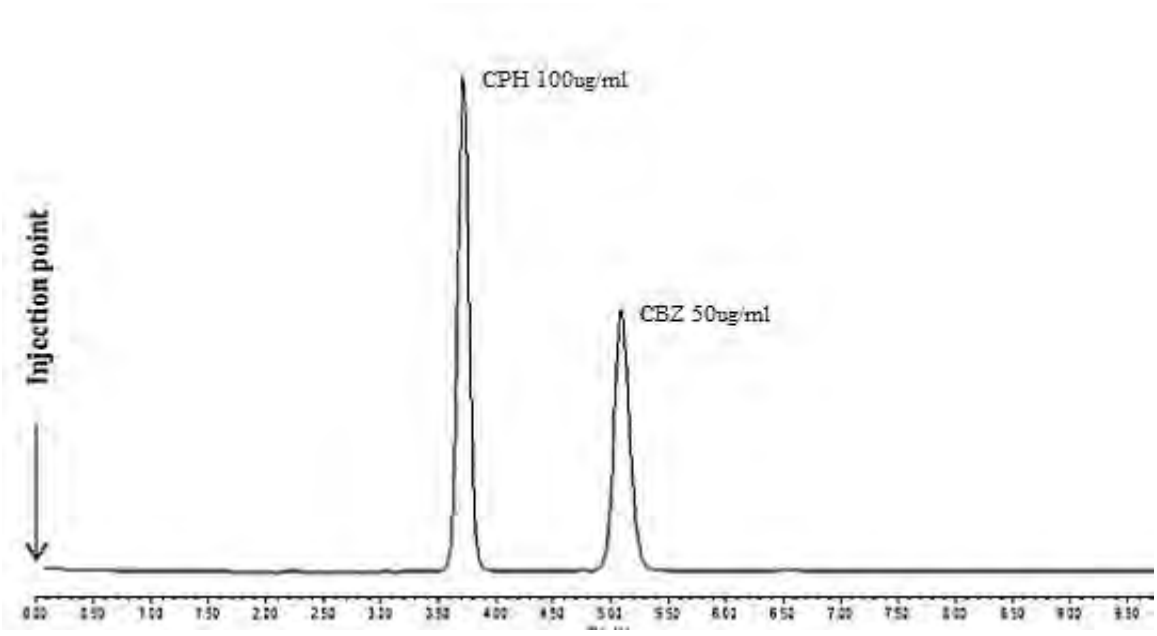

Figure 2.2 Typical chromatograph of CPH and CBZ at 278nm.

The chromatograms shown in **Figures 2.1** and **2.2** depict a peak for the IS at 5.3 minutes and CPH at 3.7 minutes. RSM was used to optimize the chromatographic conditions further and find the best conditions that meet the set requirements: $R_s \geq 2$ and asymmetry factor ≤ 1.50.

2.4.9.2 Use of CCD for the development and optimization of a RP-HPLC method for the analysis of CPH.

An essential aspect of developing a RP-HPLC method is to achieve adequate separation between peaks in the chromatogram [131]. A RP-HPLC method for analyzing CPH was developed and optimized using a CCD in which the mobile phase pH, phosphate buffer molarity, mobile phase composition, and column temperature were considered critical, independent variables. The responses monitored were R_t of CPH and CBZ, asymmetry factor, and R_s. The target was for the R_t of CPH and CBZ to be ≤ 10 minutes, the asymmetry factor ≤ 1.50, and for the R_s to be ≥ 2. The method was optimized to develop a rapid, precise, accurate, repeatable, and simple RP-HPLC method. The low and high values for each response were entered into Design Expert® Version 7.0.1 (Stat-Ease Inc., Minneapolis USA) statistical software to produce a CCD that required 29 experiments, as summarized in **Table 2.4**.

Table 2.4 Randomized experimental runs conducted to assess the impact of method parameters on the analysis of CPH.

Code standard run number	Experimental run	A: pH of mobile phase	B: Molarity mM	C: Organic solvent %	D: Column temperature ℃
11	1	3	17.5	30	40
21	2	4.5	10	30	25
14	3	4.5	25	20	32.5
4	4	6	25	30	32.5
3	5	3	25	30	32.5
15	6	4.5	10	40	32.5
12	7	6	17.5	30	40
17	8	3	17.5	20	32.5
13	9	4.5	10	20	32.5
19	10	3	17.5	40	32.5
10	11	6	17.5	30	25
23	12	4.5	10	30	40
16	13	4.5	25	40	32.5
9	14	3	17.5	30	25
8	15	4.5	17.5	40	40
27	16	4.5	17.5	30	32.5
26	17	4.5	17.5	30	32.5
25	18	4.5	17.5	30	32.5
20	19	6	17.5	40	32.5
6	20	4.5	17.5	40	25
18	21	6	17.5	20	32.5
29	22	4.5	17.5	30	32.5
24	23	4.5	25	30	40
1	24	3	10	30	32.5
2	25	6	10	30	32.5
28	26	4.5	17.5	30	32.5
5	27	4.5	17.5	20	25
22	28	4.5	25	30	25
7	29	4.5	17.5	20	40

The low and high levels for the input variables were specifically set between 0.01 and 0.025 M, organic solvent content between 20 and 40 %, pH between 3 and 6, and the column temperature between 25 and 40 ℃. To avoid experimental bias, the experiments were undertaken in the run order specified in **Table 2.4**. Design Expert® Version 7.0.1 (Stat-Ease Inc., Minneapolis USA) statistical software was used to analyze the data and predict input variables' values to produce the target responses and adequate separation of CPH and CBZ.

Fischer's statistical test was used to evaluate Analysis of Variance (ANOVA) for the response surface quadratic models used to identify significant input factors. The model's effectiveness was evaluated using the F-ratio, Coefficient of Variation (CV), adequate precision, adjusted R^2, predicted R^2, and the predicted residual error sum of squares (PRESS).

2.4.10 Method Validation

Various regulatory authorities give particular emphasis on the validation of all the processes used in the laboratory. Validation is a formal and systemic way to demonstrate the method's suitability and ensure the method gives satisfactory and consistent results. The Food and Drug Administration (FDA), the ICH, the United States Pharmacopoeia (USP), and other regulatory authorities provide a framework for undertaking method validation studies. In this study, ICH method validation guidelines were used [80].

2.4.10.1 Linearity and Range

The linearity of an HPLC method is its ability to produce test results that are directly proportional to sample concentration over a given range. To determine linearity, a calibration curve must be constructed using at least 5 different concentrations [80]. Linearity was investigated using fifteen standard CPH solutions (n = 5). The calibration standards were prepared as described in **§ 2.4.4** and were 0.1, 0.2, 0.4, 0.6, 0.8, 1, 2, 5, 10, 20, 50, 80, 120, 150, 250 µg/mL CPH. CBZ was added to all standards in a 50 µg/mL concentration. The average PAR of CPH: CBZ was plotted versus sample concentrations to construct a calibration curve. Linearity was established using least squares linear regression analysis for these data.

2.4.10.2 Precision

The precision of an analytical method is defined as the closeness of agreement between quantity values obtained by replicate measurements of a quantity under specified conditions [132]. Precision may be considered at 3 levels, *viz*, intraday precision, inter-day precision, and reproducibility. The precision data of an analytical method is usually expressed as the variance, standard deviation (SD), or CV of a series of measurements. Reproducibility of an analytical method is the ability to reproduce results using the same samples when the analysis is undertaken by different analysts, instruments, and laboratories [133]. The specifications for acceptable precision were set at SD $\leq \pm$ 1.05 and % relative standard deviation (RSD) $\leq$ 5 %.

2.4.10.2.1 *Intra-day precision*

Repeatability is the precision under the same operating conditions over a short period of time in a day. It is assessed by preparing three samples at three concentrations on triplicates covering the specified range for the procedure [132]. This precision of the RP-HPLC method was conducted in one laboratory by a single analyst using the same HPLC instrumentation over one day. CPH was analyzed in replicate (n= 6) at three different concentrations *viz*., 3 µg/mL, 50 µg/mL, and 120 µg/mL representing low, medium, and high sample concentrations in the calibration curve range. The solutions were prepared as described in **§ 2.4.4**.

2.4.10.2.2 *Intermediate or inter-day precision*

Intermediate precision focuses on the variation in analytical results that may occur in a laboratory over a period of time [132]. The studies were performed daily on three consecutive days using three concentrations *viz*., 3 µg/mL, 50 µg/mL, and 120 µg/mL. The studies were conducted in replicate (n = 6) by a single analyst in one laboratory using the same instrumentation.

2.4.10.3 Reproducibility

Reproducibility is the precision obtained by analysis between laboratories or using different instruments and is essential in collaborative studies and if a method is to be transferred to different environments and method standardization is essential [132]. In this study, reproducibility was not evaluated as the experiments were conducted by the same analyst in the same laboratory using the same instrumentation.

2.4.10.4 Accuracy

Accuracy is the degree of agreement between the experimental value obtained by replicate measurements and the accepted reference value [133]. Practically, no measurement process is ideal; therefore, the actual value cannot be precisely known in any environment. Accuracy can also be defined as the lack of bias, and an acceptable % bias is ≤ ± 5 %. The % bias is calculated using **Equation 2.6**.

$$\%\, Bias \;=\; 100\, \frac{(True\ value - measured\ value)}{Measured\ value}$$

Equation 2.6

For accuracy studies, solutions of CPH of low, medium, and high concentration within the calibration curve range were prepared as described in **§ 2.4.4** and were analyzed in replicate (n = 6).

2.4.10.5 Limits of quantification and detection

An individual analytical procedure's limit of detection (LOD) is the lowest analyte in the sample that can be detected but not necessarily quantified as an exact value. An analytical procedure's limit of quantification (LOQ) is the lowest analyte in a sample that can be detected with suitable precision and accuracy [132].

The LOQ of a method can be calculated using three approaches *viz*., signal to noise ratio, confidence interval (CI) for the line of best fit, slope of SD versus concentration of CPH, and evaluation of lowest concentration for which the value for the % RSD is ≤ 5 % SD of the response [134]. For the validation of this method, the approaches used were visual and SD. Solutions of low concentrations of CPH *viz*., 0.05, 0.1, 0.15, and 0.2 µg/mL were used, and the lowest concentration of CPH for which the response was quantifiable with the necessary accuracy and precision was considered the LOQ. The LOD was determined as 0.3 x LOQ.

2.4.11 Ciprofloxacin Assay

2.4.11.1 Method

Ten Cifran® tablets were crushed and powdered in a mortar using a pestle. Approximately 0.770 g of powder from the Cifran® tablets equivalent to 100 mg CPH was weighed directly into a 100 mL A-grade volumetric flask and dissolved in 100 mL of ACN: 0.01 M phosphate buffer adjusted to pH 3 in a ratio of 40:60 v/v and sonicated for 30 minutes. The mixture was vortexed with Model G-560E Vortex Genie-2 mixer (Bohemia, New York, USA), after which a 1 mL aliquot was filtered using a Millipore® 0.45µm PVDF hydrophilic syringe filter (Milford, Massachusetts, USA) attached to a 10 mL Neomedic® plastic syringe (Rickmansworth, Hertfordshire, England) into a 10 mL A-grade volumetric flask. The solution was made up to volume with ACN: 0.0175 M phosphate buffer adjusted to pH 3 in a ratio of 40:60 v/v. A 1.5 mL aliquot of the solution was transferred into a 2 mL Waters® amber glass screw top vial (Milford, Massachusetts, USA) and was analyzed by RP-HPLC.

2.4.11.2 *Validation of extraction method*

The extraction method for isolating CPH from dosage forms must be validated to ensure accuracy, precision, and reproducibility [135]. Assay procedures must be validated for accuracy, precision, specificity, linearity, and range, according to the ICH Q2 (R1) guideline [136]. The extraction method used was validated for repeatability and accuracy as described in **§ 2.4.10.2** and **§ 2.4.10.4**. Parameter limits were set at ± 1.05 for experimental SD, ± 2.09 for the calculated SD, ≤ 5% for the RSD to establish repeatability, and 5 % bias to establish accuracy [137].

2.4.11.3 *Repeatability*

Replicate samples (n = 6) were analyzed at low, medium, and high concentrations within the calibration range for the method. Approximately 0.0770 g of CPH was weighed, extracted, and assayed using the method described in **§ 2.4.11.1**.

2.4.11.4 *Accuracy*

The % recovery of the label claim of CPH was established to assess the accuracy of the extraction procedure. Approximately 0.0770 g of powdered CPH tablets was weighed, extracted, and analyzed (n = 6) to establish the accuracy of the extraction procedure as described in **§ 2.4.11.1**.

2.5 RESULTS AND DISCUSSION

2.5.1 System Suitability Testing

Table 2.5 System suitability results (n = 3).

Factor	Value	% RSD
Resolution factor (R_s)	5.524	2.803
Asymmetric factor	1.251	1.839
Capacity factor (K')	2.51	0.122
Number of theoretical plates (N)	6889.90	0.145

The R_s was > 2, and there was adequate resolution between the peaks. The results of all the tests are within the limits set, and therefore, the column was deemed appropriate for use as a $R_s < 1.50$ indicates inadequate separation. The column was considered suitable for the analysis of CPH.

2.5.2 Central Composite Design

Twenty-nine experiments were performed using CCD, and a summary of the results for R_t of CPH and CBZ and R_s are summarized in **Table 2.6**. The experiments were performed randomly, and simplified data sets were generated to minimize the effects of uncontrolled factors that may cause bias in the responses monitored.

Table 2.6 Responses observed for CCD input variables.

Code standard run number	Experimental run	R_t CPH min	R_t CBZ min	Asymmetric factor	R_s
11	1	2.70	1.40	1.25	2.53
21	2	2.97	1.24	2.02	3.09
14	3	5.08	8.09	1.48	1.77
4	4	3.38	1.61	2.40	2.88
3	5	2.67	1.07	1.13	3.21
15	6	2.57	5.76	1.87	9.49
12	7	3.54	0.70	2.75	4.42
17	8	4.79	13.91	1.16	4.91
13	9	4.86	2.95	2.58	3.46
19	10	2.14	5.37	1.31	1.08
10	11	3.48	17.5	2.87	4.32
23	12	3.00	10	5.41	2.66
16	13	2.34	25	1.35	1.06
9	14	2.64	17.5	1.16	4.73
8	15	2.39	5.55	1.50	1.08
27	16	2.91	0.77	1.55	3.68
26	17	2.91	0.77	1.55	3.68
25	18	2.91	0.77	1.55	3.68
20	19	3.02	5.80	2.41	7.50
6	20	2.45	5.76	1.40	1.00
18	21	5.51	9.70	3.16	4.89
29	22	2.91	0.77	1.55	3.68
24	23	2.68	9.67	1.45	1.58
1	24	2.65	1.45	1.32	2.32
2	25	4.11	1.65	2.72	3.21
28	26	2.91	0.77	1.55	3.68
5	27	5.61	12.53	1.70	3.48
22	28	2.87	2.04	1.43	1.67
7	29	4.83	3.29	1.81	4.67

The responses listed in **Table 2.6** were evaluated using Design Expert® software and were fitted to quadratic models. The quadratic models were evaluated for adequacy in describing the

relationship between independent variables and responses, and ANOVA was used to identify the significance of each parameter. Evaluation of model adequacy and ANOVA for R_t of CPH and R_s are discussed in detail, and ANOVA data for the R_t of CBZ is not discussed since CBZ was used as the IS. The relationships established were used to predict input variables that would produce predefined responses for adequate separation of CPH and CBZ. Mathematical models depicting the relationship between the input factor(s) and response(s) were used to assess the impact of organic solvent content, column temperature, molarity, and pH of mobile phase on the responses monitored in order to identify the input parameters that would ensure a rapid, accurate and robust HPLC method for the quantitative analysis of CPH was developed and validated.

2.5.2.1 Model fitting

The design space for developing the HPLC method was monitored using a quadratic order polynomial model that was adequate for navigating the design space for the data. Lack of fit testing requires a minimum of 3 degrees of freedom (df), and pure error df equals the number of center point replicates less than 1 [138]. The df of lack of fit was 10, and that of pure error was 4. Therefore, the model can detect a lack of fit adequately. The standard error of fitting for each input factor, binary combination, and squared factors was 0.29, 0.50, and 0.39, respectively. The ideal variance inflation factor (VIF) value is 1.00; VIFs above 10 cause concern, indicating that the factors are two correlated together (not independent). The VIF of individual factors, binary combination, and squared factors was 1.00, 1.00, and 1.08, respectively, indicating that the design has multi-linear constraints. The average leverage for all runs was 0.51, indicating that none of the points within the design need replicating. The G efficiency measures the average prediction variance and is presented as a percentage of the maximum prediction variance [139]. The G efficiency was 23.51 and was considered acceptable as it indicates that the model fit is robust. The condition number for the coefficient matrix was 1.93, indicating that no multi-linearity between the model terms exists.

2.5.2.2 Responses monitored

The impact of the input variables on the responses was monitored, and the results were used to optimize method parameters. The model transformations recommended for each response are listed in **Table 2.7**.

Table 2.7 Responses for CPH HPLC method and model transformations.

Response	Parameter	Unit	Minimum observed	Maximum observed	Recommended transformation
R1	CPH R_t	Min	2.14	5.61	Power
R2	Asymmetric factor	-	1.13	5.41	Power
R3	R_s	-	1.00	9.49	Natural log
R4	CBZ R_t	Min	13.91	13.91	Inverse square root

The ratio of maximum and minimum values for the R_t of CPH, asymmetric factor, and Rs were < 10.00; model transformation was recommended for this data. The ratio of maximum and minimum values for the R_t of CBZ were > 10.00 minutes; a transformation was recommended and would have a significant effect on the data. The R_t of CPH is a critical factor and was therefore used to explain how all data and response models were analyzed using Design Expert® software.

2.5.2.3 Evaluation of model adequacy for R_t of CPH

2.5.2.3.1 Transformations of R_t for CPH

Box-Cox plots are used to establish whether model transformation for a response is necessary. The green line depicted in **Figures 2.3** and **2.4** indicates the optimum lambda value for the current transformation for R_t of CPH in this case. The red lines on both plots indicate the 95 % confidence interval (CI) boundaries around the λ value, and the actual λ value indicated by a blue line should fall within the boundaries of the 95 % CI [140]. The maximum and minimum λ value ratio was 2.72; no transformation was required, but a transformation was performed since the blue line was outside the 95 % CI boundaries. The maximum and minimum λ value ratio is 2.72, and transformation has little effect on ratios less than 3. The Box-Cox plot following the recommended power transformation depicted in **Figure 2.4** indicates that the blue line is still outside the limits of the 95 % CI, revealing that the transformation recommended was not able to bring the blue line inside the 95 % CI interval.

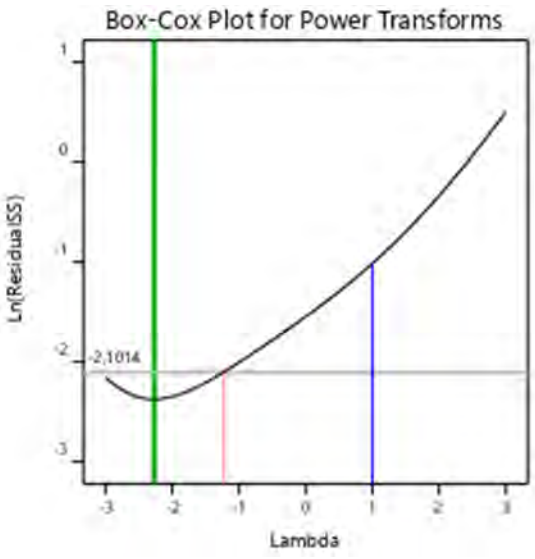

Figure 2.3 Box-Cox plot for transformation for the impact of solvent content on R_t of CPH prior to transformation.

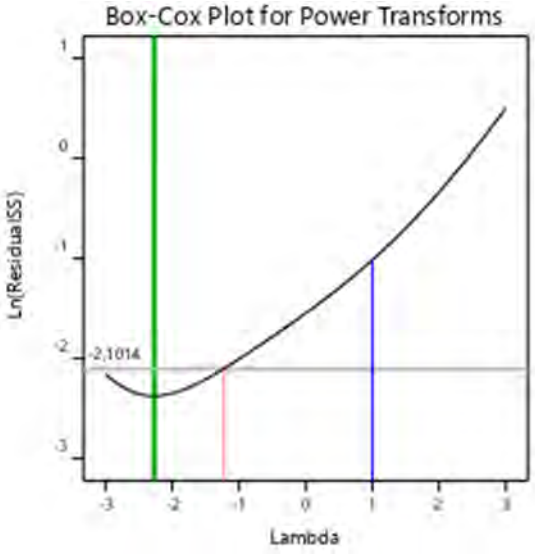

Figure 2.4 Box-Cox plot for the transformation of the impact of solvent content on the R_t of CPH following transformation.

2.5.2.4 Analysis of variance for R_t of CPH

The statistical model used was quadratic with significant terms ($p < 0.05$) were identified to define the final equation for R_t of CPH. The data generated using Design Expert® software are summarized in **Table 2.8** and include sum of squares, df, mean square, F-value, and p-value by which the significance of each term is established. The model is significant as the F-value is 138.31 and $p < 0.0001$, indicating a $< 0.01\%$ chance that the F-value is due to noise. The df value for lack of fit was 10 and fell outside the accepted range of 2 – 5.

Table 2.8 ANOVA data table for R_t of CPH.

Source	Sum of Squares	df	Mean Square	F-value	p-value	Significant
Model	0.1756	14	0.0125	138.31	< 0.0001	Significant
A-pH of mobile phase	0.0258	1	0.0258	284.44	< 0.0001	Yes
B-Buffer concentration	0.0014	1	0.0014	15.94	0.0013	Yes
C-ACN composition	0.1335	1	0.1335	1472.07	< 0.0001	Yes
D-Column temperature	0.0002	1	0.0002	1.97	0.1823	No
AB	0.0008	1	0.0008	8.51	0.0113	Yes
AC	0.0030	1	0.0030	33.15	< 0.0001	Yes
AD	3.627E-06	1	3.627E-06	0.0400	0.8444	No
BC	0.0006	1	0.0006	6.38	0.0242	Yes
BD	0.0002	1	0.0002	2.23	0.1575	No
CD	0.0001	1	0.0001	1.08	0.3159	No
A^2	0.0014	1	0.0014	15.20	0.0016	Yes
B^2	0.0000	1	0.0000	0.1830	0.6753	No
C^2	0.0089	1	0.0089	97.97	< 0.0001	Yes
D^2	2.879E-06	1	2.879E-06	0.0318	0.8611	No
Residual	0.0013	14	0.0001			
Lack of Fit	0.0013	10	0.0001			
Pure Error	0.0000	4	0.0000			
Cor Total	0.1768	28				

The predicted R^2 of 0.9587 listed in **Table 2.9** is in reasonable agreement with the adjusted R^2 of 0.9856; i.e., the difference is less than 0.2. Adequate precision measures the signal-to-noise

ratio. A ratio greater than 4 is desirable. The ratio of 44.340 indicates an adequate signal. This model can be used to navigate the design space.

Table 2.9 Statistical measures of model adequacy.

Std. Dev.	0.0095	**R^2**	0.9928
Mean	0.3223	**Adjusted R^2**	0.9856
C.V. %	2.95	**Predicted R^2**	0.9587
		Adequate Precision	44.3395

The final equation for the R_t of CPH, including significant terms, is represented as **Equation 2.7**, and was used to predict the level of input variables to produce an adequate separation.

$$(\text{CPH } R_t)^1 = -0.381531 + (0.057876 \times A) - (0.012015 \times B) + (0.040315 \times C) - (0.000868 \times D) + (0.001235 \times A \times B) - (0.001827 \times A \times C) + (0.000085 \times A \times D) + (0.000160 \times B \times C) + (0.000126 \times B \times D) - (0.000066 \times C \times D) - (0.006480 \times A^2) - (0.000028 \times B^2) - (0.000370 \times C^2) + (0.000012 \times D^2)$$

Equation 2.7

Where,

A = mobile phase pH,
B = buffer molarity,
C = organic solvent as a %, and
D = column temperature.

When evaluating **Equation 2.7**, the coefficient for the intercept, first-order main effects, higher-order effects, and interaction terms influence the R_t of CPH. The effect of the terms is quantified with a + or – operator sign and indicates that organic solvent content and mobile phase pH had positive effects on the power of R_t of CPH, which means an increase in organic solvent content and mobile phase pH will increase the R_t of CPH. The significant model terms with a negative impact on the response were buffer molarity, mobile phase pH*organic solvent, mobile phase pH^2, and organic $solvent^2$. The insignificant model terms were column temperature, mobile phase pH*column temperature, buffer molarity*column temperature, organic solvent*column temperature, $buffer\ molarity^2$, and $column\ temperature^2$. This transformation provides an accurate

analysis of the equation terms. Therefore, it is unnecessary to analyze the equation for untransformed data mathematically represented by **Equation 2.8.**

$$CPH\ R_t = 15.52257 - (0.269500 \times A) + (0.132237 \times B) - (0.685692 \times C) - (0.081230 \times D) - (0.016711 \times A \times B) + (0.002750 \times A \times C) - (0.000022 \times A \times D) - (0.001537 \times B \times C) - (0.000987 \times B \times D) + (0.002420 \times C \times D) + (0.086981 \times A^2) + (0.000241 \times B^2) + (0.008167 \times C^2) + (0.000250 \times D^2)$$

Equation 2.8

According to **Equation 2.8,** the significant model terms that positively affected the R_t of CPH were buffer molarity, mobile phase pH*organic solvent, mobile phase pH^2, and organic $solvent^2$. An increase in R_t of CPH was observed when the pH was increased. CPH is ionized in a solution of pH > 6.09, and the ionized species have an increased affinity for the polar components of the stationary phase [141]. Cyano-columns are used as stationary phases for RP-HPLC when shorter R_t for hydrophobic compounds are desired [142]. An increase in the degree of ionization of CPH increases the compound's affinity for the cyano-based stationary phase, thereby increasing the R_t as the elution of CPH from the column is delayed.

Organic solvent content was a significant factor that resulted in a decrease in R_t as it was increased. An increase in the ACN content of the mobile phase resulted in a decrease in polarity of the mobile phase and shorter R_t in the more polar environment in the column. Organic solvent content showed the most prominent overall effect as small increments in ACN content resulted in a pronounced shortening in the R_t of CPH. The buffer includes hydrogen ions, and as the concentration of H^+ ions increases, CPH ionization decreases. A low degree of ionization of CPH results in better affinity for the mobile phase and shorter separation times.

2.5.2.5 Evaluation of model fit for R_t of CPH

To confirm regression analysis using ANOVA are realistic and improves the model, residual analysis and diagnostic plots are used [143]. The normal plot of internally studentized residuals is shown in **Figure 2.5**. The points are almost located in a straight line that denotes that the error terms follow a normal distribution in terms of the mean and variance of the data.

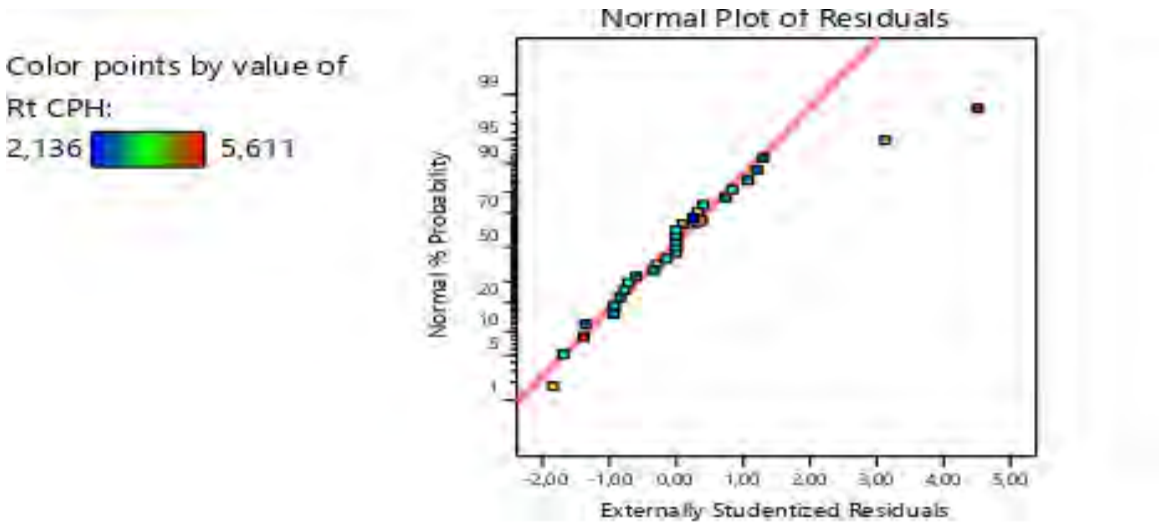

Figure 2.5 Normal plot of residuals depicting the impact of model terms on the R_t of CPH.

The residuals versus run plot for internally studentized residuals depicted in **Figure 2.6** indicates that the data points do not follow a trend indicating that more than one factor impacted the R_t of CPH. Pareto t-limits for this analysis are depicted with red lines, and an outlier indicating that not all the data was well fitted to the model is evident.

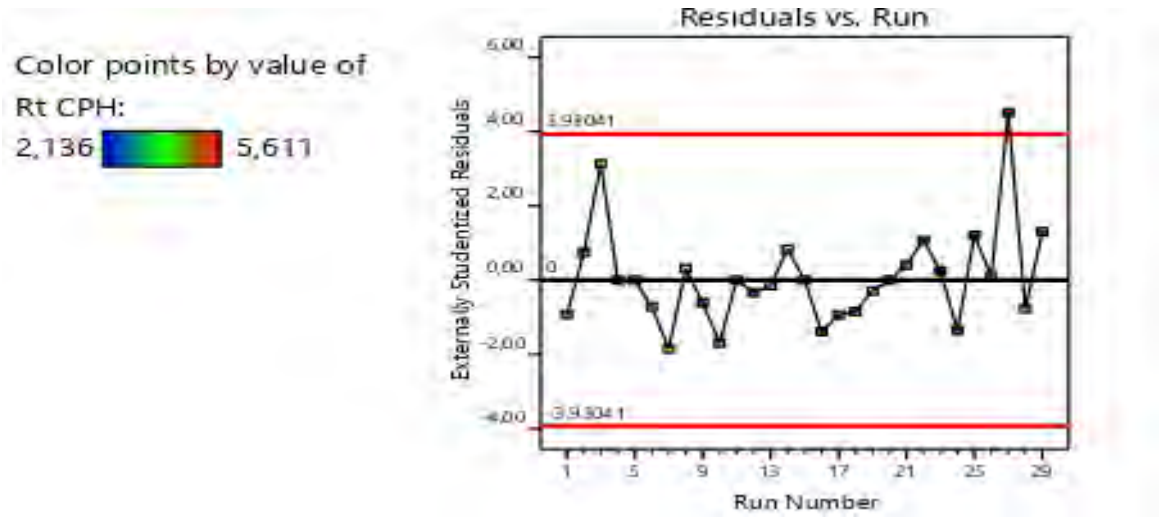

Figure 2.6 Pareto plot of residuals versus experimental runs.

The predicted value and actual response plot are depicted in **Figure 2.7**. The points are evenly located with the same number of points above and below the line, indicating that the data fits the model, and that model transformation may not be necessary.

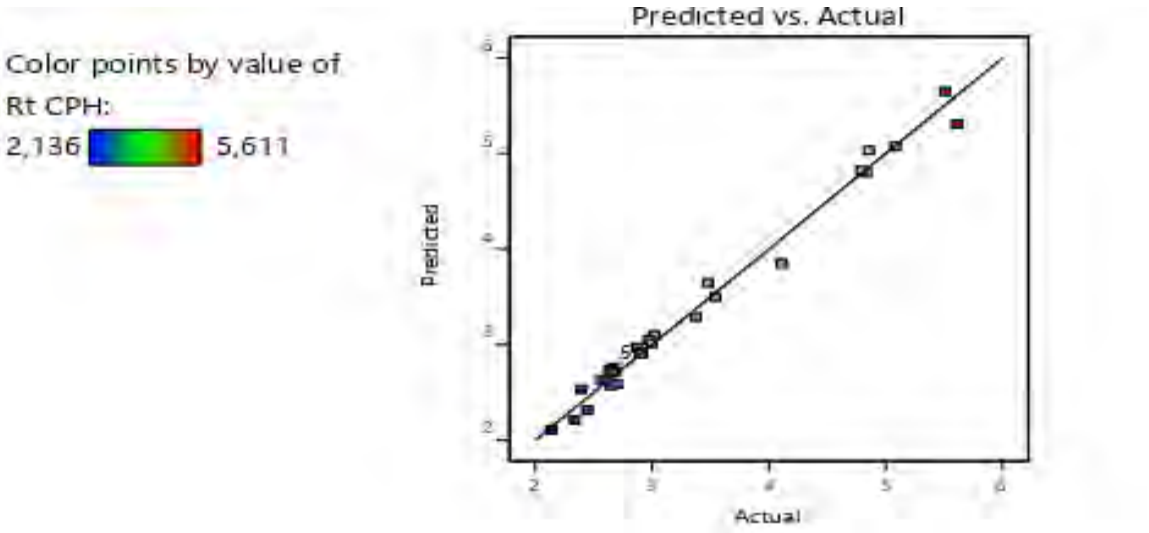

Figure 2.7 Actual versus predicted response plot for R_t of CPH.

2.5.2.6 Graphical interpretation and evaluation of the CPH model for R_t.

The response sensitivity to small changes in the model terms is demonstrated using perturbation plots that show the effect of individual input variables on a response. The perturbation plot depicted in **Figure 2.8** for R_t of CPH was used to evaluate the impact of organic solvent content, column temperature, buffer molarity, and pH on R_t. An increase in the organic solvent content has the most pronounced impact on the reduction of R_t for CPH as described in **§ 2.5.2.4**.

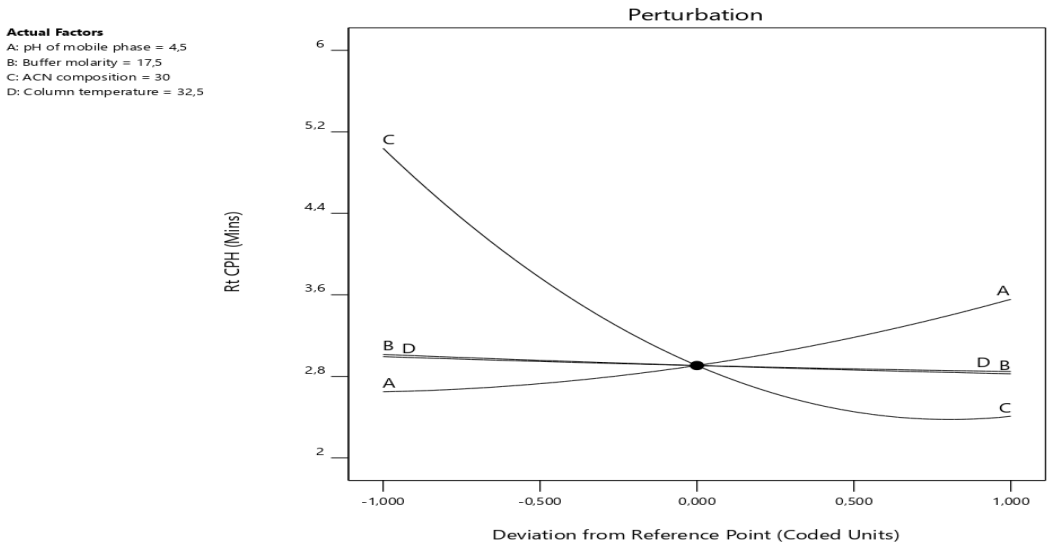

Figure 2.8 Perturbation plot demonstrating the impact of input variables on R_t of CPH.

2.5.2.6.1 *Response surface model diagnostic plots for R_t.*

The relative effects of model terms were evaluated using contour and three-dimensional (3D) response surface plots. The plots represent the effects of binary combinations of input factors on the R_t of CPH and are depicted in **Figures 2.9** and **2.10**. The 3D response surface plot gives shape to two-dimensional contour plots permitting a more thorough data analysis. The lines on the contour plot indicate a minor interaction between buffer molarity and mobile phase pH. As depicted in the contour and 3D response surface plots, the R_t of CPH decreases with a reduction in mobile phase pH and increased buffer molarity. The effects are due to the phenomena as described in section **§ 2.5.2.4.**

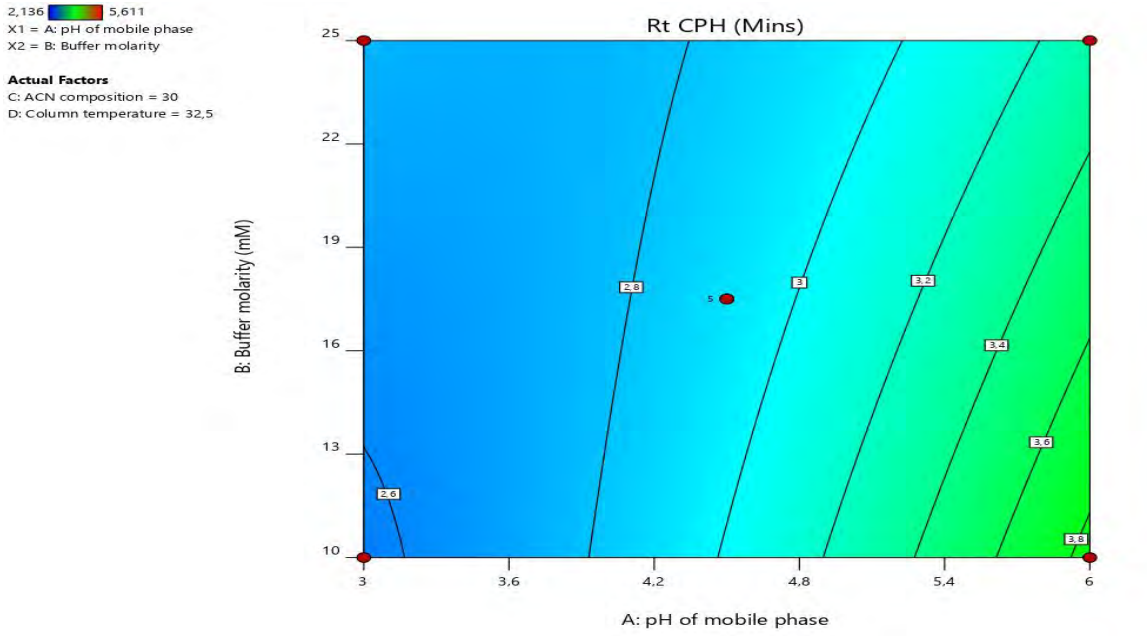

Figure 2.9 Contour plot depicting the impact of buffer molarity and mobile phase pH on R_t of CPH.

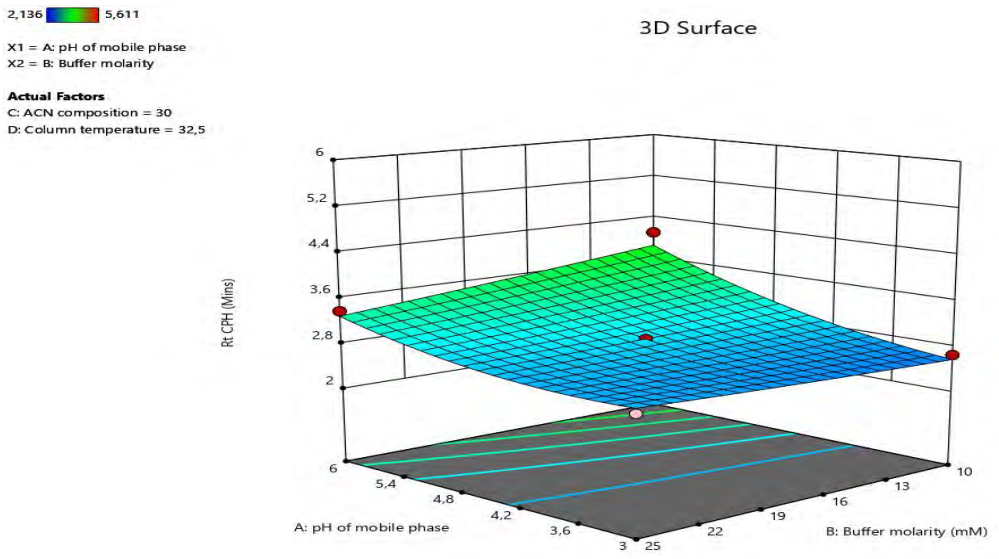

Figure 2.10 3D response surface plot depicting the impact of buffer molarity and mobile phase pH on R_t of CPH.

The binary effect of organic solvent content and mobile phase pH is depicted in the contour and 3D response surface plots in **Figures 2.11** and **2.12**, respectively. In this case, the column temperature and buffer molarity were constant. The curvature of the lines in the contour plot indicates that significant interaction between the factors exists. A reduction in the mobile phase pH and increased organic solvent content resulted in a shorter R_t of CPH.

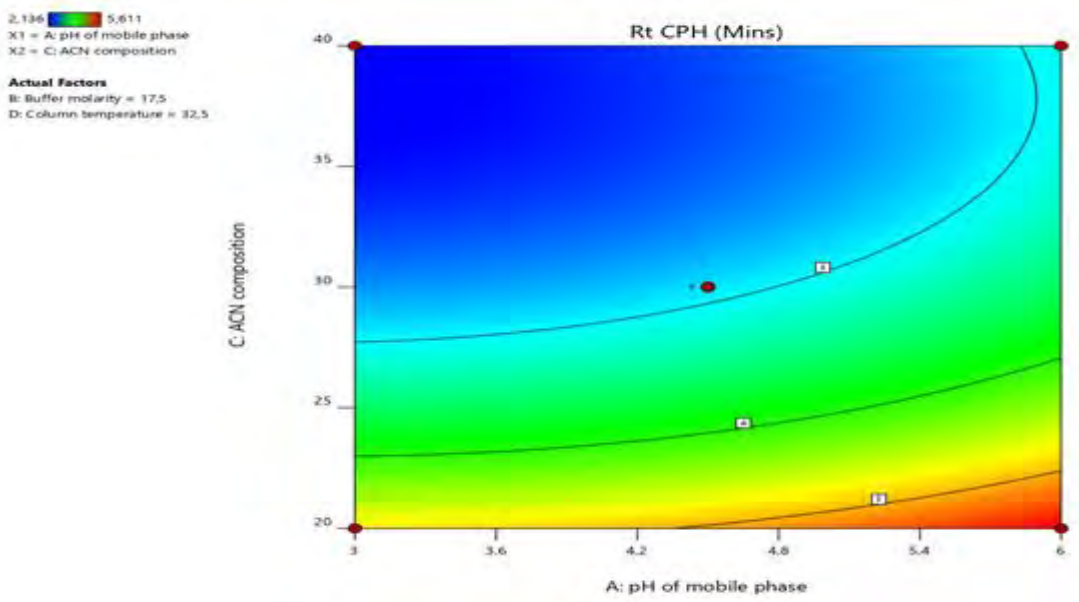

Figure 2.11 Contour plot depicting the impact of organic solvent content and mobile phase pH on R_t of CPH.

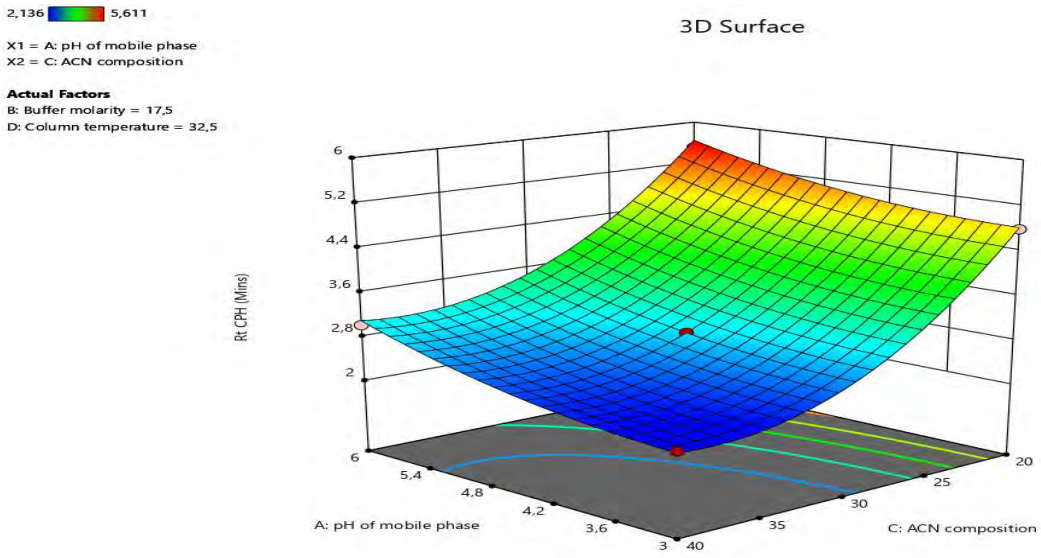

Figure 2.12 3D response surface plot depicting the impact of organic solvent composition and mobile phase pH on R_t of CPH.

The plots depicted in **Figures 2.13** and **2.14** reveal a significant interaction between organic solvent content and buffer molarity. The R_t of CPH decreases with increased ACN content in the mobile phase and an increase in buffer molarity. The minimum R_t of CPH of 2.14 minutes was obtained with an organic solvent content of 40 % and buffer molarity of 0.0175 M. The column

temperature, and mobile phase pH were maintained at 32.5 °C and 3, respectively. The longest R_t for CPH of 5.6 minutes was observed when the ACN content was 20 %; the pH was 4.5 and buffer molarity of 0.0175 M at a column temperature of 25 °C. **Figure 2.15** shows the 3D response surface plot depicting the impact of column temperature and buffer molarity on the R_t of CPH.

Column temperature had no significant effect on CPH R_t and was thus not analyzed. The interaction between column temperature and buffer molarity is moderately linear, as depicted in **Figure 2.15**. This linear interaction suggests that as the combined effect of column temperature and buffer molarity increases, there is a slight decrease in CPH R_t, as depicted in **Figure 2.15**.

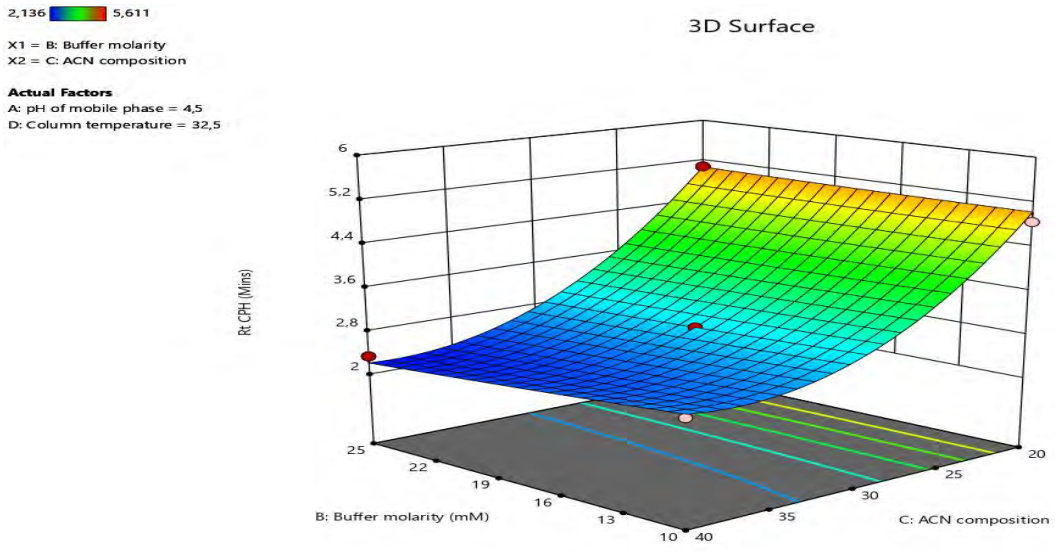

Figure 2.13 3D surface response plot depicting the impact of organic solvent content and buffer molarity on R_t of CPH.

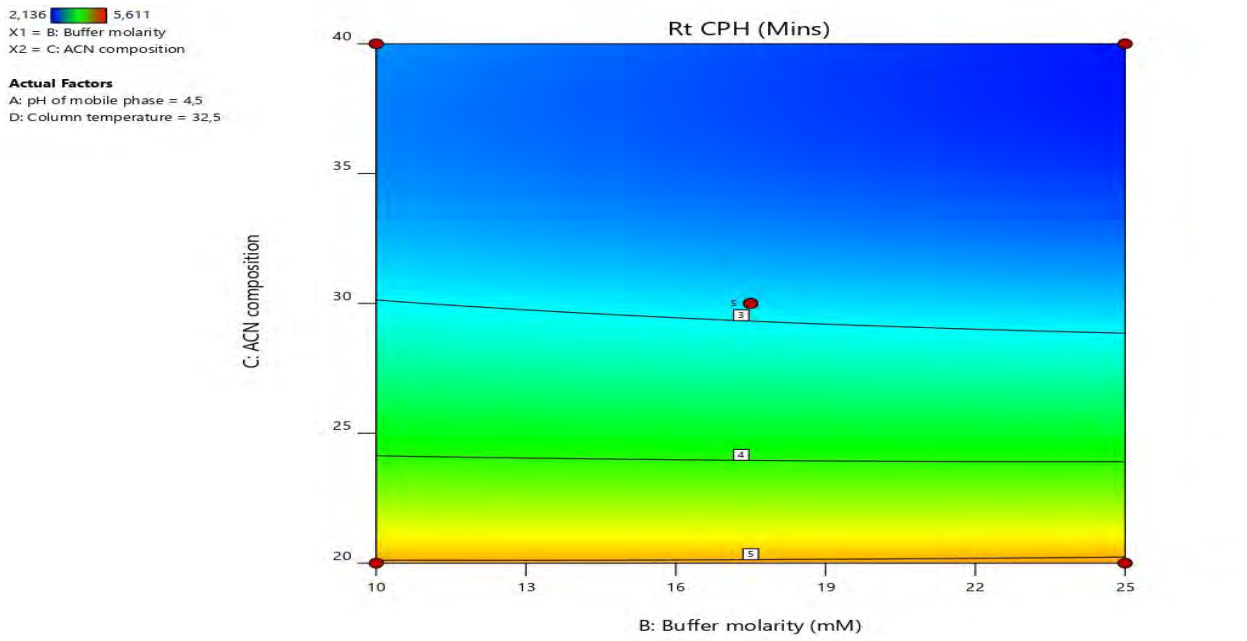

Figure 2.14 Contour plot depicting the impact of organic solvent content and buffer molarity on R_t of CPH.

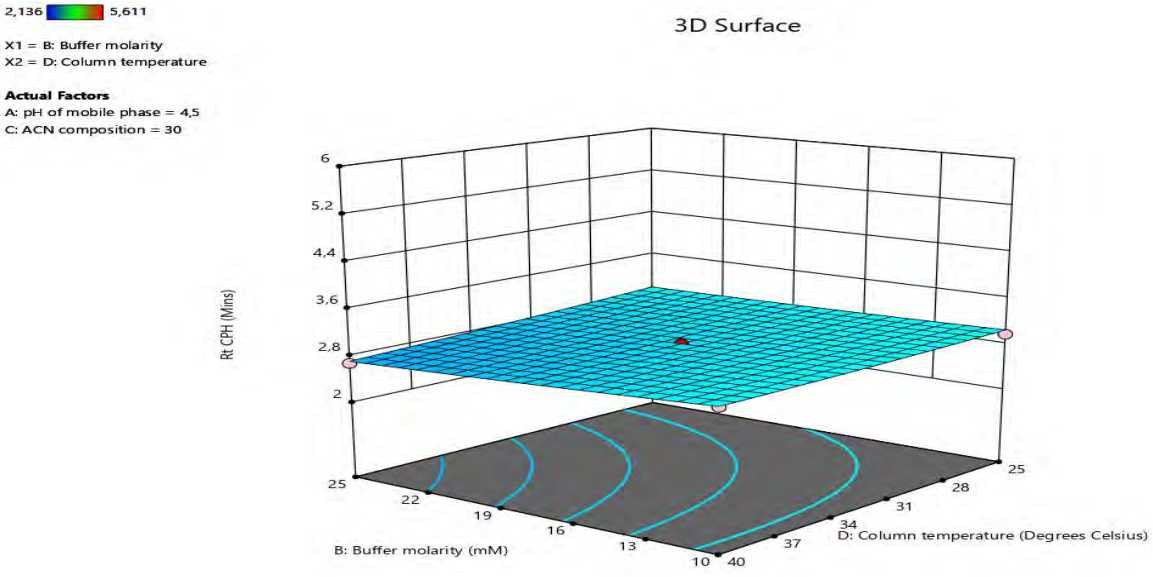

Figure 2.15 3D response surface plot depicting the impact of column temperature and buffer molarity on R_t of CPH.

2.5.2.7 Analysis of variance for R_t of CBZ

The R_t of CBZ is important as it may affect resolution and the run time for each sample analysis. The target for R_t of CBZ was < 10 minutes to ensure the RP-HPLC was rapid. The ANOVA data for the CCD model for R_t of CBZ is summarized in **Table 2.10**, revealing that organic solvent content significantly affected R_t of CBZ.

Table 2.10 ANOVA data table for R_t of CBZ.

Source	Sum of squares	df	Mean square	F-value	p-value	Significant
Model	2.90	14	0.2072	3.70	0.0100	Significant
A-pH of mobile phase	0.0003	1	0.0003	0.0062	0.9385	No
B-Buffer molarity	0.0059	1	0.0059	0.1047	0.7510	No
C-ACN composition	0.0023	1	0.0023	0.0418	0.8409	No
D-Column temperature	0.1592	1	0.1592	2.84	0.1140	No
AB	0.0038	1	0.0038	0.0676	0.7987	No
AC	0.0016	1	0.0016	0.0287	0.8679	No
AD	0.0864	1	0.0864	1.54	0.2349	No
BC	0.0150	1	0.0150	0.2678	0.6129	No
BD	0.0103	1	0.0103	0.1830	0.6753	No
CD	0.0170	1	0.0170	0.3035	0.5904	No
A^2	0.0003	1	0.0003	0.0047	0.9461	No
B^2	0.5192	1	0.5192	9.26	0.0088	Yes
C^2	2.28	1	2.28	40.68	< 0.0001	Yes
D^2	0.0908	1	0.0908	1.62	0.2237	No
Residual	0.7847	14	0.0561			
Lack of Fit	0.7847	10	0.0785			
Pure Error	0.0000	4	0.0000			
Cor Total	3.68	28				

The Model F-value of 3.70 implies that the model is significant. There is only a 1.00 % chance that an F-value this large could occur due to noise. P-values less than 0.0500 indicate model terms are significant. In this case, buffer molarity^2, ACN composition^2 are significant model terms.

A negative Predicted R^2 implies that the overall mean may be a better predictor of the response than the current model. In some cases, a higher-order model may also predict better. Adequate precision measures the signal-to-noise ratio. A ratio greater than 4 is desirable. The ratio of 6.554

in this study indicates an adequate signal. This model can be used to navigate the design space. The adequate precision measures the signal-to-noise ratio, and a value of 7.096 indicates that the model can be used to navigate the design space, as shown in **Table 2.11**. The equation for the model is mathematically represented by **Equation 2.9**.

Table 2.11 Statistical measures of model adequacy.

Std. Dev.	0.2368	**R²**	0.7870
Mean	0.7234	**Adjusted R²**	0.5741
C.V. %	32.73	**Predicted R²**	-0.2266
		Adequate Precision	6.5539

$$^{1}/_{\text{sqrt(Rt CBZ)}} = -5.88638 - (0.314524 \times A) + (0.131642 \times B) + (0.377112 \times C) + (0.072946 \times D) - (0.002736 \times A \times B) - (0.001337 \times A \times C) + (0.013062 \times A \times D) + (0.000817 \times B \times C) + (0.000900 \times B \times D) - (0.002841 \times A^2) - (0.005030 \times B^2) - (0.005929 \times C^2) - (0.002104 \times D^2)$$

Equation 2.9

The effect of organic solvent content has a negative impact on the R_t of CBZ. An increase in the content of the organic solvent reduced the R_t of CBZ significantly. The increase in the R_t of CBZ due to organic solvent content is based on the phenomenon described in **§ 2.5.2.4**. The insignificant model terms were column temperature, molarity, pH, although these exhibited positive effects according to the equation resulting in a lengthening of R_t. The most minor synergistic effects were observed for organic solvent content and mobile phase pH.

2.5.2.8 Analysis of variance for resolution factor

The R_s is a crucial response as the thorough interpretation of the chromatogram depends on two well-separated peaks to be generated. A $R_s > 2$ is desirable, and it ensures accurate quantification of the two distinct peaks. The ANOVA data for the CCD for the R_s is summarized in **Table 2.12**, revealing that organic solvent content, buffer molarity, and mobile phase pH significantly affected the R_s, with all the terms exhibiting $p < 0.05$.

Table 2.12 ANOVA data table for R_s.

Source	Sum of Squares	Df	Mean Square	F-value	p-value	Significant
Model	0.3312	4	0.0828	3.26	0.0286	Significant
A-pH of mobile phase	0.0527	1	0.0527	2.08	0.1625	No
B-Buffer molarity	0.1161	1	0.1161	4.57	0.0429	Yes
C-ACN composition	0.1613	1	0.1613	6.35	0.0188	Yes
D-Column temperature	0.0011	1	0.0011	0.0447	0.8343	No
Residual	0.6094	24	0.0254			
Lack of Fit	0.6094	20	0.0305			
Pure Error	0.0000	4	0.0000			
Cor Total	0.9406	28				

The predicted R^2 value, as listed in **Table 2.13**, is not as close to the adjusted R^2 as expected, indicating that there could be a problem with the model and the data. The adequate precision value of 11.615 indicates an adequate signal and that the model can be used to navigate the design space to determine the R_s.

Table 2.13 Statistical measures of model adequacy.

Std. Dev.	0.1593	**R²**	0.3521
Mean	0.6049	**Adjusted R²**	0.2442
C.V. %	26.34	**Predicted R²**	0.0031
		Adequate Precision	6.4775

The relationship between the model terms and the R_s is illustrated using a quadratic model, as shown by **Equation 2.10**. The equation can predict the response for different levels of the model terms, and the relationship is more accurately analyzed using untransformed data for the R_s. The recommended transformation of the natural log was not used as it made the model F-value insignificant.

$$1/\text{Sqrt (Resolution factor)} = 0.184300 - (0.044188 \times A) + (0.013116 \times B) + (0.011592 \times C) + (0.001297 \text{ x } D)$$ **Equation 2.10**

Significant positive effects were produced by organic solvent content. An increase in organic solvent content increases the R_s. The significant model terms producing a negative effect were buffer molarity and mobile phase pH. The most noticeable negative effect was produced by buffer molarity since an increase in molarity significantly reduces the R_t of CPH, thereby decreasing the resolution between the two peaks. In order to obtain an accurate analysis of the relationship between the model terms and the resolution, the untransformed data was analyzed using **Equation 2.11.**

$$\text{Resolution factor} = 10.00516 - (3.95215 \times A) + (0.610667 \times B) + (0.013037 \times C) - (0.161261 \times D) - (0.026994 \times A \times B) + (0.107500 \times A \times C) + (0.051334 \times A \times D) - (0.022425 \times B \times C) + (0.001527 \times B \times D) - (0.003712 \times C \times D)$$ **Equation 2.11**

As summarized in **Table 2.12**, organic solvent content had a significant impact on resolution. The R_s was improved as a result of increasing organic solvent content. The significant effects of buffer molarity and mobile phase pH are negative, with buffer molarity causing the most prominent effect. Ideally, according to **Equation 2.11**, the organic solvent content should be increased to ensure that the R_s is ≥ 2.

2.5.2.9 Graphical interpretation and evaluation of response model for R_s

The perturbation plot depicted in **Figure 2.16** reveals that all the input factors resulted in better resolution. The impact of organic solvent content was more significant than buffer molarity, mobile phase pH, and column temperature.

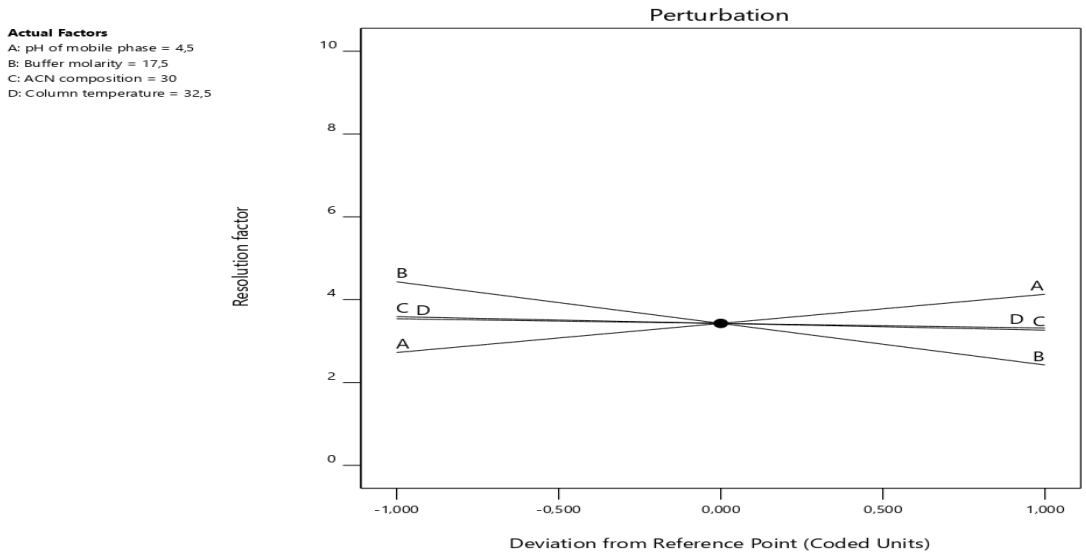

Figure 2.16 Perturbation plot demonstrating the impact of input variables on R_s.

2.5.2.10 Analysis of variance for asymmetric factor

The asymmetry factor is a measure of peak tailing and is defined as the distance from the centerline of the peak to the back slope divided by the distance from the centerline of the peak to the front slope, with all measurements made at 10% of the maximum peak height [88]. The target asymmetric factor was < 1.50 to ensure good separation between the peaks. The ANOVA data for the CCD model for the asymmetric factor is summarized in **Table 2.14**, revealing that buffer molarity and mobile phase pH significantly affected the asymmetric factor.

Table 2.14 ANOVA data table for asymmetric factor.

Source	Sum of Squares	df	Mean Square	F-value	p-value	Significant
Model	11.89	4	2.97	7.03	0.0007	Significant
A-pH of mobile phase	6.74	1	6.74	15.95	0.0005	No
B-Buffer molarity	3.72	1	3.72	8.80	0.0067	Yes
C-ACN composition	0.3523	1	0.3523	0.8333	0.3704	Yes
D-Column temperature	1.07	1	1.07	2.54	0.1240	No
Residual	10.15	24	0.4228			
Lack of Fit	10.15	20	0.5073			
Pure Error	0.0000	4	0.0000			
Cor Total	22.04	28				

The predicted R^2 value, as listed in **Table 2.15**, is in reasonable agreement with the adjusted R^2; the difference is less than 0.2. The adequate precision value of 9.679 indicates an adequate signal and that the model can be used to navigate the design space to determine the asymmetric factor.

Table 2.15 Statistical measures of model adequacy.

Std. Dev.	0.6502	**R²**	0.5396
Mean	1.91	**Adjusted R²**	0.4629
C.V. %	34.03	**Predicted R²**	0.2929
		Adequate Precision	9.6786

The relationship between the model terms and the asymmetric factor is illustrated using a quadratic model, as shown in **Equation 2.12**. The equation can predict the response for different levels of the model terms, and the relationship is more accurately analyzed using untransformed data for the asymmetric factor.

$$(\text{Asymmetric factor})^{1} = 0.178355 + (0.499795 \times A) - (0.074243 \times B) - (0.017134 \times C) + (0.039896 \times D)$$

Equation 2.12

Mobile phase pH and buffer molarity significantly affected the asymmetric factor, an increase in mobile phase pH results in an increase in the asymmetric factor. The significant model term producing a negative effect is buffer molarity. In order to obtain an accurate analysis of the relationship between the model terms and the asymmetric factor, the untransformed data was analyzed using **Equation 2.13**.

$$\text{Asymmetric factor} = 0.178355 + (0.499795 \times A) - (0.074243 \times B) - (0.017134 \times C) + (0.039896 \times D)$$

Equation 2.13

As summarized in **Table 2.15**, mobile phase pH and buffer molarity significantly affected the asymmetric factor. An increase in mobile phase pH will increase the asymmetric factor. The opposite can be said about buffer molarity; an increase in buffer molarity will increase the asymmetric factor.

2.5.2.11 Graphical interpretation and evaluation of response model for asymmetric factor

The perturbation plot depicted in **Figure 2.17** reveals that all the input factors resulted in better symmetry. The impact of organic solvent content was more significant than buffer molarity, mobile phase pH, and column temperature.

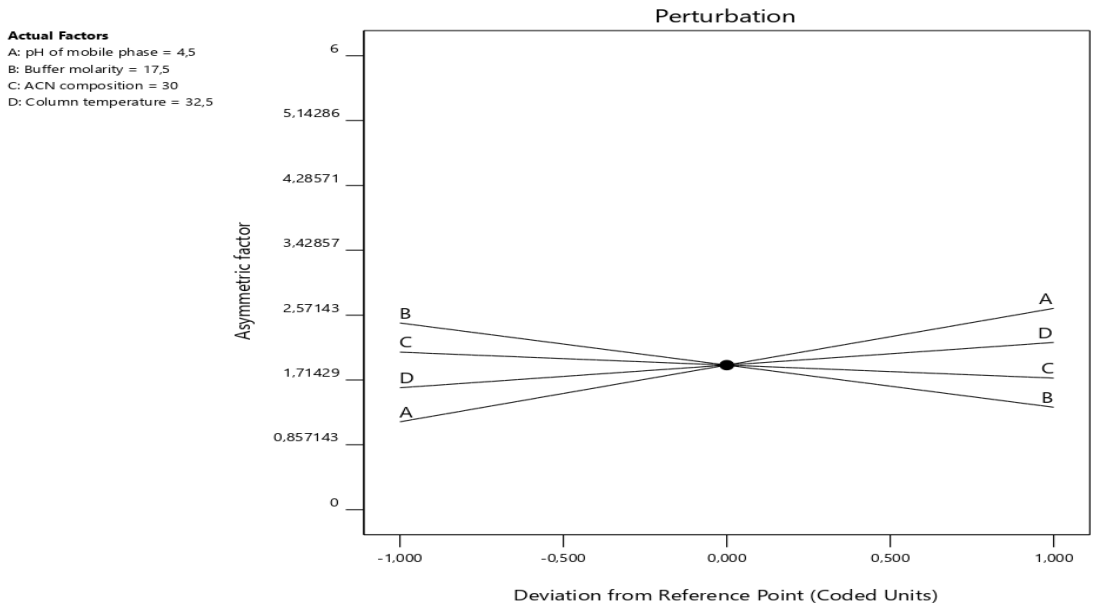

Figure 2.17 Perturbation plot demonstrating the impact of input variables on the asymmetric factor.

The insignificant factors were not analyzed in this study, all the relevant 3D plots and contour plots can be found in Appendix C.

2.5.3 Selection of chromatographic conditions

The predictions for the CCD were in reasonable agreement with the outputs observed in the trial analysis as described in **§ 2.4.9.1**. The results of the trial analysis were therefore considered when selecting the final chromatographic conditions. The chromatogram depicted in **Figure 2.2** reveals that the R_t of CPH was 3.7 minutes and for CBZ was 5.3 minutes, falling within the $2.00 < R_t < 10.00$ limits set. The R_s for the two peaks was > 2 and was therefore acceptable. The optimum chromatographic conditions selected for the analysis of CPH are listed in **Table 2.16**. The quantitative analysis of CBZ was performed using PAR.

2.5.4 Optimization of chromatographic conditions

In this study, CPH R_t was determined as a critical factor in developing a rapid and precise HPLC method. The CPH Rt was set to be > 3.5 minutes to avoid the analyte interfering with the solvent front. The R_s indicates the extent and quality of the separation between the analyte and IS peaks. The R_s is dependent on the separation conditions, instrumental effects, column, and operating conditions. A good separation is indicated by R_s values > 2.0 and poor separation by values < 1.5 [88]. The R_s was set to be > 2.0.

Peak asymmetry factor values < 1.50 are considered acceptable, and a value of 1.00 is indicative of symmetrical peaks. Values > 1.50 indicate poor peak asymmetry, which could result in the calculation of an inaccurate plate number, poor resolution, poor R_t reproducibility, and undetected minor bands located under the tail of the peak. The peak asymmetry factor was set to be between 1 and 1.20. To ensure a rapid HPLC method, the CBZ R_t was set to be < 10 minutes. **Table 2.16** below summarizes the optimizations made.

Table 2.16 The optimization parameters made on the CCD model.

Factor	Goal	Lower limit	Upper limit
Mobile phase pH	In range	3.0	6.0
Buffer molarity	In range	0.01 M	0.025 M
ACN composition	In range	20 % v/v	40 % v/v
Column temperature	Maximize	25 ˚C	40 ˚C
CPH R_t	In range	3.5 minutes	5.611 minutes
Asymmetric factor	In range	1.00	1.20
R_s	Maximize	1.00	9.49
CBZ R_t	In range	3.50 minutes	10.00 minutes

2.5.4.1 Predictive ability of the CCD model

It is essential to assess the prediction ability of a model to identify the optimum conditions for the HPLC method. The model generated 57 solutions with corresponding output predictions, and a list of the possible solutions and range of responses are summarized in **Table 2.17.**

Table 2.17 A summary of the solutions generated by the CCD model.

Solution	ACN %	Column temperature °C	Molarity mM	Mobile phase pH	CPH R_t	CBZ R_t	R_s	Asymmetric factor
11	22.13	40.00	22.04	3.00	4.15	6.50	4.16	1.20
15	22.00	40.00	21.98	3.00	4.18	6.50	4.20	1.20
1	21.89	40.00	21.94	3.00	4.22	6.48	4.30	1.20
2	29.98	40.00	22.55	3.00	4.01	6.19	3.14	1.06
3	21.82	40.00	21.82	3.02	4.12	6.50	4.03	1.17
4	22.12	40.00	20.66	3.32	4.00	6.50	3.90	1.08
8	21.72	40.00	23.00	3.23	4.14	6.50	4.23	1.19

The solutions were compared to the results generated using the HPLC method described in **§ 2.4.9.1**. With the aid of an overlay plot (**Figure 2.18**), the ability of the model to precisely predict a required output value from an input variable was investigated.

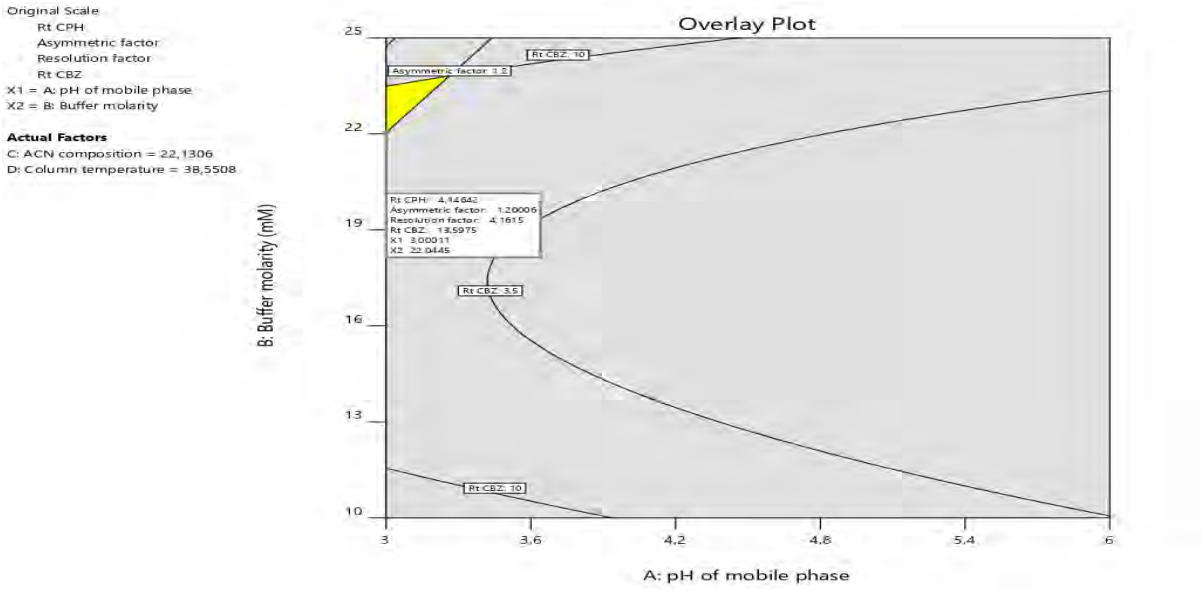

Figure 2.18 Overlay plot for the R_t of CPH, CBZ, asymmetric factor, and R_s.

The overlay plot depicted in **Figure 2.18** is for the R_t of CPH at 4.12 minutes, R_t of CBZ between 3.5 and 10 minutes, R_s of 4.16, and an asymmetric factor at 1.2. The output values are predicted for buffer molarity of between 22 and 23.5 mM, mobile phase pH of between 3 and 3.3 as indicated by the yellow region on the plot, column temperature at 38.6 °C, and ACN composition at 22.1 % v/v. The factor parameters predicted by the model are similar to those set in the method used for the trial analysis of CPH as summarized in **§ 2.4.9.1.**

2.5.5 Method validation

2.5.5.1 Linearity and range

A least squares linear regression line of best fit was plotted for PAR versus concentration, depicted in **Figure 2.19**. The relationship expressed by the equation for the line was y = 0.0157x + 0.1223 with a R^2 = 0.9999 indicating a linear relationship existed. The y-intercept was 0.1223, not necessarily satisfying the criterion for linearity, which states that the y-intercept must be < 2 %.

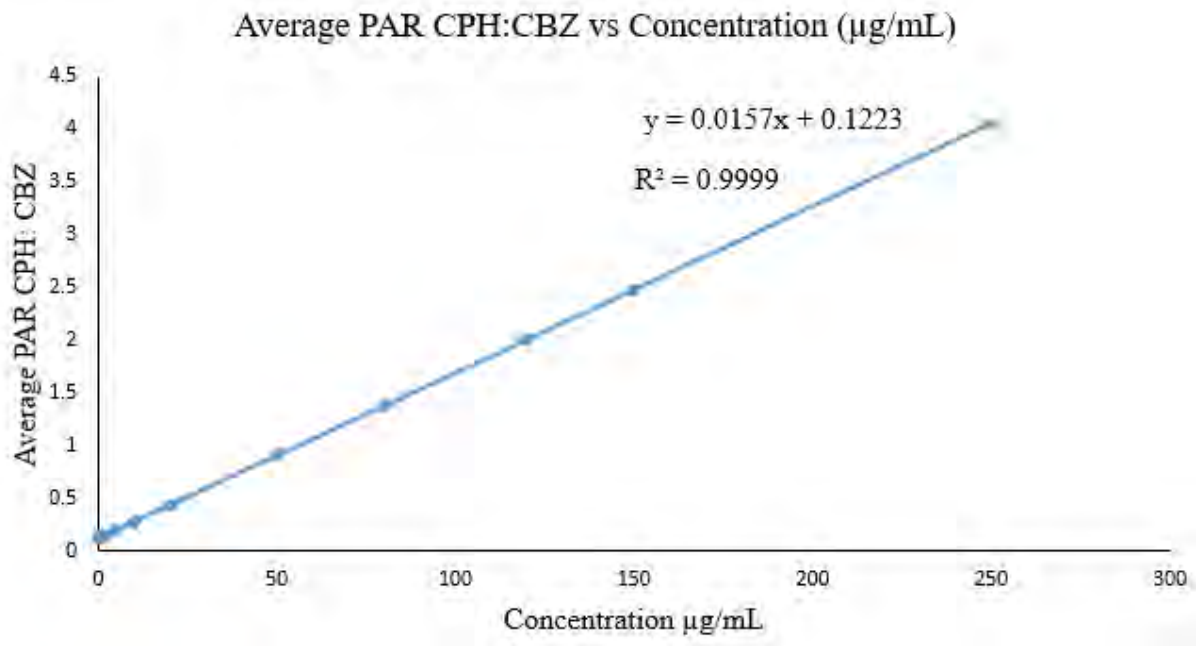

Figure 2.19 Typical calibration curve for CPH over the concentration range 0.1 - 250 µg/ml (n = 5).

The experimental SD values were ≤ ± 1.05 and % RSD values ≤ 5 % for all calibration curve points, and these data are listed in **Table 2.18**, indicating good precision.

Table 2.18 Intra-assay data for analysis of CPH.

Theoretical concentration µg/ml	Average PAR CPH: CBZ	SD	% RSD
0.1	0.1239	0.0083	6.70
0.2	0.1254	0.0001	0.08
0.4	0.1286	0.0002	0.18
0.6	0.1317	0.0001	0.08
0.8	0.1349	0.0002	0.15
1	0.1380	0.00004	0.03
2	0.1537	0.00002	0.01
5	0.2008	0.00002	0.01
10	0.2793	0.00003	0.01
20	0.4363	0.0002	0.05
50	0.9073	0.0004	0.04
80	1.3783	0.00005	0.004
120	2.0063	0.0003	0.01
150	2.4773	0.0005	0.02
250	4.0473	0.0006	0.01

2.5.5.2 Precision

2.5.5.2.1 Repeatability or intra-day precision

The results for repeatability studies are summarized in **Table 2.19** and include values for SD and % RSD. The results were within the set limits; therefore, the intra-day precision of the method was satisfactory.

Table 2.19 Intra-day precision for the analysis of CPH.

Theoretical concentration µg/ml	Actual concentration µg/ml	SD	%RSD	%Bias	%Recovery
3	3.15	0.0040	1.00	-4.46	105.00
50	50	0.0310	0.80	2.63	100.00
120	120	0.0511	0.58	2.89	100

2.5.5.2.2 Intermediate or inter-day precision

The results of inter-day precision studies are summarized in **Table 2.20.** For all results, the SD was ≤ ± 1.05, % RSD was ≤ 5 %, and the % recovery values were 100 ± 5 %, suggesting that the RP-HPLC method exhibits good intermediate precision.

Table 2.20 Inter-day precision data for the analysis of CPH.

	Theoretical concentration µg/ml	Actual concentration µg/ml	SD	%RSD	%Bias	%Recovery
Day 1	**3**	3.14	0.0012	1.29	-1.20	104.67
	50	50.0	0.0110	0.66	2.31	100.00
	120	120.2	0.0230	0.97	1.21	100.20
Day 2	**3**	3.11	0.0023	2.34	-2.11	103.67
	50	51.0	0.0409	0.94	-2.35	102.00
	120	119.5	0.0322	1.23	1.23	99.58
Day 3	**3**	3.02	0.0546	1.29	-1.45	100.67
	50	49.7	0.0354	1.90	-1.74	99.40
	120	121.0	0.0024	2.34	-3.40	101.00

2.5.5.3 Accuracy

The SD, % RSD, and % bias for accuracy studies are summarized in **Table 2.21**.

Table 2.21 Accuracy data for the analysis of CPH.

Theoretical concentration µg/ml	Actual concentration µg/ml	SD	%RSD	%Bias	%Recovery
3	3.10	0.0234	1.011	-2.45	103.33
50	50.20	0.9012	0.560	2.34	100.40
120	120.20	1.0330	0.345	1.56	100.20

2.5.5.4 Limits of quantitation and detection

The values for % RSD were used to determine the precision and accuracy. For a concentration of 1.5 µg/mL of CPH, the % RSD was 2.90 and therefore was selected as the LOQ.

The results for the determination of LOQ are summarized in **Table 2.22**.

Table 2.22 Determination of LOQ results.

Concentration µg/ml	PAR CPH: CBZ	SD	%RSD
0.05	0.001309	0.0000987	7.54
0.10	0.001880	0.0001260	6.70
0.15	0.002458	0.0000713	2.90
0.20	0.002770	0.0000022	0.08

The LOD was determined by convention as 0.3 × LOQ and was established as 0.045 µg/mL.

2.5.6 Ciprofloxacin Assay

The results following the analysis of Cifran® tablets are summarized in **Table 2.23**.

Table 2.23 Assay results for commercially available 500 mg CPH tablet.

Product	CPH recovered %
Cifran® tablets	96.8±1.23

The recovery following analysis of Cifran® tablets was 96.8 ± 1.23 % for CPH and complied with the limits set in official compendia. Therefore, the tablets are of suitable quality, and the extraction procedure was adequate for assessing CPH content in reference and test formulations. The chromatogram following analysis of the commercial product is shown in **Figure 2.20**. It is evident from the chromatogram that the method demonstrates specificity for CPH as no extra/excipient peaks were observed. The method developed has shown specificity in the analysis of CPH commercial tablets. With this information we can therefore conclude that the method could also be used in the analysis of niosomes.

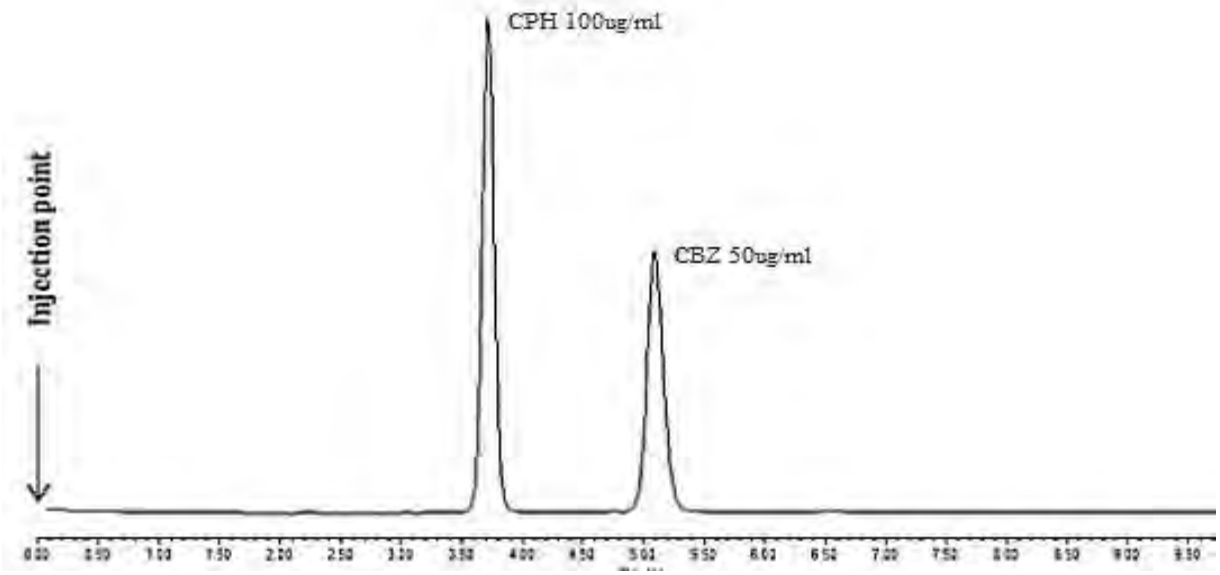

Figure 2.20 Typical chromatogram following analysis of Cifran® tablets.

2.5.6.1 Validation of the extraction procedure

2.5.6.1.1 Repeatability

The SD, % RSD, and % recovery values of CPH are listed in **Table 2.24** and were within the tolerance limits. The extraction method for the analysis of CPH in formulations is repeatable.

Table 2.24 Repeatability data for the assay of CPH in Cifran® tablets.

Product	Theoretical concentration µg/ml	Actual concentration µg/ml	SD	%RSD	%Recovery
Cifran®	3	3.09	0.0098	1.45	103.00
	50	50.60	0.0054	0.67	101.20
	100	100.89	0.0044	0.30	100.89

2.5.6.1.2 Accuracy

The accuracy of the extraction was measured using % bias and was within the limit set at ± 5 %, revealing that the extraction procedure for CPH from tablets is accurate (**Table 2.25**). Therefore, the niosomes to be developed can be accurately analyzed and CPH content quantitated during formulation development and product and process validation.

Table 2.25 Accuracy results for extraction of CPH.

Product	Theoretical concentration µg/ml	Actual concentration µg/ml	SD	%RSD	%Bias
Cifran®	50	52.34	0.1022	0.136	3.23

2.6 CONCLUSIONS

At 278 nm, a simple and rapid RP-HPLC method was developed successfully. This method may be used for the quantitative analysis of CPH in pharmaceutical dosage forms and was developed, optimized, and validated in terms of linearity, precision, accuracy, precision, robustness, and selectivity. A Phenomenex® 150 x 4.6 mm C18 column was used in a RP-HPLC method, and this was selected as the non-polar stationary phase will allow for shorter R_t of hydrophilic compounds like CPH. CBZ was selected as the IS due to its similar functional groups to CPH and the adequate resolution between CPH and CBZ.

CPH and CBZ were separated using the optimized mobile phase composition of a binary mixture of ACN and 0.0175 M phosphate buffer of pH 3 in a ratio of 20:80 v/v and a flow rate of 1.0 mL/min. The selected chromatographic conditions resulted in a R_t of 3.7 and 5.3 minutes for CPH and CBZ, respectively, with a total run-time for sample analysis of 10 minutes. Mobile pH and ACN composition significantly affected the R_t of CPH, and the R_t of CBZ was significantly affected by buffer molarity^2 and ACN composition^2. The RP-HPLC method was linear in the range of 0.1 – 250 µg/mL and had a correlation coefficient of 0.999. The validation data reveal that the RP-HPLC method was linear, precise, accurate, and selective.

The model has an F-value of 78.25, implying that the model is significant and the predicted R^2 (0.9273) is in reasonable agreement with the adjusted R^2 (0.9748), i.e., the difference is less than 0.2. The overlay plot was used to assess the predictive ability of CCD, which was shown to closely predict the outputs of a random RP-HPLC analysis of CPH using similar chromatographic conditions as those of the developed method.

The assay of CPH was used to confirm further the validity of the method using Cifran® 500mg tablets, and recovery was 96.8 %. Therefore, this method may be used for the assay of CPH in pharmaceutical dosage forms.

CHAPTER THREE

PREFORMULATION STUDIES OF CIPROFLOXACIN LOADED NIOSOMES FOR TRANSTYMPANIC DELIVERY

3.1 INTRODUCTION

Transtympanic drug delivery systems are self-contained, discrete dosage forms that deliver a predetermined amount of drug to the surface of an intact tympanic membrane and overcome the gastrointestinal system's limitation to achieve systemic effects while also avoiding the Hepatic First Pass Effect (HFPE) [144]. Preliminary studies are conducted to detect any API-excipient interactions and excipient-excipient interactions [144]. These are groups of studies that focus on the physicochemical properties that can affect API performance in the development of a pharmaceutical dosage form [145].

Preformulation studies allow the formulator to generate valuable information in developing stable, safe, and bioavailable dosage forms and maximize the chances of formulating a stable, efficacious, and safe product that provides the basis for optimization of the product [145]. Preformulation studies aim to identify potential physical and chemical interactions in API-excipient mixtures to avoid potential chemical instability, degradation, lack of safety, and bioavailability changes resulting in API inefficiency [146]. Parameters assessed include but are not limited to solid-state compatibility (thin layer compatibility, diffuse reflection spectroscopy), stability, physicomechanical properties (bulk topped density and compressibility), and thermal analysis (differential thermal analysis, differential scanning calorimetry) [145].

Fourier transform infrared spectroscopy (FT-IR) and differential scanning calorimetry (DSC) will be used in this study to identify potential API-excipient and excipient-excipient interactions. An FT-IR spectrum of a compound indicates the bond formation or breaking that could occur in API-excipient mixtures. In the IR spectral range, a compound shows characteristic absorption and emission, allowing qualitative and quantitative analysis [147]. DSC is a thermoanalytical technique in which the difference in the amount of heat required to increase the temperature of a sample and reference is measured as a function of temperature. The instrument used is a differential scanning calorimeter or DSC [148,149].

A clinically effective local delivery system that reproduces the effect of an extended systemic drug regimen should increase cumulative drug uptake and be able to maintain it over a prolonged period [150]. Niosomal drug delivery is potentially applicable to many pharmacological agents for their action against various diseases. It can also be used as vehicle for poorly absorbable drugs to design the novel drug delivery system. It enhances the bioavailability by crossing the tympanic barrier quicker, thus delivering the drug to the affected area quicker than conventional ear drops [151]. Strategies to overcome the tympanic membrane barrier have been extensively explored in transtympanic applications. These include chemical additives [152], iontophoresis [153], micro-injection [154], and CPEs [155]. CPEs have emerged as an effective means of enhancing small molecule flux across the tympanic membrane [156].

3.2 EXCIPIENTS

3.2.1 Tween® 80 (Polysorbate 80)

Tween® 80 is a viscous yellow liquid used as a surfactant in this formulation at varying concentrations. It functions as a base unit in the formation of niosomes. Polysorbates are used in cosmetics, parenteral, oral, and topical pharmaceutical formulations [157]. Polysorbates are non-toxic and non-irritant [158].

3.2.2 Cholesterol

Cholesterol (chemical name 3β-cholest-5-en-3-ol) is an organic compound belonging to the steroid family. Its molecular formula is C_{27} H_{46} O and in its pure state is a white and crystalline powder [159]. The chemical structure of cholesterol is shown in **Figure 3.1**.

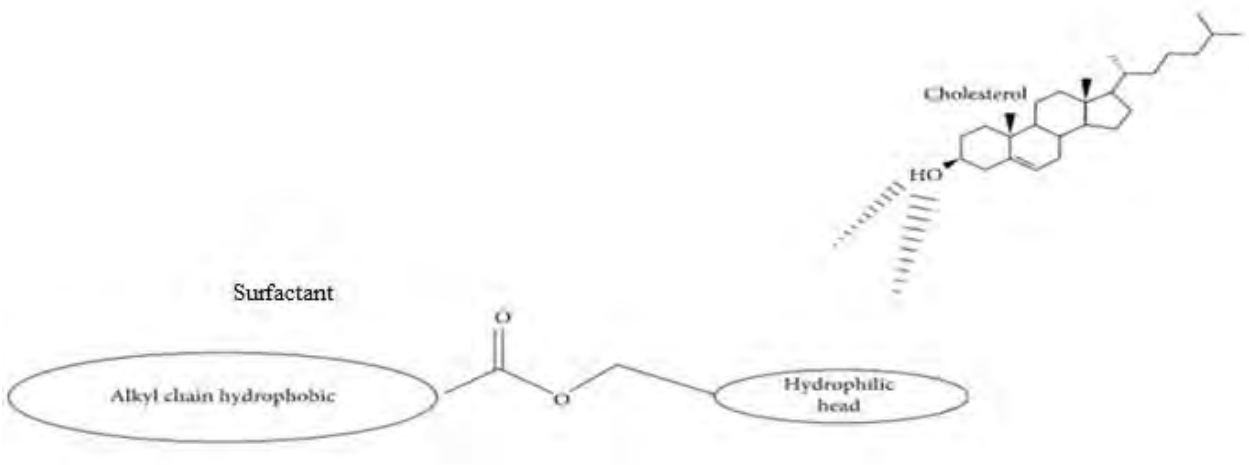

Figure 3.1 Schematic structural interaction between cholesterol and surfactants. Adapted from [160].

Cholesterol is a sterol synthesized by animal cells and is also a diet component, being present in food of animal origin. Its primary function is to maintain the integrity of cell membranes and serve as a precursor for the synthesis of substances vital for the organism, including steroid hormones, bile acids, and vitamin D [161].

In the niosome structure, cholesterol is an amphiphilic compound that can be incorporated with a surfactant to construct hydrogen bonding among hydroxyl groups of cholesterol with the hydrophilic head of the surfactant. This interaction improves the mechanical rigidity, membrane cohesion, leakiness of the membrane and finally increases the entrapment efficiency of niosomes [162, 163]. Cholesterol amount in niosomes influences the structure, physical characteristics and affects entrapment efficiency, time circulation, and payload release [164]. According to previous studies, it was revealed that cholesterol use in the preparation of niosomes, and its quantities should be adjusted depending on the physical and chemical features of surfactants [165-167]. The interface of cholesterol with surfactant in the bilayer of niosomes is based on hydrogen bonding (**Figure 3.1)**. In this study, cholesterol will be used to give rigidity to the niosome bilayer resulting in less leaky niosomes.

3.2.3 Amaranth dye

Amaranth dye is a red to maroon dye derived from the *Amaranthus* plant native to South America [168]. Amaranth leaves and grain have good nutritional value; these include several health benefits, such as antioxidant, antihyperglycemic, and antihypercholesterolemic effects [169]. Amaranth is a hydrophilic dye and will partition towards the hydrophilic core of the niosomes. Amaranth was used as a dye for microscopy studies.

3.2.4 Sodium lauryl sulfate (SLS)

Ionic detergents are strong detergents that completely disrupt cell membranes. SLS is a white to off-white, water-soluble, ionic detergent [170]. In this study, SLS was used as a detergent/surfactant in the formulation of the niosomes.

3.3 PREFORMULATION STUDIES

3.3.1 Determination of study parameter limits for design of experiment (DOE) analysis

Niosomes are non-ionic surfactant vesicles that encapsulate an aqueous volume of drug(s) with or without the addition of cholesterol and other lipid contents [171, 172]. Niosomes can encapsulate both lipophilic and hydrophilic drugs [173]. They are an alternative to liposomes, and their main benefits compared to liposomes are their lower price, higher stability, and better biodegradability [174]. By preparing niosomes, the side effects of drugs can be reduced, and the therapeutic efficacy increased [175].

The arrangement of non-ionic surfactants in bilayer or micellar form depends on the surfactants' hydrophilic-lipophilic balance (HLB). The properties of drugs, other membrane additives, and the manufacturing method also influence the structure and behaviour of niosomes [176, 177]. Hydrophilic drugs are surrounded by the bilayer of amphiphiles, while hydrophobic drugs are entrapped within the bilayer of vesicles [178]. Several non-ionic surfactants are used to produce niosomes, such as polysorbates, alkyl ethers, alkyl amides, and alkyl esters, but in many studies, only a single surfactant is used [179-182]. However, if a mixture of two or more surfactants is used, stable, small, and monodisperse niosomes can be prepared [179]. In this study, niosomes will be formulated using different concentrations and different experimental conditions to determine the limits for DOE analysis.

3.3.1.1 *Parameters examined*

3.3.1.1.1 Amount of cholesterol

Cholesterol is one of the niosomal components that can influence their physicochemical characteristics and stability [183, 184]. The influence of cholesterol percentage on the size of niosomes is markedly dependent on the type of non-ionic surfactant used. Increasing cholesterol levels leads to a significant decrease in vesicle size and the rigidity of the bilayer membranes by virtue of cholesterol's rigid structure and characteristic inverted cone shape [185]; this results in structures with a low polydispersity index (PDI) and disruption of the vesicles' bilayer structure. Such increment in cholesterol levels could also decrease the total number of bilayer vesicles available for encapsulating the drug [186, 187].

3.3.1.1.2 Sonication time

According to Uchegbu and Vyas [188], an increase in the sonication time increases entrapment efficiency, but as sonication time continues to increase beyond a certain point, a decrease in entrapment efficiency decreases will be noticed. Too long sonication time causes larger vesicles to be reformulated, which leads to drug leakage from niosomes and, accordingly, lower entrapment efficiency. The inverse relationship is observed for vesicle size and PDI vs. sonication time, as smaller niosomes with low PDI are obtained with an increase in sonication time [188, 187].

3.3.1.1.3 Amplitude

Increases in amplitude lead to an increase in the entrapment efficiency of niosomes, but with a continued increase, a decline is soon noticed. This decline is because the higher amplitude damages the vesicles, which leads to drug leakage from the niosomes. As the amplitude increases, the vesicle size and PDI also increase. The possible reason for this behaviour is that an increased energy output of the probe, which leads to excessive heat generation, causes increased vesicle size and more polydisperse niosomes [188].

3.3.2 Differential scanning calorimetry

The basic principle underlying this technique is that when the sample undergoes a physical transformation such as phase transitions, more or less heat will need to flow to it than the reference to maintain both the sample and the reference at the same temperature [189]. By observing the difference in heat flow between the sample and reference, differential scanning calorimeters can measure the amount of heat absorbed or released during such transitions [190]. Changes in the

melting endotherm such as a shift of the melting endotherm of a compound on the thermogram may reveal interactions between the API and excipients. The method is not a definite measure for incompatibilities as the dilution of CPH, or an analytical interface may also cause this shift [191, 192]. As shown in **Equation 3.1**, DSC measures the heat flow difference between the sample and the reference as a function of temperature [193, 194].

$$\Delta\left(\frac{dH}{dt}\right) = \left(\frac{dH}{dt}\right)sample - \left(\frac{dH}{dt}\right)reference$$

Equation 3.1

Where,

dH/dt = heat flow, mJ. s^{-1}

The information obtained in a DSC thermogram provides insight into the potential instability of CPH and susceptibility to chemical changes which may arise over a long period in the dosage form [178]. For thermal analysis of CPH and 1:1 w/w ratio binary mixtures of CPH and excipients, a model Q100 differential scanning calorimeter (TA Instruments, New Castle, DE, USA) coupled with an RCS (90) Refrigerated Cooling System (TA Instruments, New Castle, DE, USA) was used. Small amounts of approximately 2 - 4 mg of each sample were weighed out onto an aluminum pan, and the pans were covered with an aluminum lid. Each pan containing a sample and an empty reference pan was placed on a constantan disc inside the DSC Standard Cell FC and was heated from 30 - 450 °C at a heating rate of 10 °C/min. Analysis was conducted under an inert nitrogen atmosphere at a flow rate of 100 mL/min. The calorimeter generated thermograms which were analyzed using a Pyris Manager Analysis software (TA Instruments, New Castle, DE, USA).

3.3.3 Fourier transform infrared spectroscopy

The presence of additional bands on an FT-IR scan of API-excipient binary mixtures compared to the individual scans of the API and excipients may indicate incompatibility. Therefore, minor changes in DSC thermograms are to be accepted in cases where there are no additional bands on corresponding FT-IR scans [195, 196]. FT-IR was used to give additional information about potential API-excipient incompatibilities. A Spectrum 100 FT-IR ATR Spectrophotometer (Perkin Elmer® Ltd, Port Elizabeth, South Africa) was used to analyze CPH and investigate potential interactions between CPH and excipients. CPH and each excipient were mixed at a 1:1 ratio to make binary mixtures using a mortar and pestle. Before analyzing the powders, each binary

mixture was placed in small amounts onto a diamond crystal, and a force of approximately 90 N was applied. The resolution was 4 cm^{-1}, and the scanning range used for analysis was 4000 – 450 cm^{-1}.

3.4 EXPERIMENTAL

3.4.1 Materials

CPH was purchased from Sigma Aldrich® (St Louis, USA). Tween® 80, SLS, Pluronic F68 and amaranth red dye were purchased from Merck® Laboratories (Wadesville, Gauteng, South Africa). Cholesterol and Span (20, 60 and 80) were purchased from Saarchem-Holpro (Krugersdorp, South Africa). HPLC grade water was initially purified by reverse osmosis using a Millipore® Milli-RO 15 water purification system consisting of Organex-Q, Super-C carbon, and two Ion-X ion-exchange cartridges.

3.4.2 Preparation of CPH loaded niosomes

To produce niosomes by the probe sonication method, different surfactant/surfactant combinations were used. 150 mg CPH was first mixed with 150 mL of water with the help of a magnetic stirrer, after which 1 g cholesterol and 1 g surfactant type were added. The exact compositions of studied batches are presented in **Table 3.1**. The mixture was then subjected to probe sonication (Bandelin®, Berlin, Germany) for 6 min at 60 °C of probe temperature in a pulsatile manner (50 s sonication with 10 s pause) with 30 % amplitude. After probe sonication, niosomes were collected and stored in an amber bottle at 4 °C overnight for physicochemical characterization.

Table 3.1 Composition of different niosome formulations.

Formulation	Surfactant	Cholesterol (g)	Surfactant: Cholesterol ratio	Drug (mg)	Amplitude	Sonication time(mins)
CPH1	SLS: Span60 (1:1)	1	1:1	100	30 %	6
CPH2	Tween® 80: Span 60 (1:1)	1	1:1	100	30 %	6
CPH3	Span 60	1	1:1	100	30 %	6
CPH4	SLS: Tween® 80	1	1:1	100	30 %	6
CPH5	Tween® 80: Span 80	1	1:1	100	30 %	6
CPH6	Span20: Tween® 80	1	1:1	100	30 %	6
CPH7	Span 80	1	1:1	100	30 %	6
CPH8	Pluronic F68: Tween® 80(1:1)	1	1:1	100	30 %	6
CPH9	Span 20	1	1:1	100	30 %	6
CPH10	Pluronic F68	1	1:1	100	30 %	6
CPH11	Tween® 80	1	1:1	100	30 %	6
CPH12	SLS	1	1:1	100	30 %	6
CPH13	Pluronic F68: SLS (1:1)	1	1:1	100	30 %	6
CPH14	Pluronic F68:Span20 (1:1)	1	1:1	100	30 %	6

CPH15	Pluronic F68: Span 60 (1:1)	1	1:1	100	30 %	6
CPH16	SLS: Span20 (1:1)	1	1:1	100	30 %	6
CPH17	SLS: Span 80 (1:1)	1	1:1	100	30 %	6

The vesicle size of the niosomes (z-average), PDI, and Zeta potential were measured for all the formulations using Zetasizer Nano ZS (Malvern Instruments Ltd., UK). The niosomal dispersions (30 µL) were diluted with water up to 10 mL before the measurement to avoid multi scattering phenomenon. All the measurements were performed in triplicates. It should be noted that diluting dispersions of this nature can affect dispersion characteristics.

For determining the entrapment efficiency, the formulations were ultra-centrifuged at 12000 rpm for 30 minutes (Eppendorf, Hamburg, Germany). The supernatant was collected, the pellet at the bottom of the centrifuge tube was washed twice with water. The water was collected, and centrifugation was repeated. Drug concentration in the aqueous solution containing supernatants and water used for washing was determined. The entrapment efficiency for CPH niosomes was calculated using the following equation (**Equation 3.2**):

$$Entrapment\ efficiency = \frac{Qt - Qr}{Qt} \times 100$$

Equation 3.2

Where,

Qt is the amount of drug initially used to prepare the niosomes and

Qr is the amount of drug present in supernatant after centrifugation.

10 µL of the supernatant was then diluted up to 10 mL and analyzed using the HPLC method described in ***Chapter 2***.

The stability of the niosome formulations was determined by storing the niosomal dispersions in sealed 100 mL amber glass stock bottles at 4 °C in a refrigerator. The stored formulations' size, PDI, and Zeta potential values were evaluated at predefined time intervals (0, 1, 2, 3, and 4 weeks after preparation). Besides this, a visual examination of the physical changes on the niosomes was also done.

3.5 RESULTS AND DISCUSSION

3.5.1 Determination of parameters for DOE analysis

3.5.1.1 CPH formulation results

The results of the different CPH in terms of average vesicle size (nm), Zeta potential (mV), and entrapment efficiency are shown in **Table 3.2.** The formulations showed variable average vesicle sizes and Zeta potential. Formulation **CPH4** is most likely to be stable over an extended period compared to the other formulations as Zeta potential > -30 mV causes aggregation of particles over time, this is a minor element of the stabilization. Formulation **CPH4** was able to stay in the large uni-lamellar vesicle (LUV) range for niosomes which is between 100 and 3000 nm. It is to be noted that not all the vesicles produced are in this range. All the formulations showed good entrapment capabilities with an entrapment efficiency of at least 73 %. All results are presented as mean ±SD.

Table 3.2 CPH formulation results.

Formulation	Average vesicle size(nm) ±SD	Zeta potential average(mV) ±SD	Entrapment efficiency average (%) ±SD
CPH1	135.28±1.47	-9.27±0.54	85.21 ±0.16
CPH2	510.00±14.15	-15.60±0.64	90.91±1.94
CPH3	3397.83±403.14	-23.53±0.66	88.84±0.30
CPH4	**110.42±4.84**	**-30.40±1.28**	**90.93±4.60**
CPH5	114.78±3.60	-9.82±1.96	88.94±0.49
CPH6	556.37±15.75	-12.77±0.68	91.50±0.07
CPH7	407.67±11.61	-11.87±2.02	85.09±0.94
CPH8	748.03±200.67	-22.57±2.27	73.42±12.75
CPH9	685.93±49.28	-6.72±0.13	89.25±0.33
CPH10	770.6±179.31	-9.12±0.48	91.14±0.34
CPH11	383.18±115.57	-8.60±0.80	89.88±0.47
CPH12	221.49±15.49	-8.73±0.22	75.28±0.67
CPH13	99.86±1.83	-4.41±0.68	97.47±0.27
CPH14	348.82±11.87	-9.42±0.96	99.91±0.05
CPH15	368.67±92.24	-10.00±0.32	90.24±0.10
CPH16	136.52±2.17	-4.37±0.78	91.53±1.64
CPH17	139.67±47.74	-14.54±12.63	85.94±0.43

Formulation **CPH4** (SLS and Tween® 80 (1:1)) was the chosen formulation as it exhibited good Zeta potential (< -30 mV) and is most likely to be stable over time. Vesicles of Zeta potential > -30 mV tend to aggregate over time due to poor repulsion between the vesicles; this will affect dosing as it can lead to under or overdosing and difficulty in redispersion if required. However, Zeta potential alone is not a measure of stability for dispersions stabilized by non-ionic surfactants. The formulation showed excellent entrapment efficiency and produced niosomes in the LUV range (100 - 3000 nm). The chosen formulation was then exposed to varying levels/amounts of cholesterol, sonication time, and amplitude. **Figure 3.2** shows the structure of LUV.

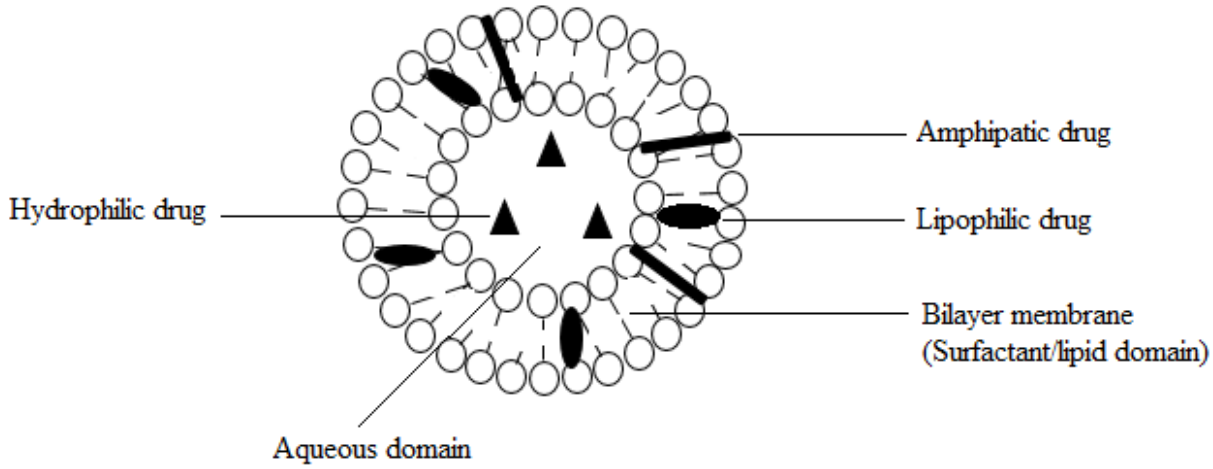

Figure 3.2 LUV structure (Adapted from [197]).

As the HLB value of surfactant increases, the alkyl chain length rises. Therefore, HLB from 14 to 17 is not suitable for niosome formulation. Tween® 80 has an HLB value of 15 and is not suitable for niosome formulation but can be used with specific additives to produce niosomes [197]. SLS, on the other hand is a water-soluble surfactant with an HLB value of 40 and forms o/w emulsions. Surfactants with a high hydrophilic–lipophilic balance (HLB) are likely to be micelle forming surfactants and need additives to achieve suitable molecular geometry and hydrophobicity for bilayer vesicle formation [197]. Membrane additives are substances added to the formulation, in order to stabilize the niosomes. The most common additive found in a niosomal system is cholesterol, which is known to alter the fluidity of the chains in the bilayer [197].

After 4 weeks, the chosen formulation **CPH4** was analyzed again for vesicle size, entrapment efficiency, PDI, and Zeta potential. The results are presented in **Table 3.3**. The formulation showed a decrease in entrapment efficiency, vesicle size, and Zeta potential. The decrease in entrapment efficiency could be attributed to the physical instability of niosomes. Niosomes are chemically stable but can be physically unstable, resulting in the leaking of the entrapped drug and consequently a decrease in vesicle size, further studies are required. Zeta potential is affected by factors like pH of the medium, concentration of additives, and temperature. The small changes in Zeta potential could be attributed to the fact that the dispersion was kept at constant temperature

for 4 weeks (4 °C). Lower temperatures slow down the rate of a reaction. The possible leakage of the drug into the medium could alter the pH of the medium. Changes in pH of the medium, in turn, affect the Zeta potential of niosomal dispersions [197]. The concentration of additives was kept constant throughout and could not significantly affect the Zeta potential.

Table 3.3 Formulation **CPH4** after 4 weeks at 4 °C.

Formulation	Average vesicle size(nm) ±SD	Average entrapment efficiency (%) ±SD	Average PDI ±SD	Average Zeta potential(mV) ±SD
CPH4	93.3±0.68	80.34±0.39	0.28±0.093	-34.54±1.71

3.5.1.2 *Amount of cholesterol*

Figure 3.3 shows the effects of different cholesterol levels used on entrapment efficiency. Irrespective of surfactant type, the higher the cholesterol concentration incorporated into niosomes, the lower the entrapment efficiency attained [197]. This effect was visible in this study as after 1 g of cholesterol, a significant drop in entrapment efficiency was noticeable. Increases in cholesterol concentration increase the rigidity of the bilayer membranes because of cholesterol's rigid structure and characteristic inverted cone shape. According to Agarwal *et al* [198], increases in cholesterol leads to an increase in entrapment efficiency due to the vesicle bilayer width increasing [198]. The opposite was seen in **Figure 3.3**, this is an area for further studies.

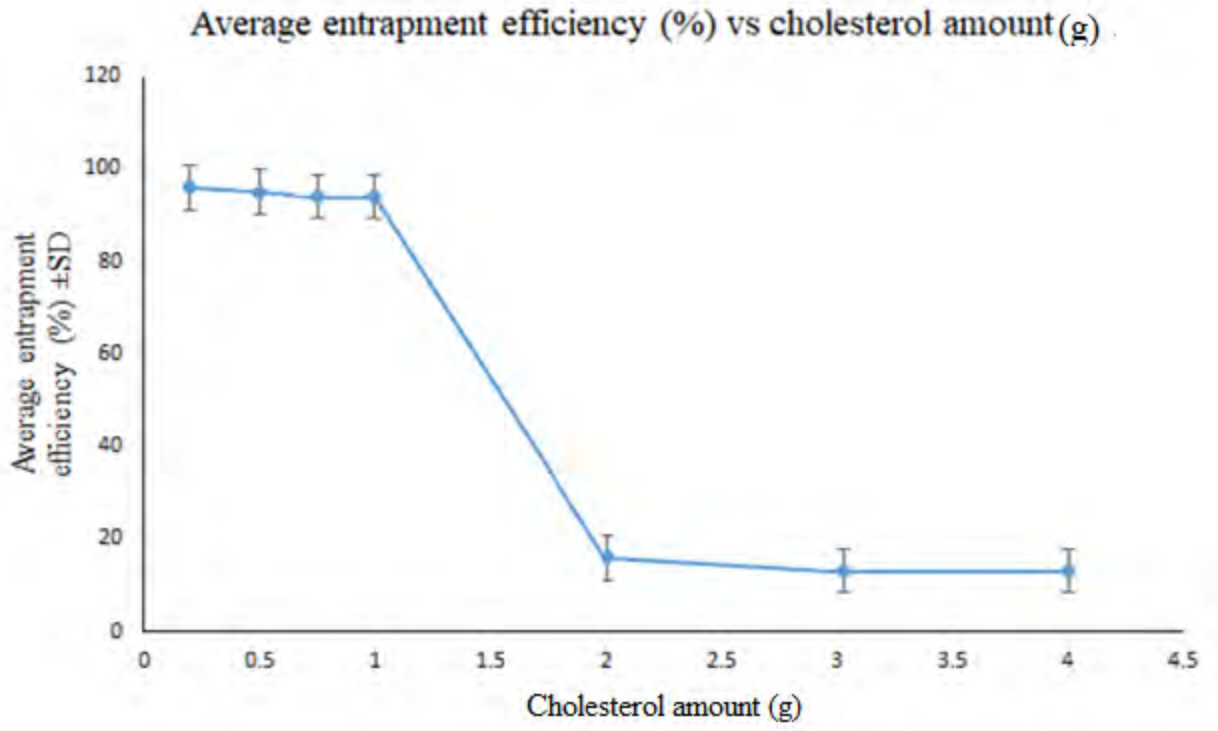

Figure 3.3 Graph shows the effect of cholesterol on entrapment efficiency (n = 3, 5 % RSD).

Cholesterol is one of the main components of niosomes that can influence their physicochemical characteristics and stability [159]. Vesicle size is an essential characteristic of vesicles from the pharmaceutical viewpoint. To study the effect of cholesterol content on niosomal vesicle size, a series of formulations containing seven different cholesterol amounts of between 0.2 and 4 g were prepared, and the results are presented in **Figure 3.4**. As it can be observed, cholesterol was found to have a significant effect on vesicle size. However, the influence of cholesterol percentage on the size of niosomes is markedly dependent on the type of non-ionic surfactant. For Tween® 60 niosomes, an increase in the cholesterol content does not significantly affect the vesicle size, while for the Brij 72 and Span 60 niosomes, increasing the amount of cholesterol causes a significant decrease in the average size of the vesicles [199]. In the case of **CPH4**, as shown in **Figure 3.4**, increasing cholesterol content causes a decrease in vesicle size. This observation may be justified because the addition of cholesterol can enhance the bilayer hydrophobicity, leading to a decrease in the surface free energy and, therefore, a decrease in vesicle size [199-201]. The accuracy of the entrapment efficiency method may have some inaccuracies, further studies are required.

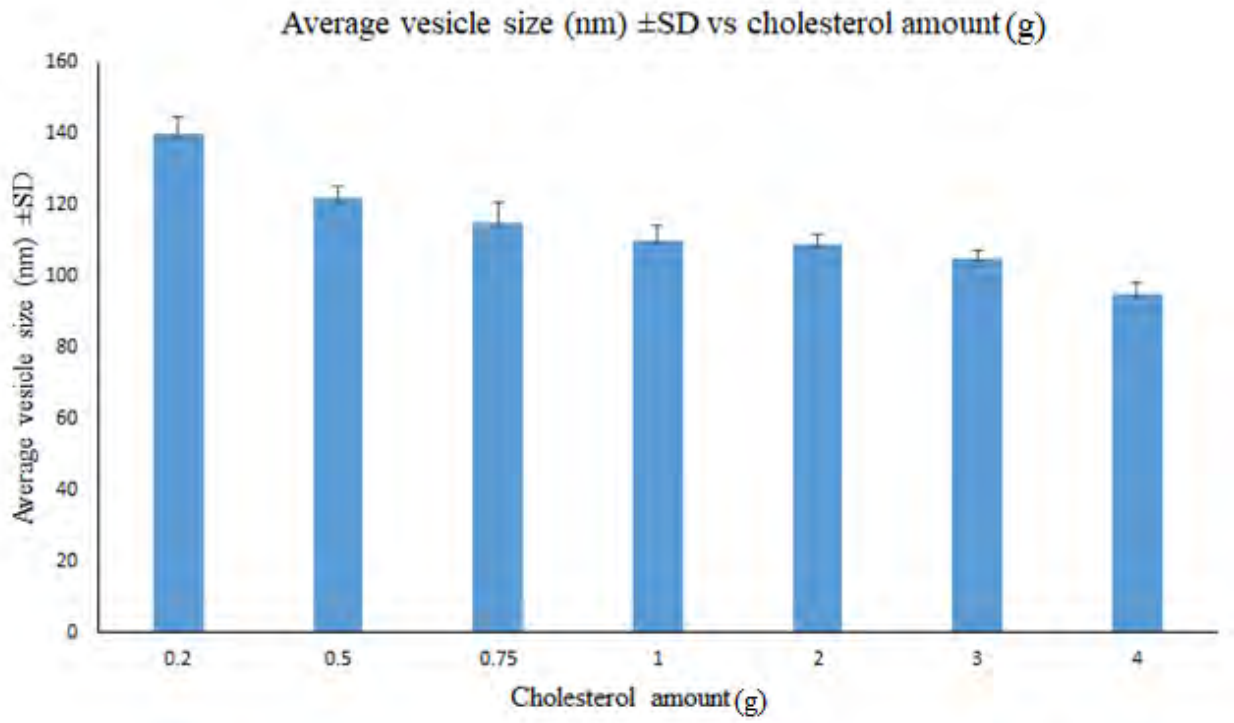

Figure 3.4 Graph showing the effect of cholesterol on average vesicle size.

All the formulations showed good homogeneity (PDI ≤ 0.30), which means that there is a slight difference in the sizes of the vesicles. The zeta potential is a prediction of the stability over time of a formulation. Zeta potential > -30 mV is an indication of potential instability over time although Zeta potential alone is not an indication of instability. Increasing cholesterol content from 1 g to 2 g showed a significant increase in Zeta potential. At 2 g, the niosomes are unlikely to be stable over a long time and would consequently aggregate or fuse. **Table 3.4** shows the effect of cholesterol amount on PDI and Zeta potential.

Table 3.4 Table showing the effect of cholesterol on Zeta potential and PDI.

Surfactant: Cholesterol ratio	Average PDI ±SD	Average Zeta potential (mV) ±SD
1:4	0.17±0.016	-1.6±0.75
1:3	0.17±0.013	-5.22±0.81
1:2	0.25±0.021	-6.72±0.55
1:1	0.22±0.032	-30.40±1.28
1:0.8	0.25±0.036	-31.04±0.91
1:0.5	0.30±0.071	-36.04±1.03
1:0.2	0.23±0.041	-32.01±2.07

3.5.1.3 *Sonication time*

The effect of sonication time on entrapment efficiency, particle size, and PDI value was studied to optimize process variables for the production of niosomes by the probe sonication method. As shown in **Figure 3.5**, when the sonication time was increased from 0 to 2 minutes, the entrapment efficiency increased, while it showed a decline when sonication was continued up to 12 minutes of sonication. Too long sonication time causes larger vesicles to be reformulated, which leads to drug leakage from niosomes and, accordingly, lower entrapment efficiencies. The inverse relationship was observed for vesicle size vs sonication time, as smaller niosomes with low PDI were obtained after sonicating for 12 minutes (**Figure 3.6**). Similar results were observed by Toshimitsu and Florence [202], where the size of resveratrol niosomes was reduced after a prolonged sonication time [201]. The smaller vesicle size on its own could cause the lower entrapment efficiency values because the drug entrapment efficiencies are typically lower with smaller vesicle sizes [202-204].

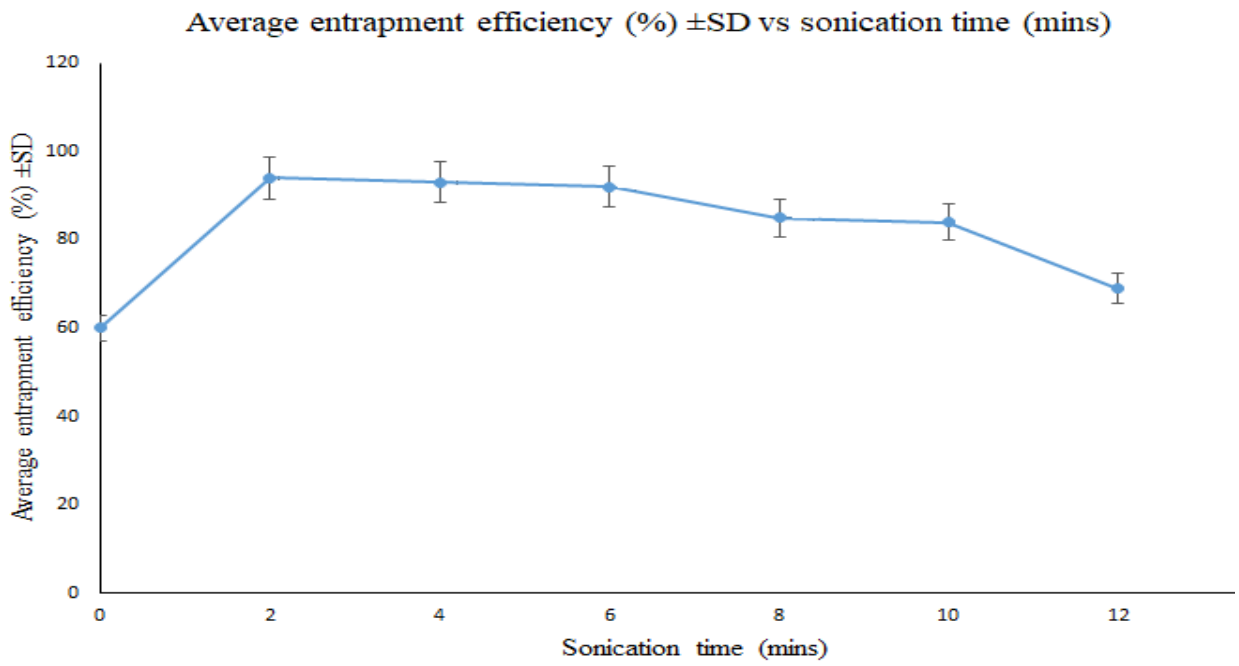

Figure 3.5 Graph showing the effect of sonication time on entrapment efficiency.

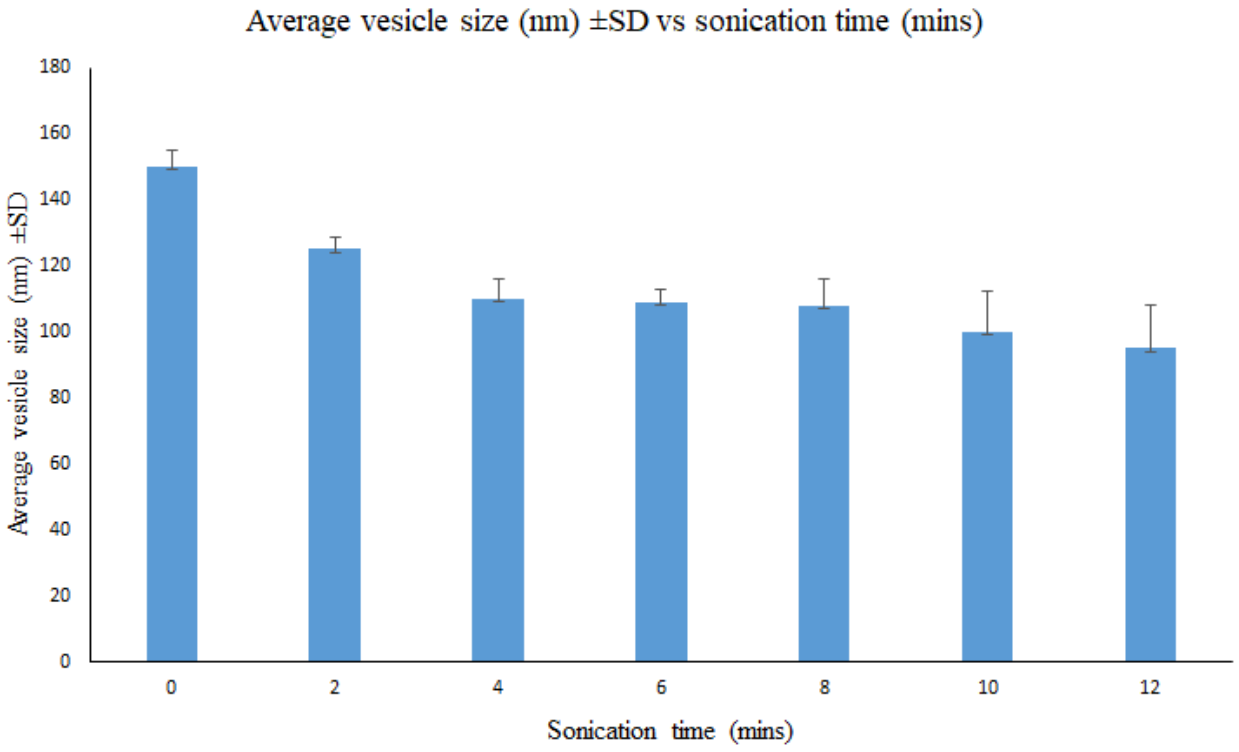

Figure 3.6 Graph showing the effect of sonication time on vesicle size.

All the formulations displayed good Zeta potential and PDI (**Table 3.5**); this shows that they will be stable over 4 weeks, and there is a slight chance of the vesicles aggregating or fusing. All formulations had a PDI of < 0.30. PDI is a measure of the dispersity of the sizes of the vesicles. A PDI as close to 0 as possible is preferred as it proves that the vesicle size is not too dispersed with a wide range of sizes.

Table 3.5 Table showing the effect of sonication time on Zeta potential and PDI.

Sonication time (min)	Average PDI ±SD	Average Zeta potential (mV)±SD
0	0.26±0.038	-12.36±1.72
2	0.26±0.024	-33.33±0.22
4	0.25±0.012	-26.38±0.14
6	0.26±0.071	-30.40±1.28
8	0.30±0.034	-32.99±1.13
10	0.28±0.038	-43.12±1.36
12	0.26±0.028	-30.14±2.15

3.5.1.4 *Amplitude*

The amplitude parameter behaved in the same way as the sonication time (**Figure 3.7**). When the amplitude was increased from 10 to 30 %, the entrapment efficiency increased, whereas it declined when going from > 30 % towards 80 % amplitude. This decline was caused by the higher amplitude damaging the vesicles, which leaked the drug from the niosomes. As the amplitude was increased from 30 to 80 %, the vesicle size and PDI were decreased (**Figure 3.8** and **Table 3.6**). The possible reason for this behaviour was increased energy output of the probe leading to excessive heat generation, which caused the decreased vesicle size and more polydisperse samples. Additionally, possible damage to the vesicles will lead to leakage, thus decreasing the vesicle size, as shown in **Figure 3.8**.

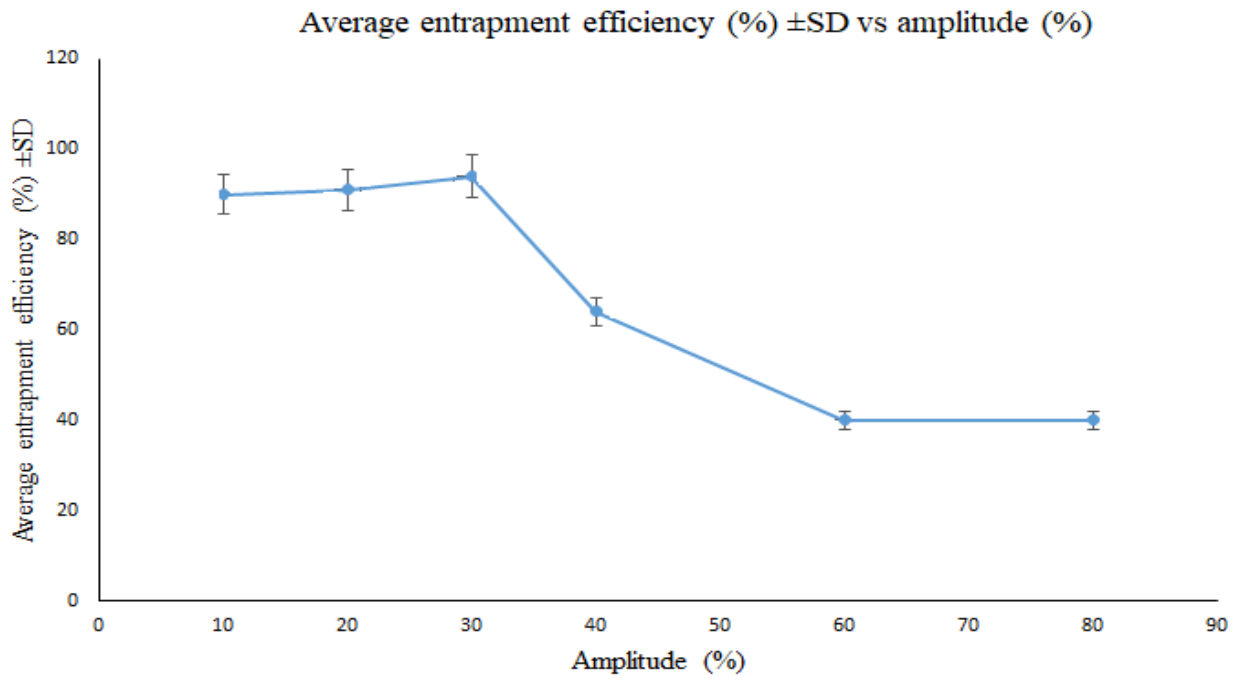

Figure 3.7 Graph showing the effect of amplitude on entrapment efficiency.

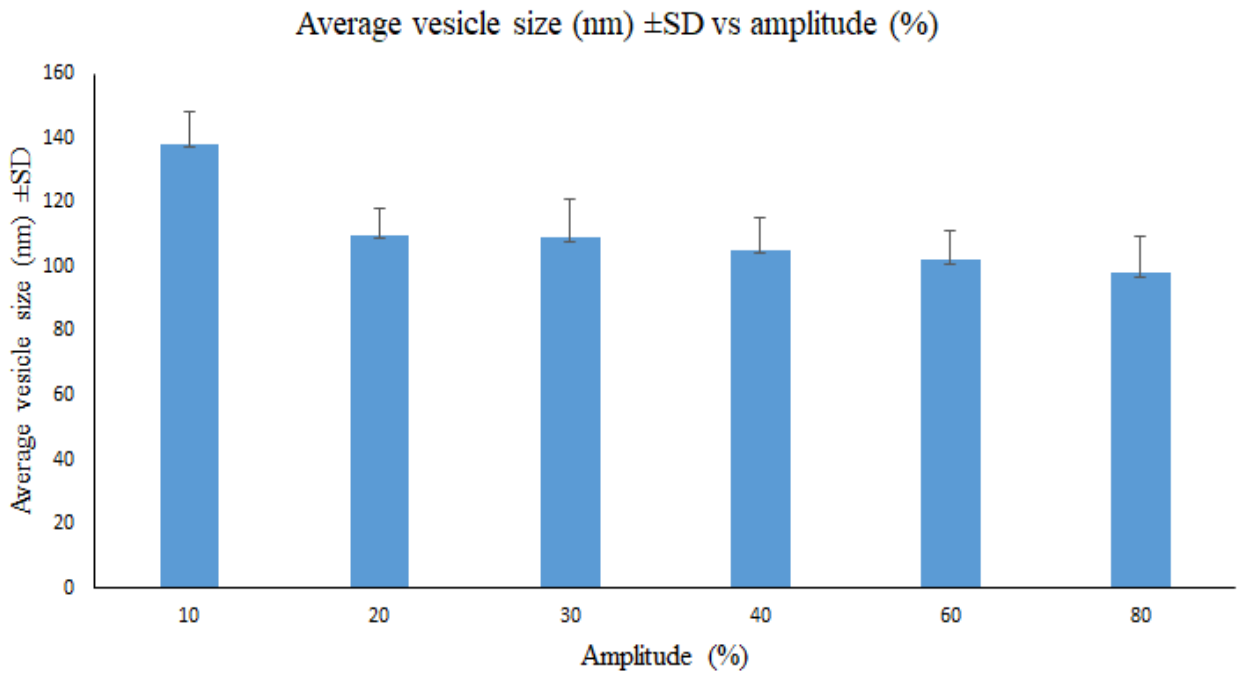

Figure 3.8 Graph showing the effect of amplitude on vesicle size.

Table 3.6 Table showing the effect of amplitude on Zeta potential and PDI.

Amplitude	Average PDI ±SD	Average Zeta potential (mV)±SD
10	0.28±0.040	-38.03±0.91
20	0.26±0.024	-33.63±2.05
30	0.26±0.038	-30.40±1.28
40	0.26±0.013	-12.44±0.36
60	0.23±0.017	-20.00±2.17
80	0.23±0.019	-15.39±3.09

Table 3.7 shows the levels that will be used for DOE analysis in ***Chapter 4***.

Table 3.7 DOE analysis levels to be used in ***Chapter 4*.**

Parameter	Low level	High level
Amount of cholesterol (g)	0.2	1
Sonication time (minutes)	2	10
Amplitude (%)	10	30

3.5.2 Differential scanning calorimetry

The surfactant combination of Tween® 80 and SLS (1:1) was selected, Tween® 80 and SLS (1:1) were used as emulsifiers to provide flexibility to the niosomes. Cholesterol will give rigidity to the niosomal bilayer to produce a bilayer that will make the niosomes less leaky. An endothermic peak indicates that the sample absorbed heat and heat flow to the sample is higher than heat flow to the reference (empty aluminum pan) and occurs in most phase transitions [205]. An exothermic peak indicates that a sample emitted heat and that heat flow is lower in the sample than in the reference. The exothermic process usually occurs for crystallization and compound decomposition [206]. DSC scans for CPH and a 1:1 binary mixture of CPH and the excipients considered are depicted in **Figures 3.9**, **3.10**, **3.11**, and **3.12**.

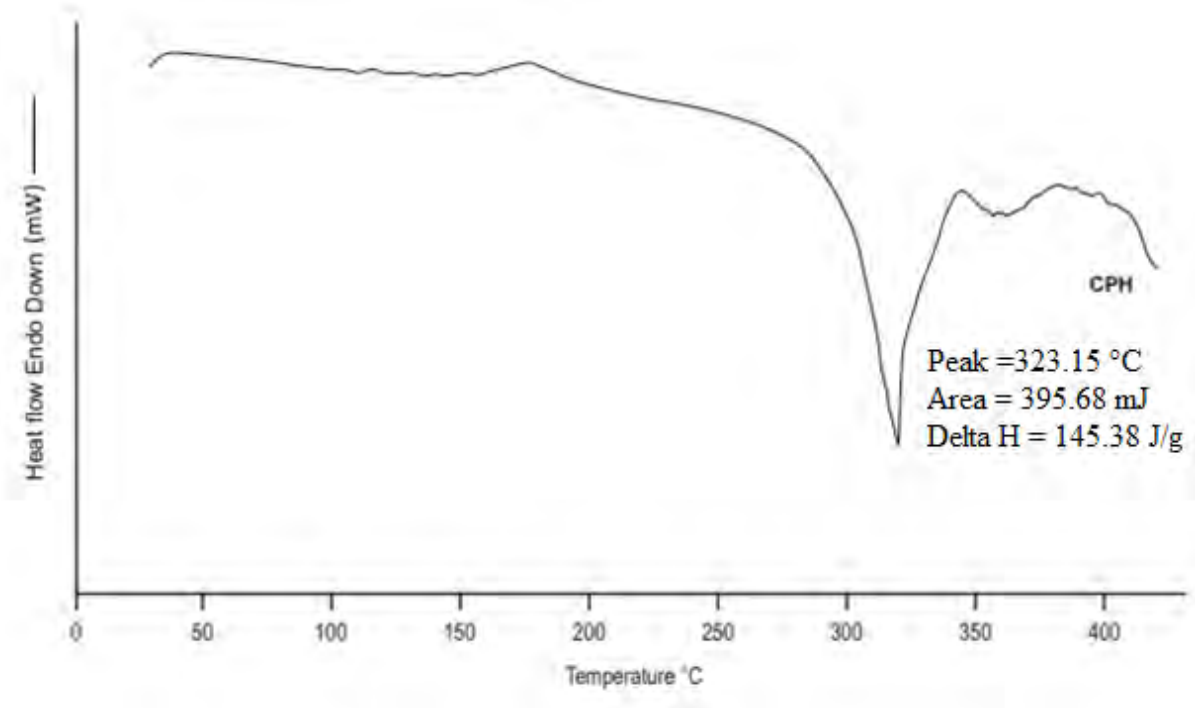

Figure 3.9 CPH DSC chromatogram.

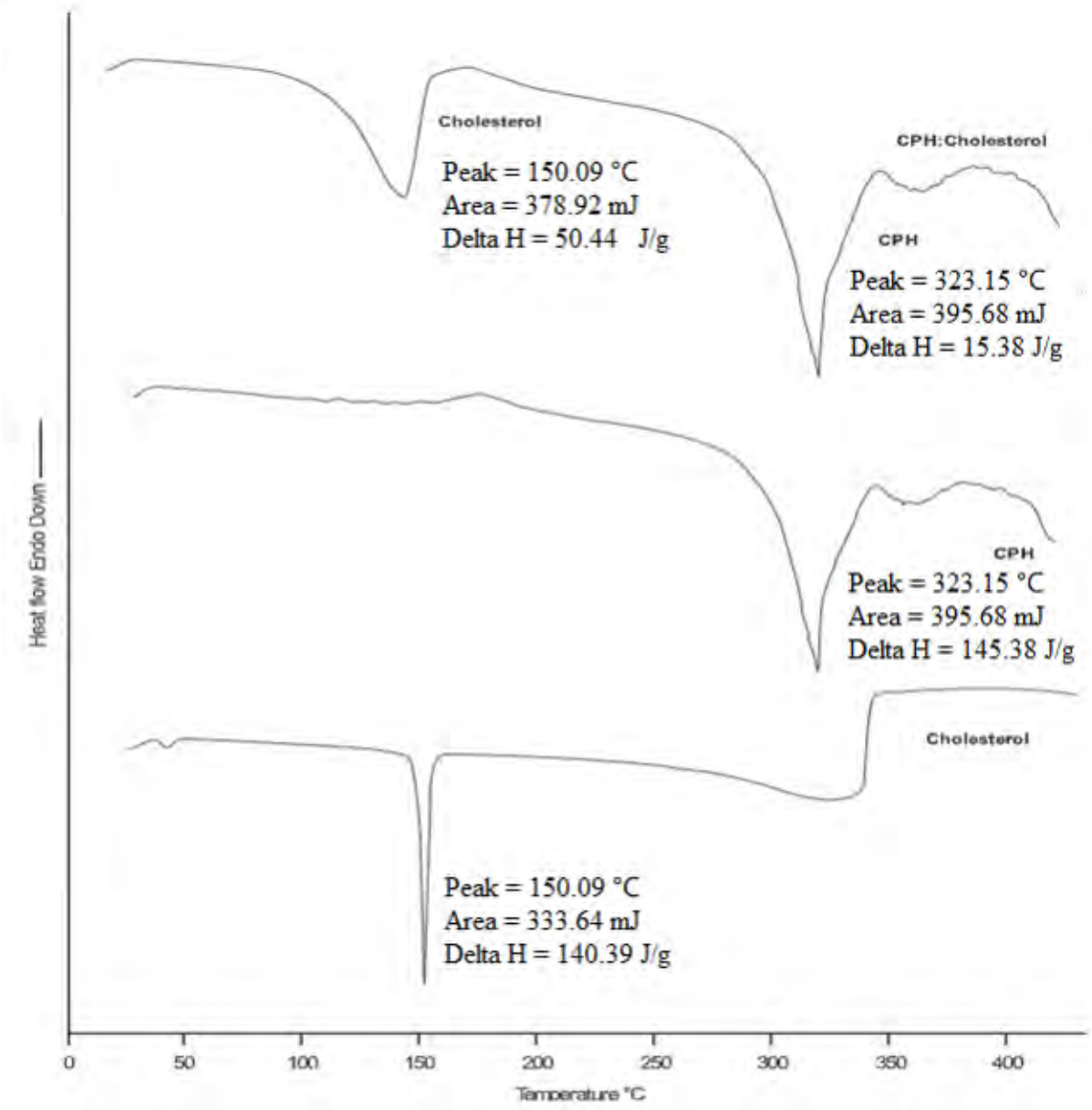

Figure 3.10 CPH and cholesterol (1:1) DSC chromatogram.

The thermograms depicted in **Figure 3.10** reveal sharp melting exothermic peaks at 323.15 ℃ for CPH and CPH: cholesterol (1:1), indicating that CPH was found in both samples. The Delta H of the CPH exothermic peak in the CPH: cholesterol thermogram is lower, which indicates a change in heat flow in CPH in the presence of cholesterol [207]. The peaks at 150.09 ℃ for cholesterol and for CPH: cholesterol confirm no incompatibilities between the CPH and cholesterol.

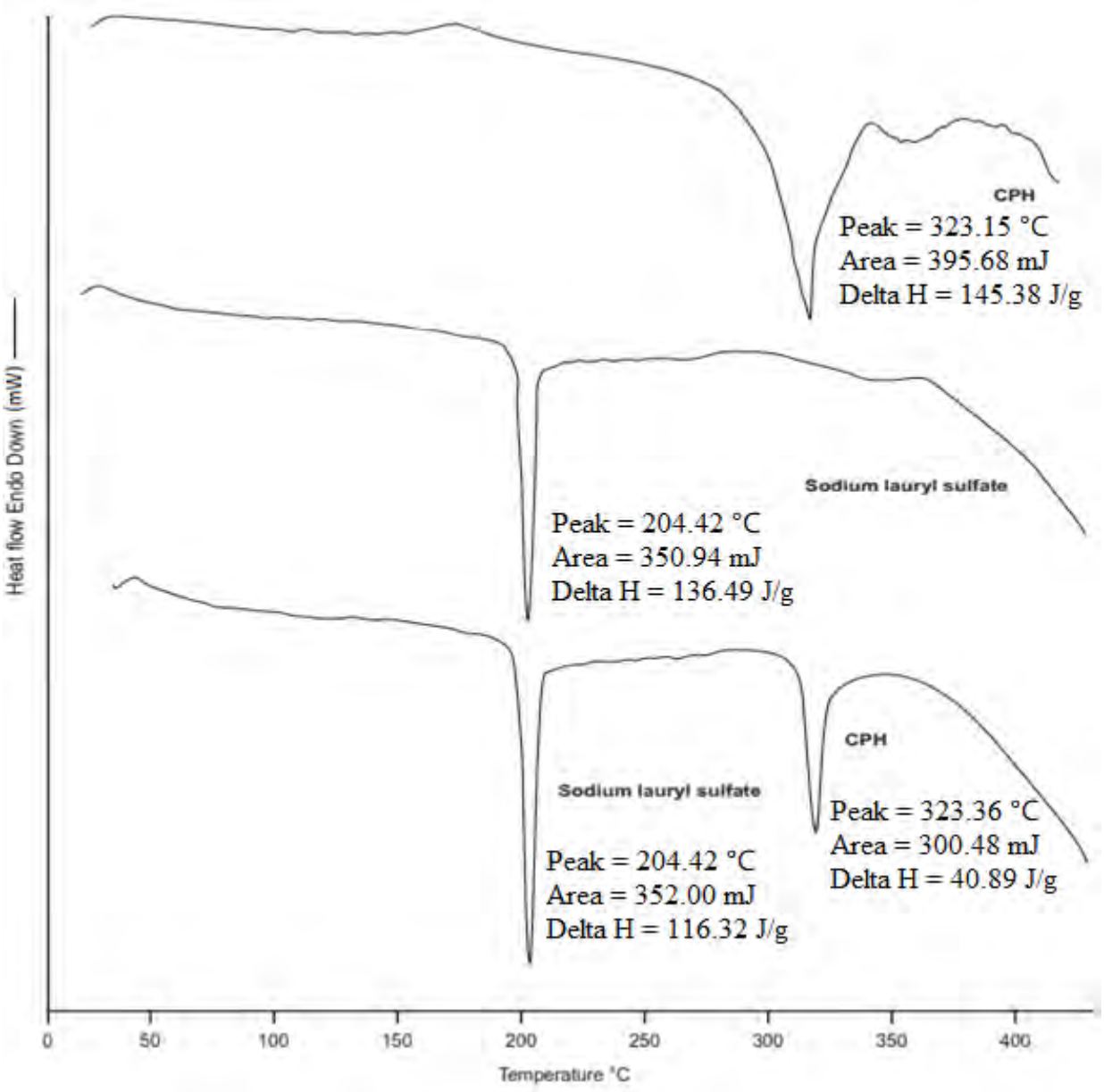

Figure 3.11 CPH: SLS (1:1) DSC chromatogram.

The exothermic peaks at 323.15 ℃ for CPH and 323.36 ℃ in the CPH: SLS binary mixture thermogram reveals the melting point of CPH. The melting point peak of CPH present in the CPH: SLS thermogram had a lower area. The existence of the melting peak of SLS in the binary mixture thermogram indicates that no incompatibilities occurred between the two compounds [208]. In the binary mixture thermogram, there was a slight shift of 0.21 ℃ in the melting peak of CPH. These shifts may be due to the binary analysis of the compounds instead of individual analysis and therefore may not suggest incompatibilities.

Additionally, a change in specific heat often occurs after the sample has gone through a transition such as curing, crystallization, or melting. Sample weight often changes during volatilization or decomposition [208]. The peak at 204.42 °C in the thermogram for SLS proves this statement.

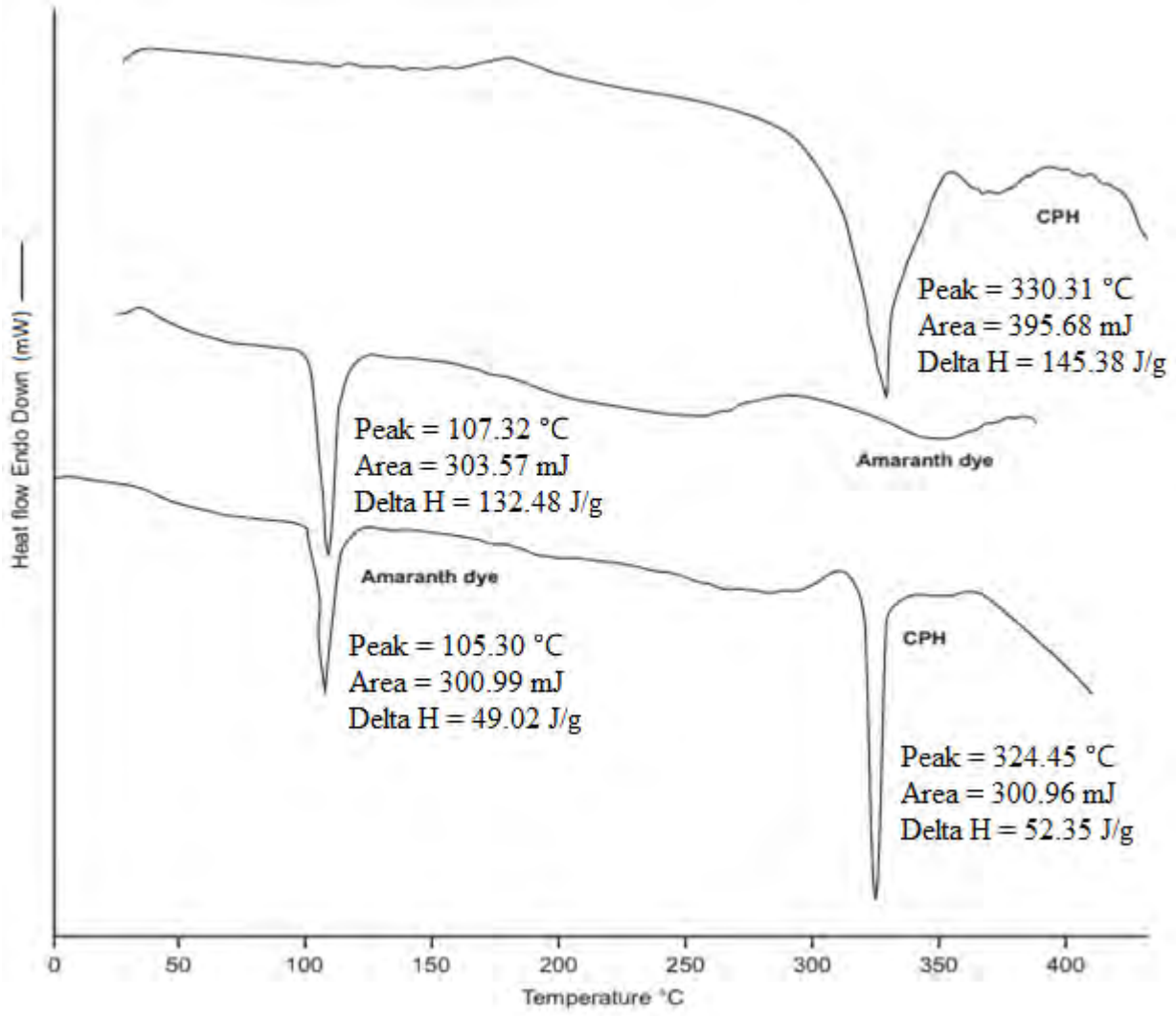

Figure 3.12 CPH: amaranth dye DSC chromatogram.

The melting point peak of CPH also occurs in the thermogram of CPH: Amaranth dye (324.45 °C with an enthalpy of 52.35 J/g) and had a slight shift of 5.86 °C to a lower temperature. The shift may be due to the analysis of CPH in a binary mixture instead of analyzing CPH alone. Baseline shifts are caused by changes in sample weight, heating rate, or the specific heat of the sample [209, 210]. The shift, therefore, does not necessarily indicate incompatibilities between the two compounds.

3.5.3 Fourier transform infrared spectroscopy (FT-IR)

IR spectroscopy possesses a qualitative aspect which is a powerful tool in analyzing compounds. IR spectra may be used to identify different compounds and can detect potential interactions between the API and excipients at a molecular level by the vibration of chemical bonds at specific frequencies. The vibrational frequencies identified for CPH in the conducted IR studies are summarized in **Table 3.8**.

Table 3.8 CPH vibrational frequencies for different functional groups.

Peaks (cm^{-1})	**Groups**	**Peak assignment**
3500-3450	Hydroxyl group	O-H stretching vibration, intermolecular H-bond
3000-2950	Aromatics and cyclic alkenes	Alkene and C-H stretching
1750-1700	CO group of acid	C = O stretching vibration
1650-1600	Quinolones	δ N-H bending vibration
1450-1400	Carbonyl group	υ C-O
1300-1250	Hydroxyl group	δ O-H bending vibration
1050-1000	Fluorine group	C-F stretching

Figure 3.13 shows the FT-IR spectrum of CPH. The absorption and frequency peaks were evaluated for a 1:1 binary mixture of CPH and the excipients used, and no additional peaks were observed. Slight shifts in the frequencies of functional group vibrations were observed in the assessed binary mixtures. These shifts could be caused by hydrogen bonding between API and excipient molecules, as opposed to chemical interactions. The FT-IR spectra of CPH, cholesterol, SLS, Tween® 80, amaranth red, and 1:1 binary mixture of CPH and excipients are depicted in **Figures 3.14, 3.15, 3.16,** and **3.17**.

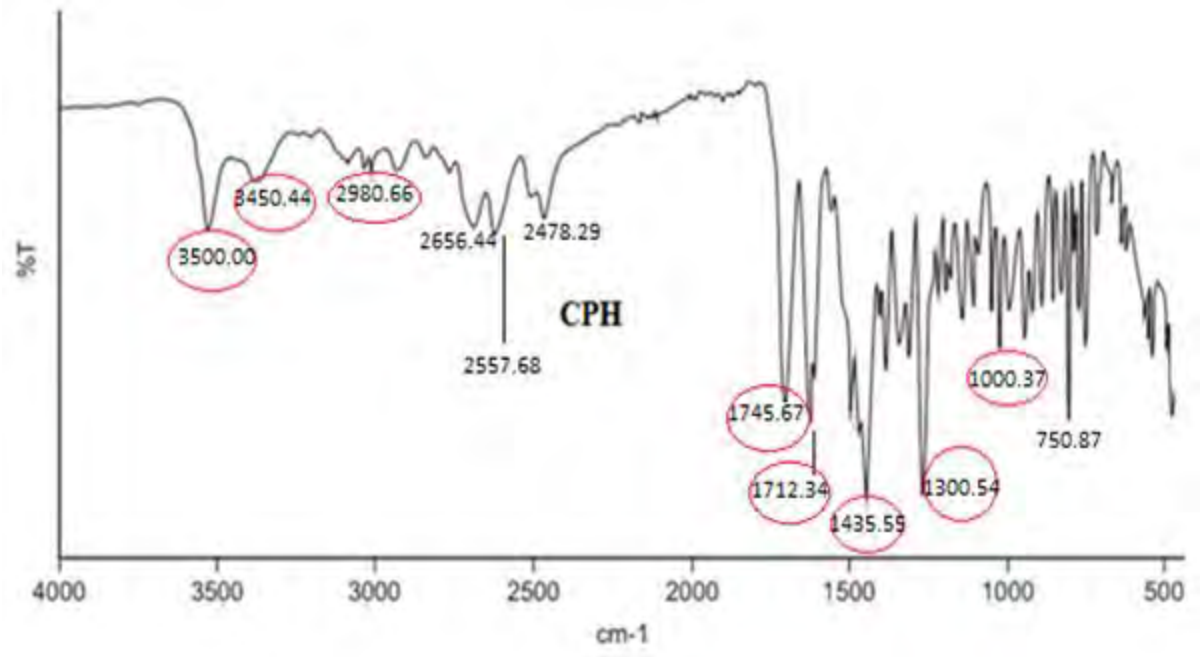

Figure 3.13 CPH FT-IR spectrum.

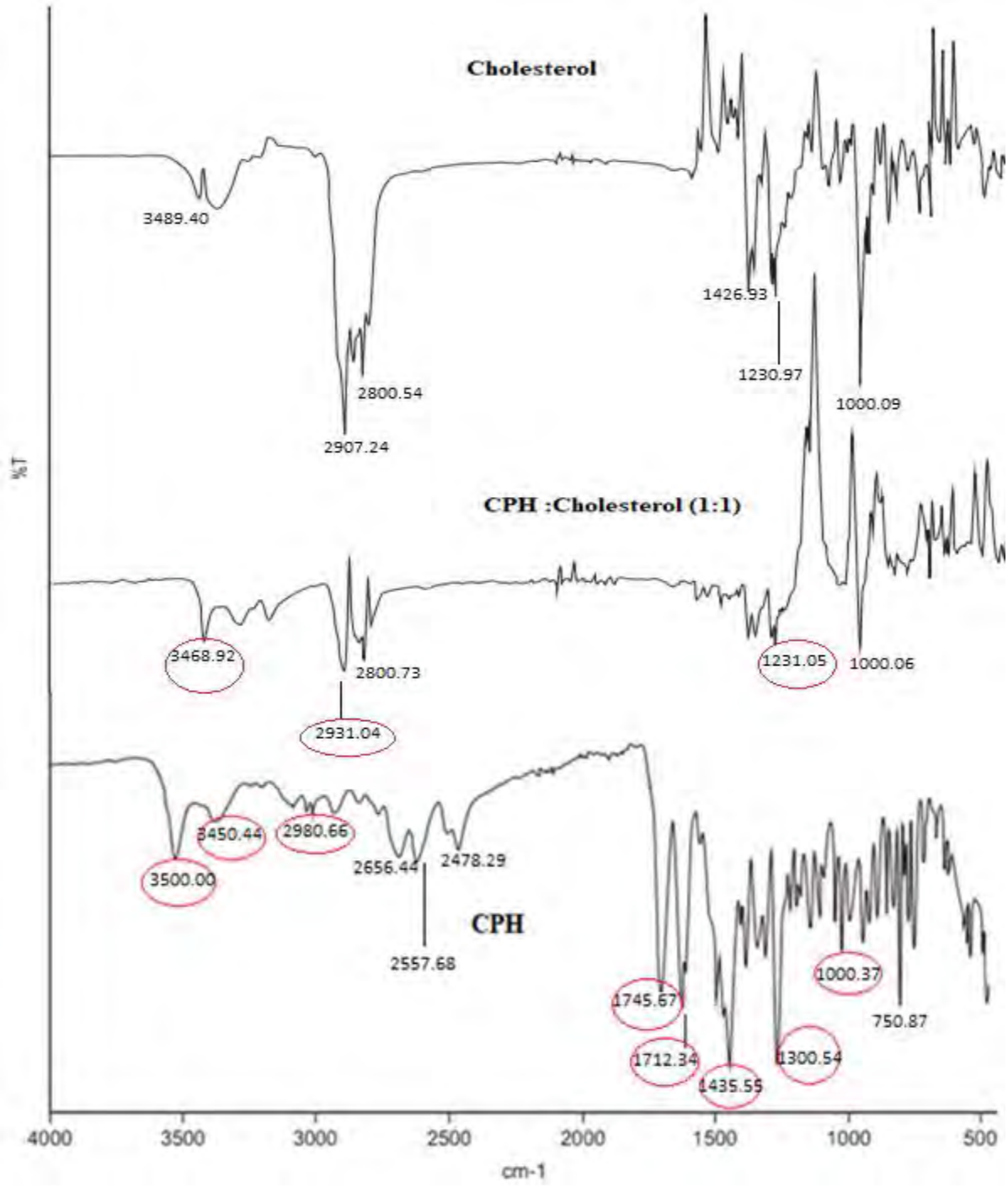

Figure 3.14 CPH and cholesterol (1:1) FT-IR spectrum.

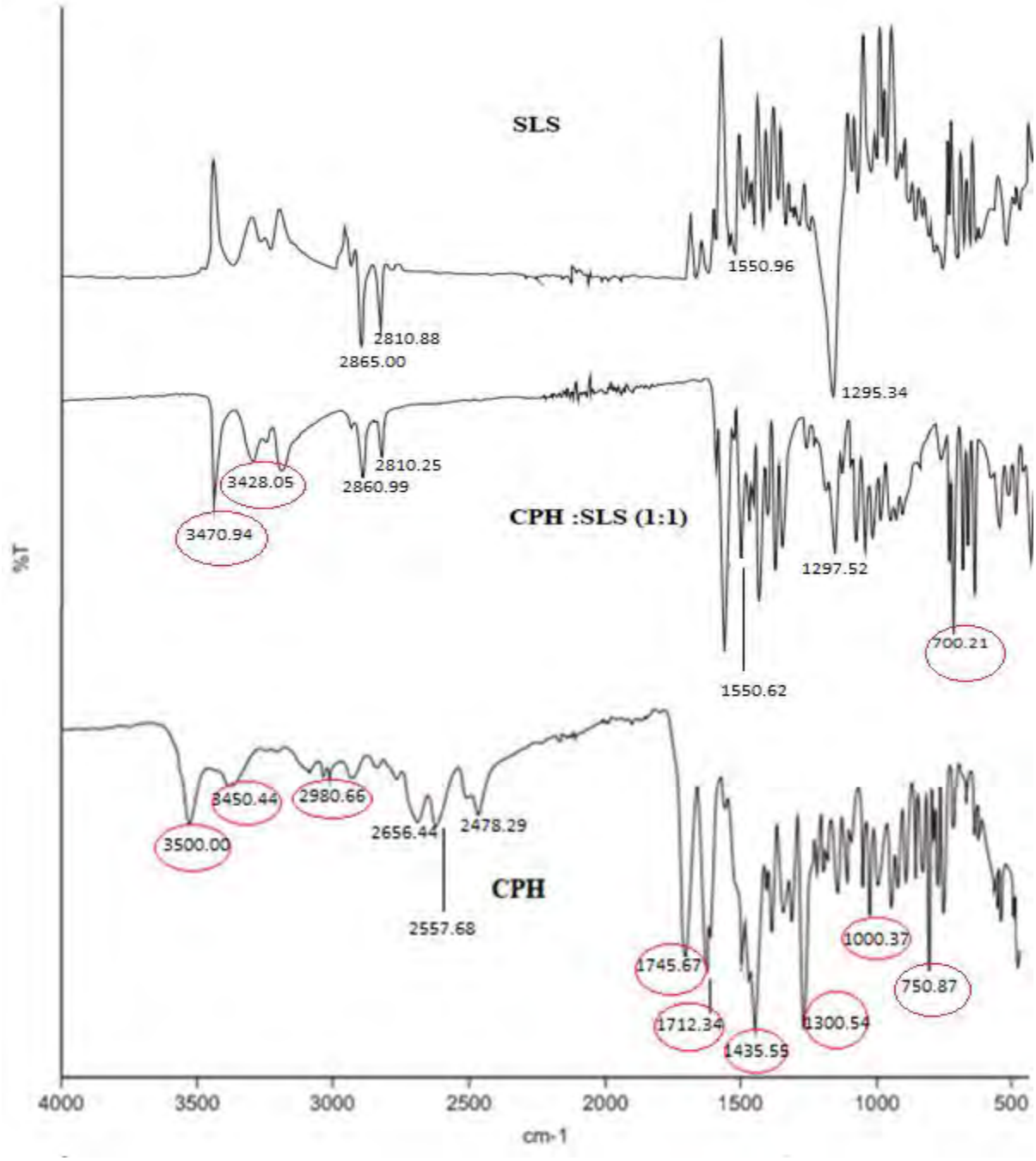

Figure 3.15 CPH and SLS (1:1) FT-IR spectrum.

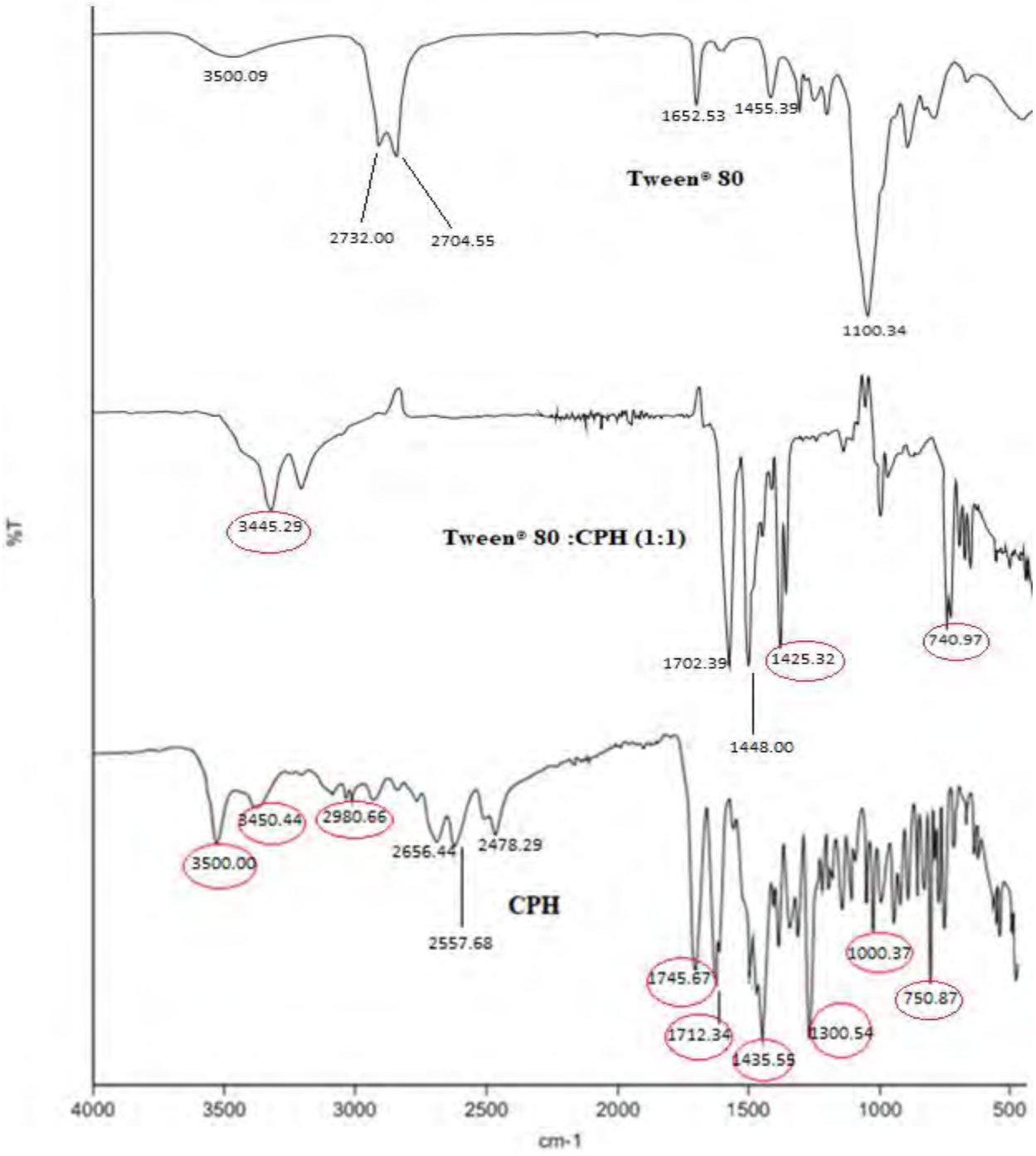

Figure 3.16 CPH and Tween® 80 (1:1) FT-IR spectrum.

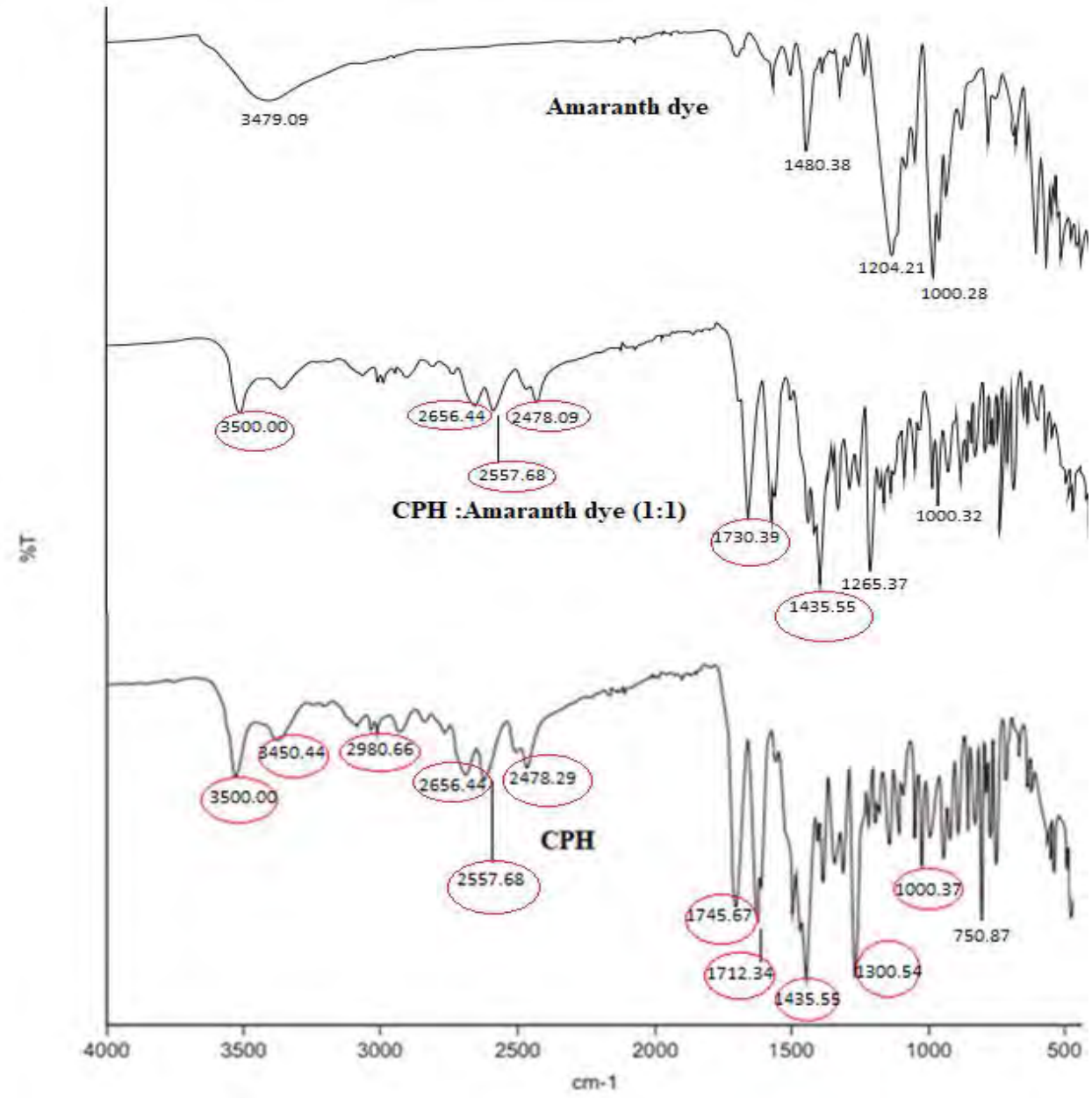

Figure 3.17 CPH and amaranth dye (1:1) FT-IR spectrum.

3.6 CONCLUSIONS

Cholesterol is an integral part of the niosomal bilayer, the addition of cholesterol results in an ordered liquid phase formation which gives rigidity to the bilayer and results in less leaky niosomes. Cholesterol up to the 1 g mark produced niosomes with entrapment efficiency > 80 %, but a very significant change was seen above 1 g of cholesterol. Therefore, for DOE analysis, cholesterol levels will be between 0.2 and 1 g. This range also produces niosomes in the LUV region (100 - 3000 nm). Niosomes between 100 - 300 nm are ideal for transtympanic delivery [211]. It should be kept in mind that the dispersion could also be made up of other vesicles outside this size range.

Sonication time is a measure of the amount of time probe sonicating the niosomal dispersion. Sonication time of 0 minutes produced entrapment efficiency < 70 %; the vesicles were not given enough time and energy to form. For these reasons, there is a significant spike in entrapment efficiency at 2 minutes and a significant drop in entrapment efficiency at 12 minutes sonication time. Additionally, after 10 minutes of sonication time, vesicle size dropped below 100 nm. With all these factors considered, sonication time will be kept between 2 and 10 minutes.

By simple definition, amplitude is a measure of how fast the probe rotates in the niosomal dispersion. These differences in speed and consequently energy affect the physicochemical properties of the niosomes, as shown. A steady increase in entrapment efficiency was visible between 10 and 30 % amplitude. Any further increases beyond 30 % amplitude showed a significant drop in entrapment efficiency and were the case up to the 80 % amplitude mark. Vesicle size stayed within the LUV niosomal range from 10 up to 40 % amplitude, but as observed, a significant drop in entrapment efficiency is seen after the 30 % amplitude mark. Therefore, with all the evidence provided, the low level for amplitude was set at 10 % and the high-level set at 30 % amplitude. The vesicles in these ranges displayed excellent zeta potential and excellent PDI. The vesicles are unlikely to fuse and aggregate over time, and the vesicle sizes will not be polydisperse with different sizes. However, it is worth noting that the dispersion formed could be niosomes but there could be other dispersion types e.g. mixed micelles and solid drug solids. Additionally, further studies are required to assess the accuracy of the method used to determine entrapment efficiency.

The DSC scans of the binary mixtures of CPH: cholesterol, CPH: SLS, and CPH: amaranth dye suggest no API-excipient incompatibilities. The scans show the micellization of CPH in melted surfactant as confirmed by the reduced area of the melting endotherm of CPH in the binary mixture. The FT-IR spectra also confirm the absence of incompatibilities. The DSC scans showed that there are no incompatibilities between CPH and the excipients. The thermograms of the binary mixtures of CPH and the excipients did not indicate any additional peaks, which could be caused by crystallization or decomposition and does not necessarily mean that the two compounds react. FT-IR was used to exclude the possibility of any potential incompatibilities between the compounds. The FT-IR scans of CPH and all the excipients further show no chemical or physical incompatibilities, as shown by the absence of additional bands on the spectrum scan of the binary mixtures. CPH is shown to be compatible with all the excipients; cholesterol, SLS, Tween® 80, and amaranth dye.

In conclusion, all the excipients showed no incompatibility with the chosen drug CPH and are not likely to cause any problems during formulation.

CHAPTER 4

FABRICATION AND CHARACTERIZATION OF CIPROFLOXACIN LOADED NIOSOMES FOR TRANSTYMPANIC DELIVERY

4.1 INTRODUCTION

Novel vesicular drug delivery systems aim to deliver a drug at a rate directed by the body's need during treatment and channel the active entity to the site of action. Vesicular drug delivery systems have improved drug molecules' therapeutic index, solubility, stability, and rapid degradation. Consequently, several systems, e.g., ethosomes, pharmacosomes, bilosomes, sphingosomes, have been developed. Each system presents its own set of benefits and challenges [212].

In the last few years, vesicular systems have been promoted as means of sustained or controlled release of drugs because of certain advantages, for example, lack of toxicity, biodegradation, the capacity of encapsulating both hydrophilic and lipophilic molecules, the capacity of prolonging the existence of the drug in the systemic circulation by encapsulation in vesicular structures, the capacity of targeting the organs and tissues, capacity of reducing drug toxicity, and increasing bioavailability of drugs [213]. The main reason behind the use of vesicles in transtympanic drug delivery is that they have been shown to act as drug carriers to deliver entrapped drug molecules across the stratum corneum because of their composition [7, 214].

As shown in **Figure 4.1**, vesicular carriers used in the transtympanic delivery of drugs can be classified based on the main excipient used, such as lipid-based and polymer-based carrier systems. Lipid-based carriers are further sub-classified into vesicular and non-vesicular lipid carriers. Vesicular lipid carriers include liposomes, niosomes, transfersomes, sphingosomes, aquasomes, and phytosomes, while non-vesicular lipid carriers include lipospheres, solid lipid nanoparticles, nano-lipid constructs, micelles, and dendrimers. Polymer-based carriers include polymeric nanoparticles, microspheres, dendrimers, polymeric micelles, nanocapsules, and nanospheres. Among these delivery carriers, vesicular systems such as liposomes, niosomes, ethosomes and elastic, deformable vesicles provide an alternative for improved skin drug delivery [215].

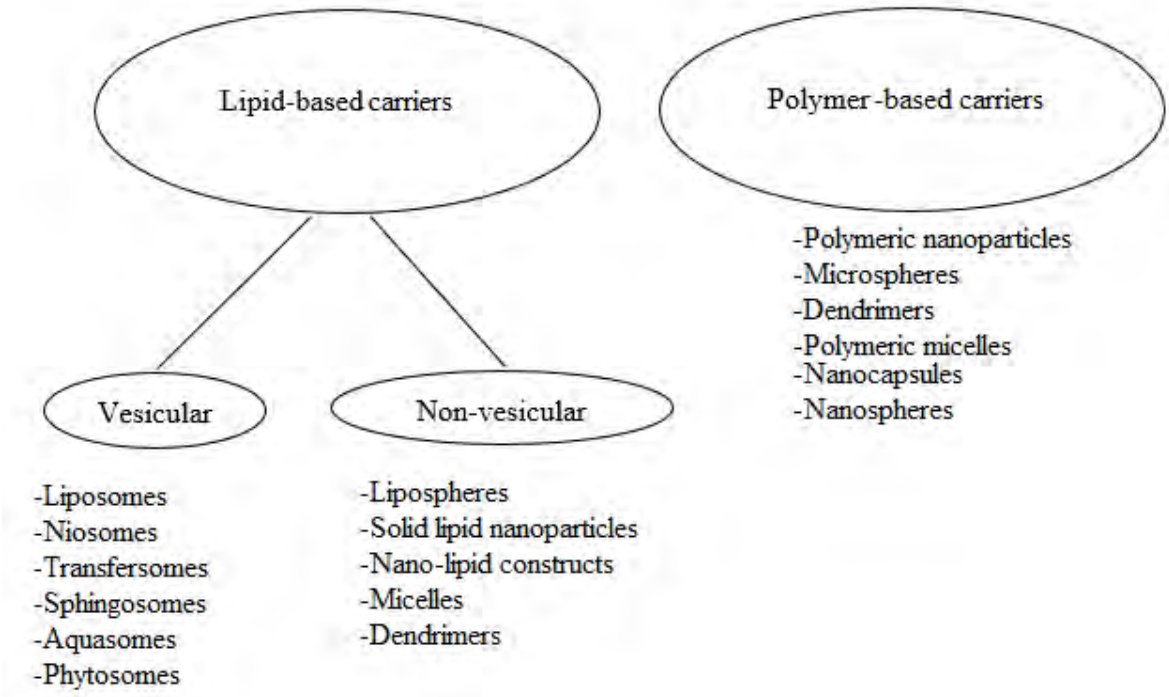

Figure 4.1 Carriers used in the trans tympanic delivery of drugs (Adapted from [215]).

Lipid vesicular systems are a novel means of drug delivery that can improve the bioavailability of encapsulated drugs and provide therapeutic activity in a controlled manner for a prolonged period [216]. The mechanism of action of lipid vesicular carriers involves:

i. Percutaneous penetration of lipid vesicular carrier comprises physiological lipids, and their nano-size range allows the close contact of the carrier with the stratum corneum, thereby increasing the percutaneous penetration (**Figure 4.2**).
ii. Disruption of tympanic membrane lipid structure by a vesicular carrier leading to an increase in fluidity and thus efficient transportation of the carrier and drug across the stratum corneum [216].

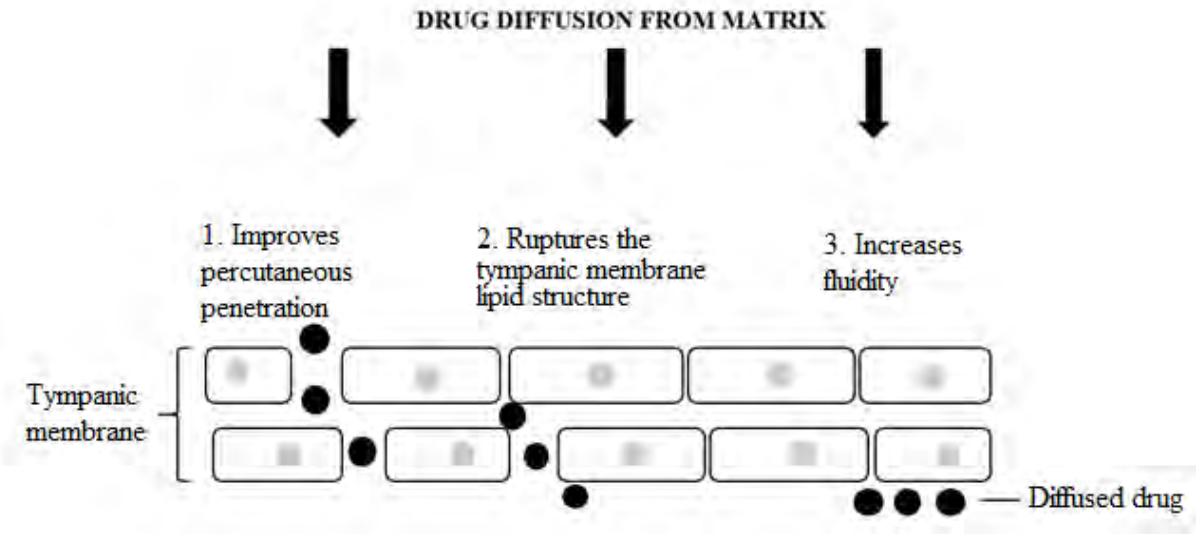

Figure 4.2 Schematic representation of lipid vesicular carriers' method of penetration (Adapted from [216]).

Niosomes are a promising drug carrier with a bilayer structure formed by the association of non-ionic surfactants and cholesterol in an aqueous phase. Niosomes are biodegradable, biocompatible, and non-immunogenic. Niosomes have a long shelf life, exhibit high stability, and enable the delivery of drugs at the target site in a controlled and sustained manner [216]. In recent years, the potential of niosomes as a drug carrier has been extensively studied. Various types of non-ionic surfactants have been reported to form niosomes and enable the entrapment of many drugs with a wide range of solubilities. The composition, size, number of lamellae, and surface charge of niosomes can be varied and optimized to enhance the performance of niosomes for drug delivery [217, 218]. Given the structural similarities between the tympanic membrane and the stratum corneum, there may be improved permeation of drug when used in the tympanic membrane. **Figure 4.3** shows the factors that affect the physical nature of niosomes.

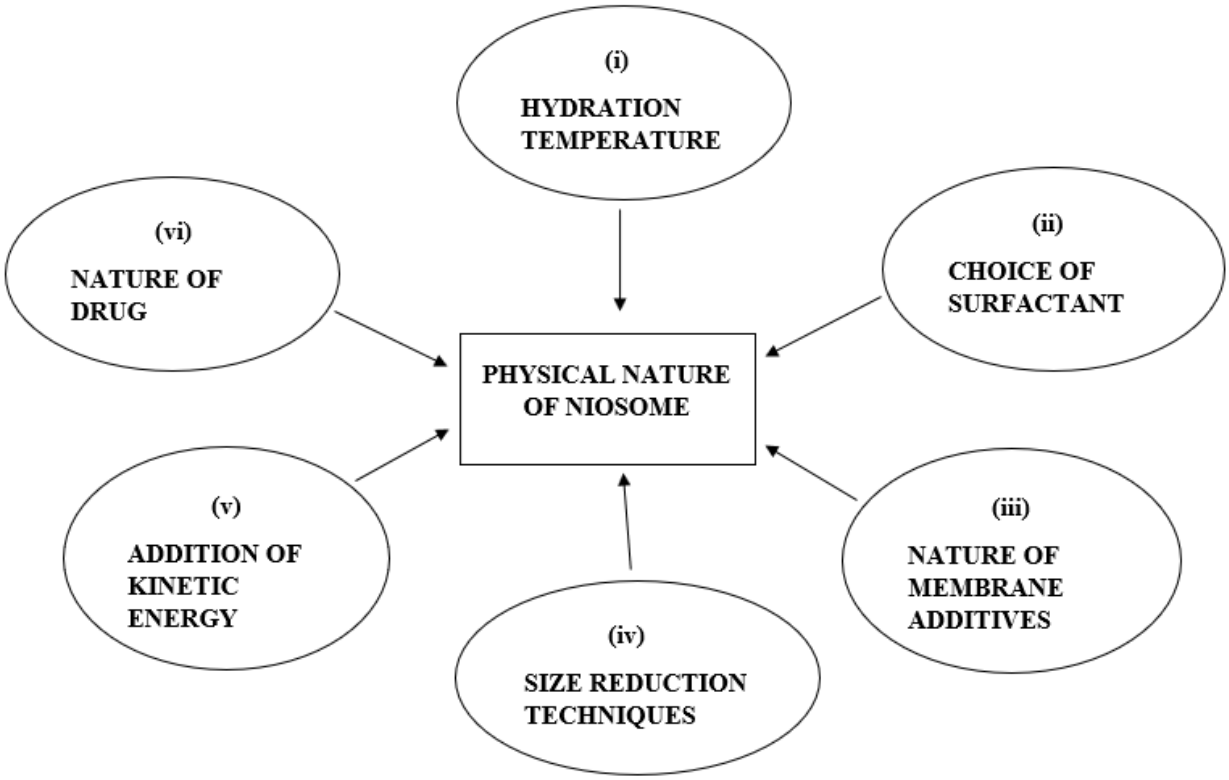

Figure 4.3 Factors that affect niosome physical characteristics [218].

The properties of drugs, other membrane additives, and the method of manufacturing influence the structure and behaviour of niosomes [219, 220]. Hydrophilic drugs are surrounded by the bilayer of amphiphiles, while hydrophobic drugs are entrapped within the bilayer of vesicles [221]. Many non-ionic surfactants are used to produce niosomes, such as polysorbates, alkyl ethers, alkyl amides, and alkyl esters, but in many studies, only a single surfactant is used [222]. However, if a mixture of two or more surfactants is used, stable, small, and monodisperse niosomes can be produced [222-225].

Niosomes act as drug depots in the body, offering drug release in a controlled manner through its bilayer, thus providing sustained release of the enclosed drug. Niosomes also provide targeted drug delivery as it delivers the drug directly to that particular part of the body where the therapeutic effect is needed. Hence it minimizes the dose required to achieve the desired therapeutic effect [226]. Niosomes have been used to deliver antibiotics, β-blockers, Ca^{2+} channel blockers, and xanthine oxidase inhibitors [227]. In the current study, a niosomal formulation will be

manufactured using the probe sonication method in the transtympanic delivery of the antibiotic CPH.

Niosomes can be formulated using different methods, including thin-film rehydration, reverse phase evaporation, and ether injection methods [228, 229]. These methods require the removal of organic solvents, and they are expensive and time-consuming, to overcome these limitations, the probe sonication method has been developed [230]. The probe sonication technique is an eco-friendly green technique with no addition of organic solvents. Besides, it is a low-cost and straightforward technique. In this method, the aqueous phase of the drug is mixed with a surfactant, cholesterol, and other surface additives and subjected to ultra-sonication with a probe [230]. In an earlier study, where probe sonication and thin-film hydration techniques were compared, both the production techniques produced spherical vesicles [230]. However, niosomes produced by the probe sonication technique were smaller with higher monodispersity and showed faster drug release rates than niosomes produced by the traditional technique [230].

The formulation was developed using design of experiment (DOE) and artificial neural network (ANN) approaches. The formulation variables and their limits were defined, determined (***Chapter 3***), and understood in relation to their attributes before using DOE and ANN. The appropriate experimental design space was established upon determining the desired limits, and the experimental matrix was defined. The defined matrix was performed in DOE, and the experimental data was collected for mathematical and statistical evaluation. Furthermore, data was analyzed and fit into a polynomial equation to define the relationship in the data mathematically. In understanding the results, the model fit of the data was evaluated, and in the case of poor fitness, the design space was optimized through data transformation to obtain a better fitting model. The data were used to train, cross-validate, and test ANN to build an architecture that best describes the relationship within data. The network that best described the relationship between the input variables and experimental responses was defined and used to establish optimal values for the analyzed factors.

4.2 EXPERIMENTAL

4.2.1 Materials

CPH was purchased from Sigma Aldrich® (St Louis, USA). Tween® 80, sodium lauryl sulfate (SLS), acetone, and amaranth red dye were purchased from Merck® Laboratories (Wadesville, Gauteng, South Africa). Cholesterol was purchased from Saarchem-Holpro (Krugersdorp, South Africa). HPLC grade water was initially purified by reverse osmosis using a Millipore® Milli-RO 15 water purification system consisting of Organex-Q, Super-C carbon, and two Ion-X ion-exchange cartridges.

4.2.2 Method

CPH loaded niosomes were prepared by the probe sonication method. 150 mg CPH was weighed on a Model AG135 Mettler Toledo® top loading balance (Mettler®, Zurich, Switzerland), and was first mixed with 150 mL of water in a 250 mL beaker with the help of a magnetic stirrer, after which 1 g cholesterol and 1 g of each of the surfactants (SLS and Tween® 80) were added. The mixture was then subjected to probe sonication (Bandelin, Berlin, Germany) for 6 min at 60 °C of probe temperature in a pulsatile manner (50 s sonication with 10 s pause) with 30 % amplitude. After probe sonication, niosomes were collected and stored in a 100 mL amber bottle at 4 °C overnight to mature [230]. **Figure 4.4** shows a schematic of the preparation of the CPH loaded niosomes.

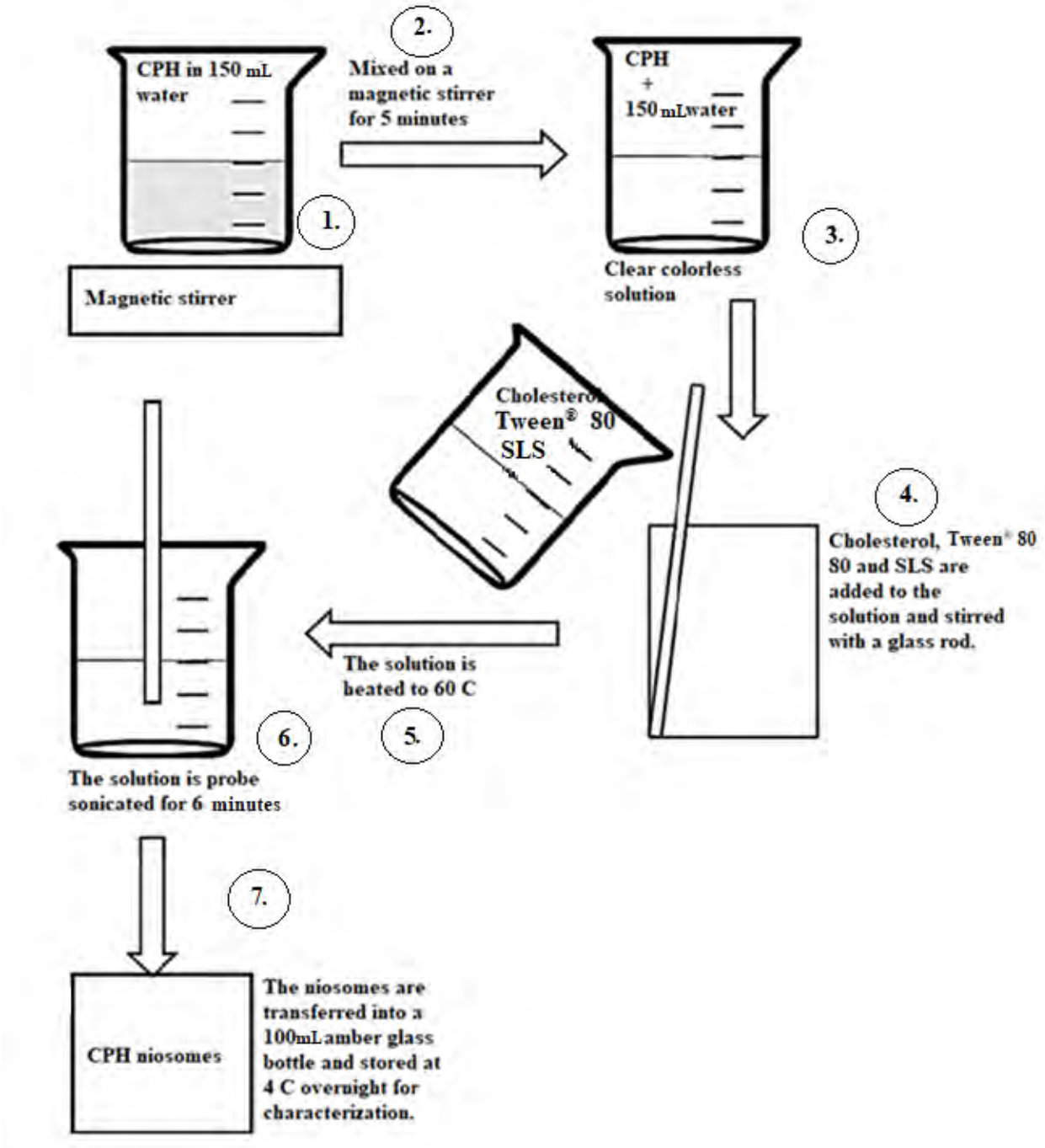

Figure 4.4 Schematic diagram showing the method used to manufacture the niosomes.

4.2.3 pH of niosomal formulation

The pH of the ear canal is approximately 5.0 - 7.8. In addition, the pH of an ear affected by otitis media ranges between 7.0 - 7.8 [231]. The pH of the niosomal formulation was monitored using a model GLP 21 Crison® Instruments pH meter (Barcelona, Catalonia, Spain). The pH meter was calibrated daily using pH 4.00, pH 7.00, and pH 9.21 standard solutions. Following calibration, the pH of each formulation was measured (n = 3) by inserting the pH electrode into 20 mL of the product and observing the pH after 60 seconds, after which the electrode was rinsed with distilled water and dried in between readings to ensure accuracy and to avoid cross-contamination.

4.2.4 Differential light scattering measurement

The size of the niosomes (z-average), PDI, and Zeta potential were measured for all the formulations using Zetasizer Nano ZS (Malvern Instruments Ltd., UK). The niosomal dispersions (30 µL) were diluted with water up to 10 mL before the measurement to avoid multi scattering phenomenon. All the measurements were performed in triplicates.

4.2.5 Entrapment efficiency

To determine the drug entrapment efficiency, the formulations were ultra-centrifuged for 30 minutes at 12000 rpm (Eppendorf, Hamburg, Germany). The supernatant was collected, the pellet at the bottom of the centrifuge tube was washed twice with water. Water was collected, and centrifugation was repeated. Drug concentration in the aqueous solution containing supernatants and water used for washing was determined. The entrapment efficiency of CPH was calculated by the following equation (**Equation 4.1**):

$$Entrapment\ efficiency = \frac{Qt - Qr}{Qt} \times 100$$

Equation 4.1

Where,

Q_t is the amount of drug initially used to prepare niosomes and

Q_r is the amount of drug present in supernatant after centrifugation.

10 µL of the supernatant was then diluted up to 10 mL and analyzed using the HPLC method described in ***Chapter 2***.

4.2.6 Drug release

The aim of conducting *in-vitro* release studies was to understand how the niosomes will behave in drug release when introduced into the biological system. The second aim of conducting *in-vitro* release studies was to compare the release of API from the niosomal formulation with formulations from different batches of the same formulation.

4.2.6.1 *Dissolution medium*

The dissolution medium used for the *in-vitro* drug release studies was a phosphate buffer solution of pH 7.8 to mimic the conditions in the ear canal. The dissolution medium was phosphate buffer saline system (PBS) prepared by transferring 5.09 g disodium hydrogen phosphate, 5.00 g sodium dihydrogen phosphate, and 16.45g sodium chloride into a 2000 mL A-grade volumetric flask and making up to volume with HPLC grade water. The pH of the PBS was adjusted to a pH of 7.8 using a 0.1 M solution of NaOH. After preparation, the dissolution medium was degassed using vacuum filtration with an Eyela® Aspirator-degasser A-2S vacuum pump (Bunkyo-Ku, Tokyo, Japan). The dissolution medium, under vacuum, was filtered using a 0.45 µm Millipore® Corporation HVLP Durapore membrane filter (Bedford, USA) to prevent the formation of air bubbles during the dissolution study. The dissolution medium was prepared daily and was stored in a 1000 mL Schott Duran® laboratory glass bottle before use.

4.2.6.2 *Dialysis bag technique*

There are no standard methods for studying drug release from niosomes *in-vitro* studies [231-234]. The proposed methods are based on separating the dissolved fraction (released drug) from the undissolved fraction (niosomal drug) [232]. The most common methods applied to niosomes are filtration, ultracentrifugation, solid-phase extraction, and dialysis-based methods [232]. The dialysis-based methods utilize the drug's diffusion across barriers to separate niosomal drugs from released drugs [233]. The niosomal formulation is placed in the donor compartment, which is separated from the acceptor compartment by a barrier that can exhibit low retention (*e.g.*, dialysis barrier) or high retention (*e.g.*, biomimetic, biologic barrier) to drug permeation [232]. The disadvantages regarding the dialysis-based methods are related to violation of sink conditions and the fact that the drug released from niosomes needs to cross an additional barrier before being quantified [232 - 235]. On the other hand, dialysis-based methods are convenient, cost-effective, and straightforward.

The *in-vitro* release of CPH was assessed using the dialysis bag diffusion technique as reported by Ross [236]. Dialysis is a technique based on the diffusion of small solutes from a concentrated solution to a lower-concentration solution of this solute through a semi-permeable membrane until equilibrium is reached and is widely used in studies of *in-vitro* drug release studies [236]. The sample and the dissolution medium are placed on opposite sides of the membrane, and the sample molecules smaller than the membrane pores freely pass through the membrane through diffusion [237]. A dialysis membrane is, therefore, a semi-permeable film consisting of various-sized pores [237]. The rate of dialysis is directly proportional to the temperature and surface area of the membrane and is inversely proportional to membrane thickness [237].

The dialysis bag technique has been used in the *in-vitro* release studies of etodolac topical niosomal gel [238], cyclosporine niosomes for prolonged delivery [239], and rifampicin niosomes [240].

A Himedia® dialysis tubing cellulose membrane bag (12000 –140000 Da molecular mass cut off) (Mumbai, India) was sealed on one end using a thread. Approximately 5 mL of the niosomal formulation equivalent to 3.3 mg of CPH was transferred into the sealed dialysis bag using an Eppendorf® Research 100 - 1000 µL micropipette. The dialysis bag was sealed on the opposite end and was then placed into a 15 mL PBS solution maintained at 37 °C in a 25 mL glass tube agitated at 200 rpm by a magnetic stirrer. The dialysis bag's glass tube was placed on a hotplate stirrer and was stirred at 200 rpm. The release of CPH was monitored over 12 hours, and samples were removed at 0, 1, 2, 4, 6, 8, 10, and 12 hours to develop the drug release profile. Approximately 1 mL aliquots were withdrawn from the glass tube at each time point using an Eppendorf® Research 100 - 1000 µL micropipette, and an equal volume of fresh buffer at the same temperature was immediately replaced maintain a constant release volume.

The aliquot and a 1 mL aliquot of 500 µg/mL CBZ solutions were transferred into a 10 mL volumetric flask. The solution was made up to 10 mL with methanol. The final solution was then transferred into a 2 mL amber vial and analyzed using the validated RP-HPLC method (***Chapter 2***).

4.2.7 Mathematical modelling and comparison of *in-vitro* release profiles

The mechanism of drug release-rate kinetics was analyzed by plotting the results of the *in-vitro* release profiles in various kinetic models, such as zero-order, first-order, Higuchi, and Korsmeyer-Peppas. Mathematical modeling increases understanding of the release mechanisms and, in turn, helps to reduce the number of experiments required to optimize the formulation. The mathematical models used in this study are described as follows.

4.2.7.1 Zero-order model

Zero-order release kinetics describe systems where the drug release rate is constant over a period of time [241]. The equation for zero-order release is shown in **Equation 4.2**.

$$Q_t = Q_0 + K_0 t$$

Equation 4.2

Where,

Q_t = cumulative amount of drug released at time t,

Q_0 = initial amount of drug,

K = release kinetic constant, and

t = time at which the drug release is calculated or measured.

The cumulative % CPH release data were fitted to the zero-order model, goodness of fit was evaluated using the R^2 value, and the release rate constant (K) was also evaluated.

4.2.7.2 First-order model

Typically utilized to describe the adsorption and elimination of certain drugs, the first-order model is derived from first-order release kinetics, which states that the change in concentration with respect to change in time is dependent only on concentration. In typical first-order release kinetics, the drug release rate depends on its concentration [242]. The first-order release equation can be explained as shown in **Equation 4.3**.

$$\ln C = \ln C_0 - Kt$$

Equation 4.3

Where,

C = concentration at time, t,

C_0 = the initial concentration of API,

t = time, and

K = first-order rate constant with units, hr^{-1}.

The cumulative % CPH release data were fitted to the first-order model, and goodness of fit was evaluated using the R^2 value, and the release rate constant (K) was also evaluated.

4.2.7.3 *Korsmeyer-Peppas model*

The Korsmeyer-Peppas model has previously been successfully used to describe the drug release [243]. This study's experimental data from the dialysis studies were fitted to **Equation 4.4** (named the Korsmeyer-Peppas equation).

$$\frac{M_t}{M\infty} = Kt^n$$

Equation 4.4

Where,

$\frac{M_t}{M\infty}$ = the fraction of the API released at time, t.

K = the dissolution constant with units, $\mu g/cm^2/hr^n$, and

n = the release exponent.

The release constant K provides information on the drug formulation, such as structural characteristics of the nanocarriers primarily, whereas n is essential since it is related to the drug release mechanism (*i.e.*, Fickian diffusion or non-Fickian diffusion). In the case of niosomes and assuming sink conditions, the flux of the drug (j) through a low retention barrier (*e.g.*, regenerated cellulose) of a constant thickness (x) can be described by **Equation 4.5** (simplified Fick's first law) [244, 245].

$$j = D\frac{(C_d^0 - C_a)}{x}$$

Equation 4.5

Where,

j = flux of the drug through a low retention barrier

x = barrier thickness

C^0_d = freely dissolved unentrapped drug concentration outside niosomes in the donor compartment,

C_a = the acceptor drug concentration, and

D = diffusion coefficient.

According to this model, the net flux of drugs through the barrier results from two diffusion mechanisms. One is the diffusion of drug molecules from the donor compartment to the acceptor compartment (experimentally measured *K*), the second is the diffusion through the phospholipid bilayer of niosomes dependent on the niosomal release rate [246].

The Korsmeyer-Peppas model was used to assess the kinetics of CPH release from experimental formulations.

4.2.7.4 *Hixson-Crowell model*

The Hixson-Crowell cube root law describes the release from systems with a change in surface area and diameter of particles or tablets. Hence, particles of regular area are proportional to the cube root of its volume [247]. Hixson-Crowell established a relationship between drug release and time from the above concept, as shown in **Equation 4.6**.

$$W_0^{1/3} - W_t^{1/3} = kt$$

Equation 4.6

Where,

W_0 = the initial amount of drug in the pharmaceutical dosage form

W_t = the remaining amount of drug in the pharmaceutical dosage form at time t

KHC = the Hixson-Crowell constant describing surface volume relation.

The CPH release data fitted the Hixson-Crowell model using the R^2 value and the release rate constant (K).

4.2.7.5 *Higuchi model*

The Higuchi model is a kinetic equation used chiefly to model controlled API release from non-eroding matrices [248, 249]. The model is based on the hypothesis that the initial concentration in the dosage form is greater than the solubility of the API in the dissolution medium [249]. It is also based on the hypothesis that one-dimensional dissolution/diffusion of the compound occurs from the system where the thickness of the formulation is larger than that of the dimension. This model represents API release which is diffusion-controlled only. A simplified mathematical expression of the model is shown in **Equation 4.7** [249]. The relationship described by the model is valid until the API is completely depleted in the dosage form.

$$Q = K_H \, x \, t^{1/2}$$

Equation 4.7

Where,

Q = amount of API release per unit area at time,

$t^{1/2}$= square root of time, and

K_H = Higuchi dissolution constant with units, μg/ cm^2/ $hr^{1/2}$

The cumulative % CPH release data were fitted to the Higuchi model, and the goodness of fit was evaluated. A linear relationship indicates that the release of CPH from the dosage form is controlled by diffusion using the R^2 value and the release rate constant (K).

4.2.8 Data analysis and statistics

Data are expressed as mean ±SD. Analysis of variation (ANOVA) was used to evaluate mean values of size of niosomes and entrapment efficiency of niosomal preparations. ANOVA was conducted at 95 % confidence interval (CI) by Design Expert® Version 7.0.1 (Stat-Ease Inc., Minneapolis USA) software. The significance was defined at p-values < 0.05.

4.3 RESULTS AND DISCUSSION

4.3.1 Formulation development and optimization using BBD

The niosomal formulation was optimized using BBD DOE, where the amount of cholesterol, sonication time, and amplitude were the varied/input variables. The dependent/output variables were vesicle size, Zeta potential, entrapment efficiency, and PDI. BBD was used to produce a niosomal formulation with optimal vesicle size, PDI, entrapment efficiency, and Zeta potential. The BBD model was generated by transferring the low and high values into the Design Expert® software. The generated BBD consisted of 17 experiments with 5 center point replicates, as summarized in **Table 4.1**.

Table 4.1 Randomized experimental runs to determine the effect of sonication time, cholesterol, and amplitude on the niosomal formulation.

SD	Run	Sonication time(mins)	Cholesterol (g)	Amplitude (%)
14	1	6	1	30
2	2	10	1	20
5	3	6	0.6	20
9	4	6	0.6	20
8	5	2	1	20
3	6	10	0.6	10
1	7	2	0.6	10
7	8	6	0.6	20
16	9	2	0.6	30
15	10	6	1	10
11	11	6	0.6	20
13	12	10	0.2	20
10	13	6	0.6	20
6	14	10	0.6	30
12	15	6	0.2	30
17	16	6	0.2	10
4	17	2	0.2	20

The variables sonication time, amount of cholesterol and amplitude levels were set at 2 - 10 minutes, 0.2 - 1 g, and 10 - 30 %. The experiments were performed in the same order as shown in **Table 4.1** to avoid experimental bias. Design Expert® Version 7.0.1 (Stat-Ease Inc., Minneapolis USA) statistical software was used to analyze the data set and predict values for input variables that would produce desired responses. Fisher's statistical test was used for ANOVA for the response surface model, and ANOVA data was used to determine the significance of each factor on the responses. The model's effectiveness was evaluated using the F-ratio, coefficient of

variation (CV), adequate precision, adjusted R^2, predicted R^2, and predicted error sum of squares (PRESS).

Mathematical models were used to describe the impact of input variables on the responses monitored to identify optimum formulation composition for acceptable vesicle size, Zeta potential, entrapment efficiency, and PDI. The experimental data for vesicle size, entrapment efficiency, Zeta potential, and PDI obtained are summarized in **Table 4.2**.

Table 4.2 Experimental results for vesicle size, Zeta potential, entrapment efficiency, and PDI.

Run	Vesicle size (nm)	Zeta potential(mV)	Entrapment efficiency (%)	PDI
1	114.78	-25.30	99.25	0.34
2	119.93	-24.30	93.74	0.30
3	118.65	-31.30	91.76	0.28
4	117.95	-31.20	94.56	0.35
5	165.97	-39.37	86.64	0.38
6	148.23	-23.80	92.25	0.31
7	220.55	-35.70	20.39	0.48
8	117.57	-32.00	92.52	0.31
9	151.75	-33.40	51.08	0.29
10	148.92	-35.50	95.87	0.37
11	116.43	-31.20	92.79	0.30
12	286.52	-20.05	54.59	0.38
13	118.68	-33.28	92.43	0.26
14	109.45	-37.03	48.01	0.32
15	231.73	-29.27	15.60	0.35
16	154.73	-26.33	19.49	0.38
17	185.05	-3.46	14.90	0.41

4.3.1.1 Model fitting

The design space was monitored using a quadratic order polynomial model for analyzing and evaluating the input values sonication time, amount of cholesterol, and amplitude. The df of lack of fit was 3 and was within the recommended limits of 2 – 5. The model was able to detect the lack of fit adequately. The standard error of model fit of each factor, binary combinations, and squared factors were 0.35, 0.50, and 0.49, respectively. The variance inflation factor (VIF) of individual factors, binary combinations, and squared factors was 1.00, 1.00, and 1.01, respectively. These VIF values indicate that the model does not contain multi-linear constraints. The average leverage of the runs was 0.5882, suggesting that none of the design points need to be replicated. G-efficiency was 43.17 % and was accepted as it revealed the robustness of model fit. The condition number of the coefficient matrix was 1.18, suggesting that no multi-linearity existed between the terms in the model.

4.3.1.2 Responses monitored

The effect of cholesterol, sonication time, and amplitude on the vesicle size, entrapment, Zeta potential, and PDI was monitored. The recommended model transformations for the output data are listed in **Table 4.3**. The PDI, vesicle size, and zeta potential had ratios of maximum and minimum values < 10 and did not require further analysis of model transformation. Entrapment efficiency had a ratio of maximum and minimum values > 10, and no model transformation was used as the model F-value is significant and any changes made drove the Box-Cox plot outside the recommended 95 % CI. The models were used for further data analysis.

Table 4.3 Responses for niosomal formulations and model transformations.

Response	Parameter	Unit	Minimum observed	Maximum observed	Transformation used
R1	Vesicle size	nm	109.45	286.52	None
R2	Zeta potential	mV	-39.47	-5.46	None
R3	Entrapment efficiency	%	1.49	99.25	None
R4	PDI	-	0.28	0.48	None

The significance of the factors was statistically evaluated and reported as probability > F at a confidence level of 0.0001 to ensure that the data obtained is usable in the design space and reliable. The accuracy of the final model was evaluated using R^2, Adjusted R^2, and lack of fit in the optimization process. R^2 values were used to measure the influence of the input variables and interactions on the variability of the observed responses. A model with an R^2 value above 90 % is considered good. A good model is well capable of explaining the variation in the observed responses. The lack of fit explains the adequacy of the model, and the lack of fit that is not significant is good as the model is required to fit [250].

4.3.1.3 *Analysis of variance for vesicle size*

Statistical modelling was conducted using a quadratic model with significant terms identified to define the final equations for vesicle size. The data generated using Design Expert®, including the sum of squares, df, mean square, F-value, p-value, and significant difference of the model terms, are summarized in **Table 4.4**. As observed, the F-value of 12.45 indicated that the model was significant, and the p-value has a 1.96 % (p = 0.0196) chance of having occurred due to noise. The df of the lack of fit 3 is a fair number as it is within the acceptable range of 2 and 5. The lack of fit F-value of 0.016 implies that the lack of fit is insignificant relative to pure error and has an 86 % (p = 0.8600) chance of having occurred due to noise. The lack of fit value indicates that the model is good and that it fits. The amount of cholesterol was found to significantly affect the vesicle size of the niosomal formulations [250].

Table 4.4 ANOVA data table for the BBD model for vesicle size of the niosomal formulation.

Source	Sum of Squares	Df	Mean Square	F-value	p-value	Significant?
Model	24495.91	9	2721.77	12.45	0.0196	Significant
A-Sonication time	437.93	1	437.93	0.3357	0.5805	No
B-Cholesterol	9690.41	1	9690.41	7.43	0.0295	Yes
C-Amplitude	150.68	1	150.68	0.1155	0.7439	No
AB	5439.80	1	5439.80	4.17	0.0805	No
AC	225.30	1	225.30	0.1727	0.6901	No
BC	1645.92	1	1645.92	1.26	0.2983	No
A^2	1818.71	1	1818.71	1.39	0.2762	No
B^2	4676.94	1	4676.94	3.59	0.1002	No
C^2	8.92	1	8.92	0.0068	0.9364	No
Residual	9130.79	7	1304.40	-	-	-
Lack of Fit	8763.48	3	2921.16	0.016	0.8600	Not significant
Pure Error	367.31	4	91.83	-	-	-
Cor Total	33626.70	16	-	-	-	-

The Model F-value of 12.45 implies the model is significant relative to the noise. There is a 1.96 % chance that an F-value this large could occur due to noise. P-values less than 0.0500 indicate model terms are significant. In this case, B (cholesterol) is a significant model term; values greater than 0.1000 indicate the model terms are not significant. The lack of fit F-value of 0.016 implies the lack of fit is not significant. There is an 86 % chance that a lack of fit F-value this large could occur due to noise. The R^2 value was close to 1, and there is a correlation between the predicted and adjusted R^2 values. The predicted R^2 of 0.7997 agrees with the adjusted R^2 of 0.7997, as summarized in **Table 4.5**.

Table 4.5 Statistical measures of model adequacy.

Squared residuals	Values
R^2	0.7285
Adjusted R^2	0.7997
Predicted R^2	0.7997
Adequate precision	5.1760
SD	36.12
Mean	161.41
%Coefficient of variation	2.38
Predicted error sum of squares	1.40E+05

The adequate precision indicates the signal-to-noise ratio, and a value > 4 is recommended; therefore, the adequate precision value of 5.1760 suggests that the model can be used to navigate the design space. CV is a measure of the closeness of the data to the mean, and a low value confirms adequate precision and reliability for CV. The value for CV was 2.38, suggesting that the data obtained is reliable.

The final equation for the vesicle size is reported in **Equation 4.8**, and the equation was used to make predictions with regard to the response for the various levels of the input variables.

$$\text{Vesicle size} = 135.26 - (7.40 \times A) - (34.80 \times B) - (4.34 \times C) - (36.88 \times A \times B) + (7.51 \times A \times C) - (20.28 \times B \times C) + (20.78 \times A^2) + (33.33 \times B^2) + (1.46 \times C^2)$$

Equation 4.8

Where,

A = Sonication time,

B = Cholesterol and,

C = Amplitude.

The quadratic equation, **Equation 4.8**, shows the coefficient for the intercept, the first-order main effects, higher-order effects, and interaction terms. To quantitate the influence of each

parameter on vesicle size, a + or – operator sign is used. According to the value of the coefficients, sonication time, cholesterol, amplitude, sonication time*cholesterol, and cholesterol*amplitude negatively impact the vesicle size of the niosomal formulation. Sonication time*amplitude, sonication time^2, cholesterol^2, and amplitude^2 positively impacted the vesicle size.

The equation for vesicle size indicates that sonication time, cholesterol, and amplitude all decrease the vesicle size. All the parameters had a negative effect on vesicle size due to the phenomenon described in **§ 3.3.1.1.** The influence of cholesterol percentage on the size of niosomes is markedly dependent on the type of non-ionic surfactant. In this study, the non-ionic surfactant was Tween® 80 with an HLB value of 15 [157]. Increasing cholesterol levels led to a significant decrease in vesicle size. Increases in cholesterol concentration increase the rigidity of the bilayer membranes because of cholesterol's rigid structure and characteristic inverted cone shape [195]. As a result, a decrease in vesicle size was seen.

The relative effect of the factors can be better evaluated using model graphs, contour, and 3D response surface plots. **Figures 4.5** – **4.8** show contour and 3D response surface plots of different variables on vesicle size.

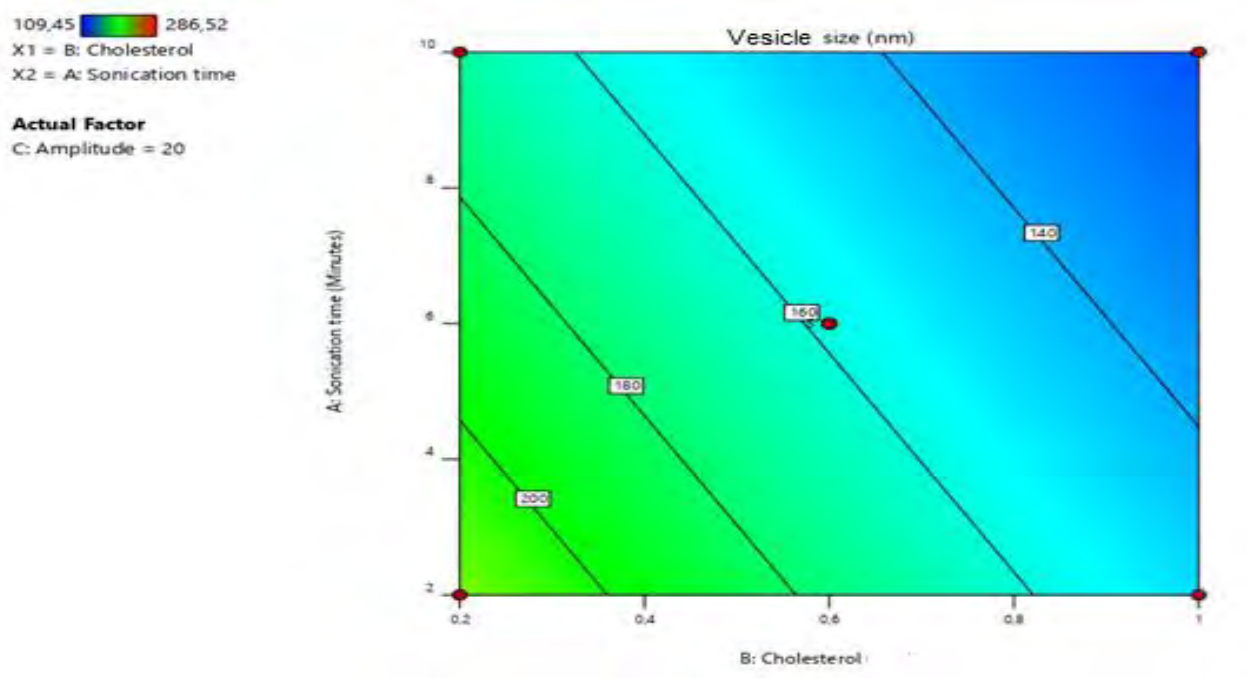

Figure 4.5 Contour plot showing the effect of sonication time and cholesterol on vesicle size.

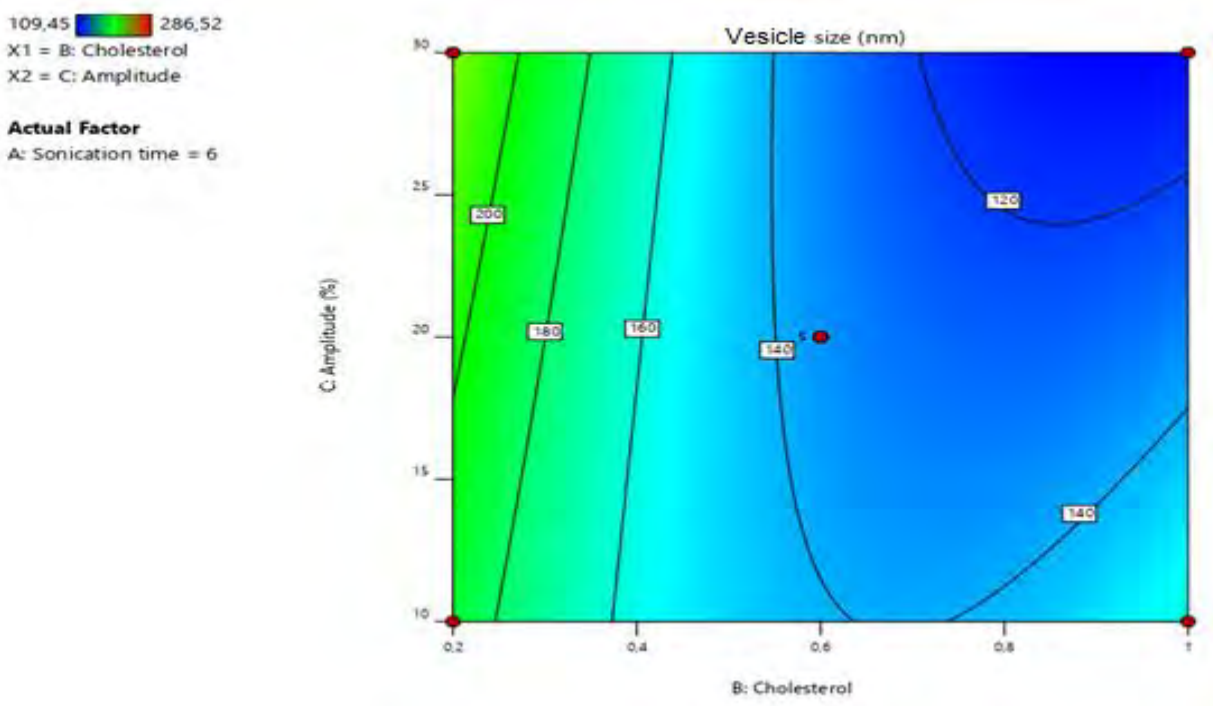

Figure 4.6 Contour plot showing the effect of amplitude and cholesterol on vesicle size.

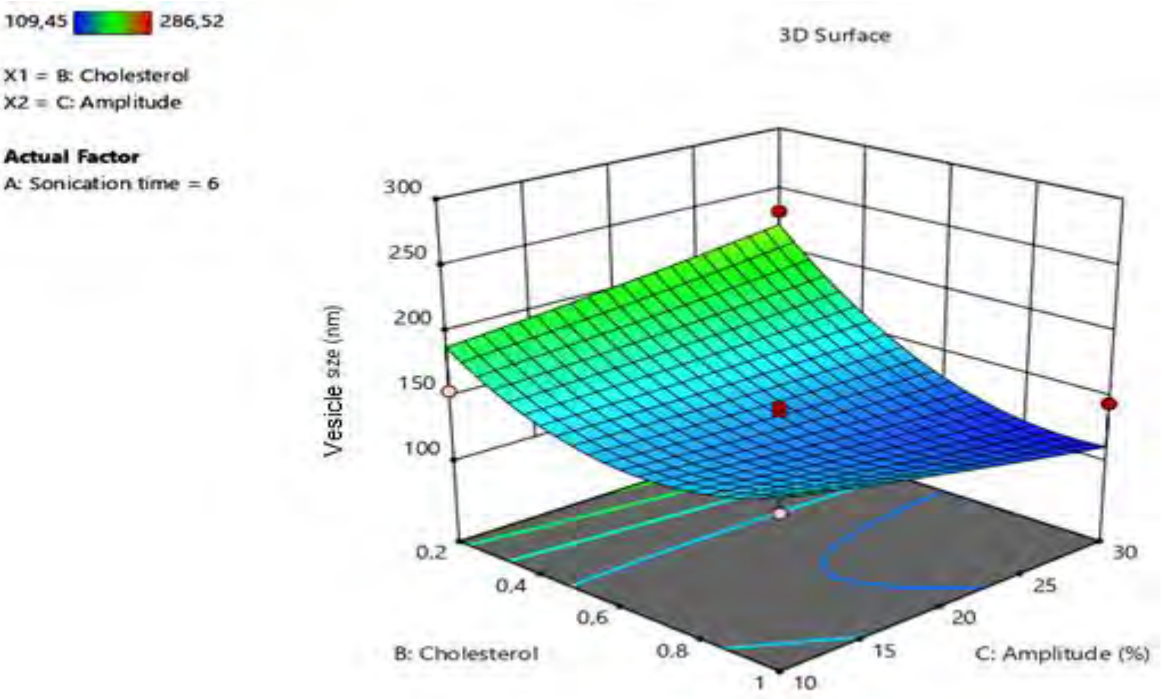

Figure 4.7 3D plot showing the effect of cholesterol and sonication time on vesicle size.

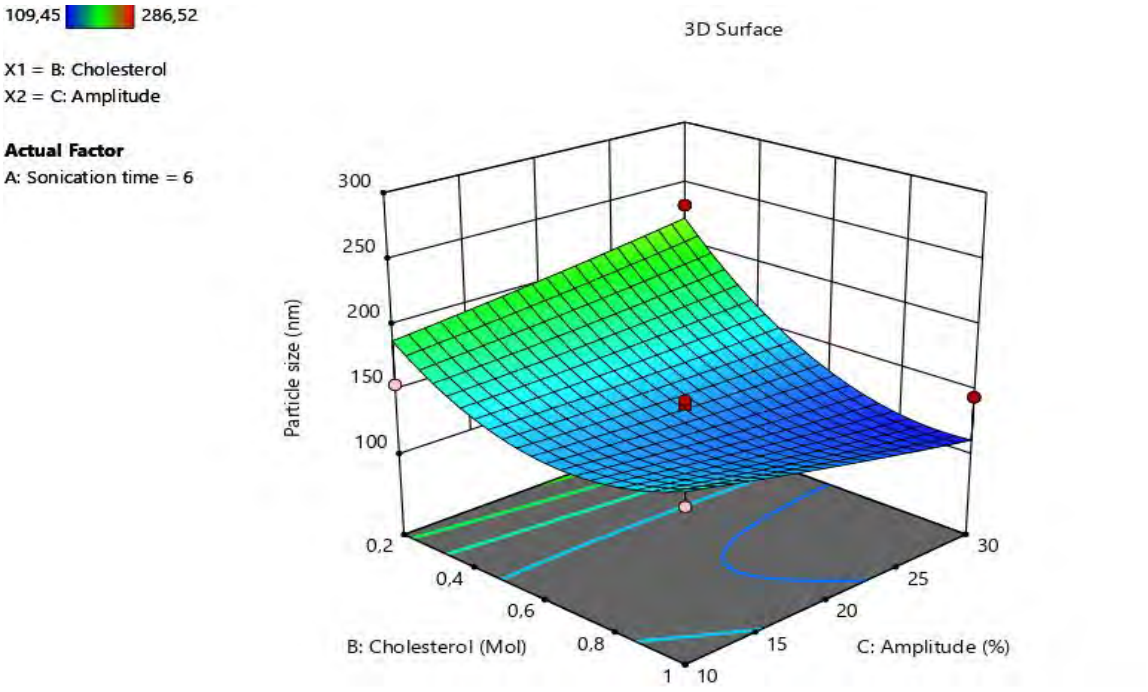

Figure 4.8 3D plot showing the effect of cholesterol and amplitude on vesicle size.

4.3.1.4 *Analysis of variance for entrapment efficiency*

Statistical modelling was conducted using a quadratic model with significant terms identified to define the final equations for entrapment efficiency. The data generated using Design Expert®, including sum of squares, df, mean square, F-value, p-value, and significant difference of the model terms, are summarized in **Table 4.6**. As observed, the F-value of 7.81 indicates that the model was significant, and the F-value has a 0.31 % (p = 0.0031) chance of having occurred due to noise. The df of the lack of fit of 3 is a fair number as it is within the acceptable range of between 2 and 5 [251, 252]. The lack of fit F-value of 0.8061 implies that the lack of fit is insignificant relative to pure error and has a 63.97 % (p = 0.6397) chance of having occurred due to noise. The lack of fit value indicates that the model is good and can be used in the design space. Cholesterol was found to have a significant effect on the entrapment efficiency of the niosomal formulation.

Table 4.6 ANOVA table for the BBD model for entrapment efficiency of the niosomal formulation.

Source	Sum of Squares	df	Mean Square	F-value	p-value	Significant?
Model	12205.90	3	4068.63	7.81	0.0031	Significant
A-Sonication time	2079.80	1	2079.80	3.99	0.0671	No
B-Cholesterol	10101.18	1	10101.18	19.38	0.0007	Yes
C-Amplitude	24.92	1	24.92	0.0478	0.8303	No
Residual	6774.60	13	521.12	-	-	-
Lack of Fit	4366.86	3	485.21	0.8061	0.6397	not significant
Pure Error	2407.75	4	601.94	-	-	-
Cor Total	18980.51	16	-	-	-	-

The predicted R^2 of 0.4523 is in reasonable agreement with the adjusted R^2 of 0.5607; the difference is less than 0.2. The adequate precision of 9.3301 shows that the model can navigate the design space and indicated an adequate signal, as shown in **Table 4.7**.

Table 4.7 Statistical measures of model adequacy.

Squared residuals	Values
R^2	0.6431
Adjusted R^2	0.5607
Predicted R^2	0.4523
Adequate precision	9.3301
SD	22.83
Mean	63.80
%Coefficient of variation	35.78
Predicted error sum of squares	1.04E+04

The final equation of the entrapment efficiency of the niosomal formulation is reported in **Equation 4.9**, and the equation was used to make predictions with regard to the response for the various levels of the input variables.

$$\text{Entrapment efficiency} = + 63.80 + (16.12 \times A) + (35.53 \times B) - (1.77 \times C)$$

Equation 4.9

Where,

A = Sonication time,

B = Cholesterol and

C = Amplitude**.**

To quantitate the influence of each parameter on the entrapment efficiency, a + or – operator sign is used. According to the value of the coefficients, sonication time and cholesterol positively impact the entrapment efficiency of the niosomal formulation. Amplitude decreased the entrapment efficiency.

Increases in cholesterol concentration increase the rigidity of the bilayer membranes because of cholesterol's rigid structure and characteristic inverted cone shape [195]. Such increases could increase the entrapment efficiency of the vesicles. Consequently, there could be an increase in the ability of the niosomes to entrap water-soluble drug molecules [195]. In this study, entrapment efficiency increased with an increase in cholesterol content, further emphasizing the points made above. The contour and 3D plots in **Figures 4.9** and **4.10** further illustrate the effect of cholesterol on entrapment efficiency.

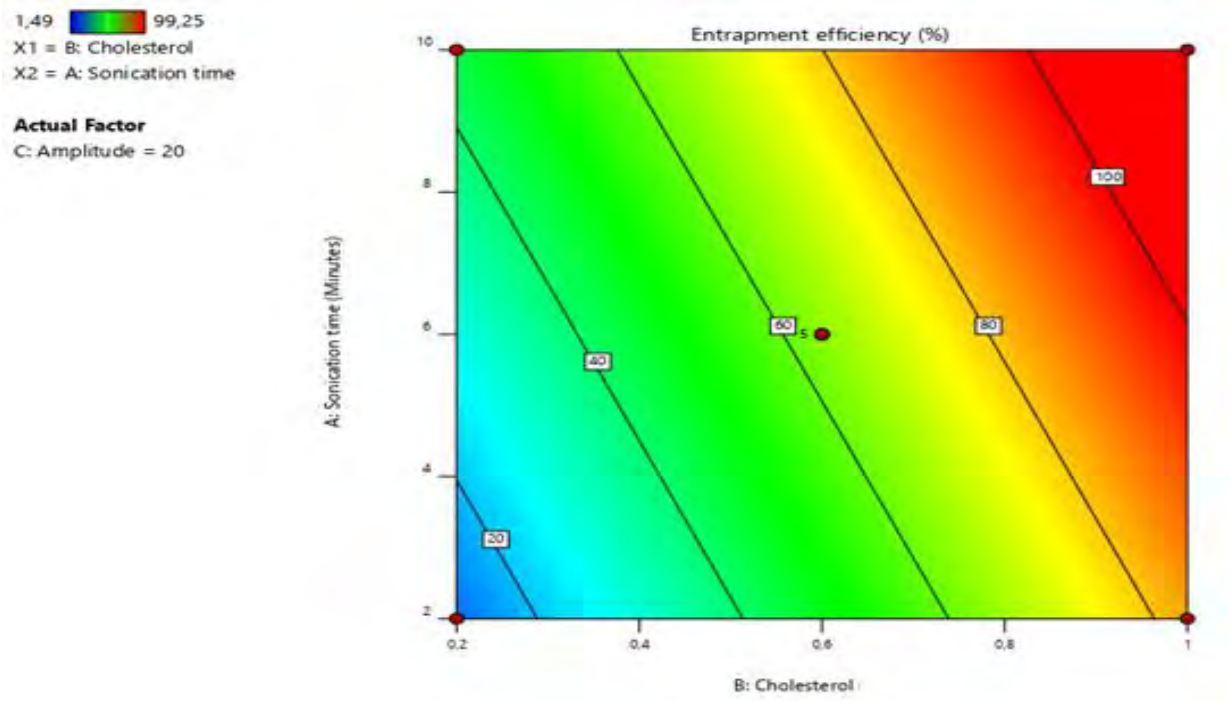

Figure 4.9 Contour plot showing the effect of cholesterol and sonication time on entrapment efficiency.

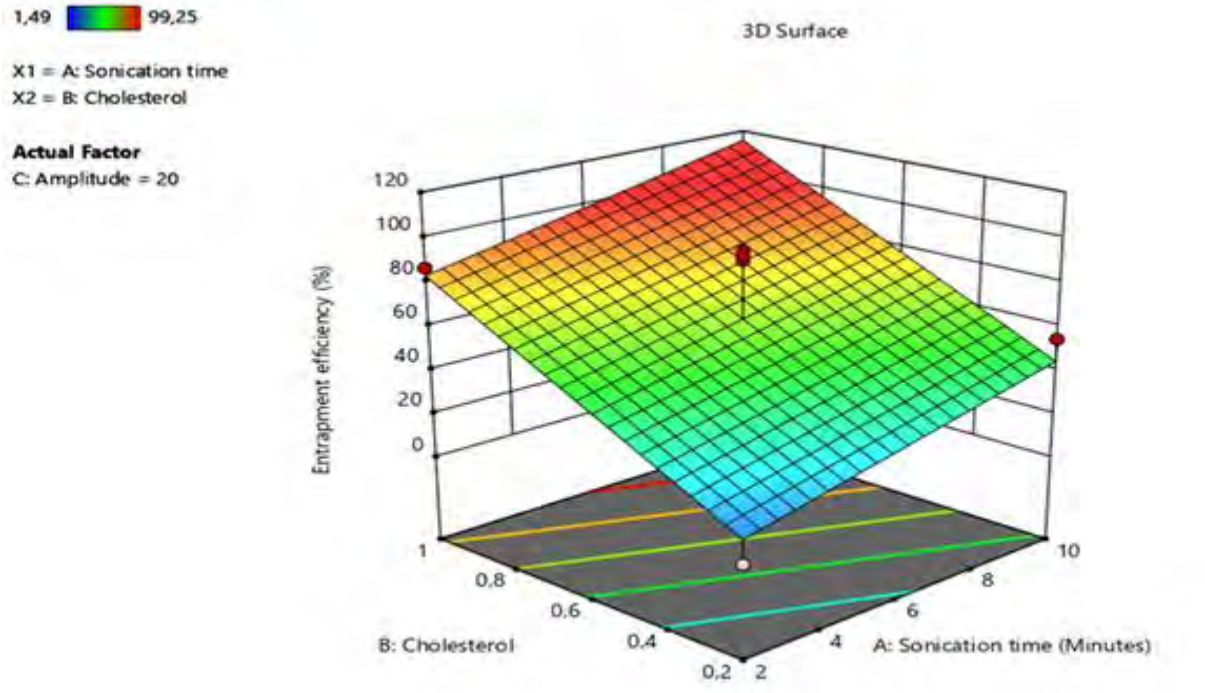

Figure 4.10 3D plot showing the effect of cholesterol and sonication time on entrapment efficiency.

4.3.1.5 Analysis of variance for PDI

The ANOVA data for the BBD is summarized in **Table 4.8.** Sonication time and amplitude was found to contribute significantly to the PDI of the niosomal formulation.

Table 4.8 ANOVA data table for the BBD model for the PDI of the niosomal formulation.

Source	Sum of Squares	df	Mean Square	F-value	p-value	Significant?
Model	0.0277	6	0.0046	3.51	0.0392	Significant
A-Sonication time	0.0078	1	0.0078	5.92	0.0352	Yes
B-Cholesterol	0.0021	1	0.0021	1.60	0.2344	No
C-Amplitude	0.0072	1	0.0072	5.46	0.0416	Yes
AB	0.0006	1	0.0006	0.4739	0.5069	No
AC	0.0100	1	0.0100	7.58	0.0204	Yes
BC	0.0000	1	0.0000	0.0000	1.0000	No
Residual	0.0132	10	0.0013	-	-	-
Lack of Fit	0.0087	6	0.0015	1.31	0.5150	not significant
Pure Error	0.0045	4	0.0011	-	-	-
Cor Total	0.0409	16	-	-	-	-

The model F-value of 3.51 implies that the model is significant. There is only a 3.92 % chance that an F-value this large could occur due to noise. P-values less than 0.0500 indicate model terms are significant. In this case, sonication time, amplitude, and sonication time*amplitude are significant model terms. The lack of fit F-value of 1.31 implies that the lack of fit is insignificant relative to the pure error. There is a 51.50 % chance that a lack of fit F-value this large could occur due to noise. **Table 4.9** summarises the statistical measures of model adequacy.

Table 4.9 Statistical measures of model adequacy.

Squared residuals	Values
R^2	0.6778
Adjusted R^2	0.1399
Predicted R^2	0.4845
Adequate precision	7.3483
SD	0.0363
Mean	0.3479
%Coefficient of variation	10.44
Predicted error sum of squares	0.0352

The predicted R^2 of 0.4845 is not as close to the adjusted R^2 of 0.1399 as expected; the difference is more than 0.2 and may indicate a possible problem with the data and the model. Adequate precision measures the signal-to-noise ratio. A ratio greater than 4 is desirable, and the ratio from the study of 7.348 indicates an adequate signal, and this model can be used to navigate the design space.

The final equation for the PDI of the niosomal formulation is shown in **Equation 4.10**.

$$PDI = 0.03479 – (0.0313 \times A) – (0.0163 \times B) – (0.0300 \times C) – (0.0125 \times A \times B) + (0.0500 \times A \times C)$$

Equation 4.10

Where,

A = Sonication time,

B = Cholesterol and

C = Amplitude.

According to the coefficients' values and the operator's associated sign, all 3 parameters had a negative effect on the PDI (decreased the PDI). The significant factors, sonication time and amplitude, had an almost identical negative effect on the PDI. Cholesterol also had a negative effect on the PDI, almost half the effect of the other two factors. **Figures 4.11- 4.16** illustrate this phenomenon.

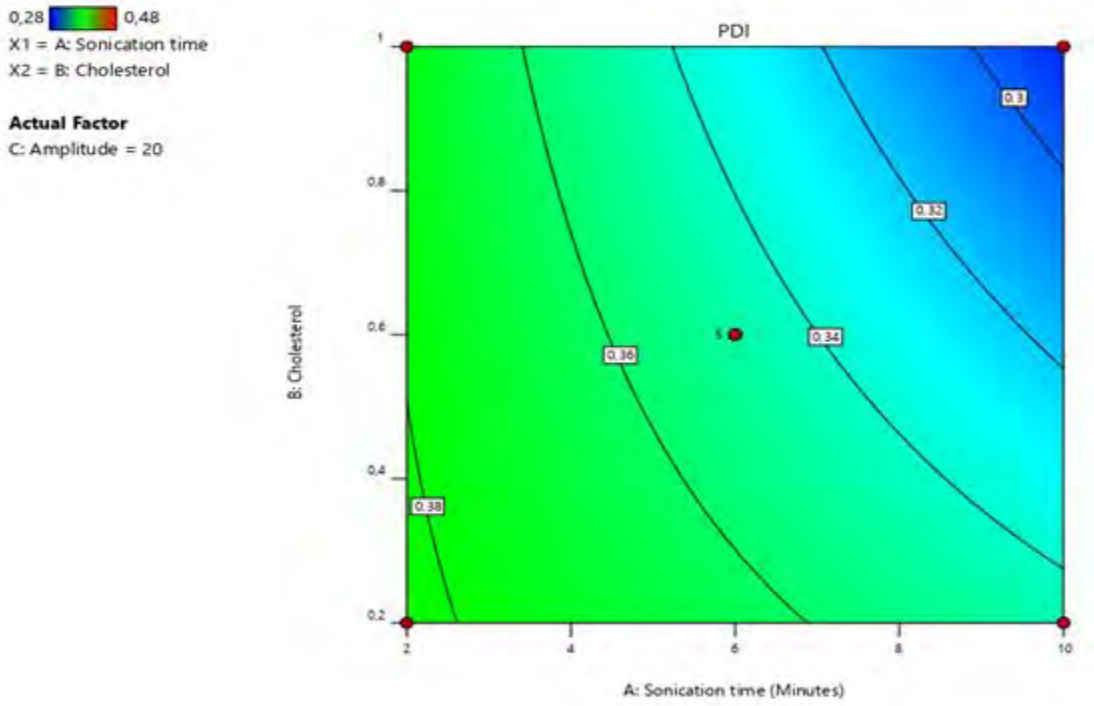

Figure 4.11 Contour plot showing the effect of sonication time and cholesterol on PDI.

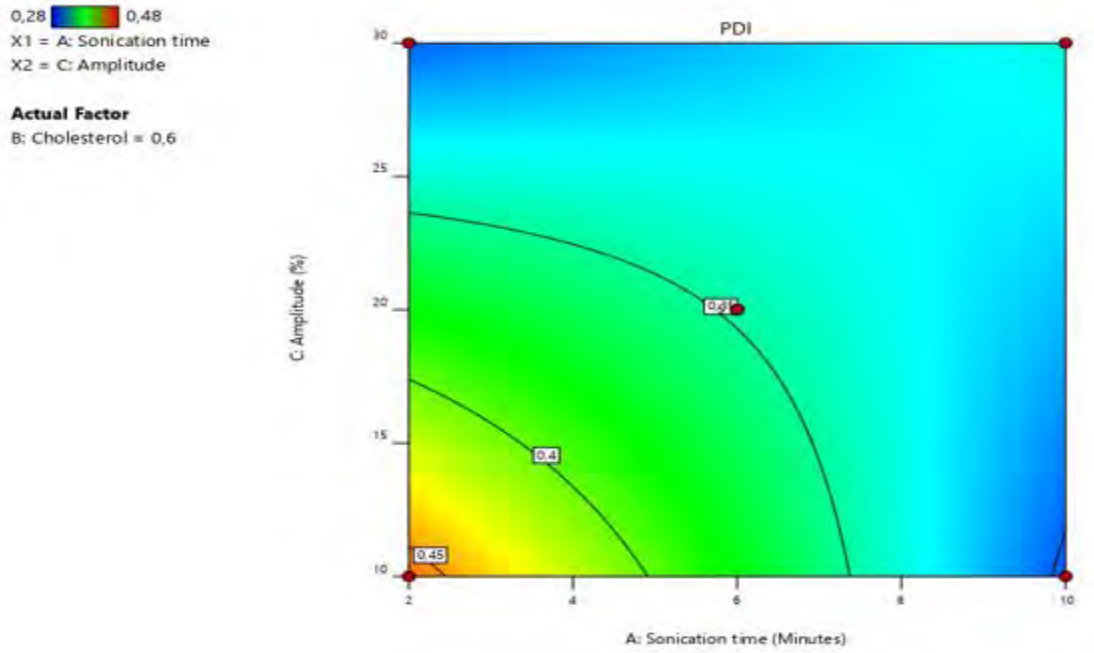

Figure 4.12 Contour plot showing the effect of sonication time and amplitude on PDI.

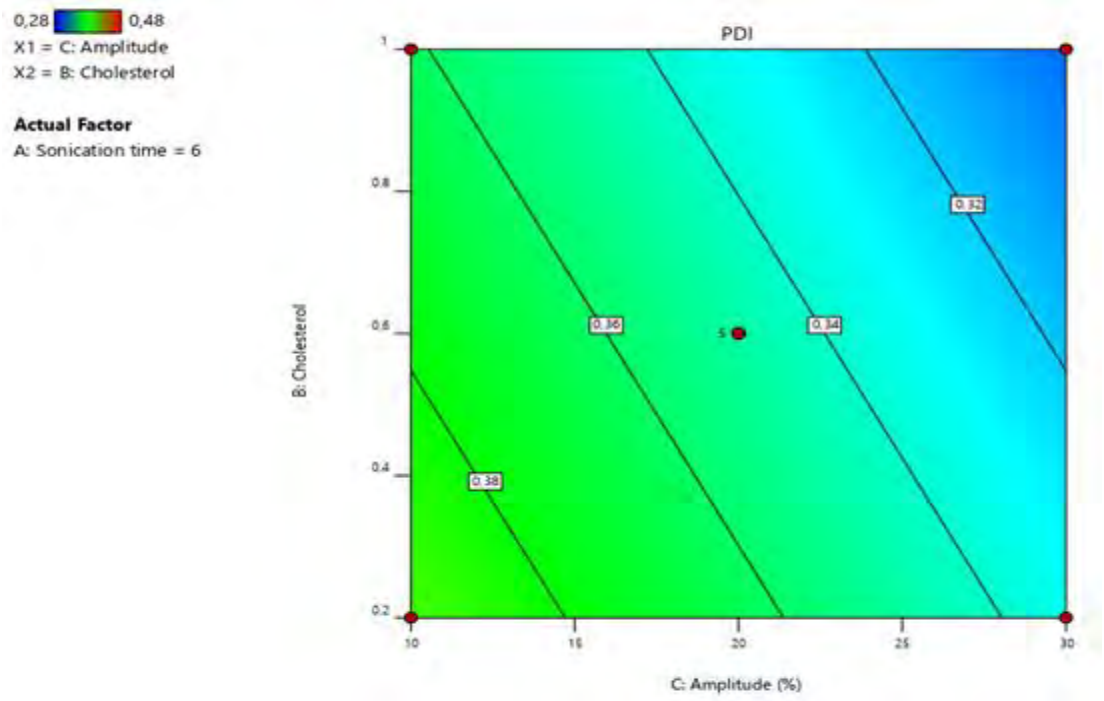

Figure 4.13 Contour plot showing the effect of amplitude and cholesterol on PDI.

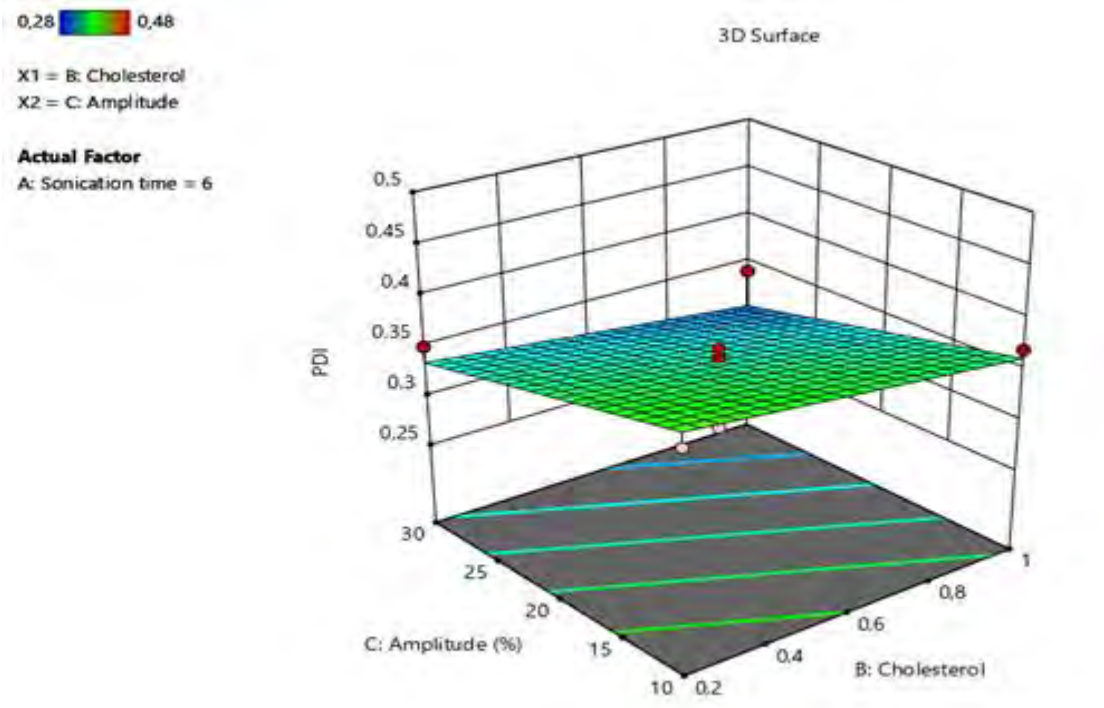

Figure 4.14 3D plot showing the effect of amplitude and cholesterol on PDI.

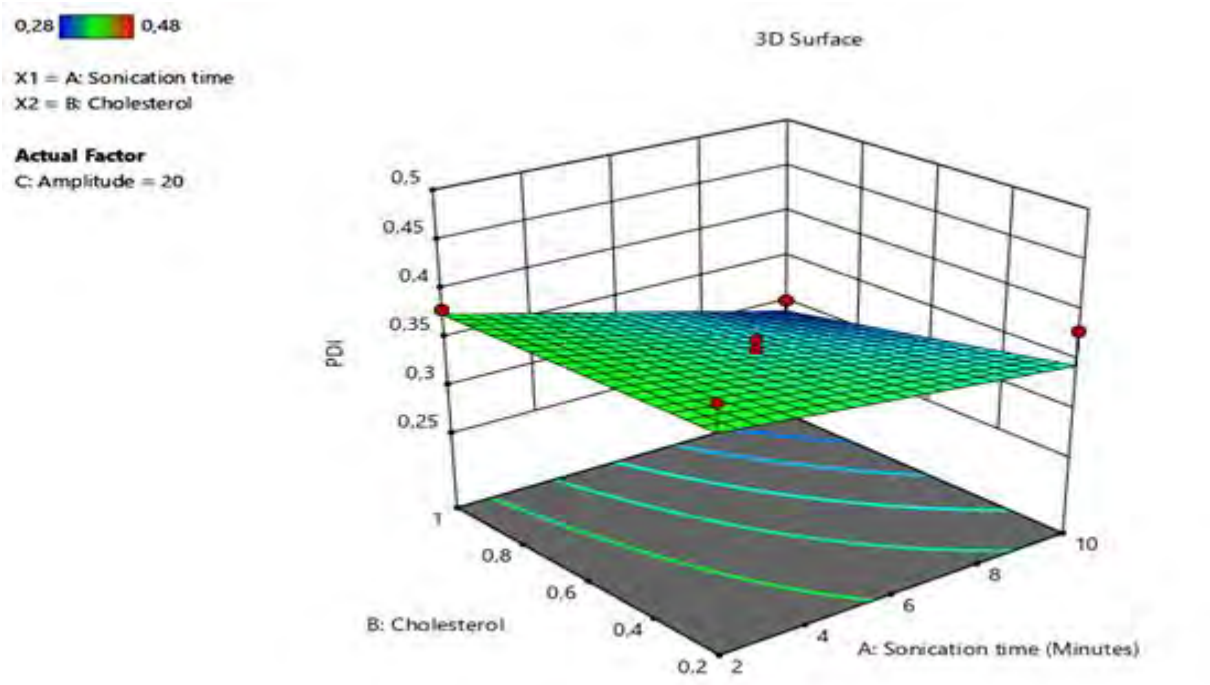

Figure 4.15 3D plot showing the effect of sonication time and cholesterol on PDI.

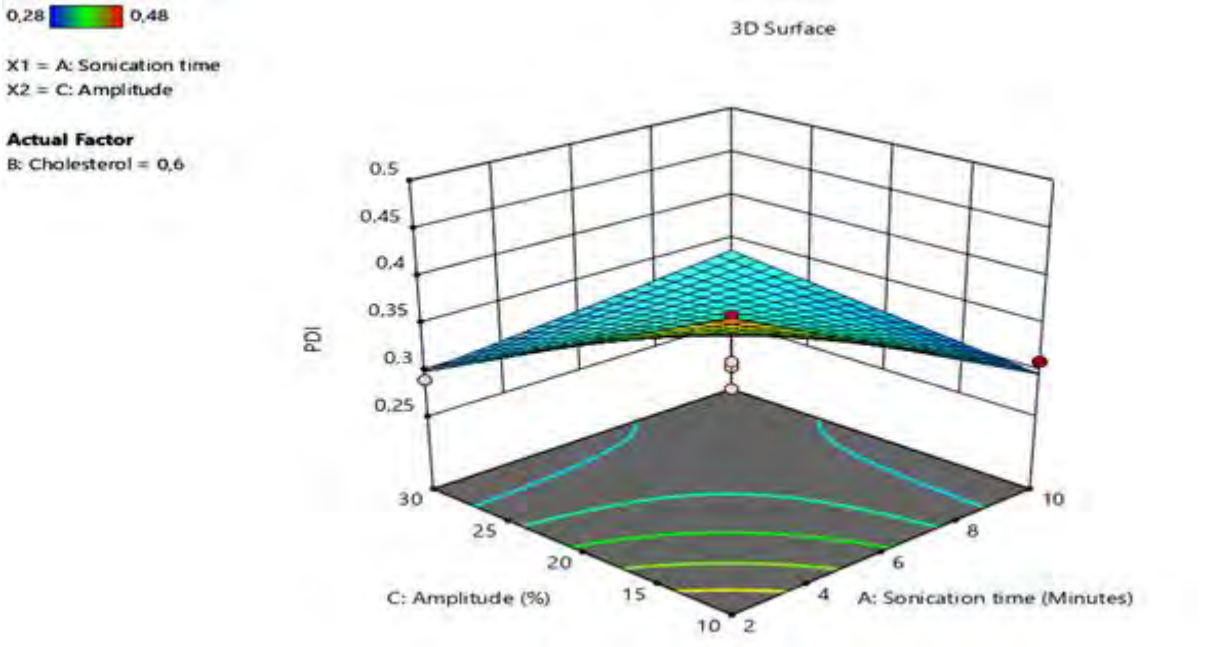

Figure 4.16 3D plot showing the effect of amplitude and sonication time on PDI.

4.3.1.6 *Analysis of variance for Zeta potential*

The ANOVA data for the BBD for the Zeta potential of the niosomal formulation is summarized in **Table 4.10**.

Table 4.10 ANOVA data table for the BBD model for Zeta potential of the niosomal formulation.

Source	Sum of Squares	df	Mean Square	F-value	p-value	Significant?
Model	788.40	9	87.60	9.61	0.0192	Significant
A-Sonication time	9.57	1	9.57	0.2146	0.6572	No
B-Cholesterol	235.01	1	235.01	5.27	0.0403	Yes
C-Amplitude	1.68	1	1.68	0.0378	0.8514	No
AB	219.93	1	219.93	4.93	0.0618	No
AC	60.30	1	60.30	1.35	0.2830	No
BC	43.16	1	43.16	0.9681	0.3579	No
A^2	11.18	1	11.18	0.2507	0.6320	No
B^2	105.76	1	105.76	2.37	0.1674	No
C^2	112.79	1	112.79	2.53	0.1557	No
Residual	312.12	7	44.59	-	-	-
Lack of Fit	184.74	3	61.58	1.93	0.6259	not significant
Pure Error	127.38	4	31.84	-	-	-
Cor Total	1100.52	16		-	-	-

The model F-value of 9.61 implies that the model is significant. There is a 1.92 % chance that an F-value this large could occur due to noise. P-values less than 0.0500 indicate model terms are significant. In this case, only cholesterol is the significant model term. The lack of fit F-value of 1.93 implies that the lack of fit is insignificant relative to the pure error. There is a 62.59 % chance that a lack of fit F-value this large could occur due to noise. **Table 4.11** shows the statistical measures of model adequacy.

Table 4.11 Statistical measures of model adequacy.

Squared residuals	Values
R^2	0.7164
Adjusted R^2	0.3517
Predicted R^2	-1.8667
Adequate precision	5.2315
SD	6.68
Mean	-28.25
%Coefficient of variation	23.64
Predicted error sum of squares	3.15E+03

A negative predicted R^2 implies that the overall mean may be a better predictor of the response than the current model. In such cases, a higher-order model is recommended as it can predict better. In this case, a higher-order model could not be used as the data contained negative numbers, and transformation was not possible/required as the ratio of maximum: minimum was < 10. The adequate precision of 5.232 is desirable as any adequate precision > 4 is desirable and shows that the model can be used to navigate the design space. The final equation for Zeta potential for the niosomal formulation is shown in **Equation 4.11**.

$$\text{Zeta potential} = -28.94 + (1.09 \times A) - (5.42 \times B) - (0.4588 \times C) + (7.42 \times A \times B) - (3.88 \times A \times C) + (3.29 \times B \times C) + (1.63 \times A^2) + (5.016 \times B^2) - (5.18 \times C^2)$$

Equation 4.11

Where,

A = Sonication time,

B = Cholesterol and

C = Amplitude.

According to the values for the coefficients and the associated sign for the operator, sonication time had a positive impact on the Zeta potential of the niosomal formulation. Cholesterol and amplitude had a negative effect on the Zeta potential of the niosomal formulation. Cholesterol had a more pronounced negative effect on the Zeta potential (> 5 times) than the amplitude. Primarily, Zeta potential is affected by the presence of counterions. Other factors that can affect Zeta potential

include ionic strength and temperature [196]. Zeta potential is mentioned as a stability indicating marker, but it is important to note that non-ionic surfactant systems are predominantly stabilized by steric stabilization, and there is only a minor electrostatic element from adsorbed hydroxyl ions [196].

According to **Equation 4.11**, sonication time increased Zeta potential; an increase in sonication time means increased Zeta potential. Sonication has no significant effect on Zeta potential [198]. However, there is no specific rule on how sonication affects Zeta potential as the effect depends on vesicles used, method of preparation and sonication method [198]. **Figures 4.17** to **4.20** show the effect of cholesterol on Zeta potential compared to other factors in the study, namely, amplitude and sonication time.

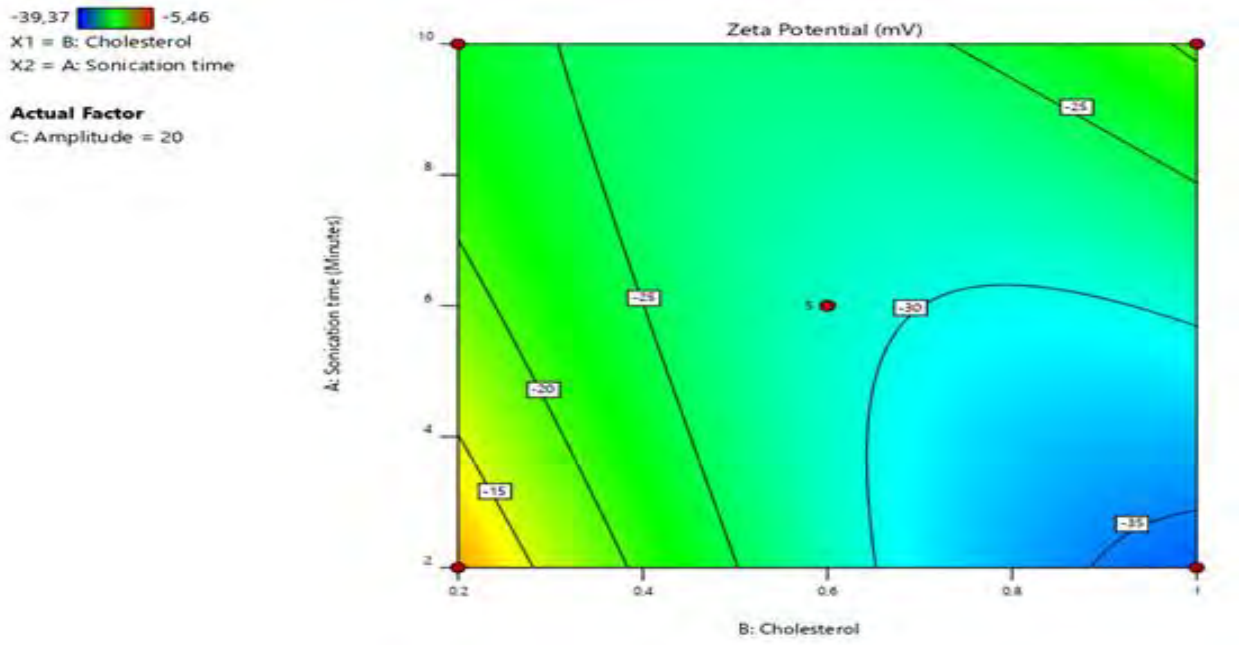

Figure 4.17 Contour plot showing the effect of cholesterol and sonication time on Zeta potential.

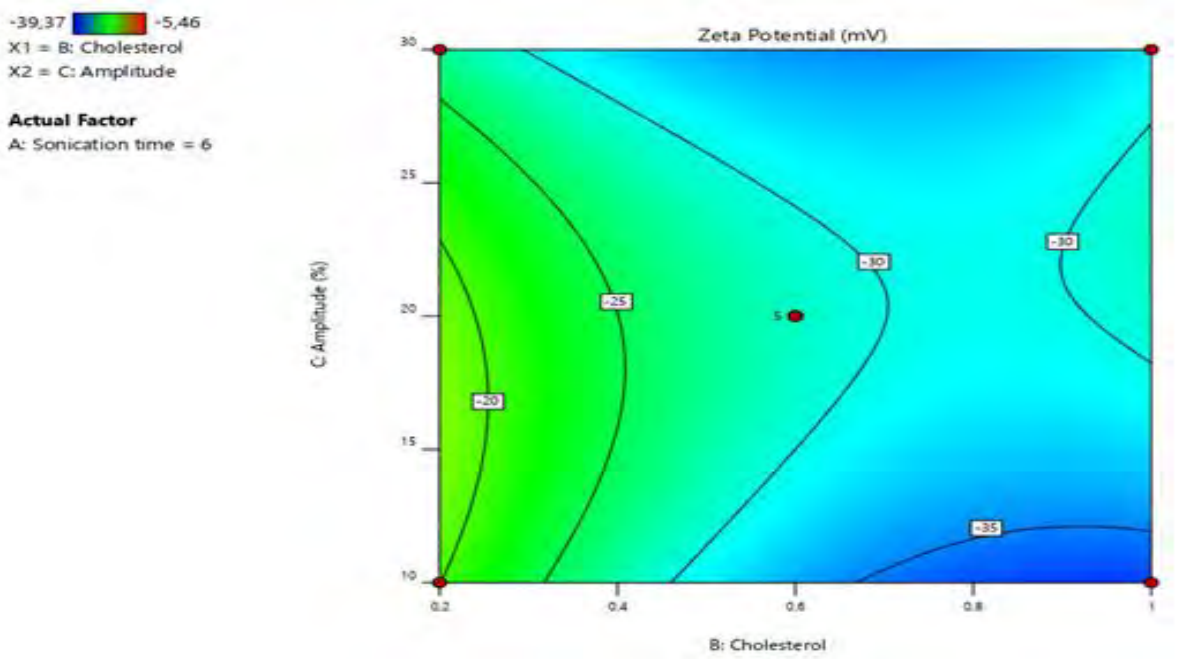

Figure 4.18 Contour plot showing the effect of cholesterol and amplitude on Zeta potential.

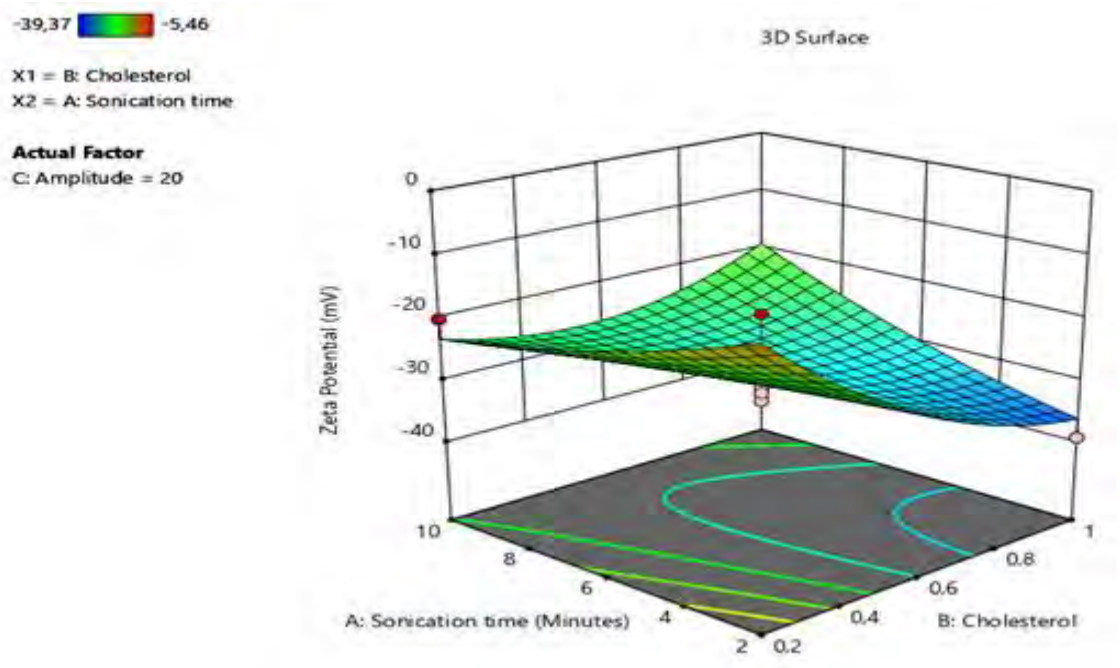

Figure 4.19 3D plot showing the effect of cholesterol and sonication time on Zeta potential.

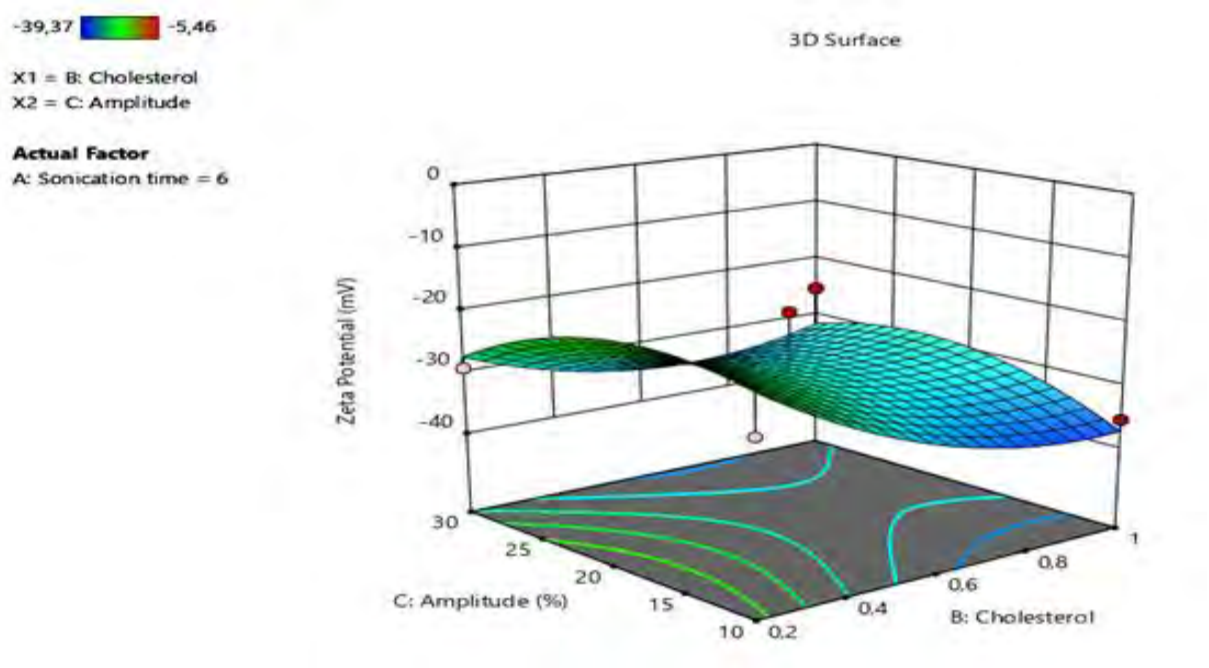

Figure 4.20 3D plot showing the effect of cholesterol and amplitude on Zeta potential.

All the 3D and contour plots belonging to insignificant variables were not analyzed and are presented in **Appendix D**.

4.3.2 Optimization of the niosomal formulation

4.3.2.1 Optimization using BBD

The optimized niosomal formulation was selected based on the specified ranges which give the most desirable characteristics. After the relationships between the factors and the responses were established and evaluated, the desirable lower and upper limits of the responses were defined and are listed in **Table 4.12**.

Table 4.12 Summary of response upper and lower limits.

Response	Lower limit	Upper limit	Criteria
Entrapment efficiency	1.46 %	99.25 %	Maximize
Vesicle size	109.45 nm	286.52 nm	In range
Polydispersity index	0.28	0.48	Minimize
Zeta potential	-39.37 mV	-5.46 mV	Minimize

The desirable responses were defined on the established BBD, and the solutions generated are summarized in **Table 4.13**. The BBD solution predicted factor values that would produce responses desirable in the optimized niosomal formulation.

Table 4.13 BBD predictions based on custom inputs.

Solution	Sonication time(mins)	Cholesterol (g)	Amplitude	Zeta potential (mV)	Entrapment efficiency (%)	Vesicle size (nm)	PDI
1	3.304	1	11.294	-39.238	90.00	200.00	0.31

4.3.2.2 *Optimization using artificial neural networks*

Artificial neural networks (ANN) offer a different way to analyze data and recognize patterns from traditional computing methods. However, they are not a solution for all computing problems. Traditional computing methods work well for problems that can be well characterized. The training of an ANN corresponds to minimizing the associated measure of error represented by the predefined error function. The literature suggests many choices of error functions. The most straightforward and commonly used error function in neural networks used for regression is the mean square error (MSE) [251].

The purpose of training a network is to identify the optimum value for weights that connect all neurons such that the input value will produce accurate outputs, necessitating training of the network as an optimization process [251]. Therefore, the training process is required to ensure changes are made to the weight values. The procedure used to carry out this function is called the training algorithm. Activation functions transform the input received to keep values within a manageable range, and error functions minimize error in the network [252].

In neural networks, a hidden layer is located between the input and output of the algorithm, in which the function applies weights to the inputs and directs them through an activation function as the output. In short, the hidden layers perform non-linear transformations of the inputs entered into the network. Hidden layers vary depending on the function of the neural network, and similarly, the layers may vary depending on their associated weights. The output layer is responsible for producing the final result. There must always be one output layer in a neural network. The output layer takes in the inputs passed in from the layers before it, performs the calculations via its neurons, and then the output is computed [252, 253].

The selection of the best ANN topology was based on the test MSE and R^2. The network that best described the relationship between the factors and the responses was MLP 3-3-4. The number of input neurons was three, which corresponds with the number of factors. The number of output neurons was four which corresponds with the number of responses. The number of hidden neurons was three and generated the lowest test MSE value as listed in **Table 4.14**.

Table 4.14 A summary of the performance and errors of active networks.

Network name	Training R^2	Training MSE	Validation R^2	Validation MSE	Test R^2	Test MSE
RBF 3-8-4	0.584	1735990000	1.00	13894700000	0.164	1258997000
MLP 3-3-4	0.701	165630000	0.700	8006100000	1.00	100429300
MLP 3-5-4	0.952	1795670000	0.700	9027800000	1.00	284222000
RBF 3-7-4	0.489	447893000	1.00	14095000000	0.164	1562298000
MLP 3-15-4	0.604	1893300000	1.00	15935600000	0.743	2560097000

The lowest test MSE is indicative of the best data fit and predictive ability. This network was trained using the Broyden-Fletcher-Goldfarb-Shano (BFGS) training algorithm, and activation functions for the hidden layer and output were exponential functions, as listed in **Table 4.15**.

Table 4.15 A summary of the error, hidden, and activation functions of the active networks.

Network name	Training algorithm	Error function	Hidden activation	Output activation
RBF 3-8-4	RBFT	SOS	Identity	Exponential
MLP 3-3-4	BFGS 12	SOS	Exponential	Exponential
MLP 3-5-4	BFGS 13	SOS	Exponential	Exponential
RBF 3-7-4	RBFT	SOS	Gaussian	Identity
MLP 3-15-4	BFGS 30	SOS	Identity	Exponential

ANN was used to predict the responses of the BBD, and the responses generated are summarized in **Table 4.16**.

Table 4.16 ANN predictions for the responses.

Formulation	ANN prediction			
	Vesicle size (nm)	Entrapment efficiency (%)	PDI	Zeta potential(mV)
1	150.09	90.00	0.34	-25.00
2	136.92	92.22	0.34	-24.30
3	118.00	88.72	0.27	-31.50
4	118.95	89.56	0.26	-31.40
5	160.00	88.60	0.40	-40.39
6	148.30	90.75	0.32	-20.80
7	200.45	88.29	0.29	-35.70
8	117.57	92.52	0.30	-32.00
9	150.20	81.05	0.30	-33.40
10	148.92	94.84	0.28	-35.50
11	118.02	88.30	0.27	-29.00
12	208.49	94.51	0.32	-20.00
13	118.68	87.93	0.27	-31.28
14	110.00	85.37	0.33	-27.05
15	245.99	86.18	0.35	-30.08
16	165.94	91.55	0.38	-36.33
17	200.70	91.10	0.31	-10.50

The predicted responses for the same formulations, F3, F4, F8, F11, and F13, showed that the network adequately learned the input-output data relationships. The formulation was optimized by defining custom inputs similar to those determined by the BBD model (**Table 4.2**), as listed in **Table 4.17**. The ANN custom inputs were made like those of the BBD to compare the two approaches of formulation optimization to determine the approach that could predict the optimized niosomal formulation results closely.

Table 4.17 Custom input predictions generated by MLP 3-3-4.

Formulation	Sonication time (mins)	Cholesterol (g)	Amplitude	Zeta potential (mV)	Entrapment efficiency (%)	Vesicle size (nm)	PDI
1	3.304	1.00	11.294	-39.00	94.50	200.00	0.31

4.3.2.3 Manufacture of the niosomal formulation

The niosomal formulation was formulated with the specified initial factors and conditions listed in **Tables 4.13** and **4.17.** They were manufactured according to the probe sonication method as described in **§ 4.2.2** (**Figure 4.4**). The niosomal formulation was assessed for vesicle size, PDI,

and Zeta potential as described in **§ 4.2.4**. The entrapment efficiency of the niosomal formulation was assessed as described in **§ 4.2.5**. The values for the responses assessed are listed in **Table 4.18**.

Table 4.18 Responses for the optimized formulation.

Solution	Average pH ±SD	Average Zeta potential (mV) ±SD	Average Entrapment efficiency (%) ±SD	Average Vesicle size (nm) ±SD	Average PDI±SD
1	7.45±0.26	-39.18±3.28	90.26±2.39	220.53±19.06	0.314±0.059

The optimized niosomal formulation had an average pH of 7.45± 0.26 and this pH alteration will not cause any irritation in the ear canal. The CPH release data were subjected to release kinetic study, and the release kinetics of the optimized formulation was best described by a zero-order model with an R^2 value of 0.932079 and an *n* value of 0.5, as shown in **Table 4.19**.

Table 4.19 Parameters for CPH release from the optimized niosomal formulation.

Formulation	Zero-order		First-order		Hixson-Crowell		Korsmeyer-Peppas			Higuchi	
	R^2	K	R^2	K	R^2	K	R^2	n	K	R^2	K
1	0.93	0.50	0.68	0.08	0.70	0.24	0.95	0.57	9.38	0.85	0.98

Figure 4.21 shows the release profile of the optimized formulation.

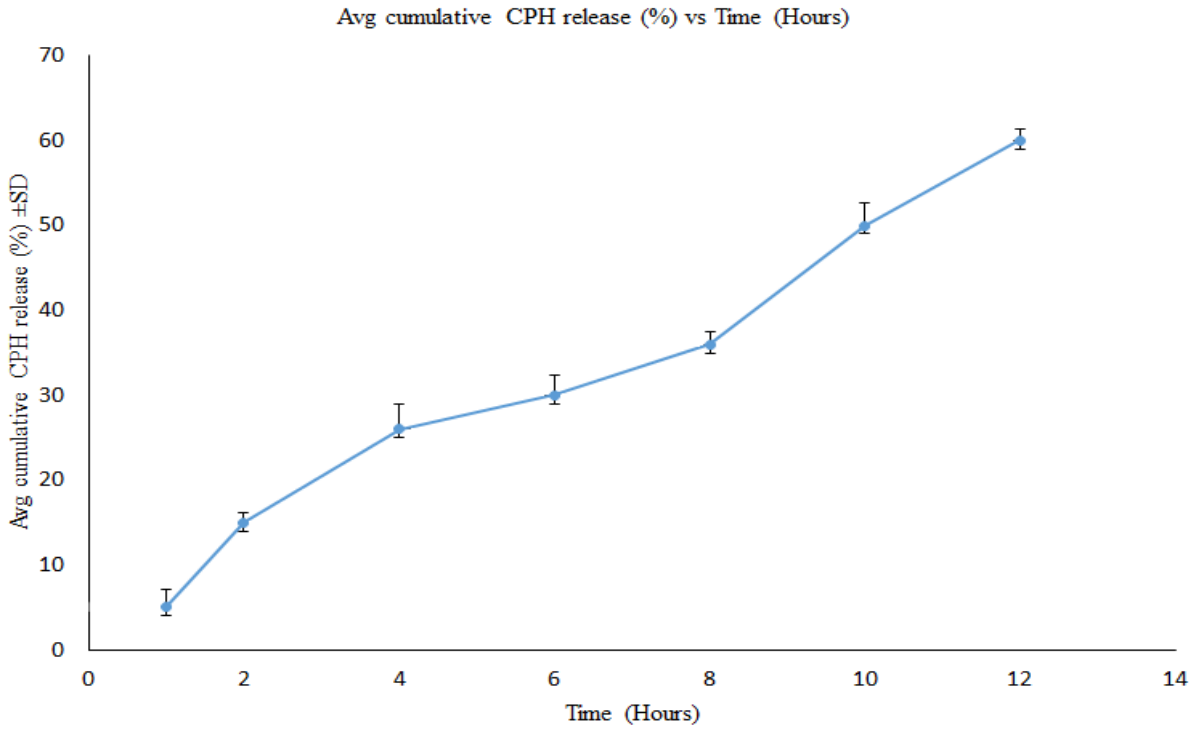

Figure 4.21 Cumulative CPH released from the optimized formulation (mean ±SD) (n=3).

According to **Figure 4.21**, 60 % of the drug (CPH) will be released after 12 hours from the time of administration. It is important to note that the formulation may be removed from the tympanic membrane before the active drug is absorbed. Therefore, studies focusing on the residence time of the formulation on the tympanic membrane would be beneficial in this study. Additionally, studies to determine if the niosomes are diffusing through the cut-off need to be investigated, molecular weight alone is not sufficient in this case.

4.4 CONCLUSIONS

A niosomal formulation for the transtympanic delivery of CPH was manufactured with surfactants (SLS, Tween® 80) and cholesterol using the probe sonication method of preparing niosomes. Using the BBD approach, various cholesterol levels, sonication time, and amplitude were determined, and their impact on vesicle size, entrapment efficiency, Zeta potential, and PDI were assessed. The impact of the input factors on the responses was explained using polynomial equations generated for each response. DOE facilitated the design and manufacture of different formulations for developing an optimized niosomal formulation considering the factors that influence the formulation's performance. Therefore, three factors were simultaneously investigated for their significance in impacting the responses using the BBD approach. The information gathered from the study was used to identify and establish possible relationships between the factors and their effect on each response. It can be concluded that the approach used in this study is helpful for the optimization of niosomal formulations for the delivery of CPH transtympanically.

The pH of the ear, when affected by otitis media, ranges between 7.0 and 7.8. The pH was not significantly affected by the excipients used in the study. The pH remained constant throughout the study. For this reason, pH was not included in the BBD as it did not show any fluctuations and would be easily controlled. On the other hand, as seen in ***Chapter 3***, responses like Zeta potential, entrapment efficiency, vesicle size, and PDI fluctuated with slight changes in the experiments. As a result, these were included in the BBD approach to control and optimize them to give the desired results.

In-vitro release of CPH was observed below from the BBD niosomal formulations as none of the formulations released 100 % of CPH after 12 hours. The low release could mean that the CPH release was retarded. This retardation of CPH release can be attributed to the entrapment of CPH in the niosomal structure, resulting in the sustained release of CPH over 12 hours. It is reported that the transtympanic dose of CPH eardrops for otitis media is 12 mg, and the eardrops take between 48 - 72 hours to start working [253]. Based on the release studies performed on the formulation and calculating backwards, the niosomal formulation reached the minimum effective concentration in almost 3 hours. However, it is impossible to correlate *in-vitro* release into a large fluid volume with *in-vivo* release from a small volume.

Additionally, the formulation was able to provide sustained release of the drug for the next 9 hours. This shows that there may be improved control of overall release.

In-vitro studies are not always an accurate predictor of what will happen once the formulation enters the biological system and there was no method used to that the vesicles are not diffusing across the cut off. Therefore, more *in-vivo* studies need to be performed to assess the formulation's performance when introduced into the biological system. Additionally, when administering the drug via the transtympanic route, some drugs can be lost to the Eustachian tube. Studies to determine the fraction of drug lost to the Eustachian tube and how, if possible, it can be avoided also need to be performed. The niosomes developed may improve drug permeation across the tympanic membrane. Further studies need to be performed to assess the rate and the factors that affect the niosomes crossing the tympanic membrane.

CHAPTER 5

STABILITY STUDIES OF CIPROFLOXACIN LOADED NIOSOMES FOR TRANSTYMPANIC DELIVERY

5.1 INTRODUCTION

Non-ionic surfactant vesicles are one of the most promising drug carriers with a bilayer structure and are formed by the association of non-ionic surfactants and cholesterol in an aqueous phase [254]. Niosomes are biodegradable, biocompatible, and non-immunogenic. They have a long shelf-life, exhibit high stability, and enable the delivery of drug at the target site in a controlled and sustained manner [254]. In recent years, the potential of niosomes as a drug carrier has been extensively studied [255, 256]. Various types of non-ionic surfactants have been reported to form niosomes and enable the entrapment of many drugs with a wide range of solubility. The composition, size, number of lamellae, and surface charge of niosomes can be varied and optimized to enhance the performance of niosomes for drug delivery [257, 258].

Non-ionic surfactant vesicles (niosomes), formulated with non-ionic amphiphiles in specific aqueous dispersions, were first used in cosmetics development [259]. In structure, niosomes are usually multi-lamellar or uni-lamellar vesicles that possess closed bilayers with hydrophilic cavities as both the internal and hydrophobic shells as the outer layers to accommodate the active agents [260]. In recent years, with the development of nanotechnologies in pharmaceutics, more and more studies have focused on niosomes as nanocarriers for drug delivery [260, 261]. Niosomes differ from liposomes and polymersomes based their composition and/or function. Unlike other nanoparticles, structurally, liposomes, polymersomes, and niosomes have many similarities, and they can all be loaded with both hydrophilic and hydrophobic drugs. Therefore, they could deliver both hydrophilic and hydrophobic drugs in one vesicle [262].

Compared with liposomes, niosomes have several advantages: good stability, low cost, ease to be formulated, and scaling-up [263]. Niosomes are much more stable because their forming materials, non-ionic surfactants, are more stable than those of other lipid-based carriers in terms of physical and chemical stability [264]. The stability of the niosomes plays an essential role in formulation development. It is affected by the preparation method, loaded drugs, and types of membrane-

forming materials [265]. For their storage, the changes in vesicle size, zeta potential, morphology, and loaded drug leakage may be measured to evaluate the stability [266, 267].

The stability of ciprofloxacin (CPH) niosomes after the probe sonication method was studied at various temperatures by storing the samples in air-tight sealed amber bottles at 2 different conditions: room temperature (25 °C) and the refrigerator (4 °C) for 28 days. Samples from each bottle were analyzed every 7 days to observe polydispersity index (PDI) changes, vesicle size, Zeta potential, pH, entrapment efficiency, colour, lamellarity, permeability, and surface morphology.

5.2 EXPERIMENTAL

5.2.1 Materials

CPH was purchased from Sigma Aldrich® (St Louis, USA). Tween® 80, acetone, SLS, and amaranth red dye were purchased from Merck® Laboratories (Wadeville, Gauteng, South Africa). Cholesterol was purchased from Saarchem-Holpro (Krugersdorp, South Africa). HPLC grade water was initially purified by reverse osmosis using a Millipore® Milli-RO 15 water purification system consisting of Organex-Q, Super-C carbon, and two Ion-X ion-exchange cartridges.

5.2.2 Method

Several different methods with varying results can be used to prepare niosomes. These include:

5.2.2.1 Ether injection method

A lipid solution in di-ethyl ether is slowly introduced into warm water. The lipid mixture is then injected into an aqueous material solution to be encapsulated (using syringe type infusion pump) at 55 – 65 °C under reduced pressure. Vaporization of ether leads to the formation of single-layered vesicles [257].

5.2.2.2 Lipid film formation

The surfactant/cholesterol mixture is dissolved in the di-ethyl ether in a round bottom flask, and ether is removed at room temperature under reduced pressure in a rotary evaporator. The dried surfactant film is hydrated with an aqueous phase at 50 – 60 °C with gentle agitation; to produce multi-lamellar vesicles [257].

5.2.2.3 Sonication method

Aqueous phase is added to the surfactant/cholesterol mixture, and the mixture is probe sonicated at 60 °C for 3 minutes to produce niosomes [257].

5.2.2.4 Reverse-phase evaporation

The novel key in this method is removing solvent from an emulsion by evaporation. Water in oil emulsion is formed by bath sonication of a mixture of two phases; the emulsion is then dried to a semi-solid gel in a rotary evaporator under reduced pressure [258]. The water droplets are then collapsed by vigorous mechanical shaking with a vortex mixer. The lipid monolayer, which encloses the collapsed vesicles, is contributed to adjacent intact vesicles to form the outer leaflet of the bilayer of large uni-lamellar vesicles (LUVs) [257].

5.2.2.5 Formation of niosomes from proniosomes

Another method of producing niosomes is to coat a water-soluble carrier such as sorbitol with surfactant. The result of the coating process is a dry formulation in which each water-soluble particle is covered with a thin film of dry surfactant. This preparation is termed “proniosomes." The niosomes are formed by the addition of the aqueous phase at T > Tm and brief agitation. Where, T = Temperature and Tm = mean phase transition temperature [257, 258].

5.2.2.6 Microfluidisation

This technique is based on a submerged jet containing micro-channels with an interaction chamber in which two fluidized streams interact with each other at ultra-velocities. The impingement of the thin liquid sheet and a common front are arranged so that the energy supplied for the formation of niosomes remains the same, and this forms uni-lamellar niosomes with better reproducibility and size uniformity [258].

5.2.2.7 Multiple membrane extrusion

In this method, niosomes are chemically prepared by extrusion through a polycarbonate membrane (0.1 µm nucleophore). By using this method, a desired size of the vesicles can be obtained [258].

In this study, the probe sonication method was used to prepare CPH loaded niosomes. CPH (150 mg) was weighed on a Model AG135 Mettler Toledo® top loading balance (Mettler®, Zurich, Switzerland) and was first mixed with 150 mL of HPLC grade water in a 250 mL beaker with the

help of a magnetic stirrer. Cholesterol (1 g) and 1 g of each surfactant (SLS and Tween® 80) were added. The mixture was subjected to probe sonication (Bandelin, Berlin, Germany) for 6 min at 60 °C of probe temperature in a pulsatile manner (50 s sonication with 10 s pause) at 11 % amplitude. After probe sonication, the niosomes were collected and stored in a 100 mL amber bottle at 4 °C overnight to allow for maturation. The niosomes were then stored at two different conditions (4 °C and 25 °C) in 100 mL amber glass bottles for 28 days with samples taken every 7 days to analyze vesicle size, PDI, Zeta potential, entrapment efficiency, pH and colour, permeability, lamellarity, and surface morphology.

5.2.3 Differential light scattering measurement

The size of the niosomes (z-average), PDI, and Zeta potential were measured every 7 days using a Zetasizer Nano ZS (Malvern Instruments Ltd., UK). To avoid multi scattering phenomenon, the niosomal dispersions (30 µL) were diluted with HPLC grade water up to 10 mL before measurement. All the measurements were performed in triplicates. The results were presented as mean ±SD.

5.2.4 Entrapment efficiency

To determine the entrapment efficiency, every 7 days, 2 mL of the formulation was withdrawn and ultra-centrifuged for 1 h at 4 °C (Eppendorf, Hamburg, Germany). The supernatant was collected, the pellet at the bottom of the centrifuge tube was washed twice with HPLC grade water. The water was then collected, and centrifugation was repeated. Drug concentration in the aqueous solution containing supernatants and water used for washing was determined. The percentage entrapment efficiency of CPH was calculated by using the following equation (**Equation 5.1**):

$$Entrapment\ Efficiency = \frac{Qt - Qr}{Qt} \times 100$$

Equation 5.1

Where,

Q_t = the amount of drug initially used for the preparation of niosomes and
Q_r = the amount of drug present in supernatant after centrifugation.

10 µL of the supernatant was then diluted up to 10 mL with HPLC grade water and analyzed using the HPLC method described in ***Chapter 2***. The results were presented as mean ±SD.

5.2.5 Fourier transform-infrared spectroscopy (FT-IR)

To prove encapsulation of the drug and the formation of niosomes, FT-IR analysis was conducted using the Perkin-Elmer FT-IR Version 10.6.2 (Llantrisant, United Kingdom). Analysis was performed on CPH loaded niosomes and the excipient mixture (CPH, Tween® 80, amaranth red, cholesterol and SLS). All analysis was performed in triplicate.

5.2.6 pH of niosomal formulation

The pH of the niosomal formulation was monitored every 7 days using a model GLP 21 Crison® Instruments pH meter (Barcelona, Catalonia, Spain). The pH meter was calibrated daily using pH 4.00, pH 7.00, and pH 9.21 standard solutions. Following calibration, the pH of each formulation was measured (n = 3) by inserting the pH electrode into 20 mL of the product and observing the pH after 60 seconds, after which the electrode was rinsed with distilled water and dried in between readings to ensure accuracy and avoid cross-contamination. The results were presented as mean ±SD. The colour of the niosomal formulations was analyzed visually.

5.2.7 Surface tension measurements

Niosomes were prepared with and without cholesterol as described in **§ 5.2.2**, and surface tension of the niosomes was measured by the Du Noüy ring method using a Krüss Tensiometer (Model K100, Germany) at 25 °C. Ten measurements were performed for each formulation every 7 days for 28 days, and the results were reported as mean ±SD.

5.2.8 Vesicle permeability

To analyze the ability of the niosomal structure to keep out other drugs from the niosomal structure, the HPLC method described in ***Chapter 2*** was used**.** Carbamazepine (CBZ) was the chosen candidate drug to be used in this study based on the following:

a) CBZ has poor water solubility (< 200 µg/mL), has a Log P of 2.77 [268] and the drug is more likely to migrate to the lamellae of the niosomes but some will migrate to the core to a level similar to the saturation solubility in water.
b) CBZ R_t has already been established in ***Chapter 2*** and is known to be 5.283 minutes.

c) CBZ is readily available.

CPH loaded niosomes were prepared as described in **§ 5.2.2**, 150 mg of CBZ was added to the niosomal formulation, and the mixture was probe sonicated for 6 minutes at 11 % amplitude. The niosomes were then stored in an amber glass bottle at 4 °C overnight for further characterization.

Every 7 days, 2 mL of the formulation was withdrawn and ultra-centrifuged for 1 h at 4 °C (Eppendorf, Hamburg, Germany). The supernatant was collected, the pellet at the bottom of the centrifuge tube was washed twice with HPLC grade water. The water was then collected, and centrifugation was repeated. Drug concentration in the aqueous solution containing supernatants and water used for washing was determined. The mixture was analyzed using a validated HPLC method (***Chapter 2***).

5.2.9 ^{1}H NMR analysis

Using a Pasteur pipette, 0.7 mL of the CPH niosome solution was transferred to a beaker, the solution was moved into the fume hood and diluted with 0.7 mL of acetone. Using a Pasteur pipette, 0.7 mL of the diluted CPH niosomes was transferred into a clean 5 mm Nuclear Magnetic Resonance Spectroscopy (NMR) tube, filling the bottom 4.5 – 5 cm. The NMR tube was capped, labelled, and inserted into the spinner, avoiding contact between the sample and the cap. The outside of the NMR tube was cleaned using 2-propanol and lab tissues. The sample was then placed in the depth gauge, and the insertion depth was calibrated. After calibration, the sample was loaded into the Bruker® 4000 NMR spectrometer, and a computer workstation was used to acquire the ^{1}H NMR spectrum; Mn^{2+} was used as a shift reagent.

5.2.9.1 ^{1}H NMR solvent selection

When selecting a solvent for running ^{1}H NMR analysis, typically, a deuterated solvent is used to minimize background signals and provide a lock signal to compensate for drifts in the magnetic field [260]. However, there are several other factors to consider for ^{1}H NMR solvent selection. These include but are not limited to:

5.2.9.1.1 Solubility

Higher solubility of samples in the chosen solvent contributes to higher sensitivity. This property assumes significance in cases where sample availability is limited. The chosen solvent must be able to solubilize the sample to be run on the NMR spectrometer [269].

5.2.9.1.2 Purity

The degree of solvent purity is one of the primary selection criteria. Chemical impurities or water content can lead to interference signals in the ^{1}H NMR spectrum. Hence, the ^{1}H NMR solvent peaks will be observed at higher chemical shifts [261]. Solvent purity is of even more significant concern as the proportion of the isotope nuclei is much less than the major isotope. Even a little moisture can incorporate water's protons into the solvent, leading to problems during the NMR run [269].

5.2.9.1.3 Solvent viscosity

The lower the sample viscosity, the better will be the spectral resolution due to better homogenization of the sample. The ideal solvent must have a viscosity lower than that of the sample; this improves resolution [269].

5.2.9.1.4 Moisture content

As mentioned earlier, the presence of traces of water will contribute to spectral interference as water itself contains two protons, this degrades the ^{1}H NMR spectra quality, but the fact that almost all solvents have some water content cannot be denied; they tend to absorb this water from the atmosphere around them [270]. In order to avoid this, the bottle of the solvent must be appropriately sealed. If the water content has already developed in the bottle, it has to be reduced by filtration of solvent through a drying agent or storing the solvent over molecular sieves [269].

5.2.9.1.5 Deuterated Solvents

^{1}H NMR solvents are distinctly different from other spectroscopic solvents as most hydrogen nuclei are replaced with deuterium to minimize interference due to protons. Though deuterium also has a nuclear spin, it does not operate on the same frequency as protons in the given magnetic field [269]. Therefore, it serves the purpose of NMR spectroscopy.

Table 5.1 shows the solvent selection parameters considered before selecting a solvent.

Table 5.1 Solvent selection for ^{1}H NMR analysis.

Solvent	Solubility	Interfering peaks	Purity	Availability	Solvent viscosity higher than sample?
Dimethyl sulfoxide	No	No	No	Yes	Yes
Deuterated water	-	No	-	No	No
Acetone	Yes	No	Yes	Yes	No
Deuterated chloroform	-	No	-	No	No

Acetone was readily available, in pure form, and was able to solubilize the sample. The solvent will show peaks at 2.2 – 2.4 ppm [271, 272] and will not interfere with the peaks from the sample. Therefore, acetone was selected as the suitable solvent to perform the ^{1}H NMR analysis.

Niosome lamellarity was calculated as reported by Jousma [273]. In the case of Mn^{2+}, lamellarity (L) was calculated by the percentage of relative loss of signal from the peak area before and after the addition of Mn^{2+}. The number of bilayers was calculated as shown in **Equation 5.2.**

$$L = 1002 \times relative\ loss\ of\ signal\ \%$$

Equation 5.2

5.2.10 Surface morphology and elasticity

The surface morphology and elasticity of the CPH loaded niosomes were examined using a transmission electron microscope (TEM). A drop of the niosome solution was stratified onto a carbon-coated copper grid and left to adhere on the carbon substrate for about 1 minute. The excess solution was removed by filter paper. The resulting thin film was stained with a drop of 2 % amaranth dye solution. The sample was air-dried and observed at 80 kV in a Zeiss Libra 210 TEM (4000 mva magnification and illumination angle = 1.00). Digital images were acquired with a Mega view Olympus SIS digital camera (1376 x 1032 x 16) [273].

To measure the elasticity, niosomal dispersions were centrifuged for 1 hour to obtain the largest fraction of vesicles residing in the pellet. Aliquots were diluted with water to obtain the minimum number of vesicles in a 0.1 ml volume of water to avoid blockage of the micropipette. A micropipette filled with 0.1 ml of diluted vesicle dispersion was connected to an electric pump via

non-expandable tubing (backfilled with water). The contents of the micropipette were constantly observed at a point just before the narrow part of the pipette. Once a vesicle was in view, the pressure was turned off, and the uncompressed vesicle image was captured using a video camera. The pressure was gradually raised, and the vesicle was forced into the narrow part of the micropipette, where the images of the deformed vesicle were captured and magnified under a TEM [273].

5.3 Results and discussion

5.3.1 Vesicle size, Zeta potential, and PDI

In colloidal delivery systems, the mean vesicle size of dispersed phases plays a vital role in stability, turbidity, and bioavailability. Colloidal systems with larger mean vesicle sizes usually show more colloidal instability (gravitational separation), higher solution turbidity, and lower bioavailability [273]. The mean vesicle sizes are shown in **Figure 5.1**, and the PDI values of the niosome formulations and Zeta potential are shown in **Table 5.2**. Over the 4 weeks, the mean size of vesicles ranged from 120.91 to 191.03 nm for the vesicles stored at room temperature (25 ℃) and 186.70 to 191.03 nm for vesicles stored at 4 ℃. Niosomes tend to aggregate over time, and this leads to an increase in vesicle size. In this study, no significant change was seen in the niosomes stored at 4 ℃; the difference in vesicle size is less than 10 nm between week 0 and week 4. The same cannot be said with the niosomes stored at room temperature. A significant drop in vesicle size is noticeable, with the difference between week 0 and week 4 > 70 nm. Size changes (**Figure 5.1**) were recorded during storage at 4 °C and 25 °C and contradicted the findings from previous research, which stated that larger vesicles would eventually form at high temperatures due to greater aggregation [273].

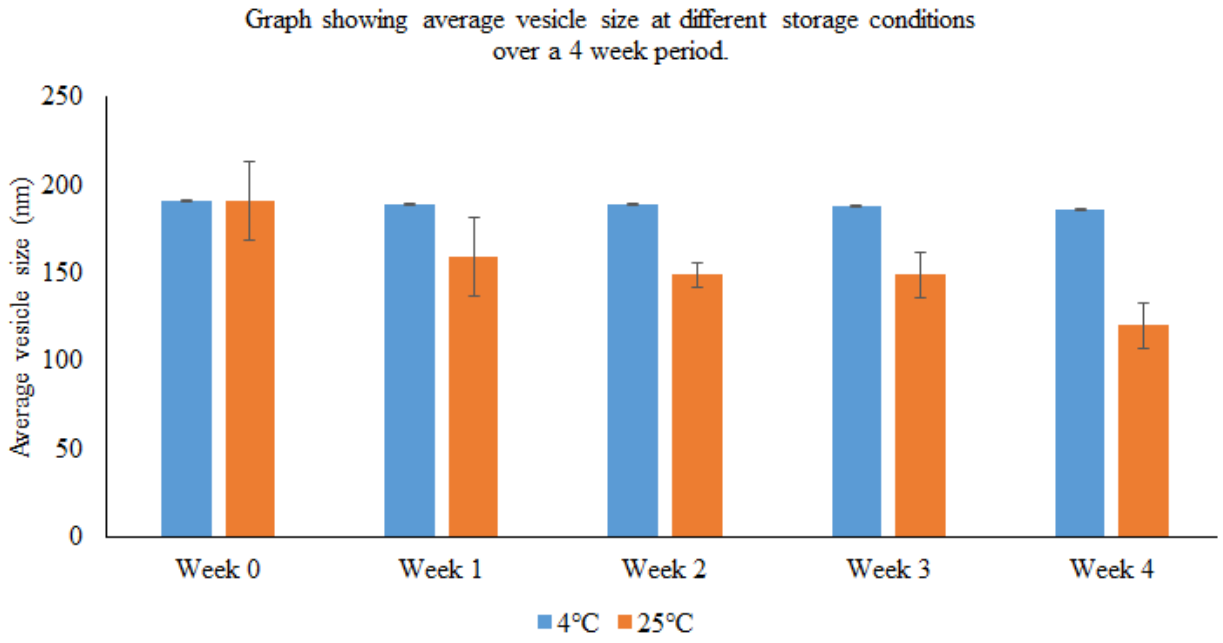

Figure 5.1 Graph showing the average vesicle size over 4 weeks.

The decrease in vesicle size coincided with a decrease in niosome entrapment efficiency of the vesicles stored at 25 °C (**Figure 5.2**). Based on the changes in entrapment efficiency and vesicle size, the decrease in vesicle size could be attributed to the drug leaking out of the niosomes, thus decreasing the vesicle size. The vesicles stored at 4 °C showed no significant change in vesicle size, and as a result, no significant change was seen in entrapment efficiency. Drug leakage could be the reason behind the decrease in vesicle size at 25 °C. The information presented by Figure 5.1 is not in agreement with literature which states that niosome size increases over time due to vesicles aggregating [273]. This area is an area of future study.

The magnitude of the Zeta potential indicates the degree of electrostatic repulsion between adjacent and similarly charged particles in dispersion [274]. For molecules and particles that are small enough, a high Zeta potential will confer stability. Attractive forces may exceed this repulsion when the potential is high, and the colloidal dispersion may flocculate. The stability of niosomes relates to a balance between the attractive van der Waals forces between vesicles and the electrical repulsion [275].

To determine electrostatic repulsion between niosomes and stability of the system, the Zeta potential of the formulation was measured every 7 days for 28 days (**Table 5.2**). The Zeta

potential of the different CPH loaded niosomes varied between −39.18 and −48.77 mV for the vesicles stored at 4 °C and −39.18 to −45.50 mV for the vesicles at 25 °C.

Table 5.2 Table showing the Zeta potential and PDI of vesicles stored at 4 °C and 25 °C.

		Week 0	Week 1	Week 2	Week 3	Week 4
Zeta potential(mV) avg ±SD	4 °C	-39.18±3.28	-41.61±0.72	-42.41±3.90	-44.53±1.76	-48.77±2.03
	25 °C	-39.18±3.28	-40.61±2.71	-42.47±0.97	-44.71±1.49	-45.50±0.31
PDI average ±SD	4 °C	0.31±0.059	0.31±0.031	0.32±0.017	0.34±0.028	0.34±0.024
	25 °C	0.31±0.059	0.36±0.027	0.35±0.025	0.35±0.030	0.36±0.037

As shown in **Table 5.2**, all the vesicles had a Zeta potential < -30 mV, this shows that the niosomes will be stable over time and will not fuse or aggregate. According to Asthana et al. [276], niosome vesicle size increases when stored at room temperature; this is because niosomes tend to aggregate and fuse, forming larger blocks that increase in vesicle size. Instead of increasing in size, the niosomes in this study decreased in size over time (4 weeks) and could be attributed to the fact that the low Zeta potential (-30 mV) did not allow the vesicles to come together and aggregate as the repulsion between the vesicles was much stronger than attraction.

PDI is a term that shows the uniformity of particle size distribution in a solution medium. Lower PDI is associated with the narrower distribution of vesicle size, which leads to lower instability, such as Ostwald ripening (mass transfer from smaller vesicles to larger ones) [277]. The colloidal system with a PDI value lower than 0.05 is considered a monodisperse system, while the dispersion with a PDI value greater than 0.70 shows a very wide particle size distribution [278]. Small vesicle size and PDI value prevent or delay Ostwald ripening, which induces higher stability in dispersion [279, 280].

The PDI values of the CPH loaded niosomes were in the range of 0.31 – 0.36. Minor changes in PDI values for both storage conditions were noticeable over 4 weeks. All the vesicles, regardless of storage condition, retained their dispersity characteristics, and the sufficient repulsion produced by the low Zeta potential is responsible for this phenomenon. The vesicles had more repulsive forces than attractive forces between them, and thus, the vesicles could not fuse and aggregate. Consequently, the PDI only showed minor changes (< 0.1).

5.3.2 Entrapment efficiency

Entrapment efficiency is expressed as the ability of the vesicle to maintain active molecules (encapsulant for core ingredient) in the bilayer membrane or the aqueous core of the vesicles [280]. In this research work, entrapment efficiency values ranged from 30.08 to 90.07 % for the niosomes stored at room temperature for 4 weeks (25 ℃) and 84.61 to 90.07 % for the vesicles stored at 4 ℃ for 4 weeks. **Figure 5.2** shows the entrapment efficiency over 4 weeks.

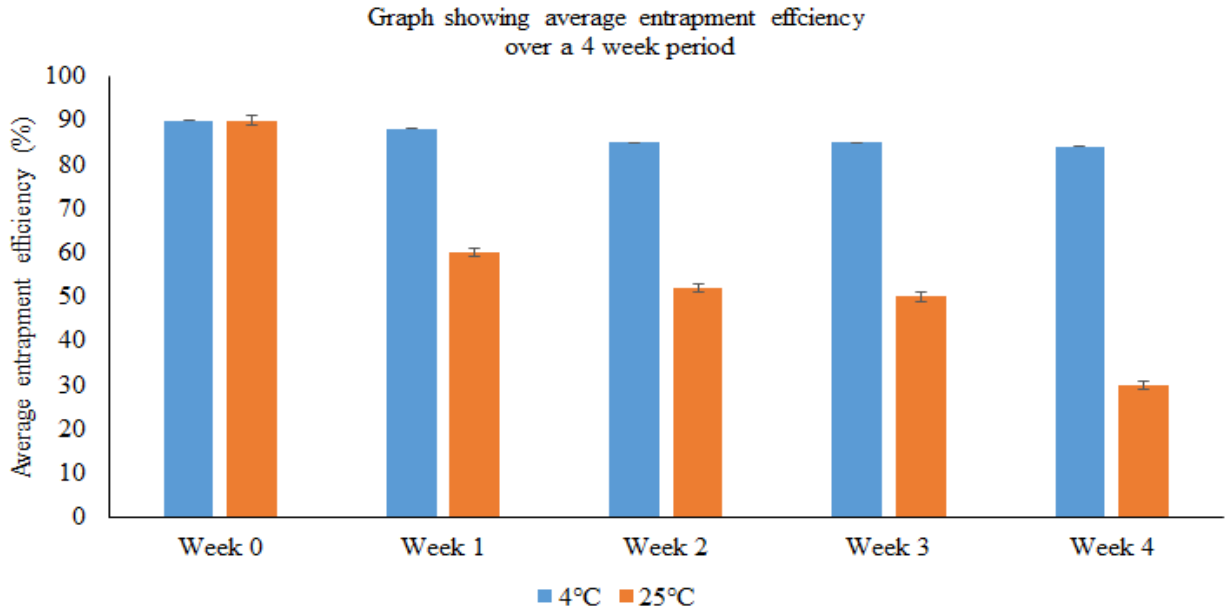

Figure 5.2 Graph showing the average entrapment efficiency of CPH niosomes at two different storage conditions over 4 weeks.

The vesicles stored at 4 ℃ for 4 weeks showed minor changes in entrapment efficiency over 4 weeks. The difference is less than 10 %. The vesicle size at 4 ℃ also remained relatively constant during this period as only minor changes were seen. The same cannot be said with the vesicles stored at 25 ℃ for 4 weeks, as a significant drop of almost 30 % in entrapment efficiency was seen after week 1. The entrapment efficiency continued dropping until the week 4 mark and could be explained by possible drug leakage from the niosomes. Cholesterol gives rigidity to the niosome bilayer, but higher temperatures tend to reduce the rigidity of the niosome bilayer, making them more fluid. In this study, when the niosomes were exposed to room temperature (25 ℃), a significant drop in entrapment efficiency was visible as the rigidity of the niosomes was compromised, most likely leading to leakage of the drug. Consequently, the niosomes also showed a decrease in vesicle size in this period, this is an area of further study.

5.3.3 Fourier-transform infrared spectroscopy

In this study, FT-IR analysis was conducted to prove encapsulation of CPH into the niosomal structure. FT-IR is an important and valuable method for identifying different molecule and interaction types and giving us helpful information about compounds' chemical structure and functional groups. FT-IR spectrum of the niosomal formulation and the excipient mixture is shown in **Figure 5.3**.

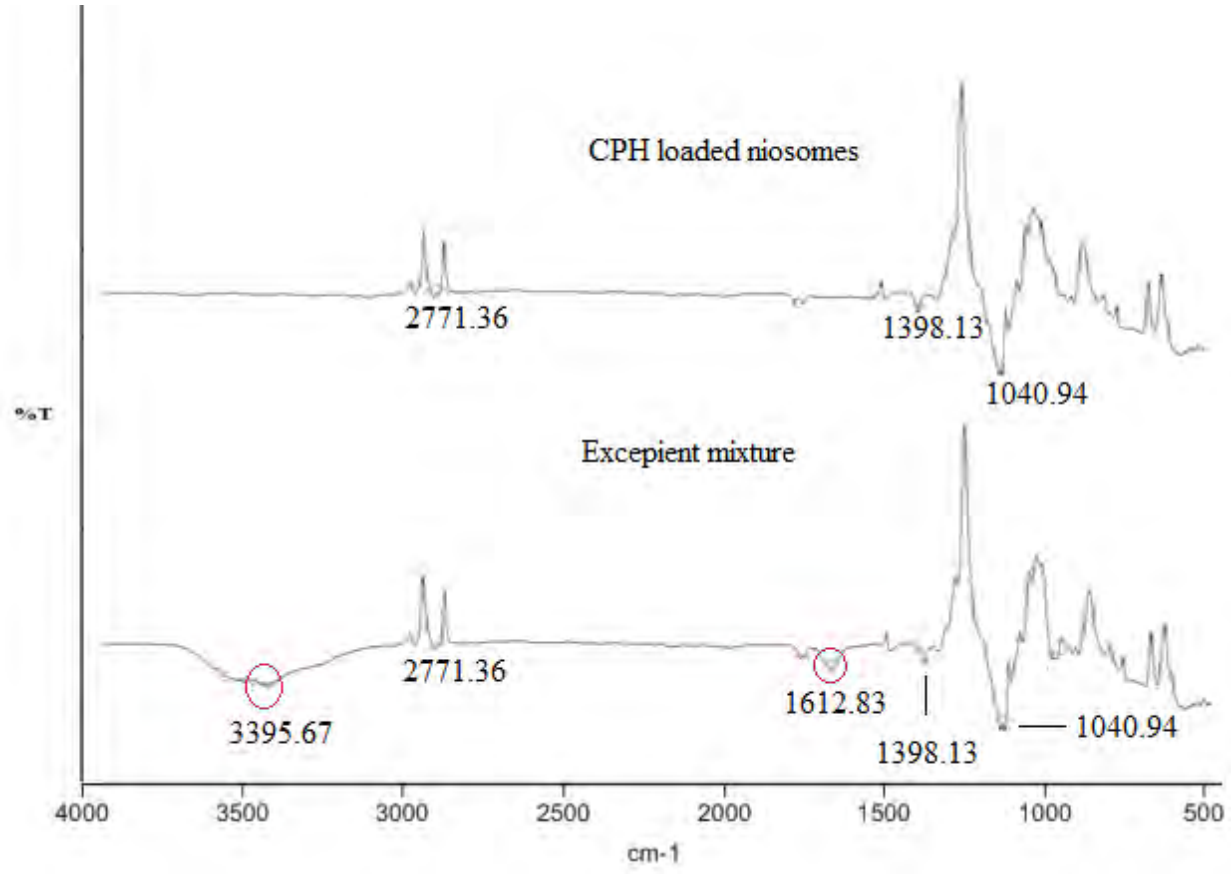

Figure 5.3 FT-IR spectrum of CPH loaded niosomes and the excipient mixture.

The changes in the structure or formation of new compounds can be identified by the displacement of bands, variations in their height, or exhibition of new bands. CPH loaded niosomes showed C-H stretching (C–H) at 2771.36 cm^{-1}, bending vibrations of OH group 1398.13 cm^{-1}, and the fluorine group at 1040.94 cm^{-1}. CPH's characteristic bands were determined in the excipient mixture at 3395.67 cm^{-1} (OH stretching vibration) and 1612.83 cm^{-1} (quinolones); both these were not visible in the CPH loaded niosomes spectrum. Venishki and Mohammad [281] studied FT-IR spectrums of CPH loaded niosomes and showed no

chemical interaction between the bioactive molecule (CPH), cholesterol, and the surfactants used SLS and Tween® 80. The FT-IR spectra of the excipient mixture and CPH loaded niosomes delineate most of the main characteristic summits of SLS, Tween® 80, and cholesterol, as shown in ***Chapter 3***. Also, the disappearance of the OH stretching vibration (3395.67 cm^{-1}) and the quinolone vibration (1612.83 cm^{-1}) of the CPH molecule in the CPH loaded niosome spectrum indicated that the drug molecule was loaded successfully into the niosomal formulation.

5.3.4 Colour and pH

Otitis media is a common problem managed by otolaryngologists and general practitioners [280, 281]. A wide variety of topical ear drop preparations is available for the treatment of this condition. These preparations include antibiotics [282], steroids [283], aluminum acetate [284], acetic acid [285], and preparations containing combinations of both an antibiotic and a steroid [286]. Previous studies have demonstrated that the acidic pH of the ear canal plays a protective role against infection [287-290] and pH remains a key consideration in the development of all otic preparations.

In this study, CPH loaded niosomes for transtympanic delivery were stored at two different storage conditions, 4 ℃, and 25 ℃. The pH and colour were monitored every 7 days for 4 weeks. The target was for the formulation to stay within the 7.1 - 7.8 pH range throughout the 4 weeks as this is the same pH as the pH of an ear canal affected by otitis media. **Table 5.3** shows the colour and pH change over 4 weeks.

Table 5.3 Table showing changes in colour and pH over 4 weeks.

		Week 0	Week 1	Week 2	Week 3	Week 4
Average pH ±SD	4°C	7.45±0.26	7.45±0.42	7.41±0.30	7.45±0.17	7.46±0.20
	25°C	7.45±0.26	7.46±0.27	7.42±0.37	7.44±0.15	7.45±0.31
Colour	4°C	Milky white	Milky white	Milky white	Milky white	Milky white
	25°C	Milky white	Milky white	Milky white	Milky white with Precipitate	Milky white with Precipitate

As shown in **Table 5.3**, the pH of the niosomal formulations at both storage conditions was able to stay within the 7.1 - 7.8 pH range; this shows that they are less likely to irritate the ear canal. The niosomal formulations in both storage conditions showed no changes in colour throughout the 4 weeks, and the formulation maintained a milky white colour with minimal precipitate. SLS and cholesterol are fine white powders; the milky white appearance of the CPH loaded niosomes is probably due to the high amounts of SLS and cholesterol used to manufacture the niosomal formulation.

Table 5.4 shows the niosomal formulations at different periods over 4 weeks. For illustrative purposes, the niosomal formulations were transferred into 100 mL clear glass bottles.

Table 5.4 CPH niosomal formulations over 4 weeks.

	25 °C	4 °C
Week 0		
Week 1		

Week 2		
Week 3		

Week 4		

5.3.5 Surface tension measurements

Surface tension is the tendency of liquid surfaces to shrink into the minimum surface area possible. Surface tension allows heavier and denser than water objects such as razor blades and insects to float and slide on a water surface without becoming even partly submerged. The du Noüy ring method is a technique for measuring the surface tension of a liquid [291]. The method involves slowly lifting a ring, often made of platinum, from the surface of a liquid. The force required to raise the ring from the liquid's surface is measured and related to the liquid's surface tension, as shown in **Equation 5.3.**

$$\gamma = \frac{1}{2} \times \frac{F}{L}$$

Equation 5.3

Where,

γ = Surface tension (N/m),

F = Force (N) and

L = Length along which the force is felt (m).

The Du Noüy method utilizes the interaction of a platinum ring with the surface of the liquid [292]. The ring is submerged below the interface by moving the stage where the liquid container is placed. After immersion, the stage is gradually lowered, and the ring pulls up the meniscus of the liquid. Eventually, this meniscus tears from the ring. Before this event, the volume (and thus the force exerted) of the meniscus passes through the maximum value and begins to drop before the actual tearing event. **Figure 5.4** shows an illustration of the Du Noüy ring method for measuring surface tension.

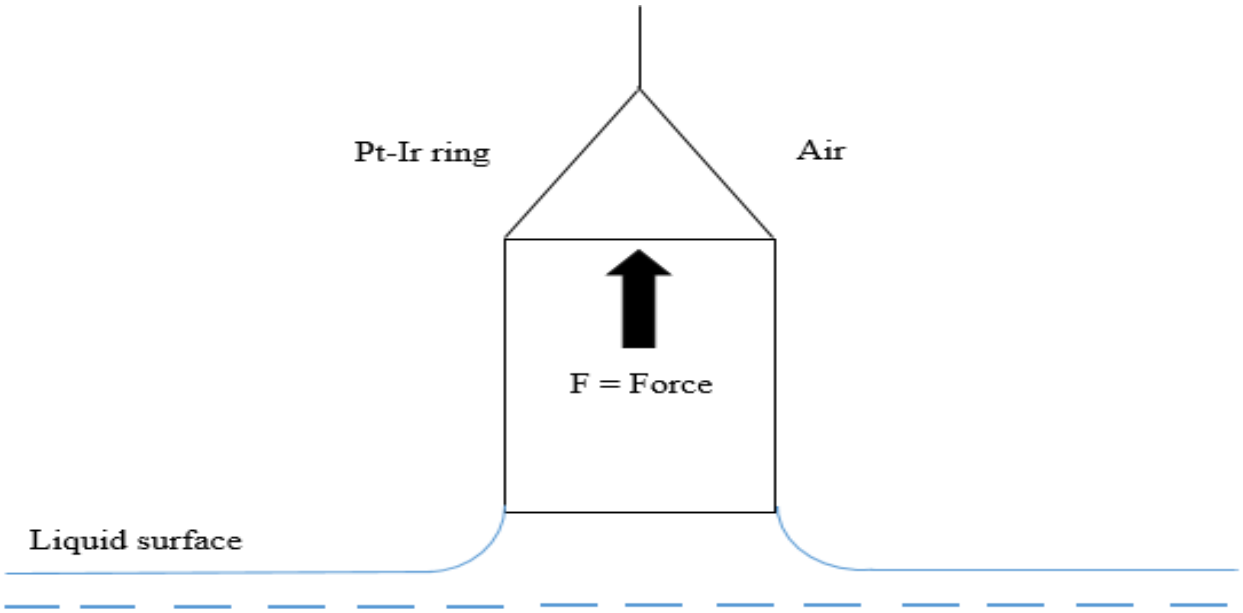

Figure 5.4 The Du Noüy ring method for measuring surface tension.

The calculation of the surface or interfacial tension by this technique is based on the measurement of this maximum force. The depth of immersion of the ring and the level to which the ring is raised when it experiences the maximum pull is irrelevant to this technique. The original calculations are based on the ring with the infinite diameter (or wire) and do not consider the excess liquid pulled up due to the proximity of one side of the ring to the other [293].

To find the maximal stability and niosome functionality, the surface tension of the niosome should be estimated [294]. The surface tension of niosomes is related to the surfactant and cholesterol content, and the results revealed that cholesterol insertion in the niosome bilayer decreases surface tension (**Figure 5.5** and **Figure 5.6**) [294-296]. The surface tension difference between CPH niosomes with cholesterol and CPH niosomes without cholesterol was significant ($P < 0.05$). As Azarbayjani *et al.* [296] and also Vargha-Butler *et al.* [297] have reported, a decrease in the surface tension value with increasing cholesterol content indicates that the surface of the bilayer becomes less hydrophilic, which leads to increased membrane integrity and rigidity and further proves that a niosomal bilayer has been formed.

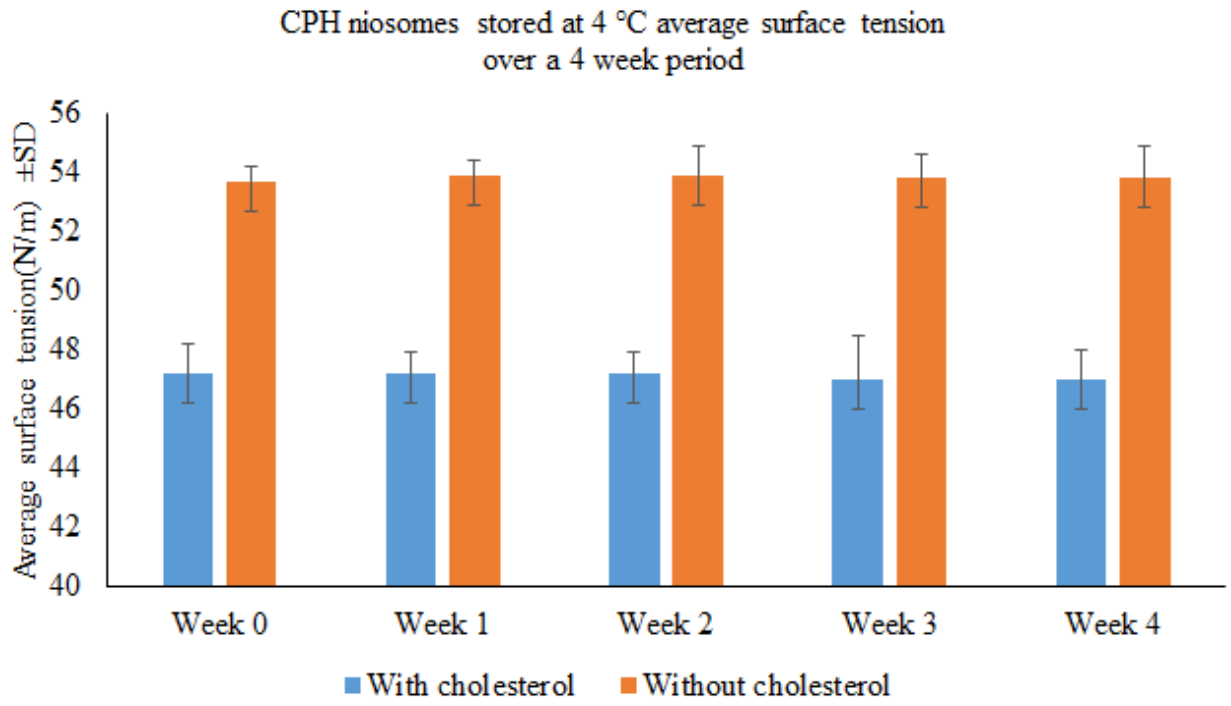

Figure 5.5 Graph showing the average surface tension for CPH niosomes at 4 °C with and without cholesterol.

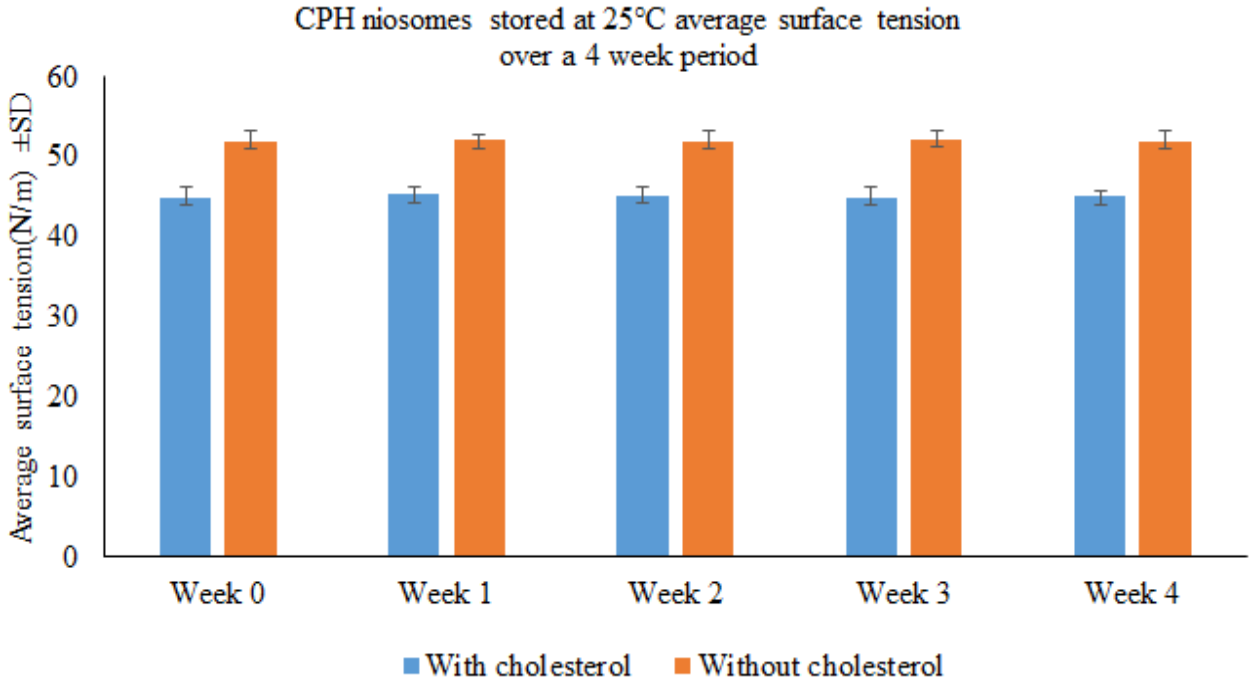

Figure 5.6 Graph showing the average surface tension for CPH niosomes at 25 °C with and without cholesterol.

As shown in **Figures 5.5** and **5.6**, CPH loaded niosomes stored at 4 °C, and 25 °C showed a decrease in average surface tension when cholesterol was added. Cholesterol is very non-polar except for the hydroxyl group attached to the first ring [297]. The addition of cholesterol makes the niosomal bilayer more hydrophobic, thus increasing niosomal rigidity and integrity, resulting in less leaky niosomes. The addition of cholesterol to the CPH niosomes showed a decrease in average surface tension over the 4 weeks, proving that the CPH loaded niosome bilayer will become more hydrophobic and will be able to maintain its integrity and rigidity and will not leak the entrapped drug.

To further emphasize the effect of cholesterol on CPH loaded niosomes, entrapment efficiency was calculated for CPH niosomes with and without cholesterol as described in **§ 5.2.4**. As shown in **Figures 5.7** and **5.8**, CPH niosomes formulated without cholesterol showed a rapid decrease in entrapment efficiency over the 4 weeks. Cholesterol adds rigidity and integrity to the niosomes. As a result, niosomes formulated without cholesterol showed a rapid decrease in entrapment efficiency.

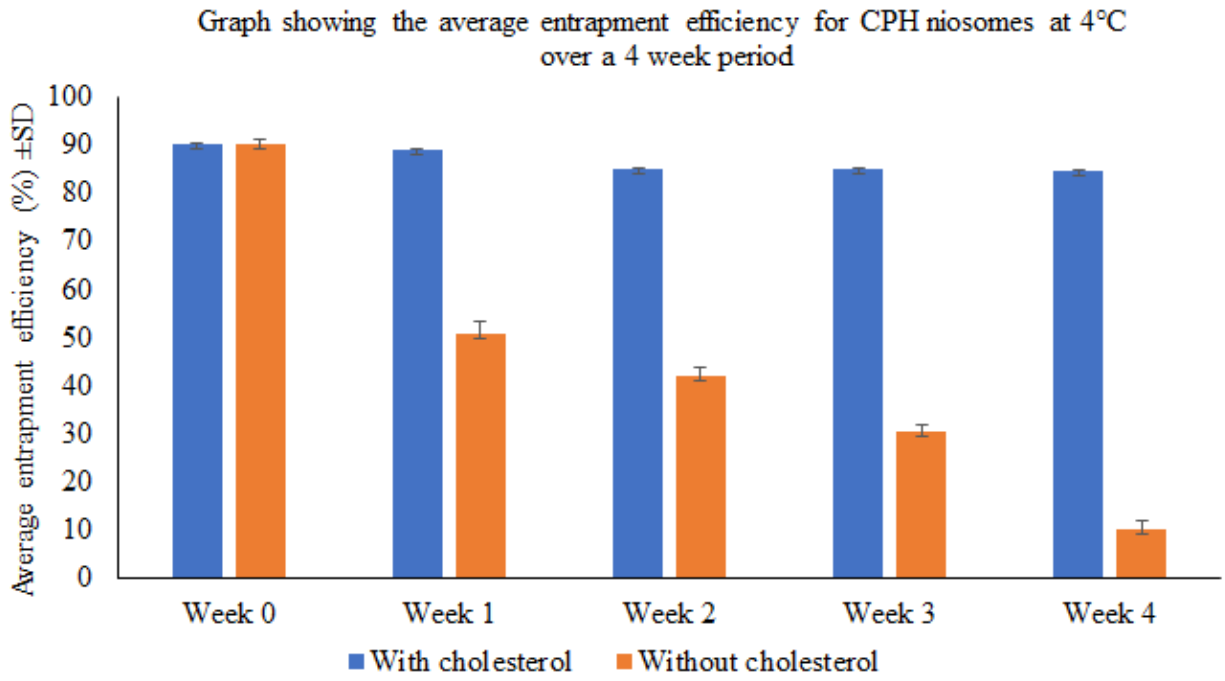

Figure 5.7 Graph showing the average entrapment efficiency of CPH niosomes at 4 °C over 4 weeks.

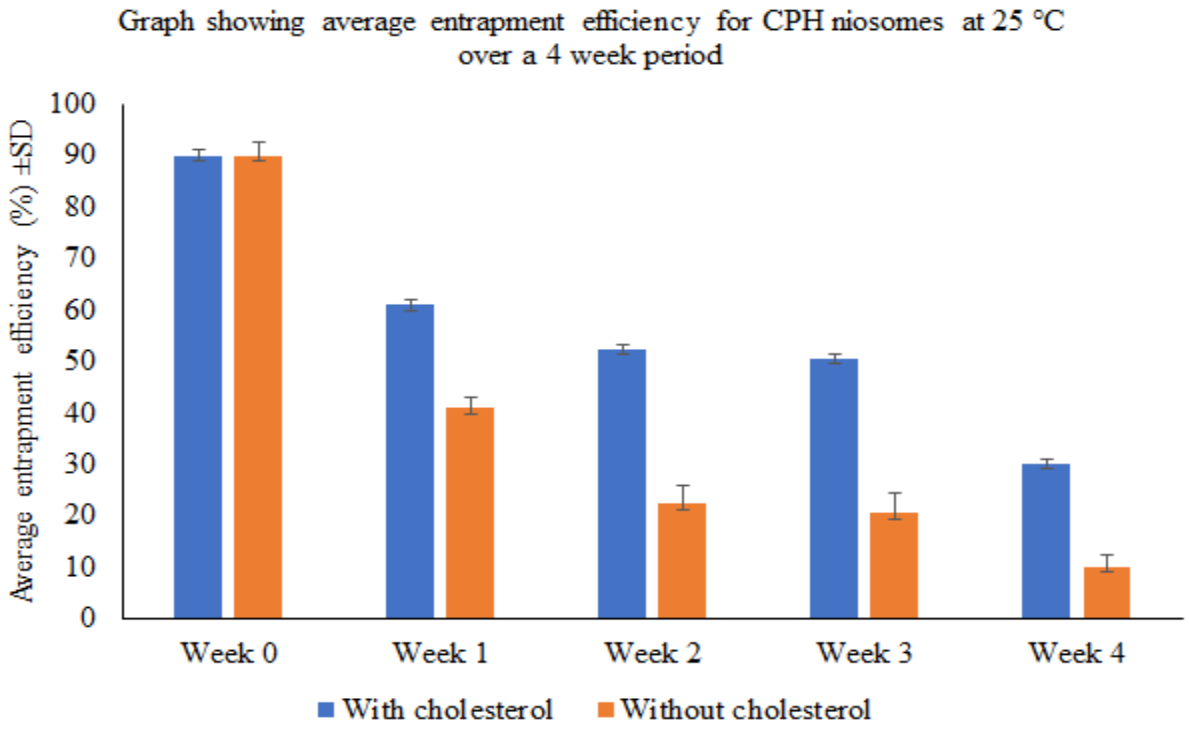

Figure 5.8 Graph showing the average entrapment efficiency of CPH niosomes at 25 ℃ over 4 weeks.

A high leakage is predictable for cholesterol-free niosomes. As shown in **Figures 5.7** and **5.8**, cholesterol-free niosomes had a higher leakage compared to cholesterol-containing niosomes. The incorporation of cholesterol caused a more ordered membrane and decreased leakage. The leakage of CPH vesicles with cholesterol at both 4 °C and 25 °C after 4 weeks was more two-fold lower than that of CPH niosomes without cholesterol, revealing that the incorporation of cholesterol into the niosomes leads to decreased vesicle leakage. Tween® 80 has a low transition temperature due to the unsaturated double bonds in their side chains [298], decreases in leakage occur through the formation of hydrogen bonds between the hydroxyl groups of cholesterol and the oxygen at the ester groups, or with the other functional oxygen groups of Tween® 80, thus enhancing the stability of the bilayer. It has been previously reported that including cholesterol in niosomes decreased the leakage of encapsulated content [294].

Figure 5.9 is a schematic diagram showing the possible hydrogen bonding interaction between the β-OH group of the cholesterol and the oxygen primarily at the ketone group of Tween® 80.

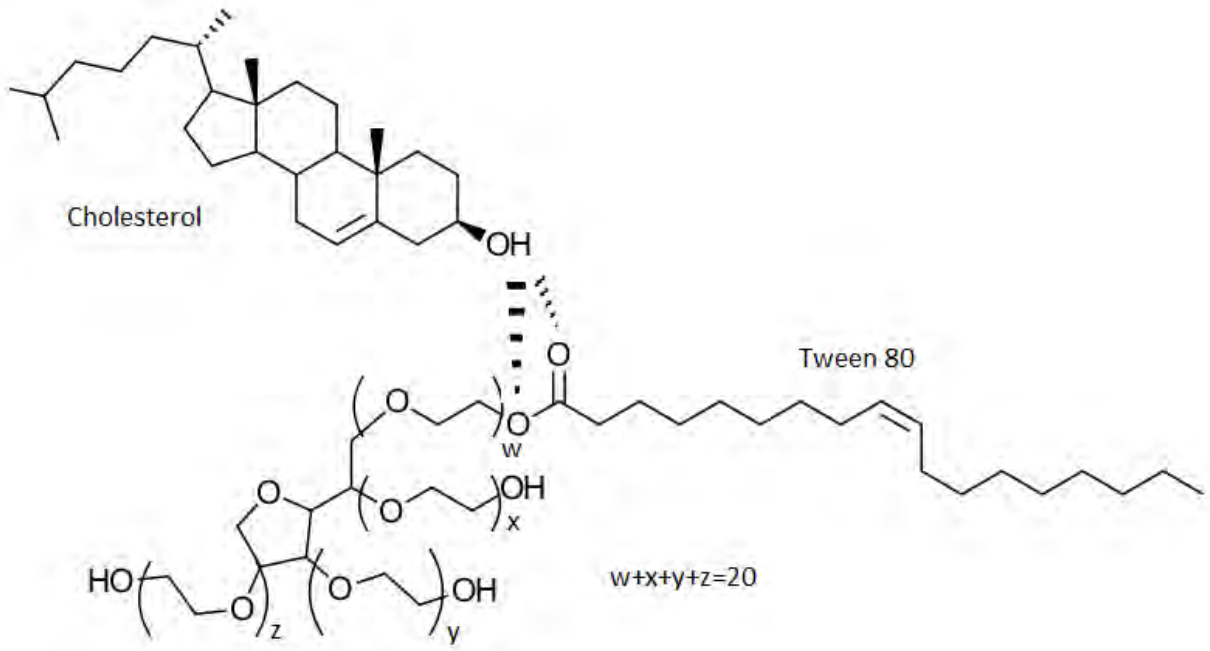

Figure 5.9 Schematic showing the possible hydrogen bonding interaction between the β-OH group of the cholesterol and the oxygen primarily at the ketone group of Tween® 80. Adapted from [299].

Figure 5.9 is a schematic showing the possible interaction between cholesterol and Tween® 80 within the bilayers of the niosome membrane. It is possible that the small hydrophilic 3 β-hydroxyl (β-OH) head group of the cholesterol in the bilayers can position itself in the vicinity of the Tween® 80 ester group the hydrophobic steroid ring orients itself parallel to the acyl chains of the non-ionic surfactant. This positioning may, in effect, restrict the movement of the acyl chains of the bilayer. As shown in **Figure 5.9**, the β-OH group could form a hydrogen bond with the oxygen at the ester group of the Tween® 80. However, it is also possible to form hydrogen bonds at the other oxygen functionalities of Tween® 80, which further enhances the stability of the bilayer. These interactions increase membrane cohesion, there is only one possible hydrogen bonding group on the cholesterol moiety. The results of this study suggest that the CPH niosomes stored at 4 °C are of sufficient integrity and rigidity and will be able to entrap and deliver the active ingredient [299, 300].

5.3.6 Vesicle permeability and rigidity

To test the permeability of CPH niosomes stored at 4 °C and 25 °C, respectively, over 4 weeks, a validated HPLC method was used. It has already been established in **§ 5.3.2** that the entrapped drug CPH can leak out the niosomal structure. Therefore, this study was performed to assess the penetrability of CPH loaded niosomes to establish whether the formulated niosomes can be penetrated by other drugs with CPH also entrapped in the niosomal structure. This is particularly important because as niosomes move through the biological system, they are exposed to different chemicals. It is paramount that these do not cross the niosomal bilayer as this affects the stability of the entrapped drug, vesicle size, and entrapment efficiency.

Figures 5.10 and **5.11** show the HPLC chromatograms of CPH niosomes stored at 4 °C and 25 °C, respectively, for 4 weeks.

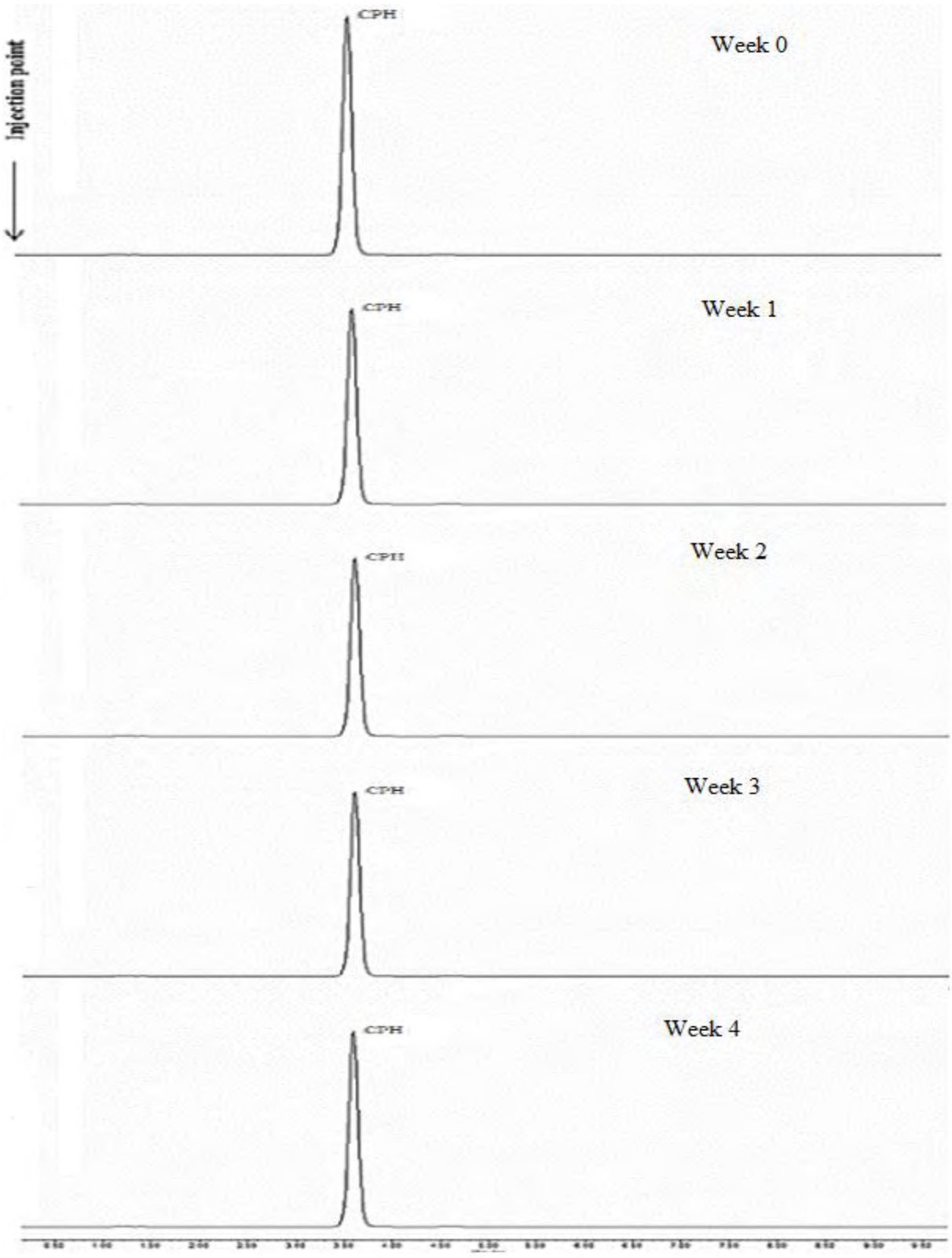

Figure 5.10 HPLC chromatograms produced by CPH niosomes stored at 4 ˚C.

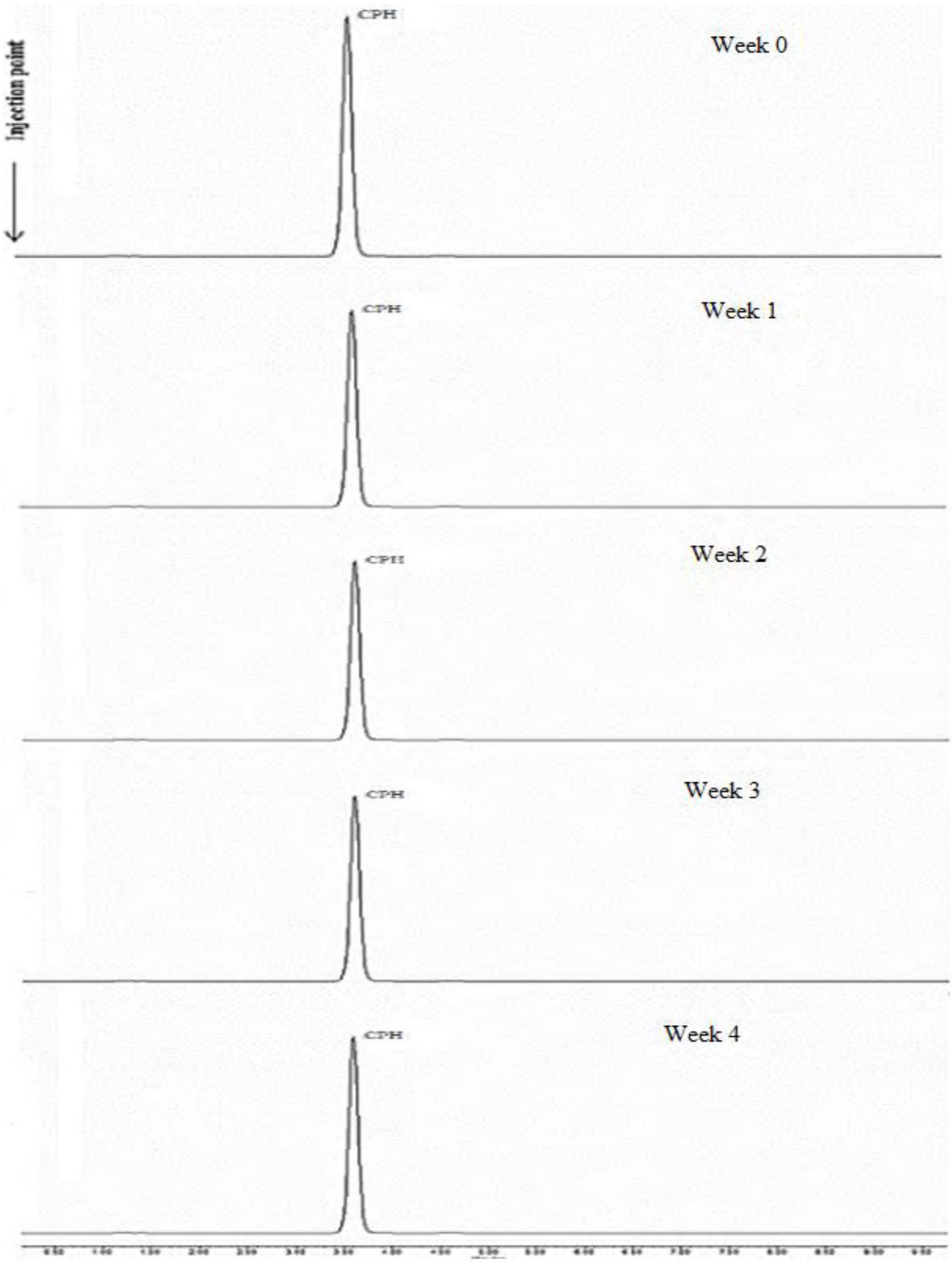

Figure 5.11 HPLC chromatograms produced by CPH niosomes stored at 25 ˚C.

As shown in **Figures 5.10** and **5.11,** CBZ could not penetrate through the niosomal structure of the formulated CPH niosomes. The results suggest that the CPH niosomes will keep out outside substances and toxins when introduced into the biological system. This impenetrability of the CPH niosomes could be attributed to the addition of cholesterol into the niosomal formulation. Cholesterol forms the bilayer in niosomes while also adding rigidity and integrity to the niosomal bilayer; this rendered the CPH niosomes impenetrable over 4 weeks.

5.3.7 ^{1}H NMR analysis

The number of lipid bilayers (lamellarity) of niosomes influences the encapsulation efficiency and the release kinetics of drugs. Additionally, when niosomes are taken up or processed in the cell, the intracellular fate of the drug is affected by the lamellarity [301]. The analysis of niosome lamellarity is, therefore, an important parameter to be considered [301, 302]. Numerous methods for determining niosome lamellarity include electron microscopic techniques (freeze-fracture), cryo-electron microscopy [302], and small-angle X-ray scattering [303]. Labelling amino-containing lipids by impermeable reagents and binding of radiolabelled ions has also been used to determine the ratio of outer-monolayer lipid to total membrane lipid [302, 304].

The usefulness of ^{1}H NMR in the study of membrane structures derives from the anisotropic nature of the molecular motion within liquid-crystalline lipid bilayers. Therefore, the motion and organization of phospholipids in membranes and even the shape of vesicles can be investigated [305]. A straightforward application of ^{1}H NMR in the quality control of niosomes is determining size and lamellarity [305]. Dispersions of large multi-lamellar vesicles (MLV's) give rise to very broad powder ^{1}H NMR spectra due to the restricted anisotropic motion, whereas small uni-lamellar vesicles (SUV's) are characterized by a narrow line spectrum [305]. The ^{1}H NMR spectra are shown in **Figures 5.12**, **5.13**, **5.14**, and **5.15.**

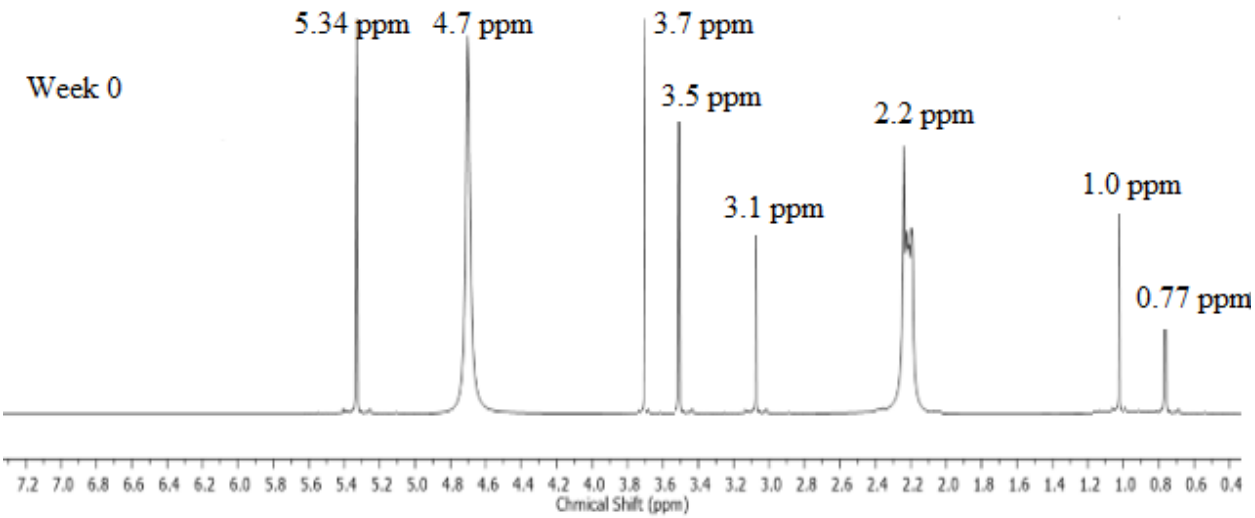

Figure 5.12 CPH niosomes stored at 4 °C ^{1}H NMR spectrum (week 0).

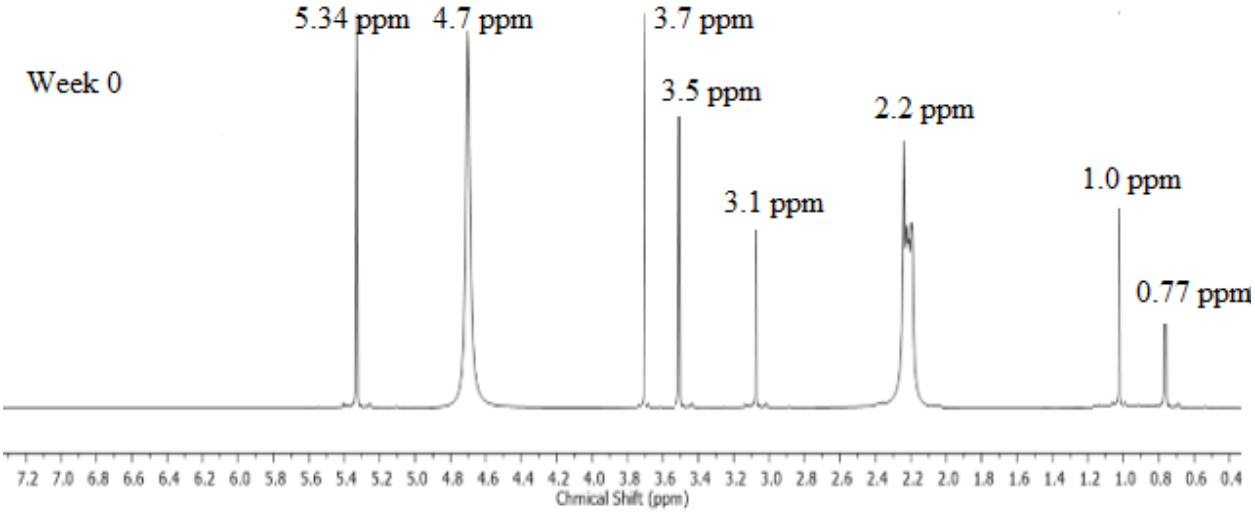

Figure 5.13 CPH niosomes stored at 25 °C ^{1}H NMR spectrum (week 0).

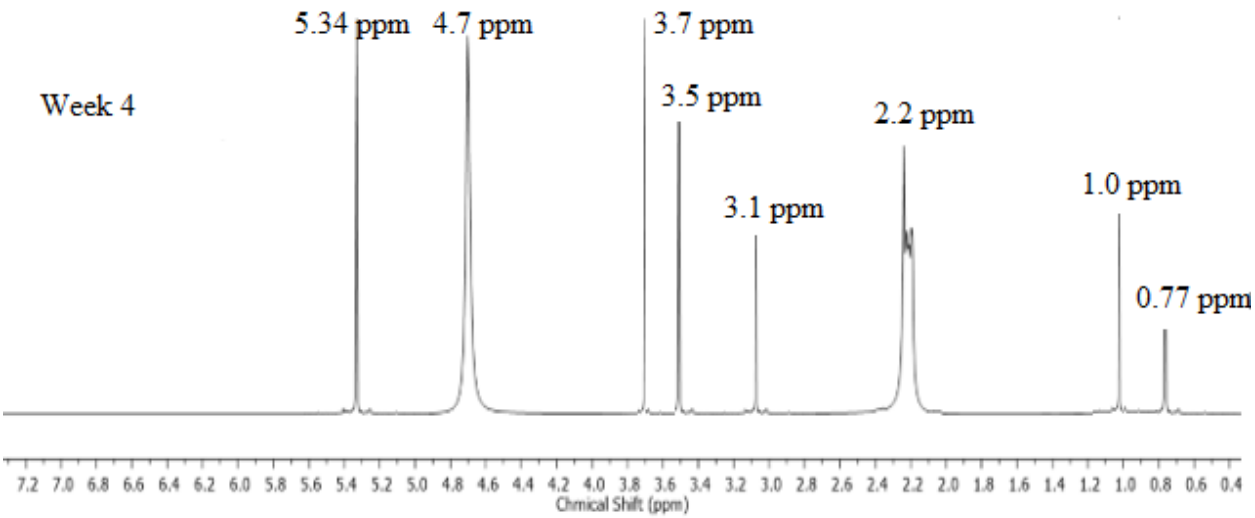

Figure 5.14 CPH niosomes stored at 4 °C ^{1}H NMR spectrum (week 4).

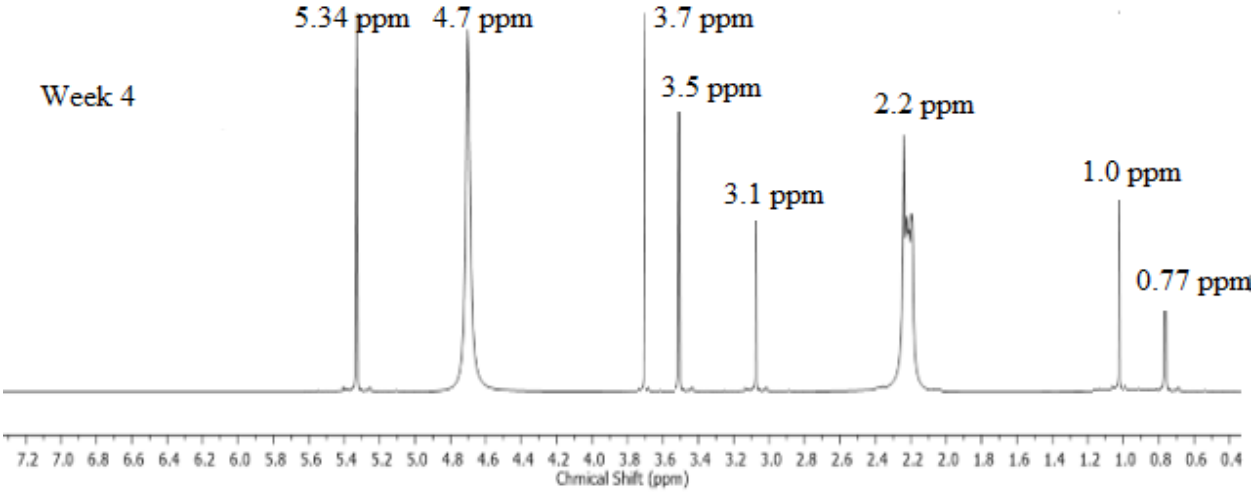

Figure 5.15 CPH niosomes stored at 25 °C ^{1}H NMR spectrum (week 4).

The multi peaks (δ = 0.77 ppm and δ = 1.0 ppm) correspond to the methyl structure on cholesterol and SLS, respectively, and the single peak (δ = 2.2 ppm) is formed by acetone which was used as a solvent. The short peak at δ = 3.1 ppm and δ = 5.34 ppm is the alcohol groups on Tween® 80 and cholesterol, respectively. Peaks at δ = 3.5 ppm and δ = 3.7 ppm were produced by the RO-CH_3 (C is attached to O) group in cholesterol and SLS. Water produced the peak at δ = 4.7 ppm [305]. **Table 5.5** shows the lamellarity of the CPH loaded niosomes over 4 weeks.

Table 5.5 Determination of niosome lamellarity using Mn^{2+} as a shift reagent.

Sample	Calculated average lamellarity ±SD
CPH niosomes stored at 4 °C (week 0)	1.23 ±0.19
CPH niosomes stored at 4 °C (week 4)	1.20 ±0.34
CPH niosomes stored at 25 °C (week 0)	1.23 ±0.52
CPH niosomes stored at 25 °C (week 4)	1.28 ±0.25

Penetration of Mn^{2+} through vesicle membranes under certain circumstances limits the use of this ion as a shift reagent for analysis of niosome lamellarity, other shift reagents such as $PrCl_3$, $Pr(NO_3)_3$, $EuCl_3$, and $Eu(NO_3)_3$ can also be considered [305, 306]. In this case, vesicle size measurements before and after adding Mn^{2+} (**Table 5.6**) agreed with the results obtained in **§ 5.3.1** and **§ 5.3.6**. The CPH niosomes prepared are impenetrable, and that LUVs were prepared as shown in **Table 5.5**.

Table 5.6 Average vesicle sizes (nm) ±SD before and after the addition of shift reagent Mn^{2+}.

Formulations	Before shift reagent	After shift reagent
CPH niosomes stored at 4 °C (week 0)	190 ±2.87	190 ±2.87
CPH niosomes stored at 25 °C (week 0)	190 ±10.33	190 ±10.33
CPH niosomes stored at 4 °C (week 4)	188 ±2.04	188 ±2.04
CPH niosomes stored at 25 °C (week 4)	110 ±6.23	110 ±6.23

5.3.8 Surface morphology and elasticity

CPH loaded niosomes were analyzed by TEM. **Figures 5.16**, **5.17**, **5.18**, and **5.19** show the results obtained.

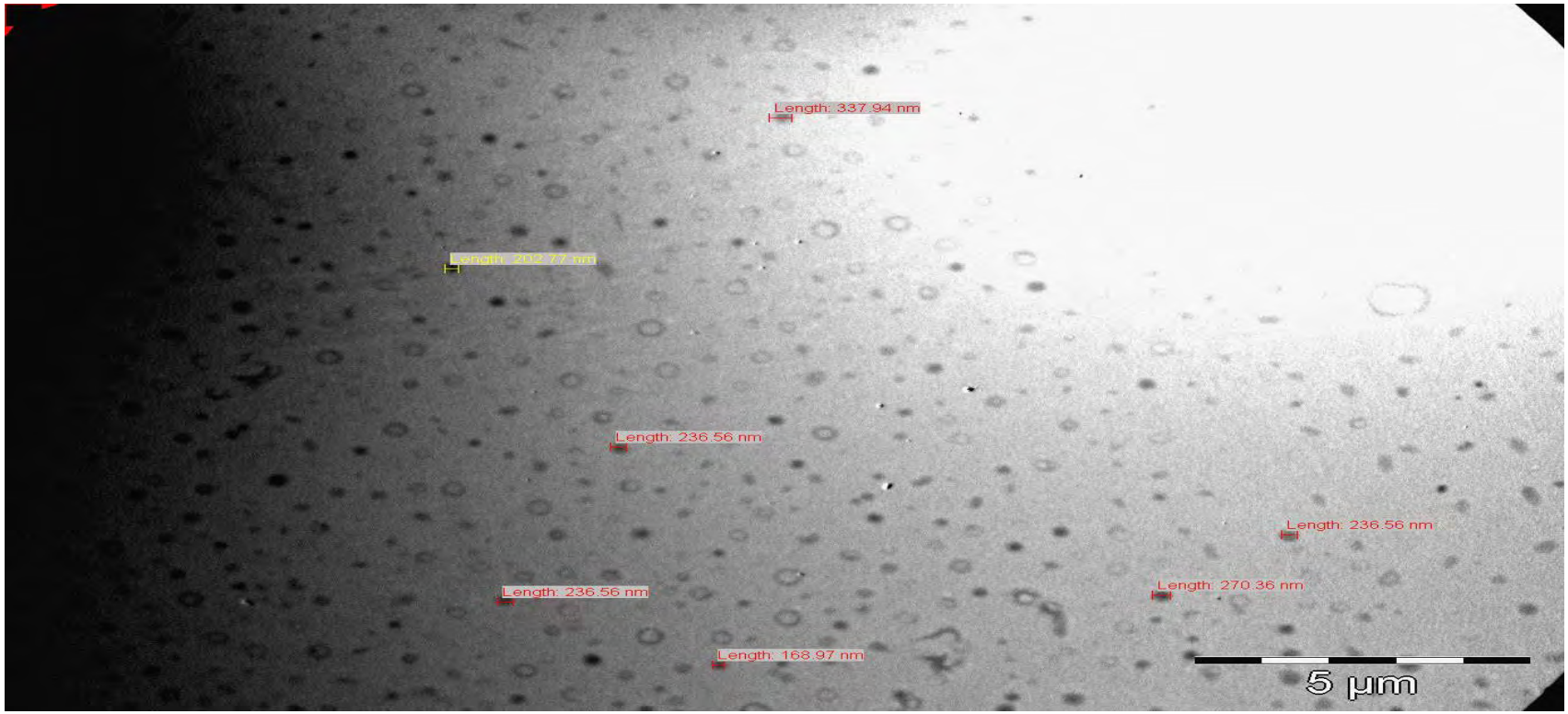

Figure 5.16 CPH niosomes stored at 4 °C (week 0).

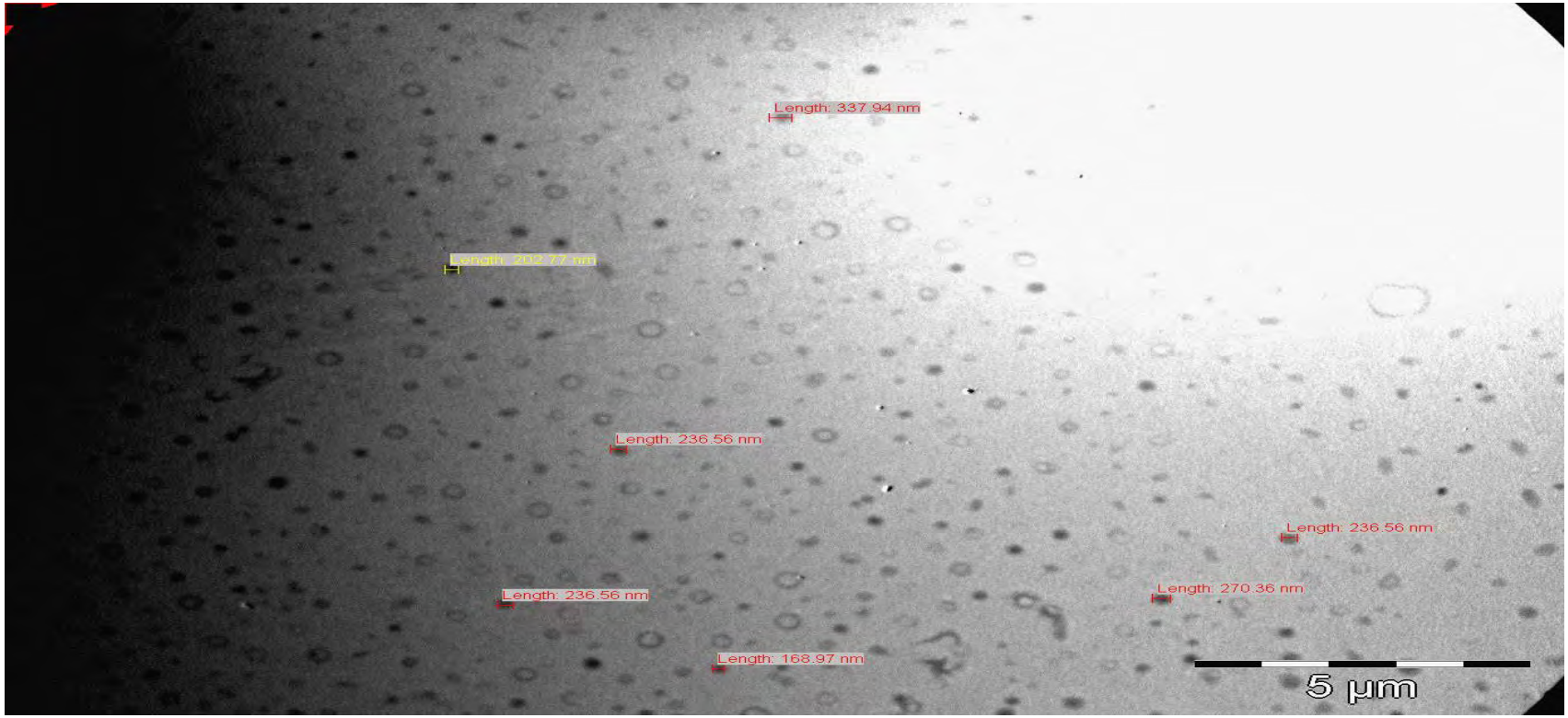

Figure 5.17 CPH niosomes stored at 25 °C (week 0).

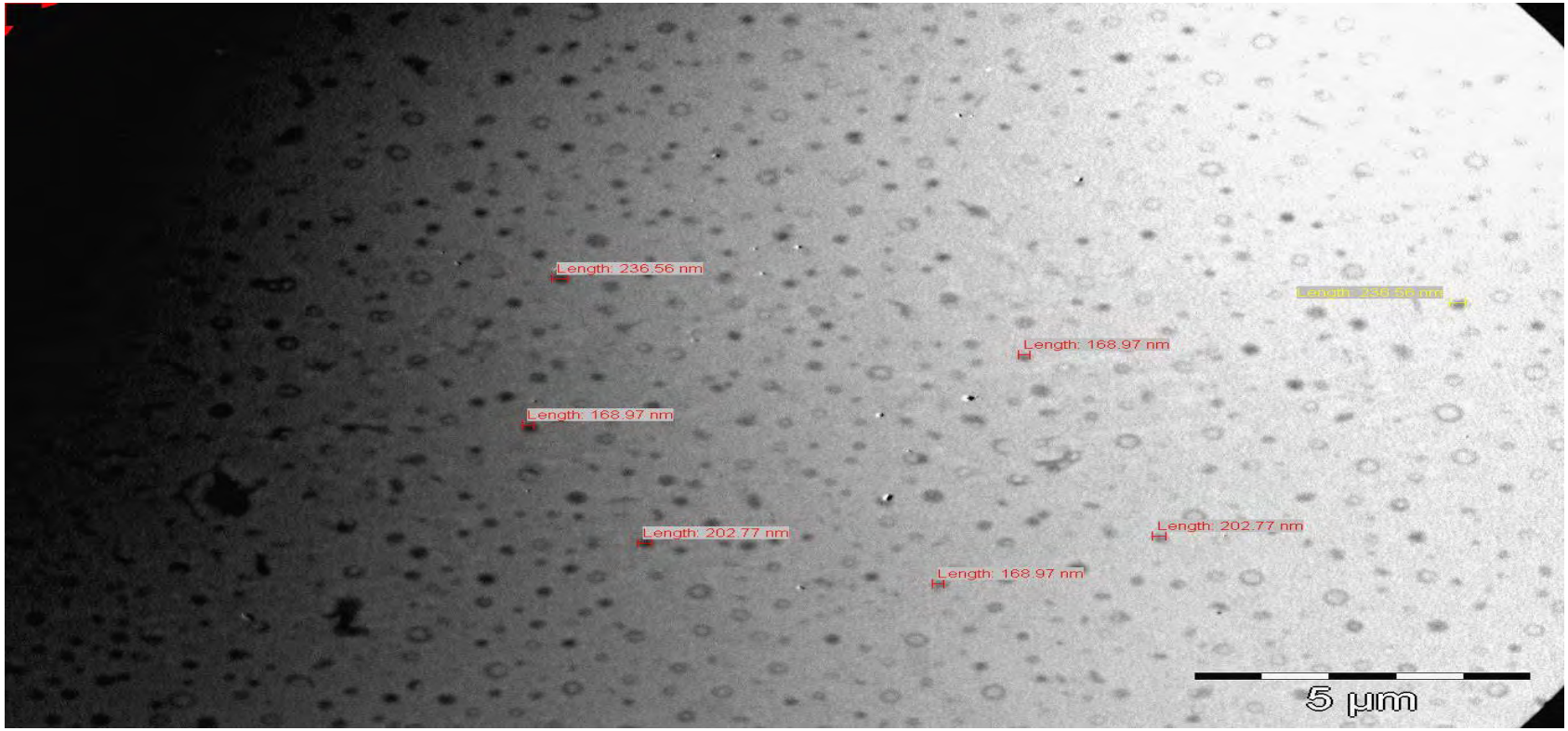

Figure 5.18 CPH niosomes stored at 4 °C (week 4).

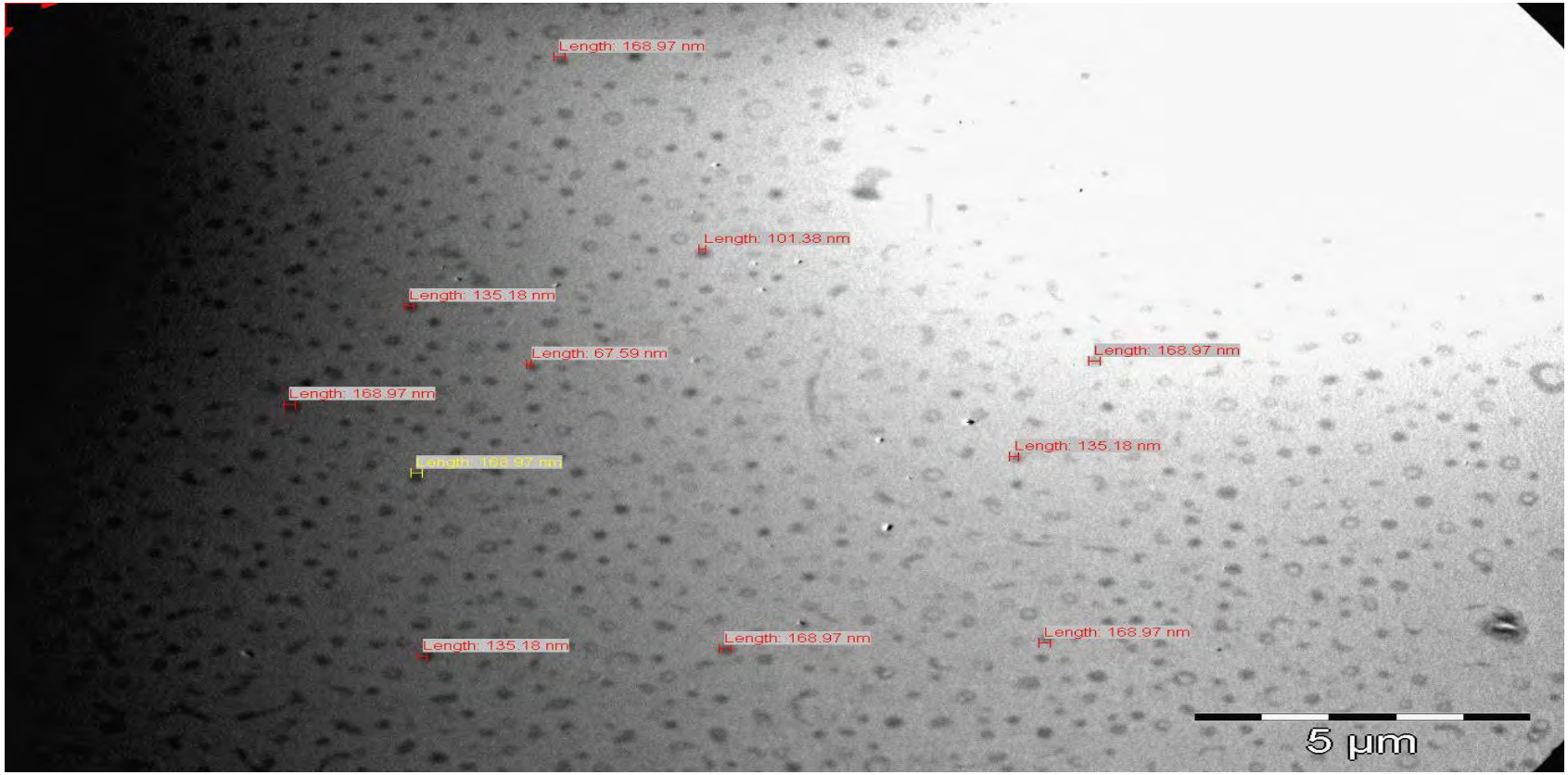

Figure 5.19 CPH niosomes stored at 25 °C (week 4).

The results obtained are in reasonable agreement with the results obtained in **§ 5.3.1**; niosomes of single lamellarity were formed. CPH niosomes stored at 25 ℃ over 4 weeks showed a decrease in vesicle size over 4 weeks, this is an area of further study. CPH niosomes stored at 4 ℃ over the same period showed no significant decrease in vesicle size. Results from the TEM confirm this phenomenon.

High membrane elasticity is suggested to be crucial for pushing a vesicle through a pore smaller than the average aggregate diameter [307], as illustrated with a niosome inside a glass micropipette in **Figure 5.20**; this is paramount for the success of the non-invasive, carrier-mediated material transport across the tympanic membrane [308]. The photomicrographs are an excellent simulation of niosomes squeezing between skin cells in the skin. From the results obtained, CPH niosomes showed good elasticity while also preserving their integrity and size.

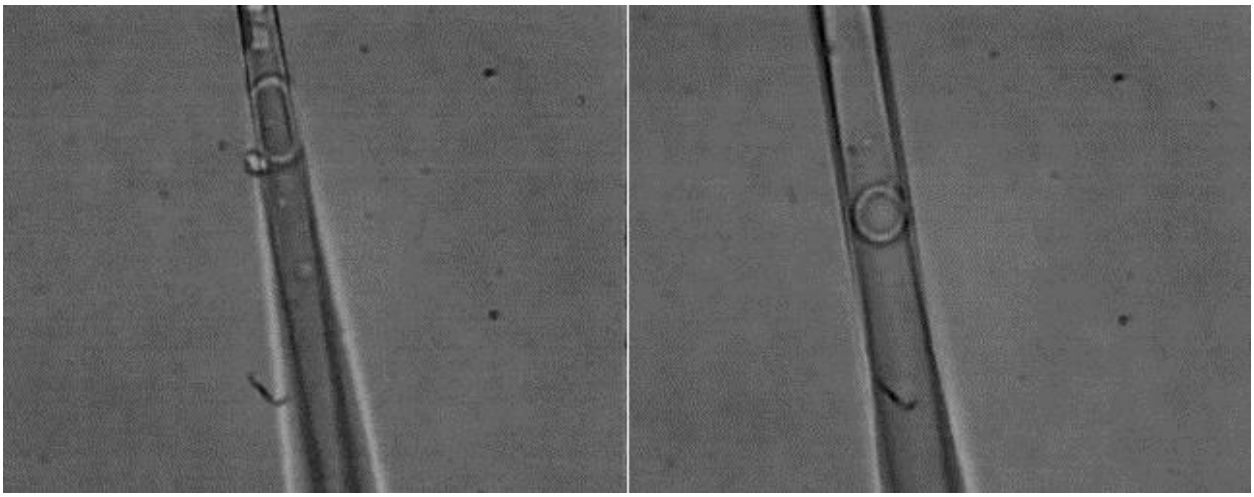

Figure 5.20 Photomicrographs showing a CPH niosome able to deform and squeeze through a glass micropipette channel smaller than its diameter, owing to its elastic properties.

5.4 CONCLUSIONS

This study used CPH loaded niosomes for transtympanic delivery to different storage conditions to test how their chemical and physical properties change over 4 weeks. The formulation proved stable at 4 ˚C as no significant changes were seen in vesicle size and entrapment efficiency. The Zeta potential and PDI were not significantly affected by the storage temperature. Additionally, FT-IR proved the encapsulation of CPH as some of the peaks were not visible when the niosomes were analyzed by FT-IR. When the niosomes are analyzed using FT-IR, the peaks belonging to the encapsulated materials tend to disappear. In this case, some of the peaks belonging to CPH disappeared when FT-IR was performed on the vesicles. This phenomenon shows that an interaction may have occurred and that CPH could be encapsulated in the niosomal structure, thus proving the formation of niosomes and encapsulation of CPH, further studies are required.

From the data obtained from the storage of the vesicles at different storage conditions over 4 weeks, we can therefore conclude that the best storage condition for the niosomal formulation is at 4 ˚C. At this storage condition, the formulation remained stable with small but expected changes in entrapment efficiency and vesicle size, these changes in entrapment efficiency may in fact be significant over 4 weeks, further studies are required. The Zeta potential continued to decrease over the 4 weeks, indicating that the formulation will remain stable and effective if stored at this temperature and will not fuse or aggregate, affecting the PDI and the vesicle size. The ear is a very sensitive part of the human body, and patients will not want to put eardrops stored at 4 ˚C in their ear. Therefore, more studies must be conducted to modify and optimize the formulation to be stable even when stored at room temperature (25 ˚C).

Additionally, owing to the large amounts of SLS and cholesterol in the formulation, the formulation had a milky white colour throughout the 4 weeks. The colour of the formulation is another aspect that could be improved. Eardrops are usually colorless; patients will not be too keen to deviate from the status quo. Therefore, more studies have to be performed to try and improve the colour. The formulation is of the same pH as the pH of the ear canal and will not cause any irritation in the ear, although pH is not the only factor that could cause irritation in the ear. Lastly, it is to be noted that placing niosomes can change the system behind recognition, further studies on lamellarity need to be performed.

In conclusion, LUVs with good flexibility and penetrability were formulated. Based on the tests performed, the vesicles will remain stable over 4 weeks while maintaining their lamellarity, flexibility, and impenetrable nature.

CHAPTER 6

CONCLUSIONS

The development of a niosomal formulation for the transtympanic delivery of CPH may minimize the dosage and frequency of CPH needed for therapeutic effect and have a slow sustained release while minimizing adverse effects.

CPH is an antibiotic used to treat several bacterial infections; this includes bone and joint infections, intra-abdominal infections, certain types of infectious diarrhea, respiratory tract infections, skin infections, typhoid fever, and UTI. CPH is a broad-spectrum antibiotic of the fluoroquinolone class. It is active against some gram-positive and many gram-negative bacteria. It functions by inhibiting a type II topoisomerase (DNA gyrase) and topoisomerase IV, necessary to separate bacterial DNA, thereby inhibiting cell division. CPH has a serum half-life of 4 - 6 hours, with 50 – 70 % of an administered dose being excreted in the urine as an unmetabolized drug. Urinary excretion excretes an additional 10 % as metabolites and is virtually complete 24 hours after administration. Dose adjustment is required in the elderly and those with renal impairment. It was realized that a cyclopropyl moiety (as seen in ciprofloxacin and sparfloxacin) conferred significant activity against gram-negative bacteria and significantly affected the mechanism of action of the API. Common side effects include nausea, vomiting, diarrhea, and rash. Minimizing the dose delivered will reduce the occurrence of these adverse effects. Therefore, it is important to develop a transtympanic API delivery system that will deliver a therapeutic concentration of CPH directly to the affected area, the ear.

An RP-HPLC method was developed, optimized, and validated to quantify CPH in solution and pharmaceutical dosage forms. A UV-Vis detector was used at 278 nm for the analysis of CPH. Experimental design using CCD was used to develop an RP-HPLC method, reducing development and optimization time. The method was developed and optimized according to the effect of ACN content in the mobile phase, column temperature, phosphate buffer molarity, and mobile phase pH on the main experimental responses *viz*., R_t of CPH and CBZ, symmetry factor, and resolution

factor between the peaks. These responses are critical as the R_t of CPH and CBZ will determine the run time of analysis, and good resolution will allow more accurate quantitation of CPH.
The input factors that had a significant impact on the responses were identified using ANOVA. Contour and response surface plots were used to illustrate the combinatory effects of the input factors. The ANOVA data showed that the R_t of CPH was significantly affected by ACN content, buffer molarity, and mobile phase pH. The resolution factor was significantly impacted by ACN content and buffer molarity. Mobile phase pH and buffer molarity had a significant impact on the asymmetric factor.

The predictive abilities of CCD were employed to optimize the chromatographic conditions. The final chromatographic conditions were a mobile phase with a pH of 3 composed of ACN: 0.0230 M phosphate buffer in a ratio of 22:78 v/v. A Phenomenex® C18 5 µm column (150 x 4.6 mm i.d) was selected as the stationary phase. The flow rate and injection volume used were 1 mL/min and 10 µL, respectively. In this method, CPH eluted at 3.753 minutes with adequate resolution between CPH and CBZ peaks. Validation of the method was performed according to ICH guidelines with respect to linearity, precision, accuracy, and specificity. The method was found to be suitable for the analysis of pure CPH and commercially available CPH products over a concentration of 0.1 - 250 µg/ml. The obtained % RSD values of < 5 % indicated that the developed method was accurate and precise for quantitative analysis of CPH.

Preformulation studies were conducted before formulation to identify any potential API-excipient interactions. The melting point of CPH was determined using DSC studies. The CPH thermogram revealed a sharp endothermic peak at 330.31 °C. The DSC analysis of a physical mixture of CPH and Tween® 80, CPH and SLS, CPH and amaranth, and CPH and cholesterol did not significantly shift in the endothermic peak, and no additional peaks appeared. The characteristic CPH absorption bands were still present in the FT-IR absorption spectrum of CPH and excipient mixtures. FT-IR cannot reveal changes in molecular structures of interacting molecules but is used to understand the behaviour of mixtures of APIs and excipients. The results of the DSC and FT-IR studies indicated compatibility between CPH and the excipients and were used together in formulating the niosomal drug delivery system targeting the delivery of CPH through the tympanic membrane. It should be noted that the DSC and FT-IR studies were performed with the excipients in solid state.

The results may not be completely accurate as the excipients are in aqueous form in the formulation, this is an area of further study. Several different surfactants/ surfactant combinations were used to prepare the niosomes using the probe sonication method. Tween® 80: SLS: cholesterol (1:1:1) was chosen as the best performing surfactant combination for entrapment efficiency and Zeta potential. The limits for the parameters, cholesterol amount, amplitude, and sonication time were determined. Cholesterol amount was determined to be between 0.2 - 1 g, sonication time was between 2 - 10 minutes, and amplitude was between 10 – 30 %.

A BBD approach was selected to investigate the effect of cholesterol amount, amplitude, and sonication time on vesicle size, Zeta potential, PDI, and entrapment efficiency. ANOVA was used to determine the significance of the input variables on the output variables. Contour and response surface plots were used to illustrate the combinatory effects of the input variables on the responses. The results of the ANOVA revealed that cholesterol amount had a significant effect on vesicle size, entrapment efficiency, and Zeta potential. Amplitude and sonication time had a significant effect on PDI. ANN and BBD were used to predict the formulation variables that would result in vesicle size between 109.45 - 286.52 nm, entrapment efficiency maximized at 99.25 %, PDI at 0.28, and Zeta potential at -39.47 mV. BBD exhibited better predictive ability for the input variables that would produce the optimized formulation as the experimentally obtained results were closest to those predicted by BBD.

Mathematical models were used to determine the release kinetics of CPH from the niosomal formulation by assessing *in-vitro* release data. The data was fitted to zero-order, first-order, Higuchi, Korsmeyer-Peppas, and Hixson-Crowell models, and R^2 values were calculated. The R^2 values and the release exponent (n) showed that CPH release occurred via Fickian diffusion and followed first-order release kinetics. Over a period of 4 weeks, stability studies on the niosomes were performed. Upon visual inspection, the niosomes retained a milky white colour over the period. The colour could be attributed to the SLS and cholesterol which were used in the formulation of the niosomes. The pH remained unchanged over the 4-week period. Although pH is the only factor that can cause irritation in the ear, on the pH front, the niosomes will not cause any irritation. When the niosomes were stored at 4 and 25 °C, the niosomes stored at 25 °C showed a much bigger decrease in vesicle size and entrapment efficiency. However, it should be noted that

the method used to measure entrapment efficiency is not completely accurate, this may have affected the results. According to the results obtained, niosomes stored at 4 ℃ were more stable than the niosomes stored at 25 ℃. This is an area of further study; patients will not necessarily be comfortable using ear drops stored at 4 ℃.

These studies are only a starting point for using niosomes to deliver CPH transtympanically for the treatment of otitis media. The formulation remained stable when stored at 4 ℃, with only slight changes in vesicle size and entrapment efficiency. The formulation showed elastic properties, maintained its lamellarity (uni-lamellar), and showed good rigidity and integrity over the 4-week period.

In conclusion, the experimental design was successfully used to develop a CPH niosomal formulation that could potentially deliver CPH through the ear via the transtympanic membrane. The formulation was optimized using experimental design and ANN. The formulation could be improved by performing *in-vivo* studies and in future models reflecting the tympanic membrane.

REFERENCES

1. Thomas JP, Berner R, Zahnert T and Dazert S. Acute otitis media-a structured approach, ***Dtsch Arztebl Int***, 151–160 (1), 2014.

2. Khoo X, Simons EJ, Chiang HH, Hickey JM, Sabharwal V, Pelton SI, Rosowski JJ, Langer R and Kohane DS. Formulations for trans-tympanic antibiotic delivery, ***Biomaterials 34***, 1281–1288 (33), 2005.

3. Koulich E, Roland PS and Pawlowski KS. Comparison of systemic and otic administration of ofloxacin, ***Laryngoscope***, 2083–2088 (12), 2001.

4. Cevc G and Blume G. Lipid vesicles penetrate intact skin owing to the transdermal osmotic gradients and hydration force, ***Biochemical Biophysical Acta***, 226–232 (11), 1992.

5. El Maghraby GM, Williams AC and Barry BW. Estradiol skin delivery from ultra-deformable liposomes: refinement of surfactant concentration, ***International Journal of Pharmacy***, 63–74 (16), 2000.

6. Paul A, Cevc G and Bachhawat BK. Transdermal immunization with an integral membrane component, gap junction protein, by means of ultra-deformable drug carriers, ***Transfersomes***, 188–195 (16), 2016.

7. Cevc G, Geber D, Stieber J, Schatzlein M and Blume G. Ultra-flexible vesicles, transfersomes, have an extremely low pore penetration resistance and transport therapeutic amounts of insulin across the intact mammalian skin, ***Biochemical Biophysical Acta***, 201–215 (43), 2013.

8. Cevc G and Blume G. Hydrocortisone and dexamethasone in very deformable drug carriers have increased biological potency, prolonged effect, and reduced therapeutic dosage, ***Biochemical Biophysical Acta (BBA) – Bio membrane***, 61–73 (6), 2011.
9. Cevc G, Vierl U and Mazgareanu S. Functional characterization of novel analgesic product based on self-regulating drug carriers, ***International Journal of Pharmacy***, 18–28 (36), 2016.
10. Hiruta Y, Hattori Y, Kawano K, Obata Y and Maitani Y. Novel ultra-deformable vesicles entrapped with bleomycin and enhanced to penetrate rat skin, ***Journal of Controlled Release***, 146–154 (133), 2013.
11. Campoli-Richards DM, Monk JP, Price A, Benfield P, Todd PA and Ward A. Ciprofloxacin: A review of its antibacterial activity, pharmacokinetic properties and therapeutic use, ***Drugs***, 373–447 (35), 1988.
12. Esposito S, D'Errico G and Montanaro C. Topical and oral treatment of chronic otitis media with ciprofloxacin, a preliminary study, ***Head and Neck Surgery***, 557–559 (116), 2016.
13. Wall GM, Stroman DW, Roland PS and Dohar J. Ciprofloxacin 0.3%/ dexamethasone 0.1% sterile otic suspension for the topical treatment of ear infections: a review of the literature, ***Paediatric Infection Journal***, 141–144 (28), 2016.
14. Moffat AC, Osselton MD and Widdop B. Clarke's Analysis of Drugs and Poisons 4th ed, ***Pharmaceutical Press***, ***London***, 1111–1113, 2016.
15. Trommer H and Neubert RH. Skin Pharmacology, ***Physiology***, 106–121 (19), 2000.
16. Yasin ZAM, Ibrahim F and Rashid NN. Drug Therapy, ***Current Pharmaceutical Biotechnology***, 864–876 (18), 2017.
17. Vrettakos PA. Middle ear structure, ***Physiology***, 1987.

18. Vejries LM. The permeability barrier in mammalian epidermis, ***The Journal of Cell Biology***, 180 (65), 1999.
19. Borenstein JT. Intracochlear drug delivery systems, ***Drug Delivery***, 1161–1174 (8), 2011.

20. Bear ZW and Mikulec AA. Intratympanic steroid therapy for treatment of idiopathic sudden sensorineural hearing loss, ***Molecular Medicine***, 352–356 (111), 2014.

21. El Kechai N, Agnely F, Mamelle E, Nguyen Y, Ferrary E and Bochot A. Recent advances in local drug delivery to the inner ear, ***International Journal of Pharmacy,*** 83–101 (494), 2015.

22. Shahzad Y, Louw R, Gerber M and du Plessis J. Breaching the skin barrier through temperature modulations, ***Journal of Controlled Release***, 1-13 (202), 2015.

23. Du Plessis LH, Lubbe J, Strauss T and Kotzé AF. Enhancement of nasal and intestinal calcitonin delivery by the novel fatty acid-based delivery system, and by N-trimethyl chitosan chloride, ***International Journal of Pharmaceutics***, 181-186 (38), 2010.

24. Williams M and Elias P. The extracellular matrix of stratum corneum: role of lipids in normal and pathological function, ***Critical reviews in therapeutic drug carrier systems***, 95-122 (3), 1986.

25. Biju SS, Talegaonkar S, Mishra PR and Khar RK. Vesicular systems: an overview, ***Indian Journal of Pharmaceutical Science***, 141-153 (2), 2006.

26. Manish G and Vimukta S. Targeted drug delivery system: a review, ***Research Journal of Chemical Science***, 135-138 (2), 2011.

27. Mujoriya R, Bodla RB, Dhamande K, Singh D and Patle L. Niosomal drug delivery system: the magic bullet, ***Journal of Applied Pharmaceutical Sciences***, 20-23 (9), 2011.

28. Malakar J, Gangopadhyay A and Nayak AK. Transferosome: an opportunistic carrier for transdermal drug delivery system, ***International Research Journal of Pharmacy***, 35-38 (3), 2012.

29. Ambarish G, Prajapati SK, Anand JP, Akhtar A and Aviral G. Ultra-deformable vesicle as a novel drug delivery system, ***International Research Journal of Pharmacy***, 116-120 (8), 2012.

30. Wise R, Andrews JM and Edwards LJ. In vitro activity of Bay 09867, a new quinolone derivative, compared with those of other antimicrobial agents, ***Antimicrobial Agents and Chemotherapy***, 559–64 (23), 2013.

31. Deshpande A, Pant C, Jain A, Fraser TG and Rolston DD. Do fluoroquinolones predispose patients to Clostridium difficile associated disease? A review of the evidence, ***Current Medical Research and Opinion***, 24 (2), 2009.

32. O'Neil MJ. The Merck Index - An Encyclopedia of Chemicals, Drugs, and Biologicals, ***Merck and Co***., 333, 2009.

33. South African Medicines Formulary (SAMF) 12th ed. ***Tandym Print***, 2016.

34. O'Neil MJ. The Merck Index - An Encyclopedia of Chemicals, Drugs, and Biologicals, ***Merck and Co***., 386, 2006.

35. Rinaki E, Valsami G, Mukhopadhyay AK and Macheras P. Quantitative Biopharmaceutics Classification System: The Central Role of Dose/Solubility Ratio, ***Pharmaceutical Research***, 20 (12), 2003.

36. Vaithianathan S, Raman S, Jiang W, Ting TY, Kane MA and Polli JE. Biopharmaceutical Risk Assessment of Brand and Generic Ciprofloxacin Tablets, ***Molecular Pharmaceutics***, 12 (7), 2015.
37. Kumar KM and Anil B. Biopharmaceutics drug disposition classification system: an extension of biopharmaceutics classification, ***International Research Journal of Pharmacy***, 3 (3), 2012.
38. Sangster J. Octanol-Water Partition Coefficients of Simple Organic Compounds, ***Sangster Research Laboratories***, 1989.
39. Jouyban A and Fakhree MAA. Drug Solubility, ***Drug Testing***, 2012.
40. Jouyban A and Fakhree MAA. Experimental and Computational Methods Pertaining to Drug Solubility, ***Toxicity and Drug Testing***, 230-233 (19), 2012.
41. Jouyban A, Soltanpour S and Acree WE. Improved prediction of drug solubilities in ethanol + water mixtures at various temperatures, ***Biomedicine International***, 1, 2010.
42. Montvale NJ. Physicians' Desk Reference 55th Ed, ***Medical Economics Co***, 852, 2001.
43. Coates J. Interpretation of infrared spectra, a practical approach, ***Encyclopedia of Analytical Chemistry***, 339-349 (12), 2000.
44. Hsu CPS. Infrared spectroscopy, ***Handbook of Instrumental Techniques for Analytical Chemistry (1st Ed)***, 20 (3), 1997.
45. Koteswari P, Sunium S, Srinivasababu P, Babu GK and Nithya PD. Formulation development and evaluation of ciprofloxacin using liquisolid technique, ***International Journal of Pharmaceutical Investigations,*** 4 (4), 2014.

46. Wang YC, Cheng XY and Guo HY. Recent Progress on Quinolone Agents in China, ***Chinese Journal of Pharmaceuticals***, 179-185 (35), 2004.

47. Zhengde T, Fengjiao T, Li Z and Junyong L. The Synthesis, Characterization and Application of Ciprofloxacin Complexes and Its Coordination with Copper, Manganese and Zirconium Ions, ***Journal of Crystallization Process and Technology***, 55-63 (2), 2012.

48. Veera RA and Pailla U. Ciprofloxacin: A Two Step Process, ***Der Pharma Chemica***, 174-178 (3), 2018.

49. Hooper DC. Drug Resistance, ***Acta Neurologica Belgica***, 38 (2), 1999.

50. Pietsch F, Bergman JM, Brandis G, Marcusson LL, Zorzet A, Huseby DL and Hughes D. Ciprofloxacin selects for RNA polymerase mutations with pleiotropic antibiotic resistance effects, ***Journal of Antimicrobial Chemotherapy***, 75-84 (1), 2017.

51. Zhang GF, Liu X, Zhang S, Pan B and Liu ML. Ciprofloxacin derivatives and their antibacterial activities, ***European Journal of Medicinal Chemistry***, 599-612 (46), 2018.

52. Takács-Novák K, Józan M and Szász H. Lipophilicity of antibacterial fluoroquinolones, ***International Journal of Pharmaceutics***, 89-96 (3), 1992.

53. Lee M, Bozzo P and Einarson A. Urinary tract infections in pregnancy, ***Publication of the College of family physicians of Canada***, 853-854 (6), 2008.

54. George MJ, Dew RB and Daly JS. Acute renal failure after an overdose of ciprofloxacin, ***Arch International Medicines***, 151 (3), 1991.

55. Lannetti P, Raucci U, Zuccaro P and Pacifici R. Lamotrigine Hypersensitivity in Childhood Epilepsy, ***Epilepsia***, 39 (5), 1998.

56. Micromedex Drug Information Application. 2019. Ciprofloxacin hydrochloride, ***Micromedex***, https://www.ibm.com/watson-health/learn/micromedex, (Retrieved on: 08/07/2019).
57. Le Bel M. Ciprofloxacin: chemistry, mechanism of action, resistance, antimicrobial spectrum, pharmacokinetics, clinical trials, and adverse reactions, ***Pharmacotherapy***, 3-33 (8), 1988.

58. Engelhard H. 2018. High Performance Liquid Chromatography, ***Chromatography***, https://www.soinc.org/sites/default/files/uploaded_files/forensics/For_Chromatography3.pdf, (Retrieved on: 20/08/2020).

59. Hamilton RJ and Sewell PA. Introduction to High-Performance Liquid Chromatography, ***Chromatography***, 187-189, 1982.

60. Warner IW. Liquid Chromatography in Pharmaceutical Development: An Introduction, ***Practical HPLC***, 1995.

61. Willard HH, Merritt G, Dean JA and Settle FA. High-Performance Liquid Chromatography: Theory and Instrumentation, ***ChemGuide***, 1111-1145, 1988.

62. Lindsay S. 2008. High-Performance Liquid Chromatography operation and applications in pharmaceutics, ***Lindegas***, https://www.lindegas.com/en/analytical_methods/liquid_chromatography/high_performance_liquid_chromatography.html, (Retrieved on: 01/09/2020).

63. Poole CF. Chromatography: An Introduction, ***Academic Press***, 2000.

64. Rubinson KA and Rubinson JF. Liquid Chromatography, ***Journal of Chromatography A***, 112-116, 2000.

65. Jung Bauer A and Hahn R. Ion Exchange Chromatography, ***Practical HPLC Method Development***, 463 (8), 2009.

66. Abbott SR. Practical Aspects of Normal-Phase Chromatography, ***Journal of Chromatographic Science***, 18 (10), 1980.

67. Barth HG, Boyes BE and Jackson C. Size Exclusion Chromatography, ***High Performance Liquid Chromatography***, 1994.

68. Aguilar MI. Reversed-Phase High-Performance Liquid Chromatography, ***Methods in Molecular Biology***, 251, 2004.

69. Watson DG. Pharmaceutical Analysis, ***Chromatography***, 1999.

70. Fisher RS, Van Emde Boas W, Blume W, Elger C, Genton P, Lee P and Engel J. Epileptic seizures and epilepsy: Definitions proposed by the International League Against Epilepsy (ILAE) and the International Bureau for Epilepsy (IBE), ***Epilepsia***, 46 (4), 2005.

71. Media Centre. 2017. Epilepsy and related conditions, ***World Health Organization***, http://www.who.int/mediacentre/factsheets/fs9965686669/en, (Retrieved on: 08/08/2019)

72. Coskun O. Separation Techniques: Chromatography, ***North Clin***, 2016.

73. Kirkland J, Dilks C and DeStefano J. Normal-phase high-performance liquid chromatography with highly purified porous silica microspheres, ***Journal of Chromatography A***, 635 (1), 1993.

74. Waters. 2014. HPLC Separation and operation modes, ***Waters Guide to HPLC***, http://www.waters.com/waters/en_ZA/HPLC-Separation, (Retrieved on: 28/08/2020).

75. Clark J. 2007. High-performance liquid chromatography - HPLC, ***ChemGuide***, http://www.chemguide.co.uk/analysis/chromatography/chem?//hplc.html, (Retrieved on: 28/08/2020).

76. Nyssola A and Alhfgren J. Microbial degradation of polyacrylamide and the deamination product polyacrylate, ***Technical Research Centre of Finland***, 2019.

77. Shabir G. 2015. Size Exclusion Chromatography, ***Bio-Rad***, https://www.biorad.com/en-za/applications-technologies/introduction-size-exclusion-chromatography?ID=MWHAXJKG4#targettext, (Retrieved on: 28/08/2020).

78. Shire JS. Analytical tools used in the formulation and assessment of stability of monoclonal antibodies, ***Woodhead publishing***, 2015.

79. Campbell MP. Protein glycosylation, ***Department of Chemistry and Biomolecular Sciences***, 2011.

80. Painthankar HV. HPLC method validation for pharmaceuticals: a review, ***MET's Institute of Pharmacy***, 2013.

81. Wolfson H. 2019. Reverse phase chromatography: Principles and Methods, ***Amersham***, www.wolfson.huji.ac.il/purification/PDF/ReservePhase/AmershamRPCManual.pdf, (Retrieved on: 28/08/2020).

82. Vervoort RJM, Debets AJJ, Claessens HA, Cramers CA and de Jong G. Optimization and Characterization of Silica-based Reversed-Phase Liquid Chromatographic Systems for the Analysis of Basic Pharmaceuticals, ***Journal of Chromatography A***, 897, (1-2), 2000.

83. Engelhardt H. High-Performance Liquid Chromatography, ***Springer***, 1989.

84. Khan academy expert panel. 2016. Principles of Chromatography, ***Khan Academy***,

https://www.khanacademy.org/test-prep/mcat/chemical-processes/separations-purifications/a/principles-of-chromatography, (Retrieved on: 28/08/2020).

85. Waters. 2014. How Does High-Performance Liquid Chromatography Work?, ***High Performance Liquid Chromatography***, http://www.waters.com/waters/en_ZA/How-Does-High-Performance-Liquid Chromatography-Work?/nav.htm?cid=10000000004905865&locale=en_ZA, (Retrieved on: 03/11/2020).

86. Van Oss CJ. The properties of water and their role in colloidal and biological systems, ***Elsevier***, 2008.

87. Berruex LG and Freitag R. Separation and purification of biochemicals, ***Polytechnique Federale de Lausanne***, 2003.

88. Snyder LR, Kirkland JJ and Glajch JL. Practical HPLC Method Development (2nd Ed), ***Wiley and Sons Inc.***, 1997.

89. Majors RE. Recent Advances in High Performance Liquid Chromatography Packings and Columns, ***Journal of Chromatographic Science***, 15 (9), 1977.

90. Chem F. Normal Phase High-Performance Liquid Chromatography Method for the Determination of Tocopherols and Tocotrienols in Cereals, ***Journal of Agricultural and Food Chemistry***, 51 (14), 2003.

91. Pharma guideline. 2019. Different types of HPLC columns used in pharmaceutical analysis, ***Pharma guideline***, https://www.pharmaguideline.com/2016/01/different-types-of-columns-used-in-hplc.html, (Retrieved on: 05/09/2020).

92. Lindsay S. Analytical Chemistry by Open Learning: High-Performance Liquid Chromatography, ***John Wiley and Sons Inc.***, 1987.

93. Chem Libre. 2010. Chromatographic columns: Chromatographic columns, ***Chem Libre,*** https://chem.libretexts.org/Bookshelves/Analytical_Chemistry/supplemental_modules, (Retrieved on: 05/09/2020).

94. Ravindranath B. Principles and practice of chromatography, ***John Wiley & sons***, 1989.

95. Ahuja S and Dong M. Handbook of Pharmaceutical Analysis by HPLC, ***Academic Press***, 6, 2005.

96. Chromacademy Chemistry. 2017. HPLC Column Chemistry, ***Chromacademy,*** https://www.chromacademy.com/lms/sco4/Theory_Of_HPLC_Column_Chemistry.pdf, (Retrieved on: 05/09/2020).

97. Meshkibaf MH, Ebrahimi A, Ghodsi R, and Ahmadi A. Chronic effects of ciprofloxacin on liver function in adult male rats, ***Indian Journal of Clinical Biochemistry***, 21 (1), 2006.

98. Brown AK and Wong S. Current trends in environmental analysis of human metabolite conjugates of pharmaceuticals, ***Department of Chemistry, University of Manitoba***, 2015.

99. Clark J. 2007. High performance liquid chromatography - HPLC, ***ChemGuide***, http://www.chemguide.co.uk/analysis/chromatography/chem-guide/hplc.html, (Retrieved on: 03/09/2020).

100. Richens A. Safety of ciprofloxacin, ***Analytical Chemistry***, 35 (5), 1994.

101. Ahuja S and Dong M (Editors). Handbook of Pharmaceutical Analysis by HPLC, Volume 6 (1st Ed), ***Academic Press***, 2005.

102. Guzzetti A. 2001. Reverse Phase HPLC Basics for LC/MS, ***Ion Source Tutorials***, http://www.ionsource.com/tutorial/chromatography/rphplc.html, (Retrieved: 08/09/2020).

103. Claessens HA, van Straten MA and Kirkland JJ. Effect of Buffers on Silica-based Column Stability in Reversed-Phase High-Performance Liquid Chromatography, ***Journal of Chromatography A***, 728 (2), 1996.

104. Ryan WR. 2018. Theory of HPLC Reverse Phase HPLC***, Chromatography*** File://E:/Theory_Of_High_Performance_LiquidChromatography_Reverse_Phase_Chromatography.pdf, (Retrieved on: 08/09/2020).

105. Hosmer DW and Lemeshow S. Applied Logistic Regression, ***John Wiley & Sons***, 2000.

106. Ramni K, Navneet K, Ashntosh U, Suri OP and Arti T**.** High performance liquid chromatography detectors- A review, ***ISF College of Pharmacy***, 2011.

107. Swartz M. HPLC Detectors, ***Taylor and Francis Group***, 2010.

108. Lagae L. The need for broad-spectrum and safe antibiotic drugs in otitis media, ***Acta Neurologica Belgica***, 109 (3), 2009.

109. Vella J, Busuttil F, Bartele NS, Sammut C, Ferrito V, Serracino-Inglott A, Azzopardi LM and LaFarla G. A simple HPLC-UV method for the determination of ciprofloxacin in human plasma, ***Msida Malta Medicine and Surgery***, 2015.

110. Weiner IW. Liquid Chromatography in Pharmaceutical Development: An Introduction, ***Aster Publishing Corporation***, 1995.

111. Lakka NS and Kuppan C. Principles of Chromatography Method Development, ***Intech Open***, 2019.

112. Kamberia M, Tsutsumi K, Kotegava T, Nakamura K and Nakano S. Determination of Ciprofloxacin in plasma and urine by HPLC with ultraviolet detection, ***Clinical Chemistry***, 1251-1255 (44), 1998.

113. Scherer R, Pereira J, Firme J, Lemos M and Lemos M. Determination of ciprofloxacin in pharmaceutical formulations using HPLC method with UV detection, ***Indian Journal of Pharmaceutical Sciences,*** 2014.

114. Scherer AS, Mmuo CC, Abdul Raheem OR, Abdul Kareem SS, Alemika TE, Sani AM and Ilyas M. High-Performance Liquid Chromatography (HPLC) Method Development and Validation, ***Journal of Applied Pharmaceutical Science***, 239-243 (8), 2011.

115. Nix DE, De Vito JM, and Schentag J. Liquid-Chromatographic Determination of Ciprofloxacin in Serum and Urine, ***Journal of Clinical chemistry***, 684-686 (31), 1985.

116. Lian Z and Wang J. Determination of ciprofloxacin in Jiaozuo Bay using molecularly imprinted solid-phase extraction followed by high-performance liquid chromatography with fluorescence detection, ***Journal of Science***, 1-7, 2016.

117. Emami J and Rezazadeh M. A simple and sensitive high-performance liquid chromatography method for determination of ciprofloxacin in bioavailability studies of conventional and gastro retentive prolonged-release formulations, ***Journal of Advanced Biomedical***, 163- 171 (5), 2017.

118. Alwayeh R, Hussein FR, Alvi NS and Hammami MM. Rapid determination of Ciprofloxacin concentration in human plasma by high-performance liquid chromatography, ***Chromatography***, 1765- 1774 (5), 2016.

119. Goyal A, Choudhary S and Singh GD. A validated RP-HPLC method for estimation of ciprofloxacin in tablet dosage form, ***Institute of Pharmaceutical Sciences***, 2015.

120. Ali SA, Mmuro CC, Abdul Raheem RO, Abdul Kareem ET, Musa AS and Ilyas M. High performance liquid chromatography (HPLC) Method Development and Validation Indicating Assay for ciprofloxacin hydrochloride, ***Pharmaceutical and Medicinal Chemistry***, 2015.

121. Dolan JW. Mobile-Phase Degassing: What, why, and how, ***LCGC North America***, 32 (7), 2014.

122. Hopkins T. The Basics of Mobile Phase Degassing, ***Chromatography Today***, 10 (3), 2017.

123. Shimadzu Corporation. 2016. Degassing Mobile Phase Solvents - Vacuum Degassing Using an Aspirator in High Performance Liquid Chromatography, ***Shimadzu***, http://www.shimadzu.com/an/hplc/support/lib/lctalk/s5/052009876566765.html, (Retrieved on: 18/10/2020).

124. Usher KM, Hansen SW, Amoo JS, Bernstein AP and McNally MEP. Precision of Internal Standard and External Standard Methods in High Performance Liquid Chromatography, ***Special Issues***, 33 (4), 2015.

125. Kelly K. 2014. Choosing an Internal Standard, ***Phenomenex - Technical tips***, https://www.phenomenex.com/Info/WebDocumentServe/gctt_internalstandard.pdf, (Retrieved on: 20/10/2020).

126. Stauffer E, Dolan JA and Newman R. CHAPTER 8- Gas Chromatography and Gas Chromatography, ***Mass spectroscopy***, 2008.

127. Vander HY, Nijhuis A, Smeyers-Verbeke J, Vandeginste BG and Massart DJ. Guidance for robustness/ruggedness tests in method validation, ***Journal of Pharmaceutical and Biomedical Analysis***, 24 (6), 2001.

128. Ringo MC and Evans CE. Effect of mobile phase composition on pressure-induced shifts in solute retention for LC separations using α-cyclodextrin stationary phase, ***The Journal of Micro column Separations***, 10 (8), 1998.

129. Ravisankar P, Anusha S, Supriya K and Kumar UA**.** Fundamental Chromatographic Parameters, ***Pharmaceutical Analysis and Quality Assurance***, 2014.

130. Agatonovic-Kustrin S, Zecevic M, Zivanovic L and Tucker IG. Application of artificial neural networks in HPLC method development, ***Journal of Pharmaceutical and Biomedical Analysis***, 1998.

131. Chesher D. Evaluating Assay Precision, ***Department of Clinical Biochemistry***, 2008.

132. Assay Validation. 2018. Assay Validation Methods-Definitions and Terms, ***Chromatography***, www.fws.gov/aah/PDF/QI-Terms%20and%20Defs.pdf, (Retrieved: 05/09/2020).

133. Paino TC and Moore AD. Determination of the LOD and LOQ of an HPLC method using four different techniques, ***Pharmaceutical Technology***, 23 (7), 1999.

134. Fauzee AFB. Development, manufacture and assessment of clobetasol 17-propionate cream formulations, ***Pharmaceutical Technology***, 16 (1), 2011.

135. International Conference on the Harmonization of technical requirements for the registration of pharmaceuticals for human use. 2005. ICH harmonized tripartite guideline, validation of analytical procedures: text and methodology, ***ICH***,

http://www.ich.org/fileadmin/Public_Web_Site/ICH_Products/Guidelines/Quality/Q2_R1/Step4/Q2_R1__Guideline.pdf, (Retrieved on: 18/10/2020).

136. Ermer J and Miller JH. Method Validation in Pharmaceutical Analysis: A Guide to Best Practice (1st Ed), ***Wiley-VCH***, 2005.

137. Sibanda W and Pretorius P. Comparative study of the application of Box Behnken Design (BBD) and Binary Logistic Regression (BLR) to study the effect of demographic characteristics on HIV risk in South Africa, ***Journal of Applied Medical Sciences***, 1 (2), 2012.

138. Dette H and Wong WK. On G-efficiency calculation for polynomial models, ***Annals of Statistics***, 23 (6), 1995.

139. Stat-Ease. 2014. Handbook for Experimenters and Researchers, ***Stat-Ease publishing***, http://www.statease.com/pubs/handbk_for_exp_sv.pdf, (Retrieved on: 19/10/2020).

140. Mashru R, Sutariya V, Sankalia M and Sankalia J. Transbuccal delivery of lamotrigine across porcine buccal mucosa: in vitro determination of routes of buccal transport, ***Journal of Pharmacy and Pharmaceutical Sciences***, 8 (1), 2005.

141. Waters. 2014. A Polar Stationary Phase for Non-Polar Compounds, ***CyanoColumns***, http://www.waters.com/webassets/cms/library/docs/720004108en.pdf, (Retrieved on: 01/11/2020).

142. Kim B. 2015. Understanding diagnostic plots for linear regression analysis, Research Data Services + Sciences, ***Data Library***, http://data.library.virginia.edu/diagnostic-plots, (Retrieved on: 2/12/2020).

143. Trommer H and Neubert RH. Skin Pharmacology and Physiology, ***Journal of Pharmaceutical Sciences***, 106–121 (19), 2006.

144. Yasin ZAM, Ibrahim F and Rashid NN. Current Pharmaceutical Biotechnology, ***Journal of Pharmaceutical Sciences***, 864–876 (18), 2017.

145. Bharate SS, Bharate SB and Bajaj AN. Incompatibilities of pharmaceutical excipients with active pharmaceutical ingredients: A comprehensive review, ***Journal of Excipients and Food Chemicals***, 1 (3), 2010.

146. Petit S and Madejova J. Developments in Clay Science, ***Encyclopedia of Analytical Science (Second Edition)***, 2005.

147. O'Neill MJ. Measurement of Specific Heat Functions by Differential Scanning Calorimetry, ***Analytical Chemistry***, 38 (10), 1996.

148. Höhne GWH, Hemminger WF and Flammersheim HJ. Differential Scanning Calorimetry (2nd Ed), ***Springer Science & Business Media***, 2013.

149. Shahzad Y, Louw R, Gerber M and du Plessis J. Breaching the skin barrier through temperature modulations, ***Journal of Controlled Release***, 1-13 (202), 2015.

150. Bouwstra J, Dubbelaar F, Gooris G and Ponec M. The lipid organization in the skin barrier, ***Acta Dermato Venereologica-Supplement***, 23-30 (2), 2005.

151. Blagden N, de Matas M, Gavan PT and York P. Crystal engineering of active pharmaceutical ingredients to improve solubility and dissolution rates, ***Advanced Drug Delivery Reviews***, 59 (7), 2007.

152. Khadka P, Ro J, Kim H, Kim I, Kim JT, Kim H, Cho JM, Yun G and Lee J. Pharmaceutical particle technologies: An approach to improve drug solubility, dissolution and bioavailability, ***Asian Journal of Pharmaceutical Sciences***, 9 (6), 2014.

153. Serajuddin AT. Salt Formation to Improve Drug Solubility, ***Advanced Drug Delivery Reviews***, 59 (7), 2007.

154. Chaudhari SP and Dugar RP. Application of surfactants in solid dispersion technology for improving solubility of poorly water-soluble drugs, ***Journal of Drug Delivery Science and Technology***, 41, 2017.

155. Geusens B, Strobbe T, Bracken S, Dynoodt P, Sanders N, Gele MV and Lambert J. Lipid mediated gene delivery to the skin, ***European Journal of Pharmaceutical Sciences***, 199-211 (43), 2011.

156. Rowe RC, Sheskey PJ and Quinn ME (Editors). Handbook of pharmaceutical excipients (6th Ed.), ***Pharmaceutical Press***, 2009.

157. Damer KM and Jung CM. Chapter 30: Vaccines, ***Side effects of drugs annual***, 307-334 (38), 2016.

158. Larry R. Textbook of Veterinary Physiological Chemistry (Third Edition), ***Engelking***, 2015.

159. Nowroozi F, Almasi A, Javidi J, Haeri A and Dadashzadeh S. Effect of Surfactant Type, Cholesterol Content and Various Downsizing Methods on the Particle Size of Niosomes, ***Iran Journal of Pharmaceutical Research***, 1-11 (2), 2018.

160. Zampelas A and Magriplis E. New Insights into Cholesterol Functions: A Friend or an Enemy, ***US National Library of Medicine***, 11 (7), 2019.

161. Pozzi D, Caminiti R, Marianecci C, Carafa M, Santucci E, De Sanctis SC and Caracciolo G. Effect of cholesterol on the formation and hydration behavior of solid-supported niosomal membranes, ***Langmuir***, 2268–73 (26), 2010.

162. Yeo PL, Lim CL, Chye SM, Ling APK and Koh RY. Niosomes: A review of their structure, properties, methods of preparation, and medical applications, ***Asian Biomedicine Journal***, 301–13 (11), 2017.

163. Nowroozi F, Dadashzadeh S, Soleimanjahi H, Haeri A, Shahhosseini S, Javidi J and Karimi H. Theranostic niosomes for direct intratumoral injection: marked enhancement in tumor retention and anticancer efficacy, ***Nanomedicine (London)***, 2201–19 (13), 2018.

164. Abd-el-Kader H, Alani AW and Alany RG. Recent advances in non-ionic surfactant vesicles (niosomes): self-assembly, fabrication, characterization, drug delivery applications and limitations, ***Drug Delivery***, 87–100 (21), 2014.

165. Salazar J, Müller RH and Möschwitzer JP. Combinative particle size reduction technologies to produce drug nanocrystals, ***Journal of Pharmacy***, 1–14, 2017.

166. Liu J, Yu M, Ning X, Zhou C, Yang S and Zheng J. PEGylation and zwitterionization: pros and cons in renal clearance and tumor targeting of near-IR-emitting gold nanoparticles, ***Chemistry (International Edition, England)***, 12572–6 (52), 2013.

167. Nam JH, Kim SY and Seong H. Investigation on physicochemical characteristics of a Nano liposome-based system for dual drug delivery, ***Nanoscale Residential Letter***, 101–20 (13), 2018.

168. Areas JAG, Carlos-Menezes ACC and Soares RAM. Amaranth, ***Encyclopedia of food and health***, 135-140, 2016.

169. Alizadeh MN, Shayanfar A and Jouyban A. Solubilization of drugs using sodium lauryl sulfate: Experimental data and modeling, ***Journal of molecular liquids***, 410-414 (268), 2018.

170. Gill P, Moghadam TT and Ranjbar B. Differential Scanning Calorimetry Techniques: Applications in Biology and Nanoscience, ***Journal of Biomolecular Technology***, 167-193 (4), 2010.

171. Sindhu R, Binod P and Pandey A. Chapter 17 - Microbial Poly-3-Hydroxybutyrate and Related Copolymers, ***Industrial Biorefineries and White Biotechnology***, 575-605, 2015.

172. Lavor EP, Navarro MVM, Freire FD, Aragão CFS, Raffin FN, Barbosa EG and De Lima e Moura TFA. Application of thermal analysis to the study of antituberculosis drugs-excipient compatibility, ***Journal of Thermal Analysis and Calorimetry***, 115 (3), 2014.

173. Talvani A, Bahia MT, De Sá-Barreto LCL, Lima EM and Da Cunha-Filho MSS. Carvedilol: Decomposition kinetics and compatibility with pharmaceutical excipients, ***Journal of Thermal Analysis and Calorimetry***, 115 (3), 2014.

174. Durowoju IB, Bhandal KS, Hu J, Carpick B and Kirkitadze M. Differential Scanning Calorimetry, ***International Journal of Pharmaceutics***, 1184 (32), 2004.

175. Zhao XY. Calorimetry — A Method for Assessing the Thermal Stability and Conformation of Protein Antigen, ***Journal of Visualized Experiments***, 121, 2017.

176. Colby S. Differential Scanning Calorimetry; First and Second-Order Transitions in Differential Scanning Calorimetry, ***Langmuir***, 23 (9), 2016.

177. Hwang PH. 2013. Differential Scanning Calorimetry of PETE, ***DSC PETE***, https://www.colby.edu/chemistry/PChem/lab/DSCPETE.pdf, (Retrieved on: 20/12/2020).

178. Abraham J, Mohammed AP, Kumar MP, George SC and Thomas S. Chapter 8 - Thermoanalytical Techniques of Nanomaterial, ***Characterization of nanomaterials***, 213-236, 2018.

179. Mukhopadhyay S and Khuri AI. Response surface methodology, ***Computational Statistics***, 2 (2), 2010.

180. Wang Y, Luo YH, Zhao J and Sun BW. Selection of excipients for dispersible tablets of itraconazole through the application of thermal techniques and Raman spectroscopy, ***Journal of Thermal Analysis and Calorimetry***, 115 (3), 2014.

181. Balestrieri F, Magri AD, Magri AL, Marini D and Sacchini A. Application of differential scanning calorimetry to the study of drug-excipient compatibility, ***Thermochimica Acta***, 285 (2), 1996.

182. Kumar S, Bhargava D, Thakkar A and Arora S. Drug carrier systems for solubility enhancement of BCS class II drugs: a critical review, ***Critical Review of Therapeutic Drug Carrier Systems***, 217-256 (30), 2013.

183. Lo CT, Jahn A, Locascio N and Vreeland WN. Controlled self-assembly of monodisperse niosomes by microfluidic hydrodynamic focusing, ***Langmuir***, 8559-8566 (26), 2010.

184. Bragagni MP, Mennini N, Furlanetto S, Orlandini S, Ghelardini C and Mura D. Development and characterization of functionalized niosomes for brain targeting of dynorphin-B, ***European Journal of Biopharmaceuticals***, 73-79 (87), 2014.

185. Kuotsu K, Karim K, Mandal A, Biswas N, Guha A, Chatterjee S and Behera M. Niosome: a future of targeted drug delivery systems, ***Journal of Advanced Pharmaceutical Technology***, 374 (1), 2010.

186. Yeo PL, Lim CL, Chye SM, Kiong Ling AP and Koh RY. Niosomes: a review of their structure, properties, methods of preparation, and medical applications, ***Asian Biomedicine Journal***, 301-314 (11), 2018.

187. Kumar GP and Rajeshwarrao P. Nonionic surfactant vesicular systems for effective drug delivery—an overview, ***Acta Pharmaceutics***, 208-219 (1), 2011.

188. Uchegbu IF and Vyas SP. Non-ionic surfactant-based vesicles (niosomes) in drug delivery, ***International Journal of Pharmacy***, 33-70 (172), 1998.

189. Mahale NB, Thakkar PD, Mali RG, Walunj DR and Chaudhari SR. Niosomes: novel sustained-release non-ionic stable vesicular systems — an overview, ***Advanced Colloid Interface Science***, 183–184, 2012.

190. Khan MI, Madni A and Peltonen L. Development and in-vitro characterization of sorbitan monolaurate and poloxamer 184 based niosomes for oral delivery of diacerein, ***European Journal Pharmaceutical Science***, 88-95, 2016.

191. Escudero I, Geanta RM, Ruiz MO and Benito JM. Formulation and characterization of Tween 80/cholesterol niosomes modified with tri-n-octyl methyl ammonium chloride (TOMAC) for carboxylic acids entrapment, ***Colloidal Surfaces***, 167-177, 2014.

192. Di Marzio L, Marianecci C, Petrone M, Rinaldi F and Carafa M. Novel pH-sensitive non-ionic surfactant vesicles: comparison between Tween 21 and Tween 20, ***Colloidal Surfaces and Bio interfaces***, 18-24 (82), 2011.

193. Moghassemi S and Hadjizadeh A. Nano-niosomes as nanoscale drug delivery systems: an illustrated review, ***Journal of Controlled Release***, 22-36 (185), 2014.

194. Basak R and Bandyopadhyay R. The encapsulation of hydrophobic drugs in Pluronic F127 micelles: the effects of drug hydrophobicity, solution temperature and pH, ***Langmuir***, 4350-4356 (29), 2014.

195. Abdelbary G and El-Gendy N. Niosome-encapsulated gentamicin for ophthalmic controlled delivery, ***AAPS Pharmaceutical Science and Technology***, 740–747 (9), 2008.

196. Essa AE. Effect of formulation and processing variables on the particle size of sorbitan monopalmitate niosomes, ***Asian Journal of Pharmacy***, 227–233 (4), 2010.

197. Escudero I, Geanta RM, Ruiz MO and Benito JM. Formulation and characterization of Tween 80/cholesterol niosomes modified with tri-n-octyl methylammonium chloride (TOMAC) for carboxylic acids entrapment, ***Colloids and Surfaces A***, 167–177 (461), 2014.

198. Agarwal S, Bakshi V, Vitta P, Raghuram AP and Pandey S. Effect of cholesterol content and surfactant HLB on vesicle properties of niosomes, ***College of Pharmaceutical Sciences,*** 2003.

199. Peltonen L. Ultrasonic Processing- Green niosome production, ***Division of Pharmaceutical Chemistry and Technology, Faculty of Pharmacy, University of Helsinki***, 2016.

200. Ghori MU, Mahdi MH, Smith MA and Conway BR. Nasal Drug Delivery Systems: An Overview, ***American Journal of Pharmacological Sciences***, 3 (5), 2015.

201. Balakrishnan P, Shanmugam S, Lee WS, Lee WM, Kim JO and Oh DH. Formulation and in vitro assessment of minoxidil niosomes for enhanced skin delivery, ***International Journal of Pharmacy***, 1–8 (1), 2009.

202. Toshimitsu Y and Florence AT. Vesicle (niosome)-in-water-in-oil (v/w/o) emulsions: an in vitro study, ***International Journal of Pharmacy***, 117–23 (2), 1994.

203. White H. 2013. Interpreting Unexpected Events and Transitions in DSC Results, ***Tainstruments***,

http://www.tainstruments.com/pdf/literature/TA039.pdf, (Retrieved on: 10/01/2021).

204. Widmann J. Interpreting DSC curves; Part 2: Isothermal measurements, ***Mettler Toledo Thermal Analysis Systems***, 2, 2000.

205. Bhongade B, Talath S and Dhaneshwar S. A Validated Method for the Quantitation of Ciprofloxacin Hydrochloride Using Diffuse Reflectance Infrared Fourier Transform Spectroscopy, ***International Journal Spectroscopy***, 2014, 2013.

206. Nasseri B. Effect of cholesterol and temperature on the elastic properties of niosomal membranes, ***International Journal of Pharmacy***, 101-300 (95), 2005.

207. Williams D, Carter K and Baillie A. Visceral leishmaniosis in the BALB/c mouse: a comparison of the in vivo activity of five non-ionic surfactant vesicle preparations of sodium stibogluconate, ***Journal of Drug Targeting***, 1–7 (3), 2005.

208. Moazeni E, Gilani K, Sotoudegan F, Pardakhty A, Najafabadi AR and Ghalandari R. Formulation and in vitro evaluation of ciprofloxacin containing niosomes for pulmonary delivery, ***Journal of Microencapsulation***, 618–27 (7), 2010.

209. Hossann M, Wang T, Wiggenhorn M, Schmidt R, Zengerle A and Winter G. Size of thermosensitive liposomes influences content release, ***Journal of Controlled Release***, 436–43 (3), 2010.

210. Taylor KMG and Craig DQM. Physical methods of study: differential scanning calorimetry. Liposomes: a practical approach, ***Oxford University Press***, 79–104, 2003.

211. Tavano L, Vivacqua M, Carito V, Muzzalupo R, Caroleo MC and Nicoletta F. Doxorubicin loaded magneto-niosomes for targeted drug delivery, ***Colloidal Surfaces and Bio interfaces***, 803–7 (102), 2013.

212. Bhardwaj P, Tripathi P, Gupta R and Pandey S. Niosomes: A review on niosomal research in the last decade, ***Journal of Drug Delivery Science and Technology***, Part A (56), 2020.

213. Tripper H and Robert RH. Skin, ***Skin Pharmacology and Physiology***, 109-111 (9), 2016.

214. Jain S, Sapre R, Tiwary AK and Jain NK. Proultraflexible lipid vesicles for effective transdermal delivery of levonorgestrel: Development, characterization, and performance evaluation, ***AAPS Pharmaceutical Science and Technology***, 513–522 (6), 2005.

215. Sinico C and Fadda AM. Vesicular carriers for dermal drug delivery, ***Taylor and Francis Online***, 813–825 (6), 2009.

216. Singh MR, Pradhan K and Singh D. Lipid matrix systems with emphasis on lipid microspheres: Potent carriers for transcutaneous delivery of bioactives, ***Current Drug Delivery***, 243–254 (9), 2015.

217. Singh MR, Singh D and Swarnlata S. Development and in vitro evaluation of polar lipid based lipospheres for oral delivery of peptide drugs, ***International Journal of Drug Delivery***, 15–26 (1), 2009.

218. Mujoriya RZ and Bodla RB. Niosomes challenge in preparation for pharmaceutical scientist, ***International Journal of Applied Pharmacy***, 11–15 (3), 2011.

219. Rogerson A, Cummings J, Willmott N and Florence AT. The distribution of doxorubicin in mice following administration in niosomes, ***International Journal of Pharmacy***, 337-342 (40), 1988.

220. Kumar GP and Rajeshwarrao P. Non-ionic surfactant vesicular systems for effective drug delivery—an overview, ***Acta Pharmacy***, 208-219 (1), 2011.

221. Barlow DJ, Ma G and Lawrence MJ. Neutron reflectance studies of a novel non-ionic surfactant and molecular modelling of the surfactant vesicles, ***Langmuir***, 3737-3741 (11), 1995.

222. Bernard MS, Arunothayanun P, Uchegbu IF and Florence AT. Rheological and morphological study of polyhedral and spherical/tubular niosomes, ***Third UKCRS Symposium on Controlled Drug Delivery***, 1996.

223. Ijeoma F, Uchegbu A, Suresh P and Vyas B. Non-ionic surfactant-based vesicles (niosomes) in drug delivery, ***International Journal of Pharmaceutics***, 33-70 (172), 1998.

224. Escudero I, Geanta RM, Ruiz MO and Benito JM. Formulation and characterization of Tween 80/cholesterol niosomes modified with tri-n-octyl methyl ammonium chloride (TOMAC) for carboxylic acids entrapment, ***Colloids Surfaces & Physicochemical Engineering***, 167-177 (461), 2014.

225. Di Marzio L, Marianecci C, Petrone M, Rinaldi F and Carafa M. Novel pH-sensitive non-ionic surfactant vesicles: comparison between Tween 21 and Tween 20, ***Colloids Surfaces and Bio interfaces***, 18-24 (82), 2011.

226. Moghassemi S and Hadjizadeh A. Nano-niosomes as nanoscale drug delivery systems: an illustrated review, ***Journal of Controlled Release***, 22-36 (185), 2014.

227. Khan MI, Madni A, Hirvonen J and Peltonen L. Ultrasonic processing technique as a green preparation approach for diacerein-loaded niosomes, ***AAPS Pharmaceutical Science and Technology***, 1554-1563 (18), 2017.

228. Baillie AJ, Florence AT, Hume LR, Muirhead GT and Rogerson A. The preparation and properties of niosomes non-ionic surfactant vesicles, ***Journal of Pharmacy and Pharmacology***, 863-868 (37), 2001.

229. Ravalika V and Sailaja AK. Formulation and evaluation of etoricoxib niosomes by thin film hydration technique and ether injection method, ***Nano Biomedicines***, 242-248 (9), 2017.

230. Kanaani L, Tabrizi MM and Khiyavi AA. Improvement the efficacy of cisplatin by niosome nanoparticles against human breast cancer Cell line BT-20: an in vitro study, ***Asian Pacific Journal of Cancer and Biology***, 25-26 (2), 2017.

231. Amiri B, Ahmadvand H, Farhadi A, Najma Afshar A, Chiani M and Norouzian D. Delivery of vinblastine-containing niosomes results in potent in vitro/in vivo cytotoxicity on tumour cells, ***Industrial Pharmacy***, 1371-1376 (44), 2018.

232. Chee-Yean E, Amged S and El-Hawrani S. The pH of commonly used topical ear drops in the treatment of otitis externa, ***Ear, Nose and Throat Journal***, 1 (1), 2011

233. Ruckmani K and Sankar V. Formulation and optimization of zidovudine niosomes, ***Aaps Pharmacy, Science and Technology***, 1119–1127 (3), 2010.

234. Ceren Ertekin Z, Sezgin Bayindir Z and Yuksel N. Stability studies on piroxicam encapsulated niosomes, ***Current Drug Delivery***, 192–199 (2), 2015.

235. Jain S, Mittal A and Jain AK. Enhanced topical delivery of cyclosporine-A using PLGA nanoparticles as carrier, ***Current Nanoscience***, 524–530 (4), 2011.

236. Ross HA. A dialysis rate method for the measurement of free iodothyronine and steroid hormones in blood, ***Experientia***, 34 (4), 1978.

237. Brodersen R. Determination of the vacant amount of high-affinity bilirubin binding site on serum albumin, ***Acta Pharmacologica et Toxicologica***, 42 (3), 1978.

238. Protein Biology Resource Library. 2011. Dialysis Methods for Protein Research, ***Thermo Fisher Scientific***, https://www.thermofisher.com/za/en/home/life-science/protein-biology/protein-biology-learning-center/protein-biology-resourcelibrary/pierce-protein-methods/dialysis-methods-protein-research.html, (Retrieved on: 23/01/2021).

239. Asthana A, Singh D and Sharma PK. Etodolac Containing Topical Niosomal Gel: Formulation Development and Evaluation, ***Journal of Drug Delivery***, 334-336 (9), 2016.

240. Al-Meshal MA. Oral administration of liposomes containing cyclosporine: a pharmacokinetic study, ***International Journal of Pharmacy***, 163–168 (2), 1998.

241. Khanab DH, Bashira S, Figueiredo H, Santos A and Imran Khan M. Process optimization of ecological probe sonication technique for production of rifampicin loaded niosomes, ***Journal of Drug Delivery Science and Technology,*** 27-33 (50), 2019.

242. Gokhale A. Achieving Zero-Order Release Kinetics Using Multi-Step Diffusion-Based Drug Delivery, ***Pharmaceutical Technology***, 5 (38), 2014

243. McMartin KE, Sebastian CS, Dies D and Jacobsen D. Kinetics and metabolism of fomepizole in healthy humans, ***Clinical Toxicology***, 375-83 (5), 2012.

244. Jain A and Jain SK. In vitro release model fitting of liposomes: an insight, ***Chemistry and Physics***, 28-40 (201), 2016.

245. Costa P and Sousa Lobo JM. Modelling and comparison of dissolution profiles, ***European Journal of Pharmaceutical Science***, 123-133 (13), 2001.

246. Yeeling I, Wua Sonali B, Škalko N and Cagno MPB. Dissolution, ***European Journal of Pharmaceutical Sciences,*** Volume 138, 1 October 2019.

247. Di Cagno M, Bibi HA and Bauer-Brandl A. New biomimetic barrier Permeapad™ for efficient investigation of passive permeability of drugs, ***European Journal Pharmaceutical Sciences***, 29-34 (73), 2015.

248. Nothnagel L and Wacker MG. How to measure release from nanosized carriers, ***European Journal of Pharmaceutical Sciences***, 199-211 (180), 2018.

249. Gouda R, Baishya H and Qing Z. Application of mathematical models in drug release kinetics of carbidopa and levodopa ER tablets, ***Journal of Developing Drugs***, 6 (2), 2017.

250. Higuchi T. Mechanism of sustained-action medication, theoretical analysis of rate of release of solid drugs dispersed in solid matrices, ***Journal of Pharmaceutical Sciences***, 52 (12), 1963.

251. Shahavi MH, Hosseini M, Jahanshahi M and Najafpour G. Optimization of encapsulated clove oil particle size with biodegradable shell using design expert methodology, ***Pakistan Journal of Biotechnology***, 12 (2), 2015.

252. Gibson A and Nicholson C. 2017. A Beginner‘s Guide to Recurrent Networks and LSTMs, ***Deep learning Textbook***, https://deeplearning4j.org/lstm.html, (Retrieved on: 26/12/2020).

253. Medscape Drugs and Diseases. 2016. Antibiotics, Medscape, https://reference.medscape.com, (Retrieved on: 07/01/2021).

254. Seleci DA, Seleci M, Walter JG, Stahl F and Scheper T. Nanostructural Biomaterials and Applications, ***Hindawi***, 2016.

255. Mahale NB, Thakkar PD, Mali RG, Walunj DR and Chaudhari S. Niosomes: novel sustained-release non-ionic stable vesicular systems—an overview, ***Advances in Colloid and Interface Science***, 46–54 (183), 2012.

256. Tavano L, Gentile L, Oliviero R and Muzzalupo R. Novel gel-niosomes formulations as multicomponent systems for transdermal drug delivery, ***Colloids and Surfaces B: Bio interfaces***, 281–288 (110), 2013.

257. Li Q, Li Z and Zeng W. Proniosome-derived niosomes for tacrolimus topical ocular delivery: in vitro cornea permeation, ocular irritation, and in vivo anti-allograft rejection, ***European Journal of Pharmaceutical Sciences***, 115–123 (62), 2014.

258. Bayindir ZS, Beşikci A and Yüksel N. Paclitaxel-loaded niosomes for intravenous administration: pharmacokinetics and tissue distribution in rats, ***Turkish Journal of Medical Sciences***, 1403–1412 (45), 2015.

259. Mehta SK and Jindal N. Tyloxapol niosomes as prospective drug delivery module for antiretroviral drug nevirapine, ***AAPS Pharmaceutical Science and Technology***, 67–75 (16), 2014.

260. Karim KM, Mandal AS, Biswas N, Guha A, Chatterjee S and Behera M. Niosomes: a future of targeted drug delivery system, ***Journal of Advanced Pharmaceutical and Technological Research (JAPTR)***, 374-380 (4), 2010.

261. Dhanvir K and Kumar S. Niosomes: present scenario and future aspects, ***Journal of Drug Delivery***, 35-43 (85), 2018.

262. Rampal R, Kalpana N, Singh SK and Mishra D. Niosomes: a controlled and novel drug delivery system, ***Biological Pharmacy***, 945-953 (34), 2011.

263. Ibrahim MM, Nair AB, Aldubiab BE and Shehata TM. Hydrogels and their combination with liposomes, niosomes or transfersomes for dermal and transdermal delivery, ***IntechOpen***, Volume 1, 2017.

264. Gannu Kumar P and Pogaku R. Nonionic surfactant vesicular systems for effective drug delivery—an overview, ***Pharmaceutics***, 208-219 (43), 2011.

265. Hamdi A, Alani WG and Alany G. Recent advances in non-ionic surfactant vesicles (niosomes): self-assembly, fabrication, characterization, drug delivery applications, and limitations, ***Drug delivery Information***, 1-14 (10), 2013.

266. Marinecci C, Di Marzio L, Rinaldi F, Celia C, Paolino D, Alhaique F, Esposito S and Carafa M. Niosomes from 80s to present: the state of the art, ***Advanced Colloid Interface Science***, 187-206 (205), 2014

267. Moghassemi S and Hadjizadeh A. Nano-niosomes as nanoscale drug delivery systems: an illustrated review, ***Journal of Controlled Release***, 22-36 (185), 2014.

268. Sharma V, Anandhakumar S and Manickam S. Self-degrading niosomes for encapsulation of hydrophilic and hydrophobic drugs: an efficient carrier for cancer multi-drug delivery, ***Mater Science and Engineering***, 393-400 (56), 2015.

269. Carbamazepine. 2019. Compound summary, ***PubChem NCBI***, https://pubchem.ncbi.nlm.nih.gov/compound/Carbamazepine, (Retrieved on: 14/04/2021)

270. NMR solvent selection. 2018. Solvent selection, ***BioChromato***, https://biochromato.com/nmrsolventselection/#:~:text=%E2%80%9CFor%201H%20NMR%2C%20it,considered%20in%20NMR%20solvent%20088786selection, (Retrieved on: 23/04/2021)

271. Hope MJ, Bally MB, Webb G and Cullis PR. Production of large uni-lamellar vesicles by a rapid extrusion procedure. Characterization of size distribution trapped volume, and ability to maintain a membrane potential, ***Biochim. Biophys. Acta***, 55-65 (812), 1985.

272. Armengol X and Estelrich J. Physical stability of different liposome compositions obtained by extrusion method, ***Journal of Microencapsulation***, 525-535 (11), 1994.

273. Jousma H, Talsma H, Spies F, Joosten JGH, Junginger HE and Crommelin DJA. Characterization of liposomes, The Influence of extrusion of multilamellar vesicles through polycarbonate membranes on particle size, particle size distribution and number of bilayers, ***International Journal of Pharmaceutics***, 263-274 (35), 1987.

274. Viriyaroj A, Ngawhirunpat T, Sukma M, Akkaramongkolporn P and Ruktanonchai U. Physicochemical properties and antioxidant activity of gamma-oryzanol-loaded liposome formulations for topical use, ***Pharmaceutical Development Technology***, 665-671 (14), 2009.

275. Samimi S, Niloufar M, Eftekhari RB and Dorkoosh F. Chapter 3 - Lipid-Based Nanoparticles for Drug Delivery Systems, ***Nanoscience and Nanotechnology in Drug Delivery***, 47-76 (1), 2019.

276. Asthana GS, Sharma PK and Asthana A. In vitro and in vivo evaluation of niosomal formulation for controlled delivery of clarithromycin, ***Hindawi***, 2016, 2016.

277. Pao D, Gutiérrez G, Coca J and Pazos C. Preparation and characterization of niosomes containing resveratrol, ***Journal of Food Engineering***, 227-234 (117), 2013.

278. Manosroi A, Jantrawut P, Akazawa H, Akihisa T, Manosroi W and Manosroi J. Transdermal absorption enhancement of gel containing elastic niosomes loaded with gallic acid from Terminalia chebula galls, ***Pharmaceutical Biology***, 553-562 (49), 2011.

279. Gutiérrez G, Matos M, Barrero P, Pando D, Iglesias O and Pazos C. Iron-entrapped niosomes and their potential application for yogurt fortification, ***LWT-Food Science and Technology***, 550-556 (74), 2016.

280. Alexander M, Lopez AA, Fang Y and Corredig M. Incorporation of phytosterols in soy phospholipids nanoliposomes: encapsulation efficiency and stability, ***LWT-Food Science and Technology***, 427-436 (47), 2012.

281. Venishki C and Mohammad V. Physical properties and stability of quercetin-loaded niosomes: Stabilizing effects of phytosterol and polyethylene glycol in orange juice model, ***Journal of Food Engineering*****,** 110-463 (296), 2020.

282. Martinez Devesa P, Willis CM and Capper JW. External auditory canal pH in chronic otitis externa, ***Allied Science***, 320-4 (28), 2003.

283. Van Balen FA, Smit WM, Zuithoff NP and Verheij TJ. Clinical efficacy of three common treatments in acute otitis externa in primary care: Randomized controlled trial, ***British Medical Journal***, 1201-5 (32), 2003.

284. Nilssen E, Wormald PJ and Oliver S. Glycerol and ichthammol: Medicinal solution or mythical potion, ***Journal of Laryngeal Otology***, 319-21 (110), 1996.

285. Ahmed K, Roberts ML and Mannion PT. Antimicrobial activity of glycerin-ichthammol in otitis externa, ***Allied Science***, 201-3 (20), 1995.

286. Slack RW. A study of three preparations in the treatment of otitis externa, ***Journal of Laryngeal Otology***, 533-5 (6), 1987.

287. Smith RB and Moodie J. Comparative efficacy and tolerability of two antibacterial/anti-inflammatory formulations ('Otomize' spray and 'Otosporin' drops) in the treatment of otitis externa in general practice, ***Current Medicine***, 661-7 (10), 1990.

288. Smith RB and Moodie J. A general practice study to compare the efficacy and tolerability of spray ('Otomize') versus a standard drop formulation ('Sofradex') in the treatment of patients with otitis externa, ***Current Medicine***, 12-18 (12), 1990.

289. Hachem JP, Crumrine D and Fluhr J. pH directly regulates epidermal permeability barrier homeostasis, and stratum corneum integrity cohesion, ***Journal of Investigative Dermatology***, 345-353 (121), 2003.

290. Fabricant ND and Perlstein MA. pH of the cutaneous surface of the external auditory canal: A study of 27 infants, 44 children and 60 adults, ***Arch Otolaryngologists***, 201-9 (49), 2009.

291. Fabricant ND. The pH factor in treatment of otitis externa, ***A.M.A Arch Otolaryngologists***, 11-12 (65), 1957.

292. Surface Tension. 2020. Surface tension and water, ***USGS***, https://www.usgs.gov/special-topic/water-science-school/science/surface-tension-and-water?qt-science_center_objects=0#qt-science_center_objects_USGS_GOV, (Retrieved on: 23/04/2021)

293. Belyadi H, Fathi E and Belyadi E. Chapter Four - Multiscale Fluid Flow and Transport in Organic-Rich Shale, ***Adhesives Technology Handbook***, 37-48 (4), 2017.

294. Nematollahi MH, Pardakhty A, Mahanai M and Asadakarim G. Changes in physical and chemical properties of niosomes membrane induced by cholesterol, ***Royal Society of Chemistry***, 49463-72, 2017.

295. Nematollahi MH, Abbas P, Mahanai M, Mehrabani M and Gholamreza A. Changes in physical and chemical properties of niosome membrane induced by cholesterol: a promising approach for niosome bilayer intervention, ***RSC Advances***, Issue 78, 2017.

296. Azarbayjani AF, Jouyban A and Chan SY. Impact of surface tension in pharmaceutical sciences, ***Journal of Pharmaceutical Sciences***, 218-228 (12), 2009.

297. Vargha-Butler EI, Foldvari M and Mesei M. Study of the sedimentation behaviour of liposomal drug delivery systems, ***Colloids and Surfaces***, 375-398 (42), 1989.

298. Popova VA and Hancho DK. Study of the sedimentation behaviour of liposomal drug delivery systems, ***Journal of Pharmaceutical Sciences***, 1204-1214 (4), 2007.

299. Schnitzer E, Kozlov M and Lichtenberg D. The effect of cholesterol on the solubilization of phosphatidylcholine bilayers by the non-ionic surfactant Triton X-100, ***Chemistry and Physics of lipids***, 69-82 (1), 2005.

300. Davis PJ and Keough KMW. Differential scanning calorimetric studies of aqueous dispersions of mixtures of cholesterol with some mixed-acid and single-acid phosphatidylcholines, ***Biochemistry,*** 6334–6340 (22), 1983.

301. Nasseri B and Florence AT. A vesicular shuttle: transport of a vesicle within a flexible microtube, ***Journal of Controlled Release***, 233-240 (92), 2003.

302. Kazi KM, Mandal AS, Biswas N, Guha A, Chatterjee S, Behera M and Kuotso K. Niosome: A future of targeted drug delivery systems, ***Journal of Advanced Pharmaceutical Technology and Research***, 374-380 (4), 2010.

303. Schubert R, Wolburg H, Schmidt KH and Roth HJ. Loading of preformed liposomes with high trapping efficiency by detergent induced formation of transient holes, ***Chemistry and Physics of Lipids***, 121-137 (58), 1991.

304. Aguilar L, Ortega-Pierres G, Campos B, Fonseca R, Ibánes M, Wong C, Farfán N, Naciff JM, Kaetzel MA, Dedman JR and Baeza I. Phospholipid specific non-bilayer

molecular arrangements that are antigenic, ***Journal of Biological Chemistry***, 25193-25196 (36), 1999.

305. Frohlich M, Bretch V and Peschka-Suss R. Parameters influencing the determination of liposome lamellarity by 31P-NMR, ***Chemistry and Physics of Lipids***, 103-112 (1), 2001.

306. ^{1}H NMR. 2021. ^{1}H NMR Chemical Shifts, ***California State Polytechnic University***, https://www.cpp.edu/~lsstarkey/courses/NMR/NMRshifts1H-general.pdf, (Retrieved on: 24/04/2021).

307. Huster D, Jin AJ, Arnold K and Gawrisch K. Water permeability of polyunsaturated lipid membranes measured by 17O-NMR, ***Biophysics Journal***, 855-864 (73), 1997.

308. Mayer LD, Hope HJ, Cullis PR and Janoff AS. Solute distributions and trapping efficiencies observed in freeze-thawed multilamellar vesicles, ***Biochim. Biophys. Acta***, 193-196 (817), 1985.

309. Fenske DB. Structural and motional properties of vesicles as revealed by nuclear magnetic resonance, ***Chemistry and Physics of Lipids***, 143-162 (64), 1993.

APPENDIX A

BATCH SET PRODUCTION RECORDS AND SAMPLE BATCH PRODUCTION RECORD FOR DEVELOPMENT AND OPTIMIZATION FORMULATIONS

Biopharmaceutics Research Laboratory
Department of Pharmaceutics, Faculty of Pharmacy
Rhodes University
Makhanda 6140, South Africa

BATCH SET PRODUCTION RECORD 1/1

Product:	**Date of Manufacture:**
Ciprofloxacin niosomes	12/12/2020
Batch set:	**Batch size:** 100ml
Optimization batches (F1 - F17)	

Batch record issued by	**Date**
Batch record verified by	**Date**
Batch record verified by	**Date**
Batch record verified by	**Date**

SIGNATURE & INITIAL REFERENCE

Full name (Print)	Signature	Initials	Date

Biopharmaceutics Research Laboratory
Department of Pharmaceutics, Faculty of Pharmacy
Rhodes University
Makhanda 6140, South Africa

BATCH PRODUCTION RECORD 1/2

Materials	Batch No	Original formula	Working formula	Dispensed by	Checked by
Ciprofloxacin	RM000402	100 mg	150 mg		
Tween® 80	P6224	1 g	1 g		
Sodium lauryl sulfate	J054016	1 g	1 g		
Cholesterol	22968	1 g	1 g		
HPLC water		100 mL	100 mL		

EQUIPMENT VERIFICATION

Description	Type/Model	Verified by	Confirmed by
Top loading analytical balance	AG135 Mettler Toledo®		
Refrigerator	Fuchs ware®		
Probe sonicator	Bandelin®		

Biopharmaceutics Research Laboratory
Department of Pharmaceutics, Faculty of Pharmacy
Rhodes University
Makhanda 6140, South Africa

BATCH SET PRODUCTION RECORD 2/2

Product:	**Date of Manufacture:**
Ciprofloxacin niosomes	12/12/2020
Batch set: F1	**Batch size:** 100ml

MANUFACTURING PROCEDURE

Steps	Description	Checked by	Verified by
1	Weigh 150 mg of ciprofloxacin on a top loading balance and first mix with 100 mL of water in a 250 mL beaker with the help of a magnetic stirrer. Add 1 g of cholesterol and 1 g of each of the surfactants (sodium lauryl sulfate and Tween® 80). Probe sonicate the mixture for 6 minutes at 60 °C of probe temperature in a pulsatile manner (50 s sonication with 10 s pause) with 30 % amplitude.		
2	After probe sonication, collect the niosomes and store in a 100 mL amber bottle at 4 °C overnight to mature.		

APPENDIX B

BATCH SUMMARY RECORDS FOR DEVELOPMENT AND OPTIMIZATION OF FORMULATION

Biopharmaceutics Research Laboratory
Department of Pharmaceutics, Faculty of Pharmacy
Rhodes University
Makhanda 6140, South Africa

BATCH SET PRODUCTION RECORD 1/1

Product:
Ciprofloxacin niosomes
Batch number: F1

Start of Manufacture: 12/12/2020 08:00
End of Manufacture: 13/12/2020 08:00
Batch size: 100 mL

FORMULATION

Materials	Batch No	Original formula	Working formula	Dispensed by	Checked by
Ciprofloxacin	RM000402	100 mg	150 mg		
Tween® 80	P6224	1 g	1 g		
Sodium lauryl sulfate	J054016	1 g	1 g		
Cholesterol	22968	1 g	1 g		
HPLC water		100 mL	100 mL		

Vesicle size: 114.78 nm
PDI: 0.34
Zeta potential: -25.30 mV
Entrapment efficiency: 99.25 %
Appearance: Milky white solution.

Biopharmaceutics Research Laboratory
Department of Pharmaceutics, Faculty of Pharmacy
Rhodes University
Makhanda 6140, South Africa

BATCH SET PRODUCTION RECORD 1/1

Product:
Ciprofloxacin niosomes
Batch number: F2

Start of Manufacture: 12/12/2020 08:20
End of Manufacture: 13/12/2021 08:20
Batch size: 100 mL

FORMULATION

Materials	Batch No	Original formula	Working formula	Dispensed by	Checked by
Ciprofloxacin	RM000402	100 mg	150 mg		
Tween® 80	P6224	1 g	1 g		
Sodium lauryl sulfate	J054016	1 g	1 g		
Cholesterol	22968	1 g	1 g		
HPLC water		100 mL	100 mL		

Vesicle size: 119.93 nm
PDI: 0.30
Zeta potential: -24.30mV
Entrapment efficiency: 93.74 %
Appearance: Milky white solution.

Biopharmaceutics Research Laboratory
Department of Pharmaceutics, Faculty of Pharmacy
Rhodes University
Makhanda 6140, South Africa

BATCH SET PRODUCTION RECORD 1/1

Product:
Ciprofloxacin niosomes
Batch number: F3

Start of Manufacture: 12/12/2020 08:35
End of Manufacture: 13/12/2021 08:35
Batch size: 100 mL

FORMULATION

Materials	Batch No	Original formula	Working formula	Dispensed by	Checked by
Ciprofloxacin	RM000402	100 mg	150 mg		
Tween® 80	P6224	1 g	1 g		
Sodium lauryl sulfate	J054016	1 g	1 g		
Cholesterol	22968	1 g	0.6 g		
HPLC water		100 mL	100 mL		

Vesicle size: 118.65 nm
PDI: 0.28
Zeta potential: -31.30 mV
Entrapment efficiency: 91.76 %
Appearance: Milky white solution.

Biopharmaceutics Research Laboratory
Department of Pharmaceutics, Faculty of Pharmacy
Rhodes University
Makhanda 6140, South Africa

BATCH SET PRODUCTION RECORD 1/1

Product:
Ciprofloxacin niosomes
Batch number: F4

Start of Manufacture: 12/12/2020 09:00
End of Manufacture: 13/12/2021 09:00
Batch size: 100 mL

FORMULATION

Materials	Batch No	Original formula	Working formula	Dispensed by	Checked by
Ciprofloxacin	RM000402	100 mg	150 mg		
Tween® 80	P6224	1 g	1 g		
Sodium lauryl sulfate	J054016	1 g	1 g		
Cholesterol	22968	1 g	0.6 g		
HPLC water		100 mL	100 mL		

Vesicle size: 117.95 nm
PDI: 0.35
Zeta potential: -31.20 mV
Entrapment efficiency: 94.56 %
Appearance: Milky white solution.

Biopharmaceutics Research Laboratory
Department of Pharmaceutics, Faculty of Pharmacy
Rhodes University
Makhanda 6140, South Africa

BATCH SET PRODUCTION RECORD 1/1

Product:
Ciprofloxacin niosomes
Batch number: F5

Start of Manufacture: 12/12/2020 09:15
End of Manufacture: 13/12/2021 09:15
Batch size: 100 mL

FORMULATION

Materials	Batch No	Original formula	Working formula	Dispensed by	Checked by
Ciprofloxacin	RM000402	100 mg	150 mg		
Tween® 80	P6224	1 g	1 g		
Sodium lauryl sulfate	J054016	1 g	1 g		
Cholesterol	22968	1 g	1 g		
HPLC water		100 mL	100 mL		

Vesicle size: 165.97 nm
PDI: 0.38
Zeta potential: -39.37 mV
Entrapment efficiency: 86.64 %
Appearance: Milky white solution.

Biopharmaceutics Research Laboratory
Department of Pharmaceutics, Faculty of Pharmacy
Rhodes University
Makhanda 6140, South Africa

BATCH SET PRODUCTION RECORD 1/1

Product:
Ciprofloxacin niosomes
Batch number: F6

Start of Manufacture: 12/12/2020 09:25
End of Manufacture: 13/12/2021 09:25
Batch size: 100 mL

FORMULATION

Materials	Batch No	Original formula	Working formula	Dispensed by	Checked by
Ciprofloxacin	RM000402	100 mg	150 mg		
Tween® 80	P6224	1 g	1 g		
Sodium lauryl sulfate	J054016	1 g	1 g		
Cholesterol	22968	1 g	0.6 g		
HPLC water		100 mL	100 mL		

Vesicle size: 148.23 nm
PDI: 0.31
Zeta potential: -23.80 mV
Entrapment efficiency: 92.25 %
Appearance: Milky white solution.

Biopharmaceutics Research Laboratory
Department of Pharmaceutics, Faculty of Pharmacy
Rhodes University
Makhanda 6140, South Africa

BATCH SET PRODUCTION RECORD 1/1

Product:
Ciprofloxacin niosomes
Batch number: F7

Start of Manufacture: 12/12/2020 09:40
End of Manufacture: 13/12/2021 09:40
Batch size: 100 mL

FORMULATION

Materials	Batch No	Original formula	Working formula	Dispensed by	Checked by
Ciprofloxacin	RM000402	100 mg	150 mg		
Tween® 80	P6224	1 g	1 g		
Sodium lauryl sulfate	J054016	1 g	1 g		
Cholesterol	22968	1 g	0.6 g		
HPLC water		100 mL	100 mL		

Vesicle size: 220.55 nm
PDI: 0.48
Zeta potential: -35.70 mV
Entrapment efficiency: 20.39 %
Appearance: Milky white solution.

Biopharmaceutics Research Laboratory
Department of Pharmaceutics, Faculty of Pharmacy
Rhodes University
Makhanda 6140, South Africa

BATCH SET PRODUCTION RECORD 1/1

Product:
Ciprofloxacin niosomes
Batch number: F8

Start of Manufacture: 12/12/2020 10:00
End of Manufacture: 13/12/2021 10:00
Batch size: 100 mL

FORMULATION

Materials	Batch No	Original formula	Working formula	Dispensed by	Checked by
Ciprofloxacin	RM000402	100 mg	150 mg		
Tween® 80	P6224	1 g	1 g		
Sodium lauryl sulfate	J054016	1 g	1 g		
Cholesterol	22968	1 g	0.6 g		
HPLC water		100 mL	100 mL		

Vesicle size: 117.57 nm
PDI: 0.31
Zeta potential: -32.00 mV
Entrapment efficiency: 92.52 %
Appearance: Milky white solution.

Biopharmaceutics Research Laboratory
Department of Pharmaceutics, Faculty of Pharmacy
Rhodes University
Makhanda 6140, South Africa

BATCH SET PRODUCTION RECORD 1/1

Product:
Ciprofloxacin niosomes
Batch number: F9

Start of Manufacture: 12/12/2020 10:15
End of Manufacture: 13/12/2021 10:15
Batch size: 100 mL

FORMULATION

Materials	Batch No	Original formula	Working formula	Dispensed by	Checked by
Ciprofloxacin	RM000402	100 mg	150 mg		
Tween® 80	P6224	1 g	1 g		
Sodium lauryl sulfate	J054016	1 g	1 g		
Cholesterol	22968	1 g	0.6 g		
HPLC water		100 mL	100 mL		

Vesicle size: 151.75 nm
PDI: 0.29
Zeta potential: -33.40 mV
Entrapment efficiency: 51.08 %
Appearance: Milky white solution.

Biopharmaceutics Research Laboratory
Department of Pharmaceutics, Faculty of Pharmacy
Rhodes University
Makhanda 6140, South Africa

BATCH SET PRODUCTION RECORD 1/1

Product:
Ciprofloxacin niosomes
Batch number: F10

Start of Manufacture: 12/12/2020 10:25
End of Manufacture: 13/12/2021 10:25
Batch size: 100 mL

FORMULATION

Materials	Batch No	Original formula	Working formula	Dispensed by	Checked by
Ciprofloxacin	RM000402	100 g	150 mg		
Tween® 80	P6224	1 g	1 g		
Sodium lauryl sulfate	J054016	1 g	1 g		
Cholesterol	22968	1 g	1 g		
HPLC water		100 mL	100 mL		

Vesicle size: 148.92 nm
PDI: 0.37
Zeta potential: -35.50 mV
Entrapment efficiency: 95.87 %
Appearance: Milky white solution.

Biopharmaceutics Research Laboratory
Department of Pharmaceutics, Faculty of Pharmacy
Rhodes University
Makhanda 6140, South Africa

BATCH SET PRODUCTION RECORD 1/1

Product:
Ciprofloxacin niosomes
Batch number: F11

Start of Manufacture: 12/12/2020 10:45
End of Manufacture: 13/12/2021 10:45
Batch size: 100 mL

FORMULATION

Materials	Batch No	Original formula	Working formula	Dispensed by	Checked by
Ciprofloxacin	RM000402	100 mg	150 mg		
Tween® 80	P6224	1 g	1 g		
Sodium lauryl sulfate	J054016	1 g	1 g		
Cholesterol	22968	1 g	0.6 g		
HPLC water		1 00 mL	100 mL		

Vesicle size: 116.43 nm
PDI: 0.30
Zeta potential: -31.20 mV
Entrapment efficiency: 92.79 %
Appearance: Milky white solution.

Biopharmaceutics Research Laboratory
Department of Pharmaceutics, Faculty of Pharmacy
Rhodes University
Makhanda 6140, South Africa

BATCH SET PRODUCTION RECORD 1/1

Product:
Ciprofloxacin niosomes
Batch number: F12

Start of Manufacture: 12/12/2020 11:00
End of Manufacture: 13/12/2021 11:00
Batch size: 100 mL

FORMULATION

Materials	Batch No	Original formula	Working formula	Dispensed by	Checked by
Ciprofloxacin	RM000402	100 mg	150 mg		
Tween® 80	P6224	1 g	1 g		
Sodium lauryl sulfate	J054016	1 g	1 g		
Cholesterol	22968	1 g	0.2 g		
HPLC water		100 mL	100 mL		

Vesicle size: 286.52 nm
PDI: 0.38
Zeta potential: -20.05 mV
Entrapment efficiency: 54.59 %
Appearance: Milky white solution.

Biopharmaceutics Research Laboratory
Department of Pharmaceutics, Faculty of Pharmacy
Rhodes University
Makhanda 6140, South Africa

BATCH SET PRODUCTION RECORD 1/1

Product:
Ciprofloxacin niosomes
Batch number: F13

Start of Manufacture: 12/12/2020 11:10
End of Manufacture: 13/12/2021 11:10
Batch size: 100 mL

FORMULATION

Materials	Batch No	Original formula	Working formula	Dispensed by	Checked by
Ciprofloxacin	RM000402	100 mg	150 mg		
Tween® 80	P6224	1 g	1 g		
Sodium lauryl sulfate	J054016	1 g	1 g		
Cholesterol	22968	1 g	0.6 g		
HPLC water		100 mL	100 mL		

Vesicle size: 118.68 nm
PDI: 0.26
Zeta potential: -33.28 mV
Entrapment efficiency: 92.43 %
Appearance: Milky white solution.

Biopharmaceutics Research Laboratory
Department of Pharmaceutics, Faculty of Pharmacy
Rhodes University
Makhanda 6140, South Africa

BATCH SET PRODUCTION RECORD 1/1

Product:
Ciprofloxacin niosomes
Batch number: F14

Start of Manufacture: 12/12/2020 11:25
End of Manufacture: 13/12/2021 11:25
Batch size: 100 mL

FORMULATION

Materials	Batch No	Original formula	Working formula	Dispensed by	Checked by
Ciprofloxacin	RM000402	100 mg	150 mg		
Tween® 80	P6224	1 g	1 g		
Sodium lauryl sulfate	J054016	1 g	1 g		
Cholesterol	22968	1 g	0.6 g		
HPLC water		100 mL	100 mL		

Vesicle size: 109.45 nm
PDI: 0.32
Zeta potential: -37.03 mV
Entrapment efficiency: 48.01 %
Appearance: Milky white solution.

Biopharmaceutics Research Laboratory
Department of Pharmaceutics, Faculty of Pharmacy
Rhodes University
Makhanda 6140, South Africa

BATCH SET PRODUCTION RECORD 1/1

Product:
Ciprofloxacin niosomes
Batch number: F15

Start of Manufacture: 12/12/2020 11:45
End of Manufacture: 13/12/2021 11:45
Batch size: 100 mL

FORMULATION

Materials	Batch No	Original formula	Working formula	Dispensed by	Checked by
Ciprofloxacin	RM000402	100 mg	150 mg		
Tween® 80	P6224	1 g	1 g		
Sodium lauryl sulfate	J054016	1 g	1 g		
Cholesterol	22968	1 g	0.2 g		
HPLC water		100 mL	100 mL		

Vesicle size: 231.73 nm
PDI: 0.35
Zeta potential: -29.27 mV
Entrapment efficiency: 15.60 **%**
Appearance: Milky white solution.

Biopharmaceutics Research Laboratory
Department of Pharmaceutics, Faculty of Pharmacy
Rhodes University
Makhanda 6140, South Africa

BATCH SET PRODUCTION RECORD 1/1

Product:
Ciprofloxacin niosomes
Batch number: F16

Start of Manufacture: 12/12/2020 12:10
End of Manufacture: 13/12/2021 12:10
Batch size: 100 mL

FORMULATION

Materials	Batch No	Original formula	Working formula	Dispensed by	Checked by
Ciprofloxacin	RM000402	100 g	150 mg		
Tween® 80	P6224	1 g	1 g		
Sodium lauryl sulfate	J054016	1 g	1 g		
Cholesterol	22968	1 g	0.2 g		
HPLC water		100 mL	100 mL		

Vesicle size: 154.73 nm
PDI: 0.38
Zeta potential: -26.33 mV
Entrapment efficiency: 19.49 %
Appearance: Milky white solution.

Biopharmaceutics Research Laboratory
Department of Pharmaceutics, Faculty of Pharmacy
Rhodes University
Makhanda 6140, South Africa

BATCH SET PRODUCTION RECORD 1/1

Product:
Ciprofloxacin niosomes
Batch number: F17

Start of Manufacture: 12/12/2020 12:30
End of Manufacture: 13/12/2021 12:30
Batch size: 100 mL

FORMULATION

Materials	Batch No	Original formula	Working formula	Dispensed by	Checked by
Ciprofloxacin	RM000402	1000 g	150 mg		
Tween® 80	P6224	1 g	1 g		
Sodium lauryl sulfate	J054016	1 g	1 g		
Cholesterol	22968	1 g	0.2 g		
HPLC water		100 mL	100 mL		

Vesicle size: 185.05 nm
PDI: 0.41
Zeta potential: -3.46 mV
Entrapment efficiency: 14.90 %
Appearance: Milky white solution.

APPENDIX C

3D RESPONSE SURFACE PLOTS USED FOR THE DEVELOPMENT AND OPTIMIZATION OF A RP-HPLC FOR THE ANALYSIS OF CIPROFLOXACIN

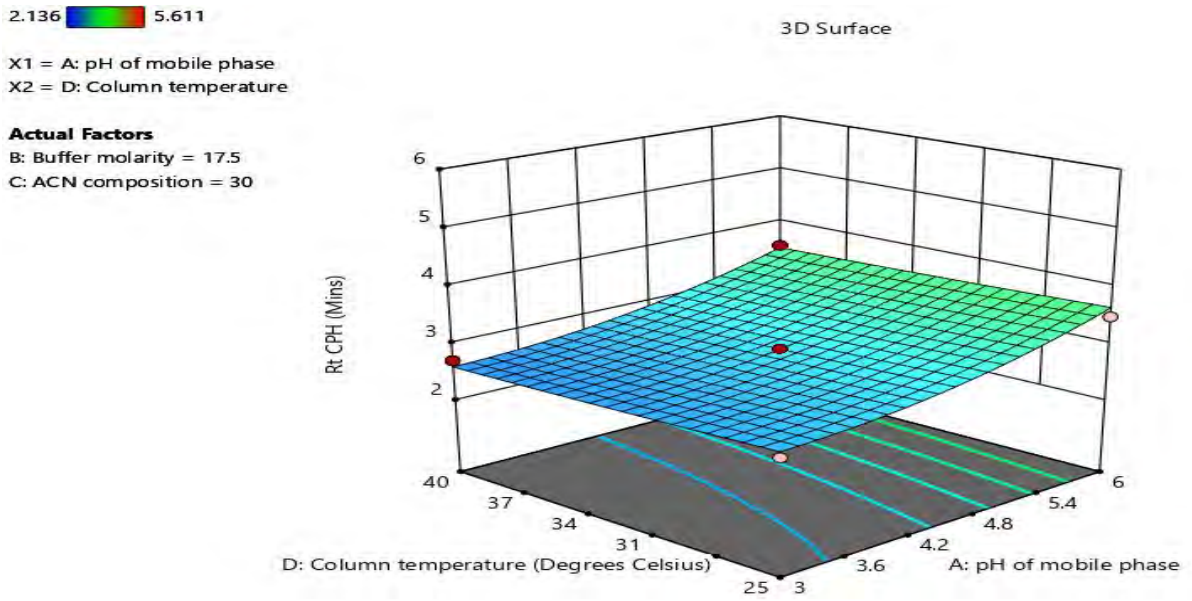

Figure C1 3D plot depicting the effect of column temperature and mobile phase pH on CPH R_t.

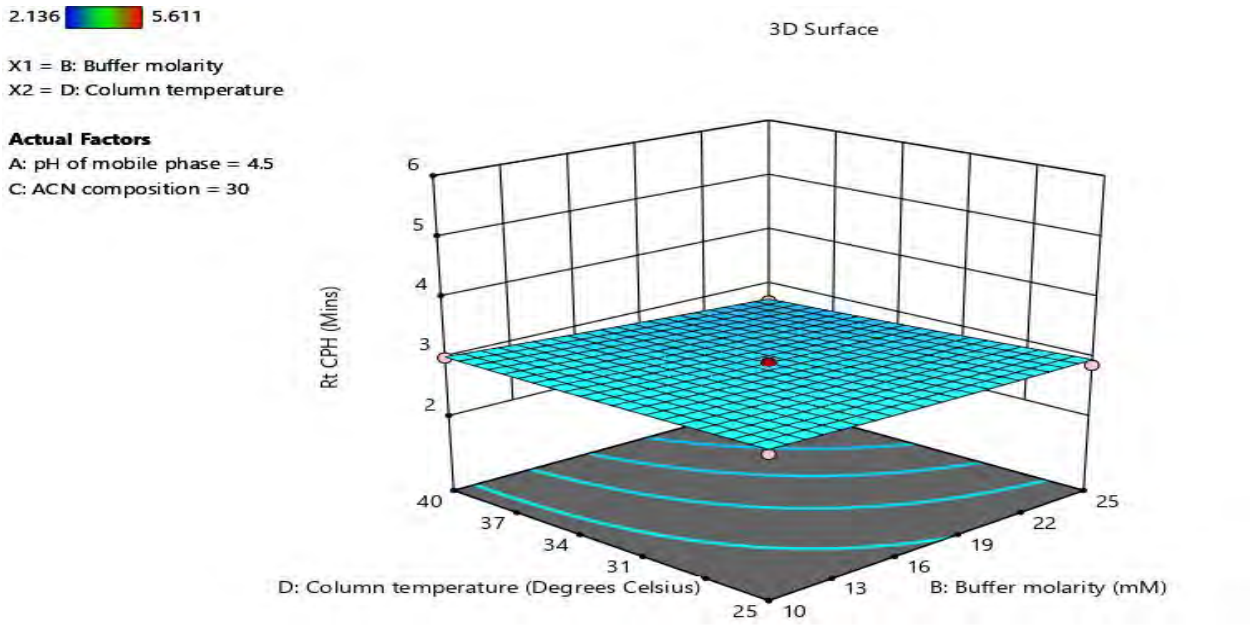

Figure C2 3D plot depicting the effect of buffer molarity and column temperature on CPH R_t.

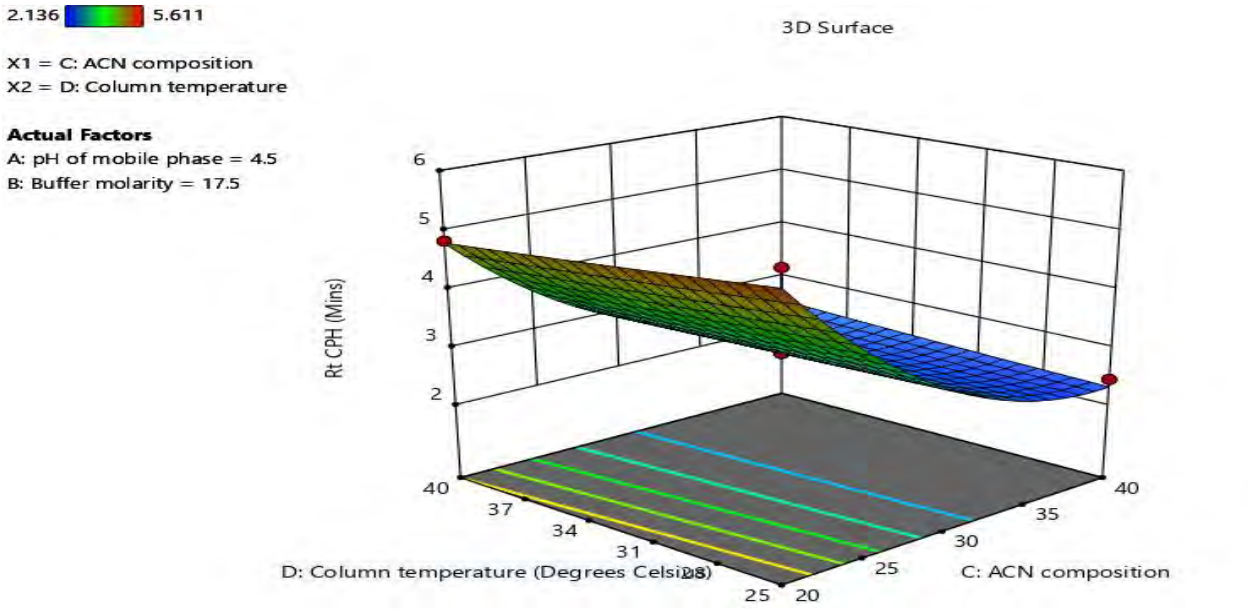

Figure C3 3D plot depicting the effect of column temperature and ACN composition on CPH R_t.

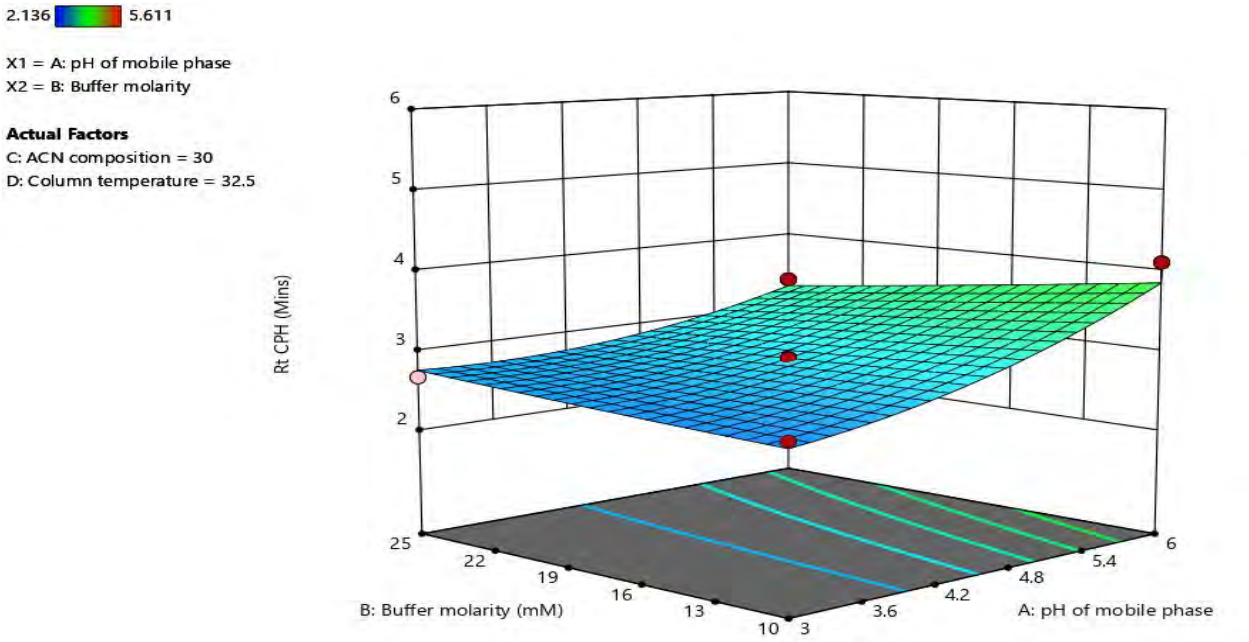

Figure C4 3D plot depicting the effect of buffer molarity and mobile phase pH on CPH R_t.

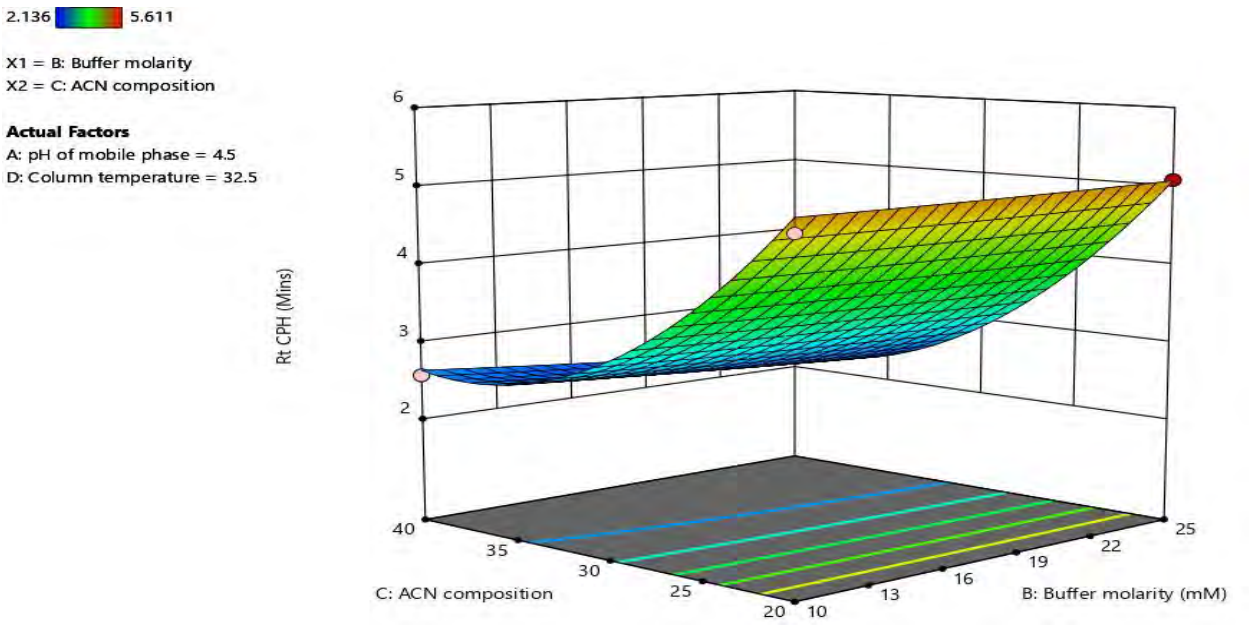

Figure C5 3D plot depicting the effect of ACN composition and buffer molarity on CPH R_t.

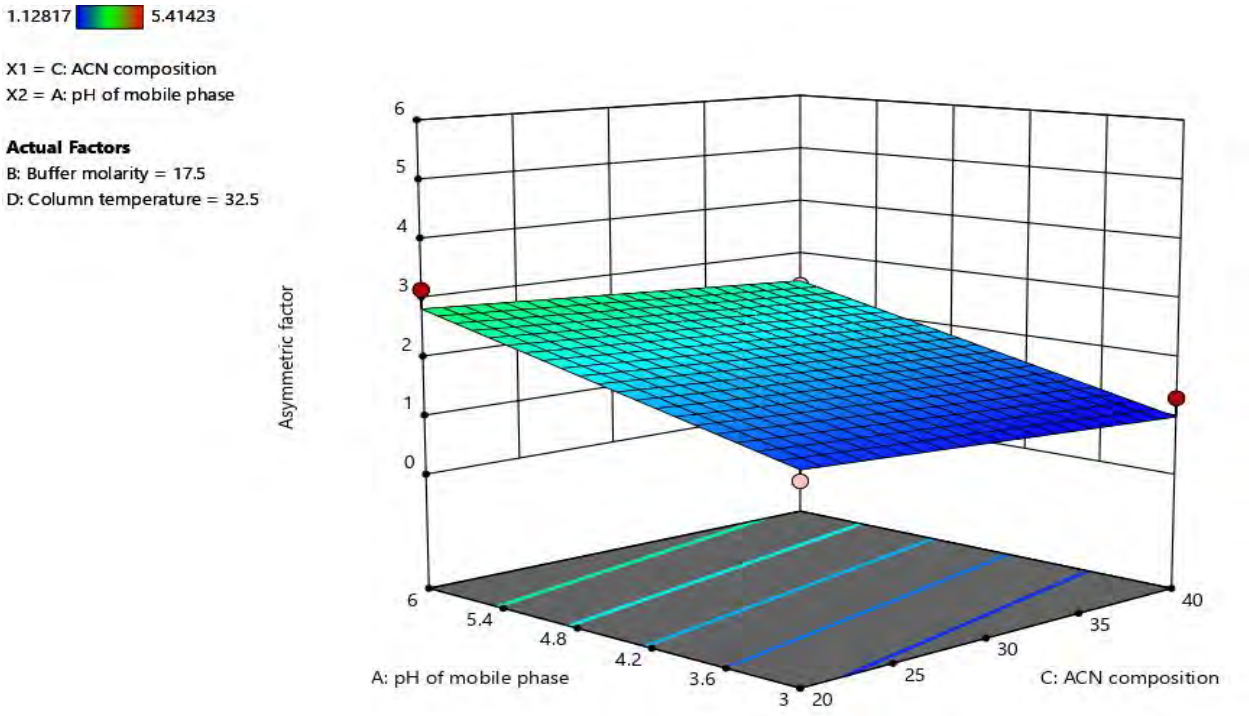

Figure C6 3D plot depicting the effect of mobile phase pH and ACN composition on asymmetric factor.

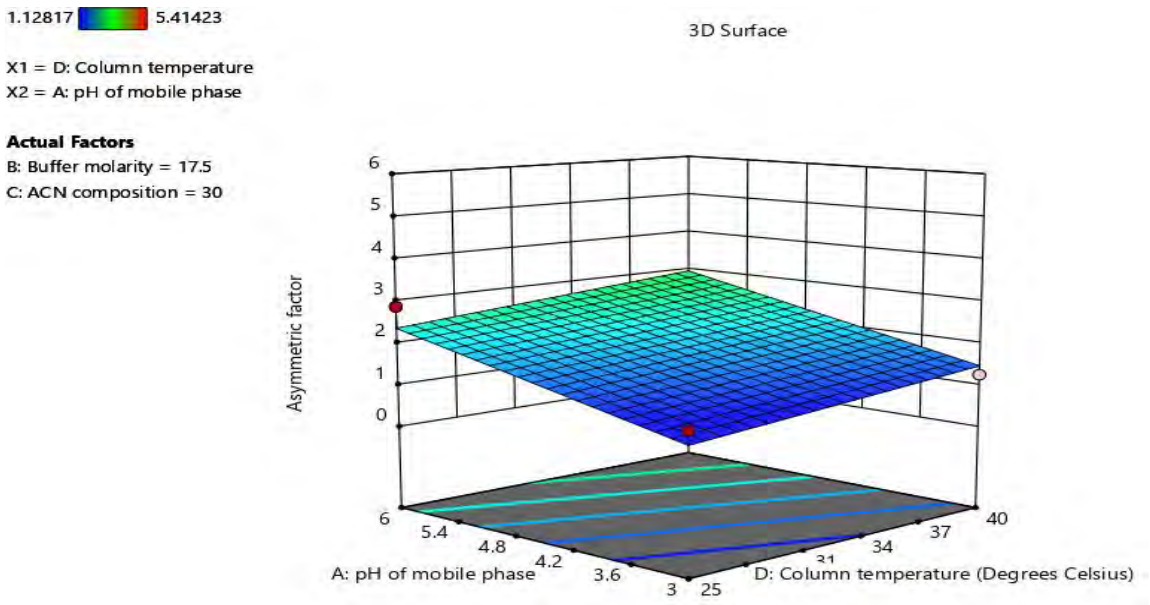

Figure C7 3D plot depicting the effect of mobile phase pH and column temperature on asymmetric factor.

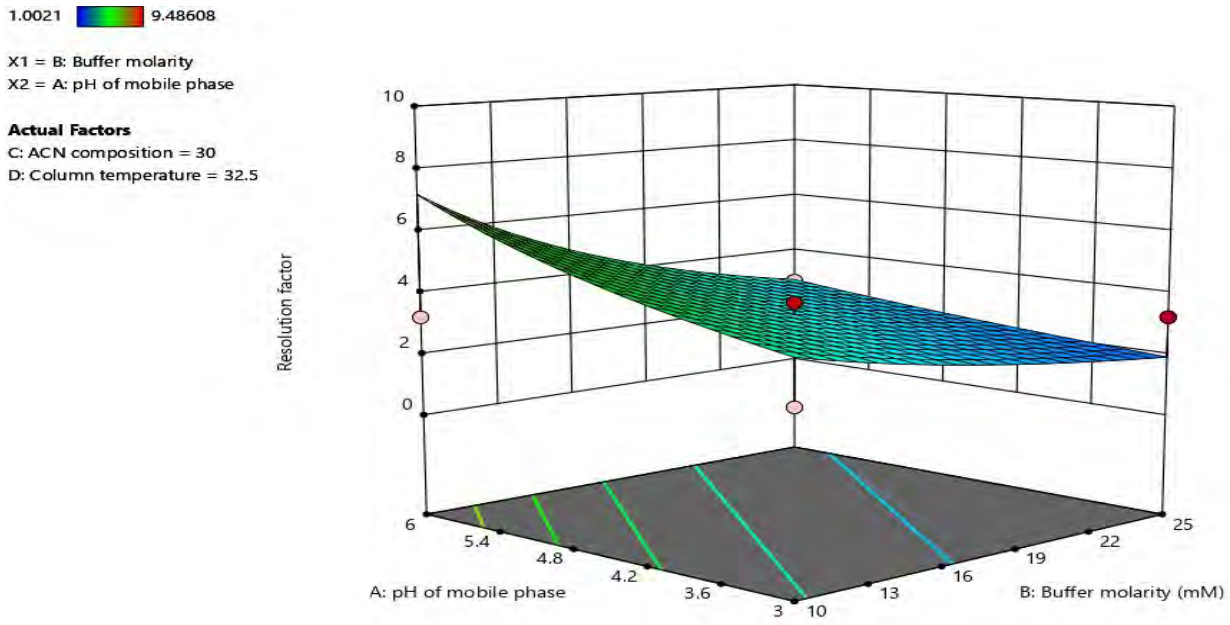

Figure C8 3D plot depicting the effect of mobile phase pH and buffer molarity on R_s.

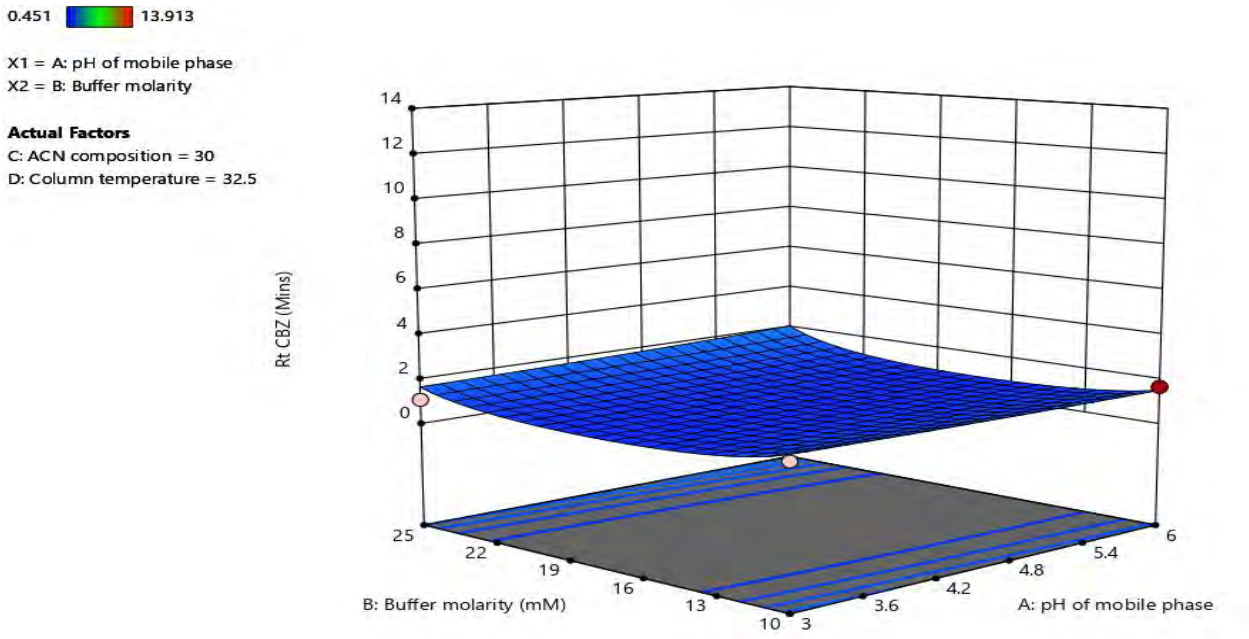

Figure C9 3D plot depicting the effect of buffer molarity and mobile phase pH on CBZ R_t.

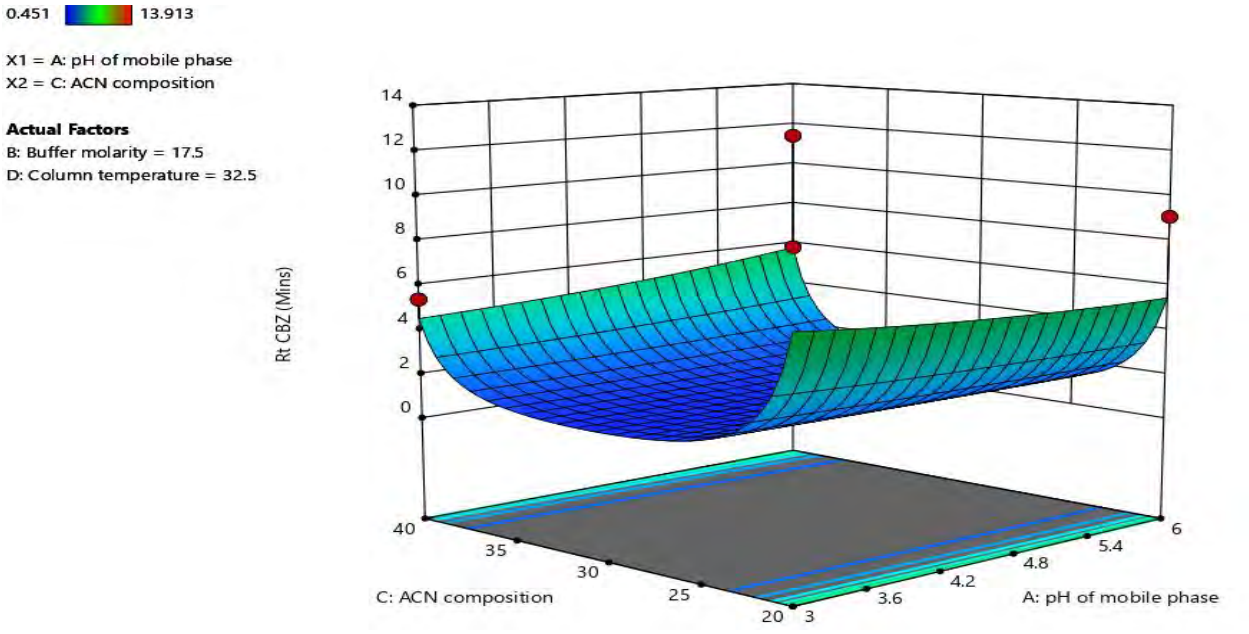

Figure C10 3D plot depicting the effect of ACN composition and mobile phase pH on CBZ R_t.

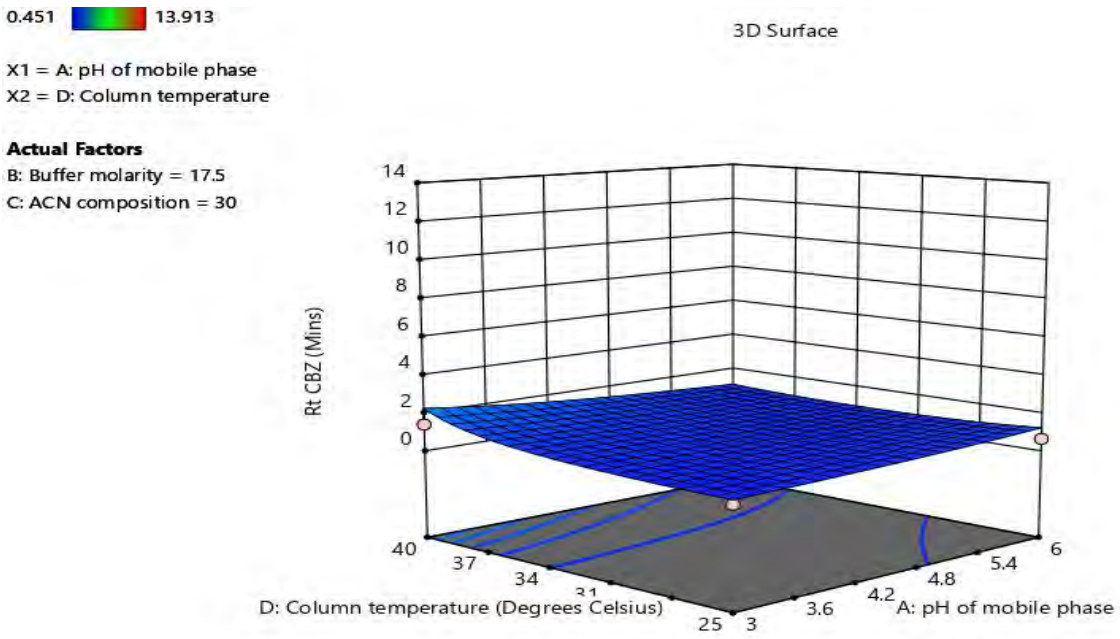

Figure C11 3D plot depicting the effect of column temperature and mobile phase pH on CBZ R_t.

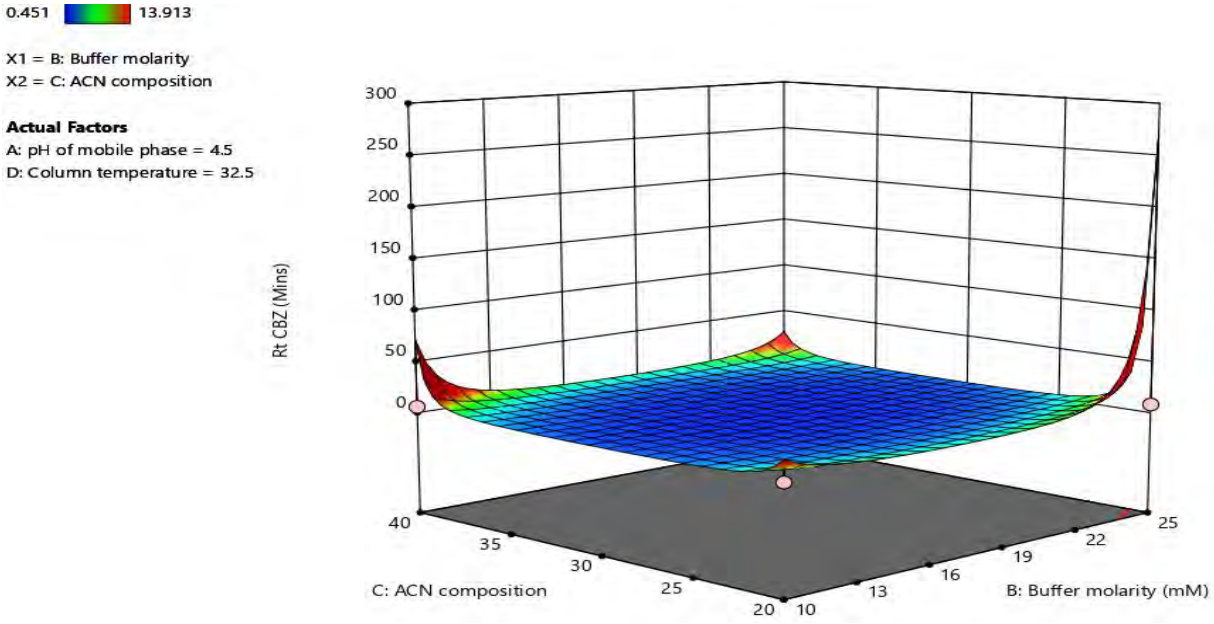

Figure C12 3D plot depicting the effect of ACN composition and buffer molarity on CBZ R_t.

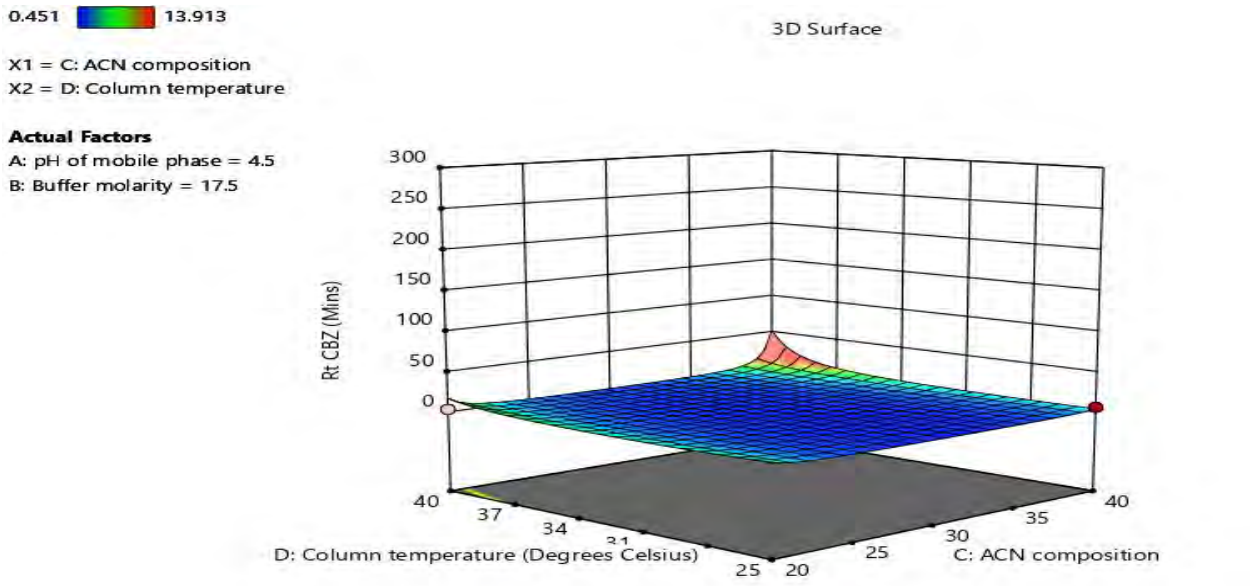

Figure C13 3D plot depicting the effect of column temperature and ACN composition on CBZ R_t.

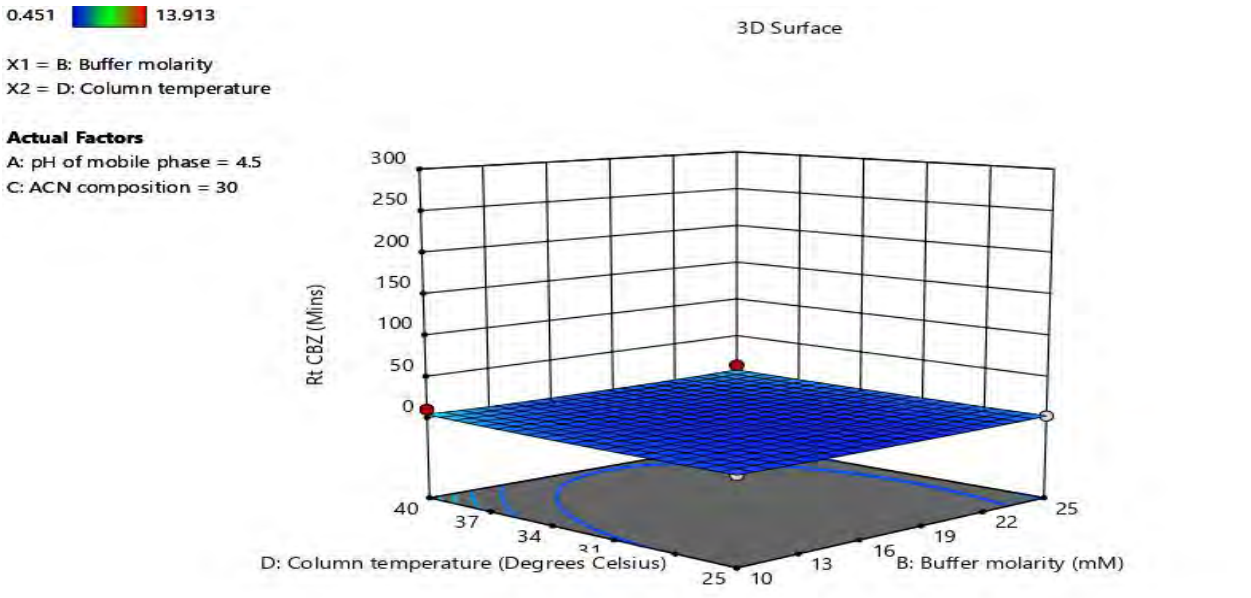

Figure C14 3D plot depicting the effect of column temperature and buffer molarity on CBZ R_t.

APPENDIX D

CONTOUR AND 3D RESPONSE SURFACE PLOTS FOR FORMULATION DEVELOPMENT AND OPTIMISATION STUDIES

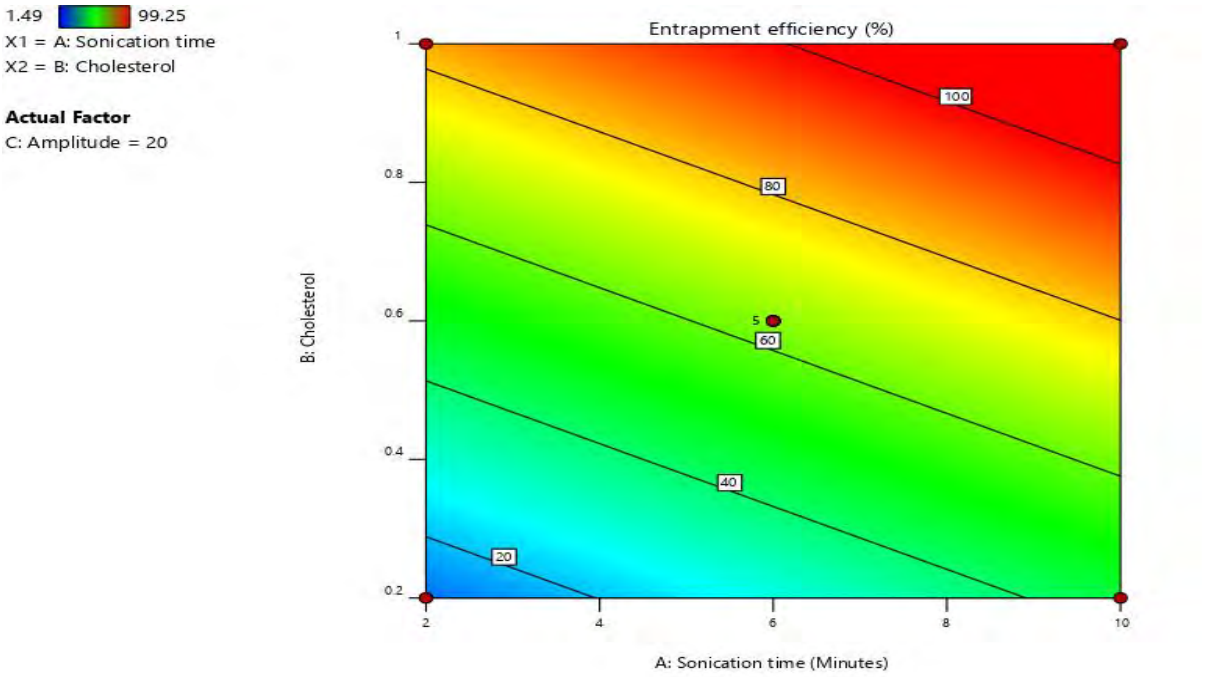

Figure D1 Contour plot depicting the effect of cholesterol and sonication time on entrapment efficiency.

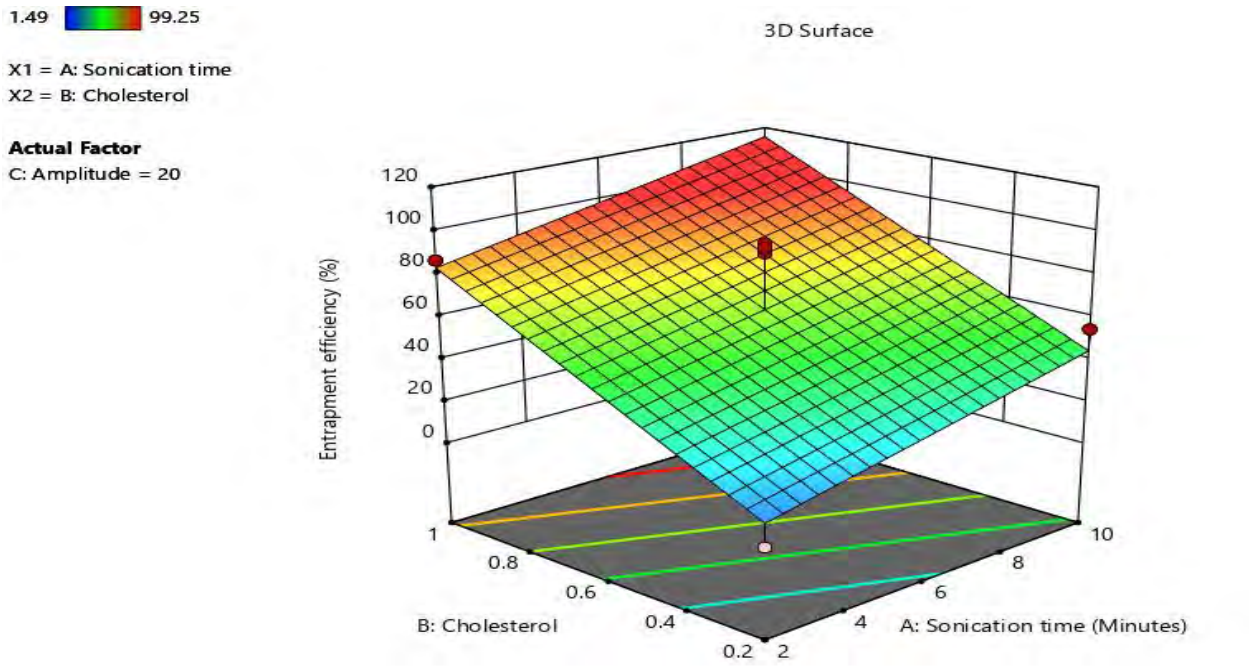

Figure D2 3D plot depicting the effect of cholesterol and sonication time on entrapment efficiency.

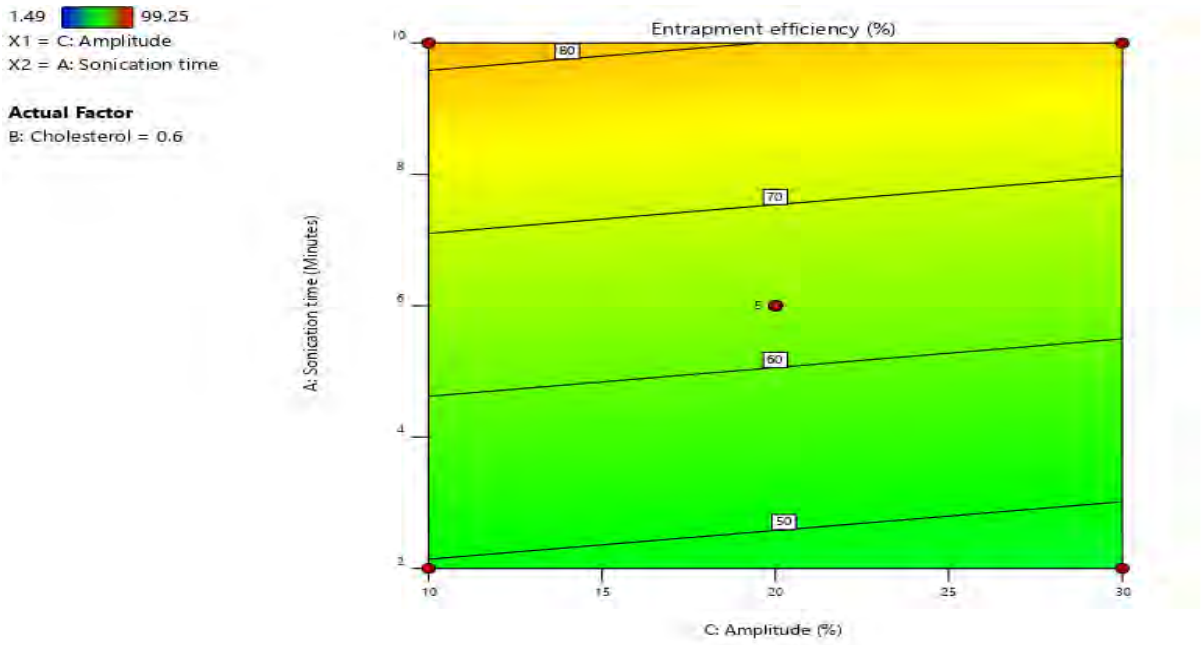

Figure D3 Contour plot depicting the effect of sonication time and amplitude on entrapment efficiency.

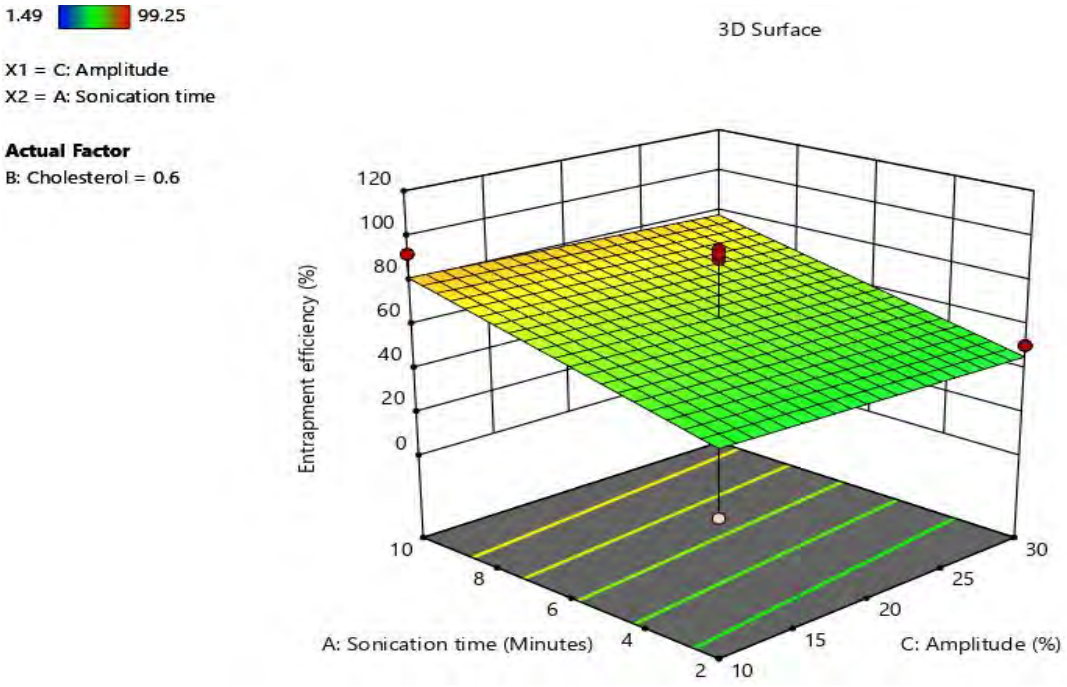

Figure D4 3D plot depicting the effect of sonication time and amplitude on entrapment efficiency.

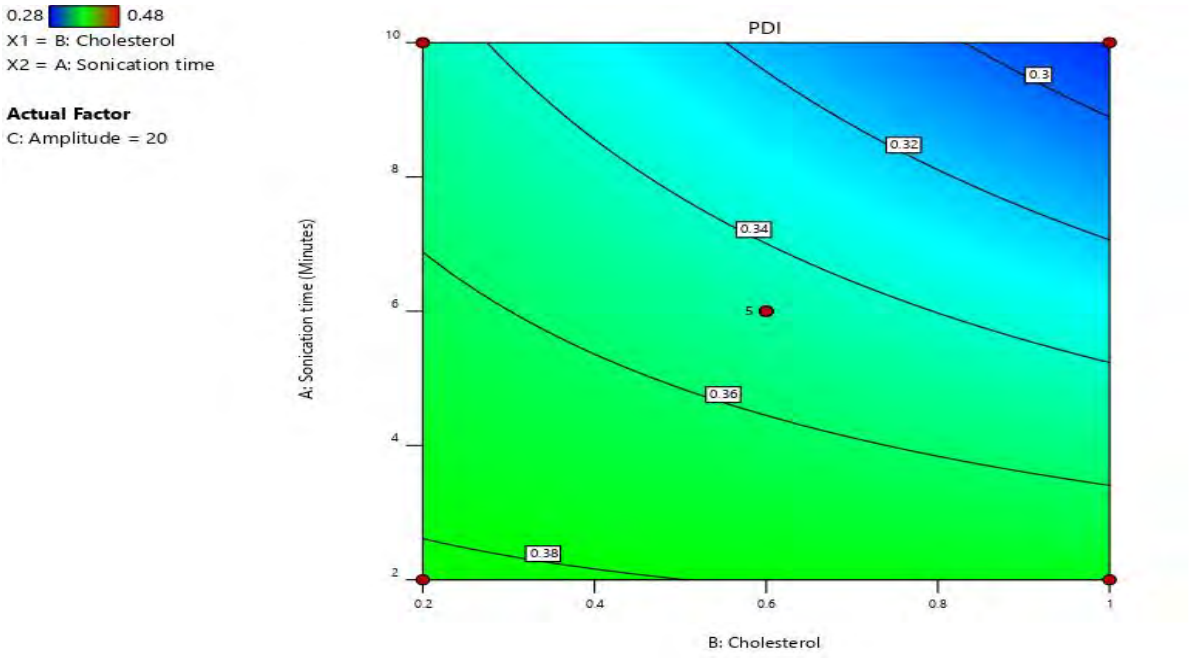

Figure D5 Contour plot depicting the effect of sonication time and cholesterol on PDI.

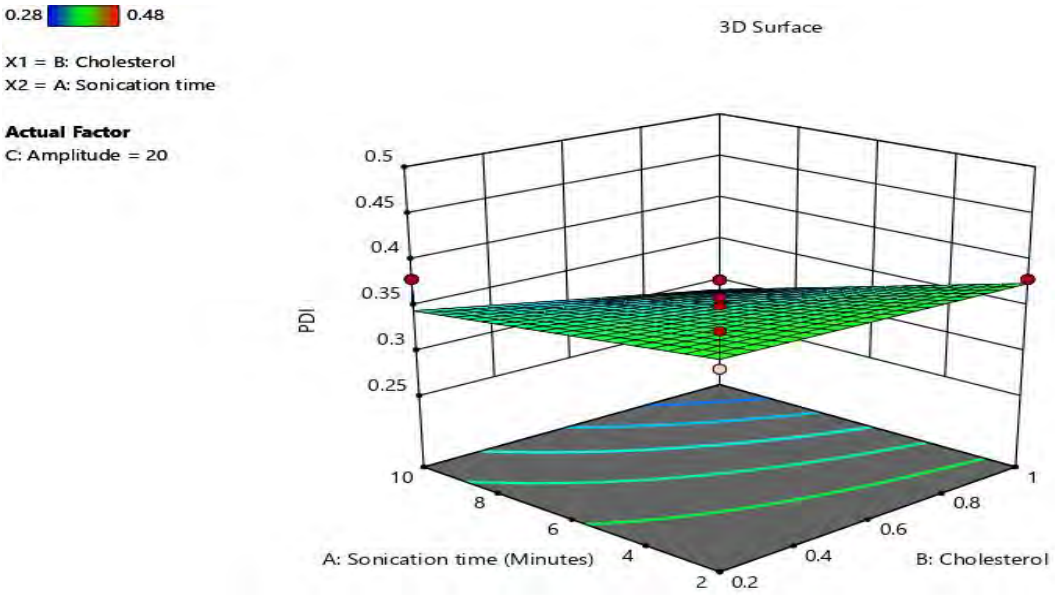

Figure D6 3D plot depicting the effect of sonication time and cholesterol on PDI.

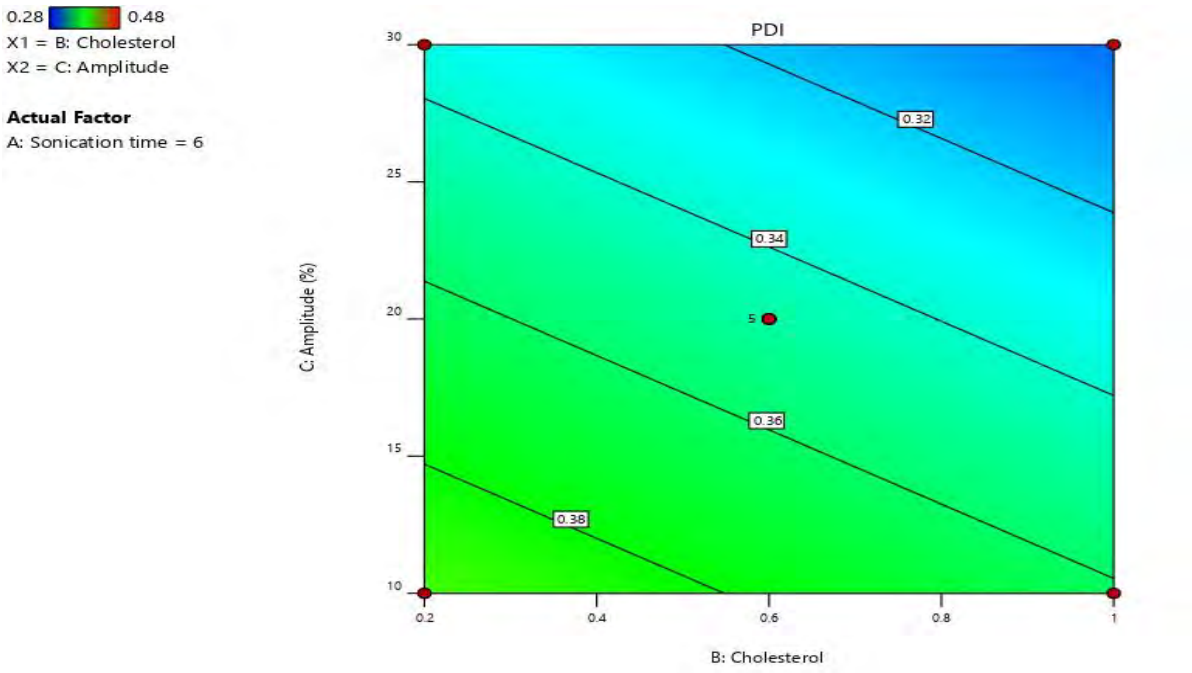

Figure D7 Contour plot depicting the effect of cholesterol and amplitude on PDI.

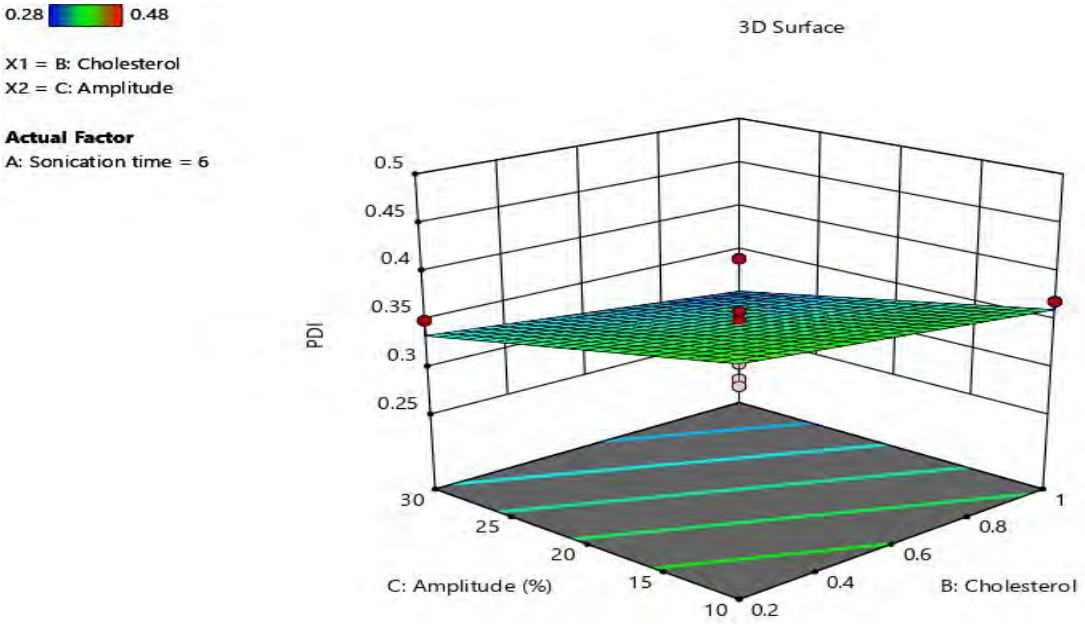

Figure D8 3D plot depicting the effect of amplitude and cholesterol on PDI.